

**STRUCTURE-ACTIVITY RELATIONSHIPS ANALYSIS OF (+)-DISCODERMOLIDE  
AND THE SYNTHESIS OF PRECURSORS FOR FURTHER ANALOGUE STUDIES**

by

**Amy Lynn Short**

B.S. Xavier University, 2008

Submitted to the Graduate Faculty of the  
Kenneth P. Dietrich School of Arts and Sciences in partial fulfillment  
of the requirements for the degree of  
Master of Science

University of Pittsburgh

2014

UNIVERSITY OF PITTSBURGH  
Dietrich School of Arts and Sciences

This thesis was presented

by

Amy Lynn Short

It was defended on

April 16, 2014

and approved by

Kay M. Brummond, Professor, Department of Chemistry

W. Seth Horne, Assistant Professor, Department of Chemistry

Dissertation Director: Dennis P. Curran, Distinguished Service Professor of Chemistry and  
Bayer Professor, Department of Chemistry

Copyright © by Amy Lynn Short

2014

# **STRUCTURE-ACTIVITY RELATIONSHIPS ANALYSIS OF (+)-DISCODERMOLIDE AND THE SYNTHESIS OF PRECURSORS FOR FURTHER ANALOGUE STUDIES**

Amy Lynn Short, MS

University of Pittsburgh, 2014

In 1990, the natural product discodermolide was isolated from a marine sponge and later found to have exceptional antiproliferative activity in cancer cells. Further studies showed discodermolide to stabilize microtubules via the taxoid binding site on  $\beta$ -tubulin. Unlike paclitaxel, it is not a substrate for P-glycoprotein transport, is potent in paclitaxel-resistant cell lines with  $\beta$ -tubulin mutations, exhibits better water solubility, and can act synergistically when combined with paclitaxel treatment. For this reason, discodermolide has been the focus of many synthetic and biological studies, culminating in a 60 gram-scale synthesis and Phase I/II clinical trials carried out by Novartis in 2004. Despite the great level of interest from the scientific community, much about this compound's behavior *in vivo* is still unknown. An extended analysis of known structure-activity relationships for discodermolide is presented herein. Also reported are the syntheses of a series of discodermolide fragments, which are designed to enable the formation of a novel analogue library via late-stage multicomponent reactions. Fragments to be synthesized prior to coupling are streamlined alternatives to the discodermolide framework that have shown promise in prior analogue and HQSAR studies. Overall, these modifications have been designed to improve the efficiency of synthetic efforts and to represent a wholly unique series of analogues for biological study.

## LIST OF ABBREVIATIONS

9-BBN	9-borabicyclo[3.3.1]nonane
Ac	Acyl
ACS	Accelerated Cell Senescence
Bn	Benzyl
CHO	Chinese hamster ovary
DAPI	6-diamidino-2-phenylindole
DIPEA	<i>N,N</i> -Diisopropylethylamine, Hünig's base
DM1A	Drugs and mouse monoclonal antibody
DMSO	Dimethyl sulfoxide
DNA	Deoxyribonucleic acid
EI	Electron ionization
equiv	Equivalent
ESI	Electrospray ionization
Et	Ethyl
EtOAc	Ethyl acetate
FT	Fourier transform
h	Hour
HDX	Hydrogen-deuterium exchange
HQSAR	Hologram quantitative structure activity relationship
HRMS	High resolution mass spectroscopy
HWE	Horner Wadsworth Emmons
IR	Infrared spectroscopy
L	Liter
LRMS	Low resolution mass spectroscopy
M	Molar
MCR	Multi-component reaction
MDR	Multi-drug resistant
MAP	Microtubule-associated protein
Me	Methyl
Mes	4-morpholineethanesulfonate
Mol	Mole
MS	Mass spectroscopy
MT	Microtubule
NAMFIS	Nuclear magnetic resonance analysis of molecular flexibility in solution
NMO	4-Methylmorpholine <i>N</i> -oxide
NMR	Nuclear magnetic resonance
Pgp	P-glycoprotein
PMB	<i>para</i> -Methoxy benzyl ether
Ph	Phenyl
r.t.	Room temperature
SA- $\beta$ -gal	Senescence-associated $\beta$ -galactosidase
SAR	Structure-activity relationship

sec	Second
TBS	<i>tert</i> -Butyl dimethylsilyl
TBSOTf	<i>tert</i> -Butyldimethylsilyl trifluoromethanesulfonate
THF	Tetrahydrofuran

## TABLE OF CONTENTS

<b>1.0</b>	<b>INTRODUCTION .....</b>	<b>1</b>
<b>1.1</b>	<b>TARGETING MICROTUBULES IN THE TREATMENT OF CANCER .....</b>	<b>3</b>
<b>1.2</b>	<b>BIOLOGICAL ACTIVITY OF DISCODERMOLIDE.....</b>	<b>7</b>
	<b>1.2.1 Immunosuppressive Activity.....</b>	<b>7</b>
	<b>1.2.2 Antiproliferative Properties Due to Microtubule Stabilization.....</b>	<b>8</b>
	<b>1.2.3 Discodermolide’s synergism with Paclitaxel .....</b>	<b>14</b>
	<b>1.2.4 Accelerated Cell Senescence and Resistance Mechanisms.....</b>	<b>17</b>
<b>1.3</b>	<b>PREVIOUS TOTAL SYNTHESSES OF DISCODERMOLIDE.....</b>	<b>18</b>
	<b>1.3.1 The Smith Group Fourth-Generation Synthesis.....</b>	<b>20</b>
	<b>1.3.2 The Paterson Group Third-Generation Synthesis.....</b>	<b>25</b>
	<b>1.3.3 The Novartis 60-g Scale Synthesis .....</b>	<b>30</b>
<b>1.4</b>	<b>STRUCTURE ACTIVITY RELATIONSHIPS FOR DISCODERMOLIDE ..</b>	<b>31</b>
	<b>1.4.1 Overview .....</b>	<b>31</b>
	<b>1.4.2 Carbamate Fragment Analogues.....</b>	<b>32</b>
	<b>1.4.3 Linker Fragment Analogues .....</b>	<b>36</b>
	<b>1.4.4 Lactone Fragment Analogues .....</b>	<b>37</b>
	<b>1.4.5 Analogues with Multiple Regions of Alteration .....</b>	<b>41</b>
	<b>1.4.6 SAR Summary.....</b>	<b>46</b>

<b>1.5</b>	<b>MODELING STUDIES OF DISCODERMOLIDE .....</b>	<b>47</b>
<b>2.0</b>	<b>RESEARCH PROJECT OVERVIEW.....</b>	<b>52</b>
	<b>2.1.1 Hypothesis.....</b>	<b>52</b>
	<b>2.1.2 Planned Research Approach.....</b>	<b>54</b>
<b>3.0</b>	<b>RESULTS AND DISCUSSION.....</b>	<b>59</b>
<b>3.1</b>	<b>CONFORMATIONAL MODELS OF DISCODERMOLIDE ANALOGUES</b>	<b>59</b>
<b>3.2</b>	<b>SYNTHESIS OF A CARBAMATE FRAGMENT COMMON PRECURSOR</b>	<b>61</b>
<b>3.3</b>	<b>SYNTHESIS OF LACTONE FRAGMENT PRECURSORS .....</b>	<b>62</b>
	<b>3.3.1 Summary of Fragment Syntheses.....</b>	<b>62</b>
	<b>3.3.2 Synthesis of the 3-(2-Hydroxypropyl)phenol Fragment 206.....</b>	<b>63</b>
	<b>3.3.3 Synthesis of 3-Propylphenol Fragments .....</b>	<b>65</b>
	<b>3.3.4 Synthesis of Coumarin Fragments .....</b>	<b>67</b>
	<b>3.3.5 Synthesis of 6,2-Normethyl-2,3-anhydro Lactone Fragments .....</b>	<b>69</b>
<b>4.0</b>	<b>SUMMARY .....</b>	<b>73</b>
<b>5.0</b>	<b>EXPERIMENTAL .....</b>	<b>75</b>
	<b>APPENDIX A .....</b>	<b>100</b>
	<b>APPENDIX B .....</b>	<b>111</b>
	<b>BIBLIOGRAPHY.....</b>	<b>158</b>

## LIST OF TABLES

Table 1: Summary of acid and amine lactone fragments syntheses. ....	63
Table 2. Characterization of cell lines used in discodermolide SAR studies. ....	101
Table 3. IC <sub>50</sub> values for carbamate fragment analogues, presented as a ratio of analogue to parent.....	102
Table 4. IC <sub>50</sub> values for linker fragment analogues, presented as a ratio of analogue to parent.	102
Table 5. IC <sub>50</sub> values for lactone fragment analogues, presented as a ratio of analogue to parent. .....	103
Table 6. IC <sub>50</sub> values for analogues with multiple regions of alteration, presented as a ratio of analogue to parent. ....	104
Table 7. Analogues with measured GI <sub>50</sub> values, rather than IC <sub>50</sub> values, presented as a ratio of analogue to parent. ....	105
Table 8. IC <sub>50</sub> values (nM) for discodermolide (left) and carbamate fragment analogues (right). .....	106
Table 9. IC <sub>50</sub> values (nM) for discodermolide (left) and linker fragment analogues (right). ....	107
Table 10. IC <sub>50</sub> values (nM) for discodermolide (left) and lactone fragment analogues (right)..	108
Table 11. IC <sub>50</sub> values (nM) for discodermolide (left) and analogues with multiple modifications (right). ....	109

Table 12. GI<sub>50</sub> values (nM) for discodermolide (left) and analogues with multiple modifications (right). ..... 110

## LIST OF FIGURES

Figure 1. The structure of (+)-discodermolide and other microtubule-stabilizing agents. ....	2
Figure 2. The structure of the microtubule and its tubulin subunits. ....	4
Figure 3. Immunofluorescence assay showing the effects of vinblastine on CHO cells. ....	6
Figure 4. The binding of paclitaxel to $\beta$ -tubulin (left) increases MT stability and bundling (right). .....	7
Figure 5. Cancer cells (left) treated with discodermolide (right) display MT bundling and hypernucleation. ....	8
Figure 6. Stimulation of MT assembly by discodermolide and paclitaxel. ....	9
Figure 7. Differences in tubulin binding contacts between paclitaxel and discodermolide. ....	13
Figure 8. Synergistic effects of A549 cell treatment with discodermolide and paclitaxel. ....	15
Figure 9. A summary of completed total syntheses of discodermolide, 1993-2007. ....	20
Figure 10. A summary of the approach taken by Novartis in their large-scale synthesis of <b>1</b> . ....	31
Figure 11. Distinctive regions of discodermolide for SAR analysis. ....	32
Figure 12. Modifications to the terminal diene. ....	33
Figure 13. Modifications to the C19 carbamate group. ....	34
Figure 14. Modifications to the carbamate fragment. ....	36
Figure 15. Cyclization of the linker region of discodermolide. ....	37

Figure 16. Synthetic analogues of the lactone group.....	39
Figure 17. Streamlined analogues of the lactone group containing aromatic rings.....	40
Figure 18. Truncation of the discodermolide backbone. ....	41
Figure 19. Saturation of discodermolide olefins.....	42
Figure 20. Acetylation of alcohol groups present in discodermolide. ....	42
Figure 21. Investigation of lactone modifications coupled with C14 and/or C23-24 alterations. ....	43
Figure 22. Carbamate and linker region modifications paired with a ring-opened lactone.....	44
Figure 23. Carbamate and lactone fragment modifications.....	46
Figure 24. Summary of the SAR profile for discodermolide.....	47
Figure 25. Conformational preferences are determined by strain minimization. ....	48
Figure 26. Conformational models of discodermolide. ....	49
Figure 27. Proposed binding conformation of discodermolide. ....	51
Figure 28. Discodermolide compared to the top performing hits from Day group HQSAR experiments. Modified regions are circled on the analogues. <sup>114</sup> .....	53
Figure 29. Reaction summary for (a) Ugi and (b) van Leusen MCR approaches. ....	54
Figure 30. Design of discodermolide analogues joined by a linker through MCR. ....	55
Figure 31. Fragments initially identified for this project's analogue studies. ....	56
Figure 32. Sample analogues resulting from (a) van Leusen and (b,c) Ugi reactions.....	57
Figure 33. Overlay of sample MCR analogues <b>198-200</b> and discodermolide (white). ....	60

## LIST OF SCHEMES

Scheme 1. Smith's fourth-generation retrosynthetic plan, with stereotriad locations labeled.....	21
Scheme 2. Smith's fourth-generation synthesis of fragment <b>2</b> .....	22
Scheme 3. Smith's fourth-generation synthesis of common precursor <b>6</b> .....	22
Scheme 4. Smith's fourth-generation synthesis of lactone intermediate <b>5</b> .....	23
Scheme 5. Smith's fourth-generation synthesis of linker fragment <b>4</b> .....	24
Scheme 6. Smith's fourth-generation coupling of advanced intermediates to form <b>1</b> .....	25
Scheme 7. Paterson's third-generation retrosynthetic plan.....	26
Scheme 8. Paterson's third-generation synthesis of $\beta$ -ketophosphonate <b>19</b> .....	27
Scheme 9. Paterson's third-generation synthesis of aldehyde intermediate <b>23</b> .....	28
Scheme 10. Paterson's third-generation synthesis of aryl ester <b>22</b> .....	28
Scheme 11. Endgame coupling strategy of Peterson's third-generation synthesis.....	30
Scheme 12. Transformation of common precursor <b>196</b> into an advanced carbamate fragment. <sup>114</sup> .....	58
Scheme 13. Synthesis of a discodermolide common precursor lactone. ....	61
Scheme 14. First-generation synthesis of fragment <b>206</b> via dihydroxylation. ....	64
Scheme 15. Second-generation synthesis of $\beta$ -hydroxyamine <b>206</b> via an epoxide intermediate. ....	65
Scheme 16. Synthesis of acid fragment <b>207</b> . ....	66

Scheme 17. Two routes towards the synthesis of amine fragment <b>208</b> . .....	67
Scheme 18. Synthesis of the 7-carboxycoumarin fragment <b>209</b> .....	68
Scheme 19. Synthesis of the 7-aminocoumarin fragment <b>210</b> . .....	69
Scheme 20. Synthesis of the 2-normethyl-2,3-anhydro fragment. ....	70

## 1.0 INTRODUCTION

Marine life has long been established as a leading source of a diverse and potent array of potent biologically active natural products.<sup>1</sup> Consequently, marine bioprospecting has yielded numerous promising targets for future biomedical research and application. One of these compounds, (+)-discodermolide (Figure 1) was first isolated from the marine sponge *Discodermia dissoluta* in 1990 by the Harbor Branch Institution, Inc. and shown to have immunosuppressive activity.<sup>2-5</sup> Later studies established discodermolide as an extraordinarily potent microtubule (MT) stabilizer. MTs are essential and dynamic cellular structures, involved in multiple critical functions including signaling, intracellular transport, and division. Because cancer cells often rely heavily on these mechanisms for growth and proliferation, MTs and their tubulin subunits are viable targets for cancer therapeutics.<sup>6</sup> With potency rivaling that of the industry standard of the time, paclitaxel, discodermolide garnered significant interest in the scientific community.

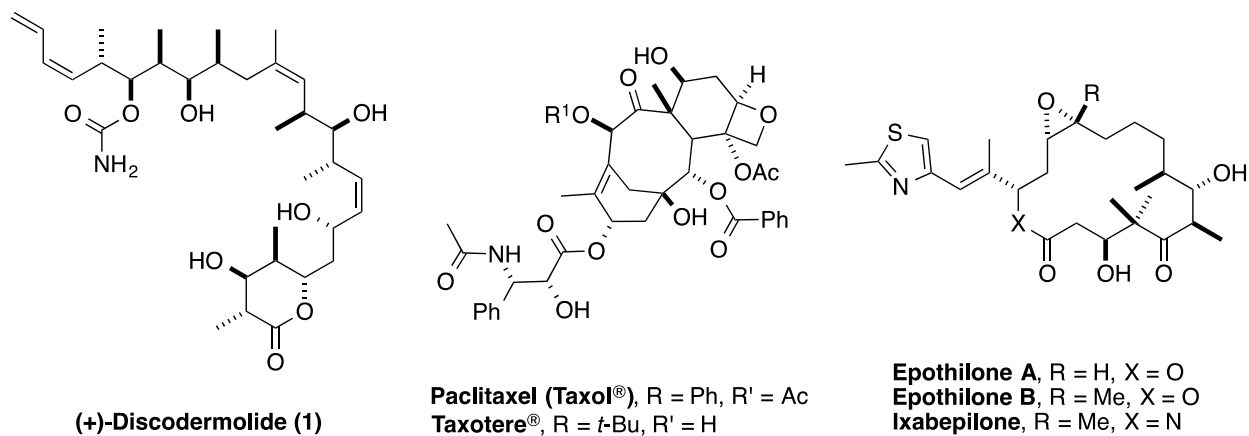


Figure 1. The structure of (+)-discodermolide and other microtubule-stabilizing agents.

Several total syntheses were completed in succeeding years to circumvent natural supply limitations and allow for more thorough biological studies.<sup>7,8</sup> It was found that discodermolide acted as a MT-stabilizing agent with impressive potency, drawing comparisons to paclitaxel and the more recently established epothilone series (Figure 1).<sup>9</sup> Altogether, discodermolide contains 13 stereogenic centers, a tetrasubstituted  $\delta$ -lactone, a di-substituted and tri-substituted (*Z*)-olefin, a terminal (*Z*)-olefin, and a carbamate moiety. This complex functionalization made total synthesis efforts challenging. Overcoming this challenge, efforts towards total synthesis of the compound culminated in the production of over 60 g of the natural product by Novartis for preliminary clinical trials. In 2004, these initial Phase I/II trials were halted due to pneumotoxic effects experienced by 3 patients in the course of the study, possibly due to metabolite formation.<sup>10,11</sup>

Herein are reported efforts towards the design and synthesis of simplified analogues of discodermolide for biological evaluation. Total syntheses attempts in the past have yielded gram quantities of the compound, but have also highlighted the difficulties inherent in the synthesis of such a complex polyketide. By simplifying the structure of discodermolide, it is hypothesized that a more facile synthesis can be obtained without significantly sacrificing MT stabilizing

activity. A multicomponent reaction (MCR) approach will be carried out for late-stage coupling of analogue fragments that will increase the potential for structural diversity and enable a more complete structure-activity relationship (SAR) profile to be developed for this promising drug target.

## 1.1 TARGETING MICROTUBULES IN THE TREATMENT OF CANCER

The cytoskeleton of eukaryotic cells is composed of three distinct types of structural proteins: microtubules, microfilaments such as actin, and intermediate filaments.<sup>6</sup> Diverse cellular functions of MTs include key roles in structural support, mitosis, meiosis, motility, and the transport of macromolecules. They are a polymeric species comprised of alpha and beta tubulin heterodimers, which are in a constant state of dynamic instability. The polymerization and organization of the MT strands differ by the needs of the individual cell, which are determined by location, type, and phase in the cell cycle.

Generally, eukaryotic MT spindles contain 12-13 linear chains of tubulin heterodimers called protofilaments (Figure 2a).<sup>12</sup> Protofilaments nucleate and are then held together through lateral bonds to form a hollow cylinder about 25 nm in diameter. The heterodimer subunits within each protofilament have the same orientation, so at one end (designated as minus),  $\alpha$ -tubulin is exposed and at the opposite end (designated as plus),  $\beta$ -tubulin is exposed (Figure 2b).<sup>12</sup> GTP attached to the  $\beta$ -tubulin at the exchangeable nucleotide site (E-site) provides requisite energy for assembly and disassembly. Once a heterodimer is incorporated into the growing MT, this  $\beta$ -tubulin GTP is hydrolyzed to GDP after a brief delay by the  $\beta$ -tubulin. Exposure of GDP-tubulin at the + end of the tubulin strand leads to the rapid dissociation of the

heterodimers, a process designated as catastrophe (Figure 2c).<sup>12</sup> MT dynamics are characterized by abrupt and asynchronous periods of catastrophe and recovery, allowing them to act as rigid structural support while simultaneously being capable of sudden depolymerization.

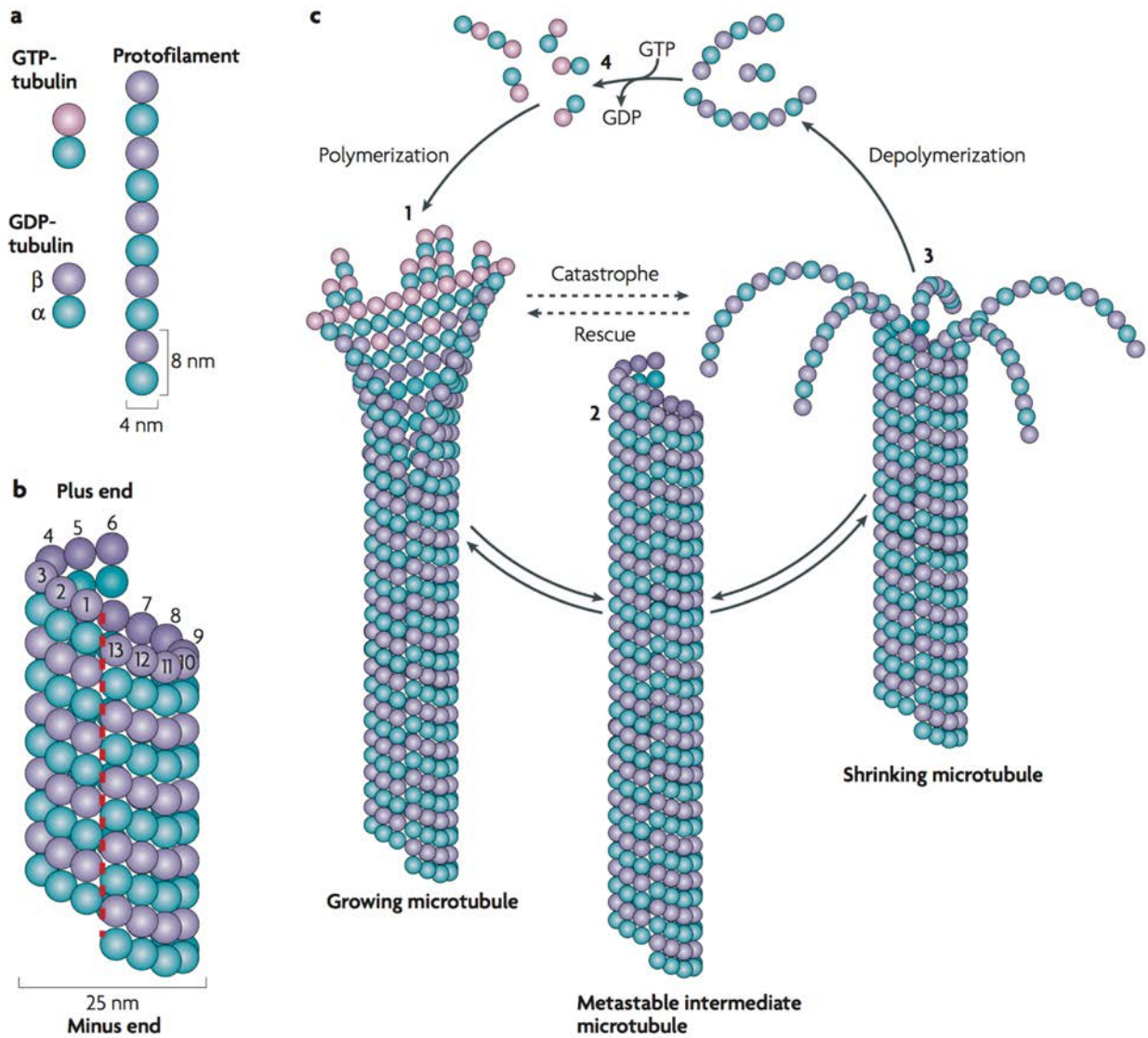


Figure 2. The structure of the microtubule and its tubulin subunits.

a) The MT protofilament is composed of repeating  $\alpha\beta$ -tubulin dimers; b) Parallel protofilaments align to form the hollow MT; c) the process of MT growth and catastrophe, via hydrolysis of GTP. *Reprinted with permission from Macmillan Publishers Ltd: Ref. 12, copyright 2008.*

Notably, MTs are responsible for the quick reorganization of replicated chromosomes during mitosis. The lengthy interphase MT strands disassemble at the onset of mitosis and become 4-100 times more dynamic, exhibiting half-times of 10-30 sec.<sup>13-15</sup> After the breakdown of the nuclear envelope, MTs probe the cytoplasm for chromosomes and converge at the spindle poles once the MT is attached to the chromosomal kinetochore. Finally, duplicated chromosomes separate and move towards the cell periphery as the daughter cells divide. Deviation from this carefully regulated process often results in cell cycle arrest in a prometaphase/metaphase-like state that leads to apoptosis.

Mitotic inhibition has proven itself to be a powerful tool for cancer treatment. Because MT dynamics are so critical for proper cell division, interruption of this process through stabilization or destabilization of the polymers can have a dramatic effect on cell populations.<sup>16</sup> Many types of cancer cells divide more frequently than healthy cells, and therefore have a substantial vulnerability to this type of interruption. The mechanisms of specific anti-mitotic agents on MT polymerization vary, but they are generally designated as either MT-stabilizing or MT-destabilizing agents. Depending on the individual drug's mechanism of action, it may bind to the MT directly and/or to soluble tubulin. An additional point of difference between anti-mitotic drugs may be their binding site along the MT framework.

A good example of the general diversity of these drugs lies in a comparison of the popular drugs vinblastine and paclitaxel. Vinblastine binds to  $\beta$ -tubulin at the "plus" end of the MT, causing the protofilaments to begin curling and suppressing further polymerization.<sup>17-19</sup> MT dynamics are slowed dramatically, and mitosis stalls with chromosomes unable to segregate at the spindle poles. The dramatic influence of vinblastine on the MT network can be seen in

Figure 3.<sup>20</sup> As more drug is added, cells experience difficulties with chromosomal separation and appear misshapen and multinucleated, reentering G<sub>1</sub> phase without dividing.

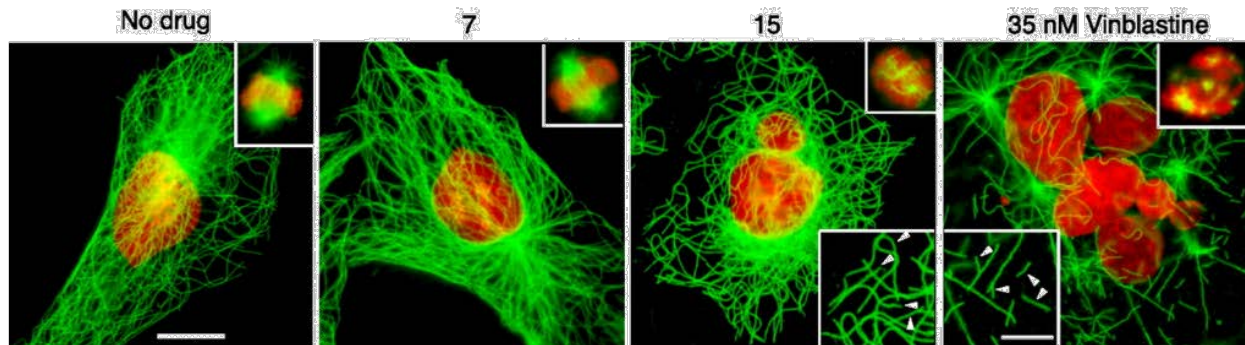


Figure 3. Immunofluorescence assay showing the effects of vinblastine on CHO cells.

Cells were treated 2 days with the indicated concentration of vinblastine, and then stained with DM1A for tubulin (green) and DAPI for DNA (red). Upper inserts show representative mitotic cells. *Adapted with permission from the American Society for Biochemistry and Molecular Biology, Ref. 20, copyright 2010.*

In contrast to the behavior of vinblastine, paclitaxel is known as an MT stabilizer. It preferentially binds to the inner surface of the  $\beta$ -tubulin with a 1:1 stoichiometry when at high concentrations of paclitaxel (Figure 4, left).<sup>21,22</sup> Even though the typical MT contains 10,000 tubulin subunits, just one molecule of paclitaxel per several hundred tubulin subunits is required to reduce MT shortening by about 50%.<sup>23</sup> Interaction with paclitaxel stabilizes the MT polymer, interrupting mitosis by forming MT bundles during interphase and preventing spindle asters from disassembling (Figure 4, right).<sup>24</sup> Despite its promising activity, the low aqueous solubility and development of cancer cell resistance to paclitaxel – typically through overexpression of P-glycoprotein (Pgp) or  $\beta$ -tubulin mutations – leaves much room for improvement for this type of therapeutic agent.

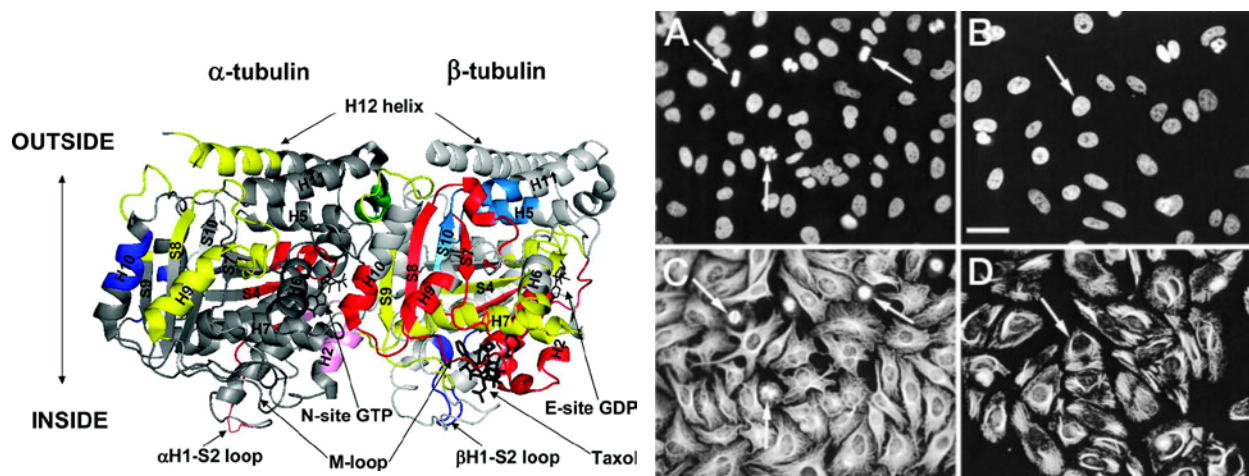


Figure 4. The binding of paclitaxel to  $\beta$ -tubulin (left) increases MT stability and bundling (right).

Left: Paclitaxel in the  $\beta$ -tubulin binding site of the tubulin heterodimer. Right: HeLa cells were incubated for 14.5 h in the presence of either drug vehicle (A and C) or 1  $\mu$ M paclitaxel (B and D). Images depict either labeled nuclei (A and B) or immunolocalized tubulin (C and D). Arrows identify subpopulations experiencing different stages of mitosis when treated with drug vehicle (A and C) or those with MT bundling when treated with drug (B and C).

*Image at left reprinted with permission from Cell Press, Ref. 22, copyright 2009; image at right reprinted with permission from The American Association for Cancer Research, Ref. 24, copyright 2002.*

## 1.2 BIOLOGICAL ACTIVITY OF DISCODERMOLIDE

### 1.2.1 Immunosuppressive Activity

Shortly after its isolation in 1990, scientists at the Harbor Branch Oceanographic Institute, Inc. found discodermolide to exhibit immunosuppressive activity in murine *in vitro* and *in vivo* graft versus host splenomegaly studies.<sup>3-5</sup> Its activity was comparable to that of cyclosporine A, and in these studies activity was attributed to a general antiproliferative effect on lymphoid cells at low nM concentrations. Cell cycle studies showed that treatment with discodermolide resulted in reversible G<sub>2</sub>/M cell cycle arrest.<sup>5</sup> At the same time, Gunesequera and co-workers at Harbor

Branch elucidated the structure and relative stereochemistry of the compound through an array of 1- and 2-dimensional NMR experiments, as well as X-ray crystallography.<sup>2</sup>

### 1.2.2 Antiproliferative Properties Due to Microtubule Stabilization

By 1996, a collaboration between Day and ter Haar demonstrated that the observed cell cycle arrest of discodermolide-treated cells was related to MT binding and stabilization.<sup>8</sup> In their seminal study, it was shown that the MTs of MCF-7 cells exhibited significant morphological changes in the presence of discodermolide. The IC<sub>50</sub> after 48 h of continuous drug exposure was found to be 2.4 nM, whereas that for the benchmark MT stabilizer paclitaxel was 2.1 nM. The cytotoxicity of paclitaxel and discodermolide were found to be quite similar, although further comparison to paclitaxel with *in vitro* models revealed several notable differences between the two. Discodermolide prompted a more rapid and significant bundling of the MT network when compared to paclitaxel, as shown in Figure 5.<sup>25</sup>

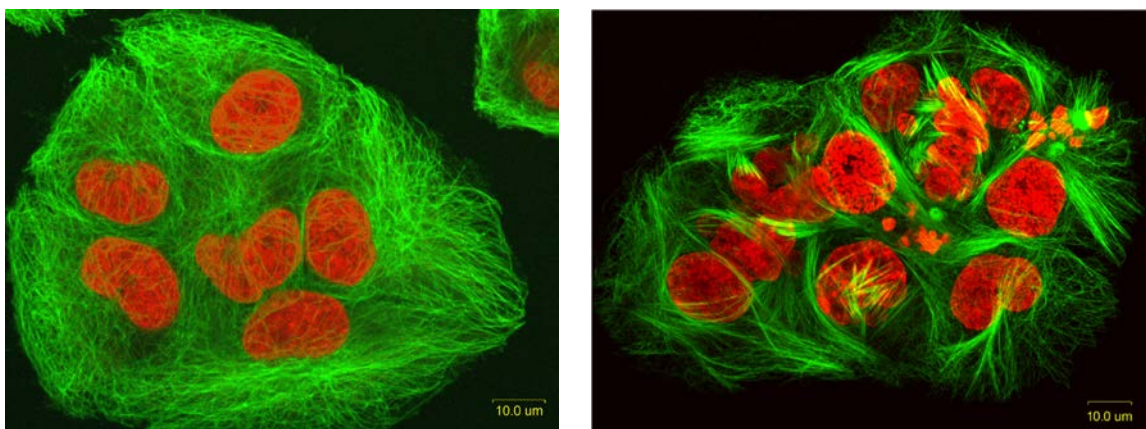


Figure 5. Cancer cells (left) treated with discodermolide (right) display MT bundling and hypernucleation. Immunofluorescence staining shows the reorganization of cellular DNA (red) and tubulin (green) within the cells. Reprinted with permission from Ref. 25, Florida Atlantic University, Harbor Branch Oceanographic Institute.

Turbidity studies with purified tubulin demonstrated the superior ability of discodermolide to promote the hypernucleation of tubulin assembly in conditions that typically favor depolymerization. An experiment highlighting this phenomenon is depicted in Figure 6, where tubulin polymerization was monitored in the absence of drug (curve 1), with 10  $\mu$ M paclitaxel (curve 2), or with 10  $\mu$ M discodermolide (curve 3). Here, a higher level of absorbance correlates to an increase in turbidity brought about by tubulin assembly.

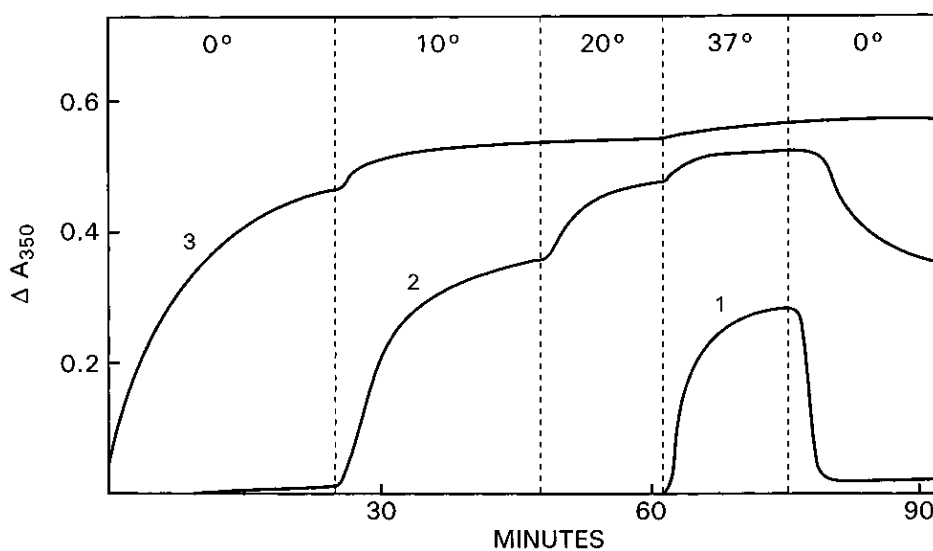


Figure 6. Stimulation of MT assembly by discodermolide and paclitaxel.

Reaction mixtures contained 0.1 M Mes buffer, 4% DMSO, 10  $\mu$ M tubulin, 100  $\mu$ M GTP, 5  $\mu$ M heat-treated MAP.  
Reprinted with permission from Ref. 8, copyright 1996 American Chemical Society.

A separate series of experiments in the same study showed that discodermolide polymers persisted even with minimal concentrations of drug and in conditions typically favoring depolymerization. These conditions included low temperatures, addition of up to 5 mM of catastrophe-promoting  $\text{Ca}^{2+}$  salts, and the omission of stabilizing microtubule-associated proteins (MAPs). Additionally, the number and length of tubulin polymers produced was quantified through electron microscopy studies. MT length in discodermolide-treated cells was proven to

be independent of temperature, with 0.5-0.6  $\mu\text{m}$  average lengths at temperatures between 0°C and 37°C. Paclitaxel was unable to hypernucleate tubulin assembly as significantly, and polymers averaged over 1.6  $\mu\text{m}$  in length in the same conditions. These exciting results demonstrated the potential for discodermolide as a novel therapeutic agent in neoplastic disease.

Concurrent to this work, the Schreiber group carried out studies to determine the specific binding affinities of discodermolide compared to paclitaxel.<sup>26</sup> A series of experiments exposing tubulin to radiolabelled [<sup>3</sup>H]-paclitaxel and then [<sup>3</sup>H]-discodermolide enabled the group to perform competitive binding studies. They found that discodermolide treatment initiated cell cycle arrest in the metaphase-anaphase transition in mitosis by binding to tubulin dimers with a 1:1 stoichiometry. In a final experiment, a solution containing 10  $\mu\text{M}$  of purified tubulin dimers were exposed to an equal concentration of [<sup>3</sup>H]-paclitaxel or [<sup>3</sup>H]-discodermolide and allowed to undergo polymerization until saturated. Increasing amounts of unlabeled discodermolide or paclitaxel, respectively, were added as competitors for each system. They found that while unlabeled discodermolide was able to effectively displace [<sup>3</sup>H]-paclitaxel, unlabeled paclitaxel was unable to do the same with [<sup>3</sup>H]-discodermolide. Even at concentrations of up to 50  $\mu\text{M}$  unlabeled paclitaxel, discodermolide was not displaced. The results clearly demonstrated the higher affinity of discodermolide compared to paclitaxel. The two compounds bound to mutually exclusive locations on tubulin, but it was uncertain whether they bound to the protein at the same or overlapping sites, or whether binding induced a conformational change that made simultaneous association impossible.

Amidst growing interest in discodermolide, the compound was assayed against colon and ovarian carcinoma multi-drug-resistant (MDR) cell lines (SW620AD-300, A2780AD) and cell lines that exhibit  $\beta$ -tubulin mutations (1A9PTX10, 1A9PTX22).<sup>9</sup> All four of these cell lines

were known to be paclitaxel-resistant, so this provided a further opportunity to explore potential differences in activity between the compounds. The IC<sub>50</sub> values of the drug-resistant cell lines were compared to the parent drug-sensitive cell line in order to quantify the degree to which potency was diminished between the two. In all cell lines studied, discodermolide was significantly more potent than paclitaxel. Interestingly, further studies of cells containing  $\beta$ -tubulin mutations revealed that discodermolide did not exhibit cross-resistance in epothilone- and paclitaxel-resistant cell lines. An impressive example was that the potency of paclitaxel was diminished 930-fold in SW620AD-300 cells whereas similar treatment with discodermolide resulted in only 25-fold drop in potency. Similarly, discodermolide retained its full potency in the drug-resistant 1A9 lines but paclitaxel was 23- and 29-fold less potent. A major contributing factor for this is hypothesized to be discodermolide's minimal affinity for Pgp and lesser sensitivity to  $\beta_1$ -tubulin isotype mutations.<sup>9,27</sup>

In the past decade, there have been several notable studies to elucidate the mechanism of action for discodermolide. In 2003, Jordan and colleagues investigated MT dynamics and determined them to be altered in a concentration-dependent manner.<sup>28</sup> Dynamicity, which is the total length grown and shortened divided by the lifespan of the MT population, was used as a measure to reflect overall exchange of tubulin. At 7 nM in A549 cells, the measure of dynamicity (an IC<sub>50</sub> value for proliferation) was reduced by 23%. At the value for 50% maximal mitotic block (83 nM), most MTs were non-dynamic, no cells arrived at anaphase, all spindles were abnormal, and 62% reduction of dynamicity was observed. This suggests that reduction of dynamicity of MTs is an essential mechanism for inhibiting proliferation.<sup>29</sup> The group postulated that reduced MT lengths limited the ability of the strands to probe the cytoplasm for chromosomal kinetochores during pro-metaphase and for chromosomal separation in anaphase.

In 2009, Horwitz and colleagues elaborated upon the MT stabilization studies using hydrogen-deuterium exchange (HDX) studies in the presence of GTP and free tubulin.<sup>22</sup> This type of experiment identifies specific residues on the tubulin binding site that are protected from deuterium incorporation after ligand association. Paclitaxel was shown to stabilize interprotofilament binding through contacts with the  $\beta$ -tubulin M-loop, as well as reducing deuterium incorporation on the  $\beta$ -face of the interdimer region (Figure 7). In contrast, discodermolide stabilized the interprotofilament region at the  $\beta$ -tubulin H1-S2 loop and protected the interdimer region more strongly on the  $\alpha$ -face. In this way, the binding of discodermolide appears to be complementary to that of paclitaxel. Unique to discodermolide was additional protection in the exchangeable nucleotide binding site (E-site) that is responsible for stabilization of GTP binding, and in the region on  $\alpha$ -tubulin containing Glu254, which is involved in GTP hydrolysis. This suggests discodermolide may have a more extensive ability to hinder GTP hydrolysis, the primary cause of catastrophe.

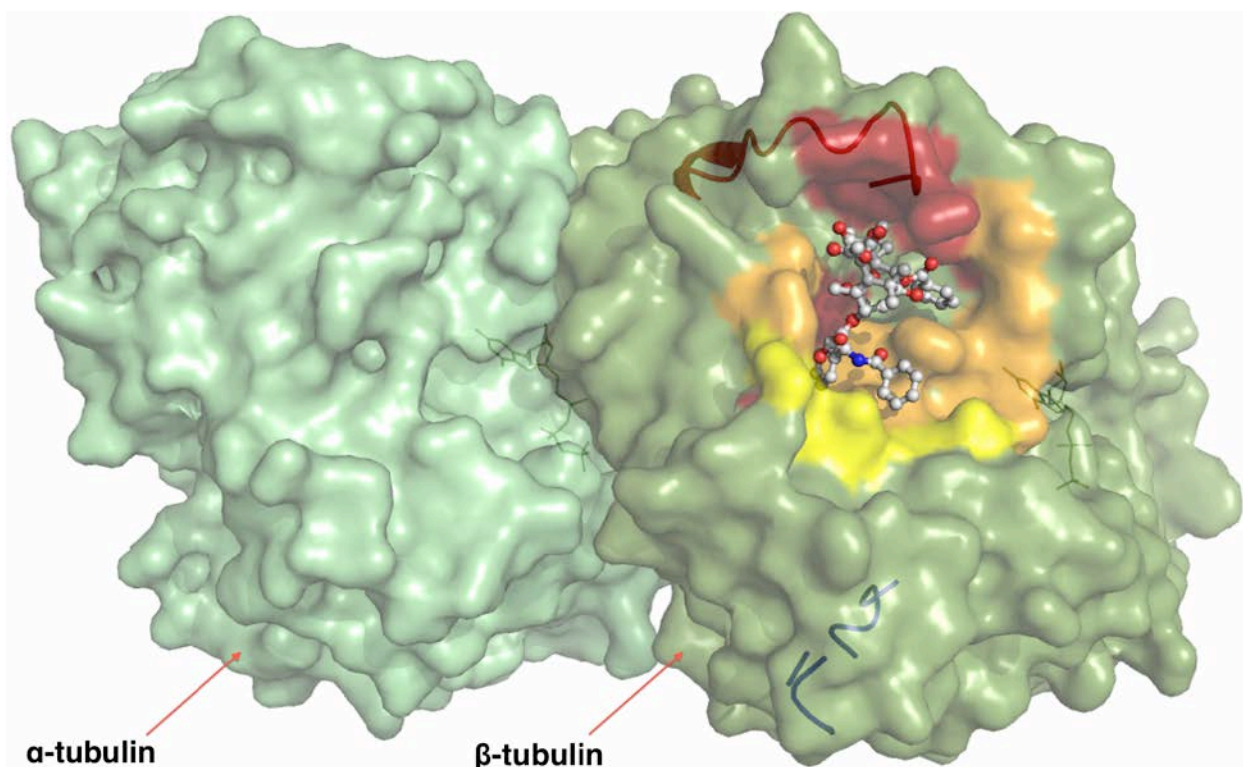


Figure 7. Differences in tubulin binding contacts between paclitaxel and discodermolide.

Paclitaxel is shown in the binding site on the tubulin dimer. Binding contacts unique to paclitaxel or discodermolide are shaded (red and yellow, respectively) and shared contacts are shown in orange. Also included are structures of GDP and GTP in their respective binding sites (dark green), and cartoon representations of the M-loop (red) and H1-S2 loop (blue) within  $\beta$ -tubulin. Three-dimensional structural data and protein sequence were obtained from the Protein Data Bank (PDB) ID: 1JFF and MacPyMOL was used to render and visualize the structure. The author used data from Horwitz's HDX studies to assign binding contacts for both discodermolide and paclitaxel.

Using an integrated NMR spectroscopy and computational approach, the binding mechanism of MT stabilizing agents (MSAs) was further explored by Díaz and colleagues in 2011.<sup>30</sup> MSAs were detected interacting with unpolymerized tubulin heterodimers, suggesting that the compounds may help to promote polymerization of dimers in addition to stabilizing the polymerized MT structure. Further saturation transfer difference NMR (STD) and TR-NOESY experiments allowed researchers to elaborate on a 2-step mechanism for binding.<sup>31</sup> It was known at the time that paclitaxel and its biomimetics were able to bind to one or two internal (luminal) sites in addition to an external pore site. Because of the 1:1 binding stoichiometry for

discodermolide to tubulin, these sites must be mutually exclusive, but may occur in sequence.<sup>31-</sup>

<sup>33</sup> First, the group found that the MSAs studied bind to an external site on the tubulin and quickly dissociate, internalizing themselves toward a secondary luminal binding site. Dissociation of the MSA from the tubulin occurs in a reverse process, in which the MSA slowly dissociates from the luminal site and is transported to an external pore site, followed by rapid release of the ligand from the pore. It had been previously shown that this process occurs within 2 minutes and that the rate-determining step was the first slow step of dissociation.<sup>34</sup> Because both NMR techniques rely on rapid dissociation that fit within the relaxation time scale, it was expected that the very high-affinity binding of MSAs to the luminal site would be NMR-silent. The result of this study corroborated what had already been predicted for the MSA-tubulin system. Even with this data, however, there is still some ambiguity about the precise binding sites of the individual compounds studied.

### **1.2.3 Discodermolide's synergism with Paclitaxel**

Drugs that behave synergistically show great promise in the realm of chemotherapeutics. The enhanced potency of the drugs when given in combination allows for lower dosing of each drug, reduced likelihood of resistance mechanisms, less severe negative side effects, and potential for non-overlapping toxicity profiles.<sup>35</sup> Despite the noted differences in the behavior of paclitaxel- and discodermolide-treated cells, it was still surprising when researchers found that they represent a synergistic drug combination for the treatment of cancer.

In 2000, it was first found that the treatment of four separate human carcinoma cell lines with both drugs resulted in a schedule-independent synergistic interaction.<sup>27</sup> The group began their study using A549-T12 cells, which are known to be 9-fold resistant to paclitaxel, but also

dependent on low levels of it (2-6 nM) for growth. Discodermolide was distinguished from epothilones A/B (Figure 1) and eleutherobin early in the study when it was shown to be an insufficient substitute for paclitaxel in this cell line. This has since been confirmed in other experiments with cell lines that have similar dependencies.<sup>36</sup> Surprisingly, discodermolide was then found to be significantly more potent in the presence of paclitaxel in all four other cell lines, while the potency of the epothilones and eleutherobin was unaffected (Figure 8). Synergism has been observed with combinations of MT-perturbing agents, although in these cases the agents had either independent mechanisms of action or binding sites.<sup>37-43</sup> This was unexpected for two drugs with a similar apparent binding site and mode of action; it was expected that the combination would be either additive or antagonistic.

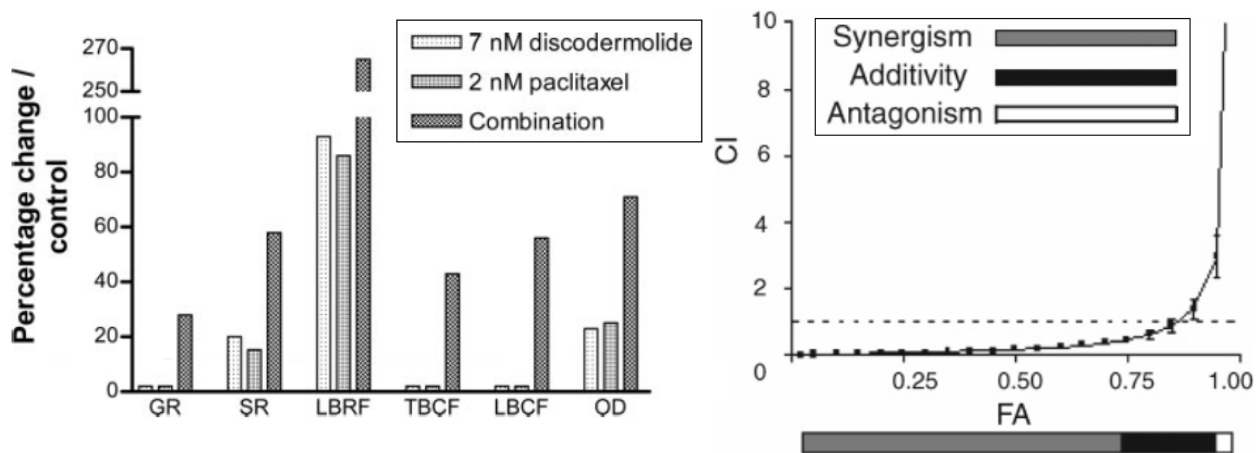


Figure 8. Synergistic effects of A549 cell treatment with discodermolide and paclitaxel.

Left: Percentage changes in the parameters of dynamic instability that were altered by treatment of A549 cells by 7 nM discodermolide and 2 nM paclitaxel. *GR*, growth rate; *SR*, shortening rate; *LBRF*, length-based rescue frequency; *TBCF*, time-based catastrophe frequency; *LBCF*, length-based catastrophe frequency; *OD*, overall dynamicity. Right: Mean combination index values as a function of cells killed, calculated after treating A549 cells with a drug combination of equipotent molar ratios (1:20 paclitaxel:discodermolide) for 72 h. *FA*, fraction affected, synergism at  $CI < 1$ , additivity at  $CI = 1$ , antagonism at  $CI > 1$ . Image at left reprinted with permission from Ref. 44, copyright 2004, American Chemical Society; image at right reprinted with permission from Ref. 45, copyright 2006, American Chemical Society.

A follow-up study by Jordan and co-workers in 2004 further investigated the synergism of the two drugs with relation to their effects on MT dynamic instability.<sup>44</sup> When tested separately at their IC<sub>50</sub> values (7 nM discodermolide, 2 nM paclitaxel), dynamic instability parameters for the A549 cells appeared qualitatively and quantitatively similar. However, at concentrations inducing 80% maximal G<sub>2</sub>-M arrest (IC<sub>80</sub>: 83 nM for discodermolide, 6 nM paclitaxel), they noted that discodermolide had no effect on length-based catastrophe frequency whereas it was increased by 80% for paclitaxel. This suggests that paclitaxel selectively stabilizes the center of the MT while allowing the ends to experience frequent brief catastrophes and rescues. When cells were treated with both compounds, synergism could be observed in various measures of dynamicity (Figure 8A).<sup>46</sup> While the mechanism for discodermolide binding was still unknown, they postulated that synergism could be the result of: occupancy on multiple sites of a single MT, cooperative binding of paclitaxel that enhances that of discodermolide, preferential binding to differing tubulin isotypes, conformational changes that influence cellular regulators of MT dynamics, or an additional antiproliferative mechanism that was at that time unknown.

In addition to cell cultures, the synergistic phenomena has also been observed in an ovarian xenograft tumor model in nude mice.<sup>35</sup> Tumor volume, xenograft vascularization, and angiogenic effects were all assessed. This study validated previous *in vitro* studies, clearly showing that combination therapy in this case was highly effective at low concentrations (< 20 nM) and significantly superior to treatment with one drug alone. While suppression of cell proliferation was identified as the primary mode of cell death, other contributing factors were also presented including: cell senescence, caspase activation, differences in affinity across

tubulin isotypes, and antiangiogenic effects. Pleasingly, due to the low dosage, no side effects such as toxicities or weight loss were observed.

#### **1.2.4 Accelerated Cell Senescence and Resistance Mechanisms**

A 2005 collaborative study between Horwitz and Smith demonstrated that in addition to mitotic aberrations, discodermolide treatment led to accelerated cell senescence (ACS) in multiple cell lines.<sup>47</sup> ACS occurs when tumor cells initiate proliferation arrest as a response to cellular stress such as chemotherapeutic treatment.<sup>48,49</sup> Biomarkers for these cells include a flattened morphology and elevated levels of senescence-associated  $\beta$ -galactosidase (SA- $\beta$ -gal) activity.<sup>50</sup> Interestingly, treatment with paclitaxel resulted in mitotic arrest, but little or no observed senescence. In fact, the researchers noted that the effects of discodermolide more closely resembled that of doxorubicin, a DNA-damaging drug. This was the first time that a MT-stabilizing drug had ever been observed using accelerated senescence as a means of suppressing tumor cell growth.

It was hypothesized that paclitaxel and discodermolide, though both MT-stabilizing drugs, had unique and disparate effects on the MAPK signaling pathway that is involved in mitogenic activation.<sup>47</sup> This finding may explain apparent pharmacokinetic differences between the two drugs.<sup>51</sup> For instance, discodermolide has a higher affinity for and ability to nucleate MTs, but generally exhibits a lower overall cytotoxicity than paclitaxel. Additionally, discodermolide does not always appear resistant in cell lines containing  $\beta$ -tubulin mutations or elevated Pgp levels that affect paclitaxel and the epothilones. Finally, inhibition of cell proliferation required seven times the concentration of discodermolide compared to paclitaxel over a short time period (3 days), but over a longer period (6 days), equal concentrations of drug

resulted in equivalent levels of apoptosis. This delayed response exhibited by discodermolide-treated cells may be explained through an alternate mechanism where abnormal cells are allowed to continue dividing until cellular stress levels bring about senescence. It is also possible that discodermolide has one or more other targets in addition to the MTs, which would help to explain the synergism observed between the two drugs.

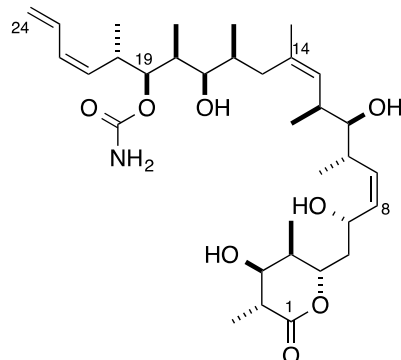
Later investigations identified 4E-BP1 mRNA as a regulator of ACS initiated by discodermolide treatment.<sup>49</sup> In fact, discodermolide was shown to be seven-fold resistant to AD32 cells, which underexpress 4E-BP1 and therefore escape ACS. Differing resistance mechanisms between discodermolide and other MT stabilizing agents offer additional motivation for discodermolide development. While a patient who has been previously treated with taxane-based chemotherapeutics may experience future resistance to both taxanes and epothilones, the  $\beta$ -tubulin and/or Pgp mutations of their cells should not mitigate the efficacy of discodermolide treatment.<sup>36</sup> These findings are all very exciting, but raise many questions regarding the relationship between ACS and tumor cell proliferation.

### **1.3 PREVIOUS TOTAL SYNTHESSES OF DISCODERMOLIDE**

Despite initial interest in discodermolide, the extremely low abundance (0.002 wt%) of the compound obtained from marine sponge samples made further studies impractical. Unable to develop a robust fermentation process to alleviate the supply shortages, scientists turned to total synthesis. The densely functionalized nature of discodermolide also created additional challenges.

The first total synthesis of the unnatural (-)-discodermolide was completed by the Schreiber group in 1993.<sup>52</sup> A year later, its natural antipode, (+)-discodermolide (**1**), was obtained by the group.<sup>53</sup> The early work of Schreiber was particularly significant in that it led to the unambiguous assignment of absolute stereochemistry, the first SAR studies of the compound, and culminated in the realization of distinct roles of natural and unnatural discodermolide in cell cycle arrest.<sup>7</sup>

Over subsequent years, several other groups completed total syntheses of discodermolide. Notably, in 1995, the Smith group took advantage of the repeating 1,2-*anti*-2,3-*syn* stereotriad found in three key subunits of the backbone: at C1-C8, C9-C14, and C15-C21 (Figure 9).<sup>54</sup> By synthesizing a common precursor for these three subunits, a more convergent approach was possible. Additionally, the synthesis of this precursor could be executed on up to a 50 g scale, so large quantities of each fragment could be obtained prior to coupling. Later strategies by Smith and many other groups similarly used a common precursor approach such as this one.<sup>55,56</sup> To date, there have been 13 unique total syntheses of discodermolide, which are summarized in Figure 9 below.<sup>7,52-54,57-76</sup> From these, three representative syntheses are highlighted below: the fourth-generation synthesis by the Smith group, the third generation synthesis by the Paterson group, and the Novartis 60 g scale synthesis.



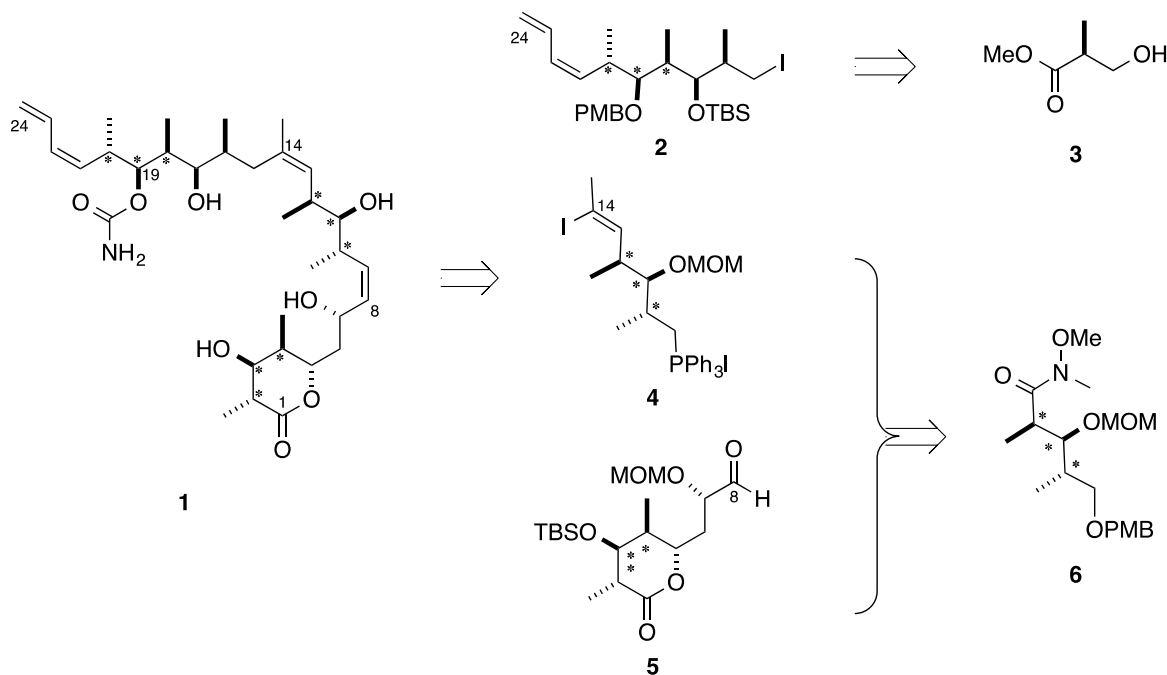
Research Group	Year	Steps in the Longest Linear Sequence	Overall Yield (%) <sup>a</sup>	Ref.
Schreiber	1993	24	4.3	52 <sup>b</sup> ,7,53
Smith (I)	1995	28	2.2	54 <sup>b</sup>
Myles	1997	22	1.1	57 <sup>b</sup>
Marshall	1998	29	2.2	58
Smith (II)	1999	24	6.0	59
Paterson (I)	2000	27	7.7	60
Paterson (II)	2003	24	5.1	74
Smith (III)	2003	24	1.9	70
* Novartis	2004	26	1.1	61–65
* Paterson (III)	2004	21	11.1	75,76
Panek	2005	27	2.1	67
* Smith (IV)	2005	17	9.0	68
Ardissou	2007	21	1.6	73,137

<sup>a</sup> Overall yield as reported by the author(s).  
<sup>b</sup> Synthesis of the unnatural antipode, (-)-discodermolide.

Figure 9. A summary of completed total syntheses of discodermolide, 1993-2007.

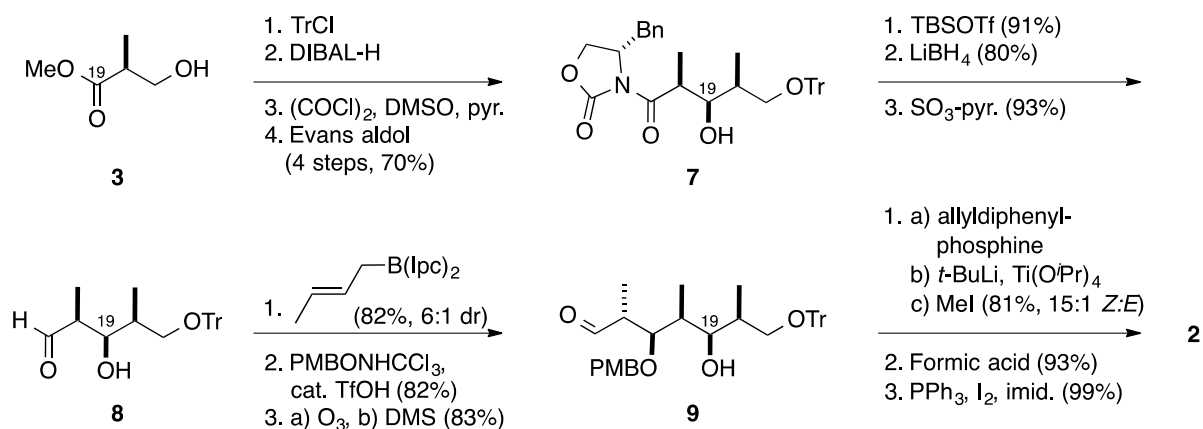
### 1.3.1 The Smith Group Fourth-Generation Synthesis

The fourth-generation synthesis developed by the Smith group in 2005 highlights the variety of improvements that were made over the course of a decade, making the overall strategy more convergent and more amenable to scaling up.<sup>77</sup> Smith's ultimate goal was the development of a scheme that would permit larger-scale production of the compound, making it more viable for clinical development. Earlier schemes suffered from a variety of problems that reduced their practicality on a large scale, including a key Wittig coupling that required ultra-high-pressure conditions and led to a variety of undesired side products.<sup>59</sup> Building on the success of their gram-scale synthesis, the group maintained a convergent approach that involved the formation of three advanced intermediates from a common precursor (**6**) containing the requisite stereotriad (Scheme 1).<sup>69</sup>



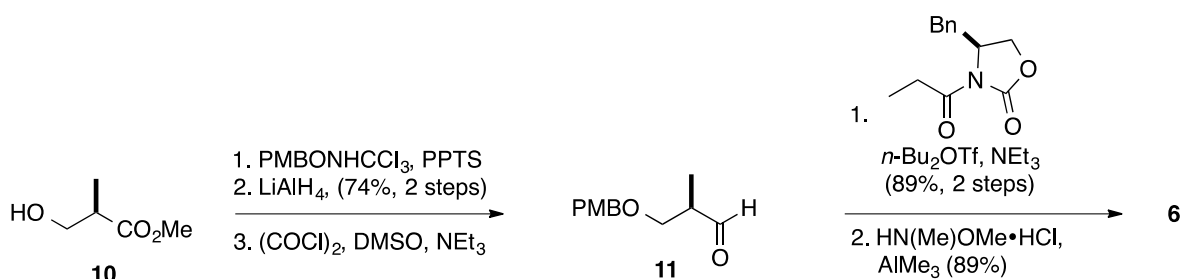
Scheme 1. Smith's fourth-generation retrosynthetic plan, with stereotriad locations labeled.

Although construction of **2** could be accomplished from **6**, a shorter route from Roche's ester **3** was used instead (Scheme 2). A sequence of steps including protection, reduction, oxidation, and Evans aldol reaction with chiral auxiliary afforded **7**, which established the stereocenters at C17-C18. Further protection, reductive removal of the auxiliary, and Parikh-Doering oxidation to the aldehyde led to **8**. Subsequent Brown crotylation led to the formation of the final two stereocenters, at C19-C20. Protection of the secondary alcohol and ozonolysis of the terminal olefin provided aldehyde **9**. Finally, the completed fragment **2** could be obtained under Yamamoto's conditions followed by trityl deprotection and iodination.<sup>78</sup> This sequence required a total of 13 linear steps, and provided **2** in 19% overall yield.



Scheme 2. Smith's fourth-generation synthesis of fragment **2**.

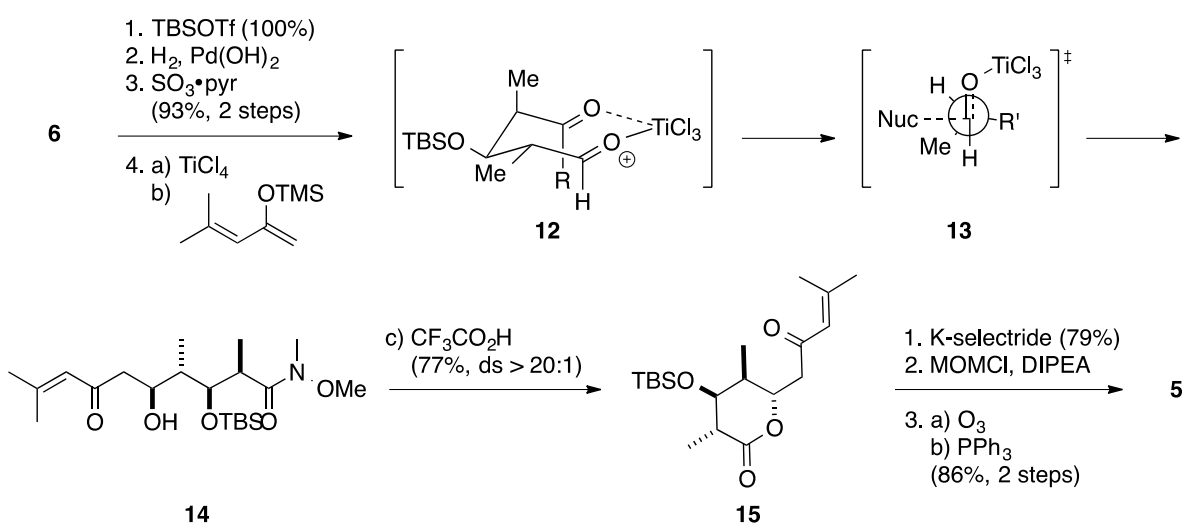
The synthesis of the other two fragments relied on the common precursor **6**, which was developed in the first-generation scheme for the group (Scheme 3).<sup>54</sup> This efficient 5-step process relied on a succession of protection, reduction, and oxidation steps leading to intermediate **11**. From here, Evans *syn*-aldol addition of **11**, followed by Weinreb transamidation, yielded the common precursor. This route was highly scalable, allowing for up to 50 g quantities of **6** to be synthesized at a time.



Scheme 3. Smith's fourth-generation synthesis of common precursor **6**.

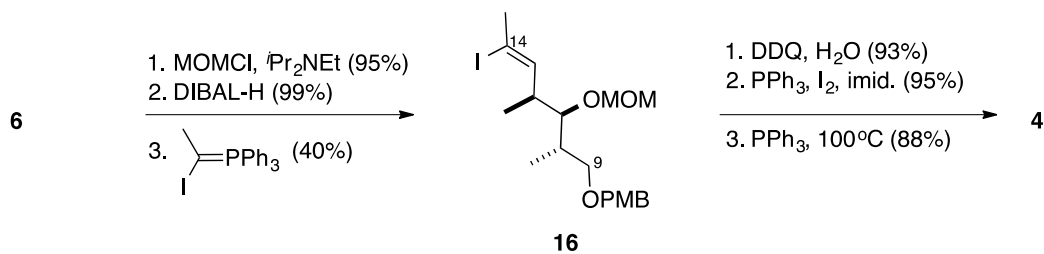
The lactone fragment was constructed from a scheme that was modified from the group's first-generation synthesis as well (Scheme 4). From the common precursor (**6**), protection with TBS

was followed by deprotection of the terminal alcohol and subsequent oxidation to the aldehyde. A chelation-controlled Mukaiyama aldol reaction established the configuration at C5 by using  $\text{TiCl}_4$  as an external asymmetric promoter.<sup>79</sup> The eight-membered ring chelate (**12**) ensured the desired formation of the anti-Felkin addition product **14** (via **13**). Treatment with acid afforded the ring-closed **15**, whose enone could then undergo directed reduction to form an allylic alcohol. From there, protection and ozonolysis furnished the completed lactone fragment **5**.



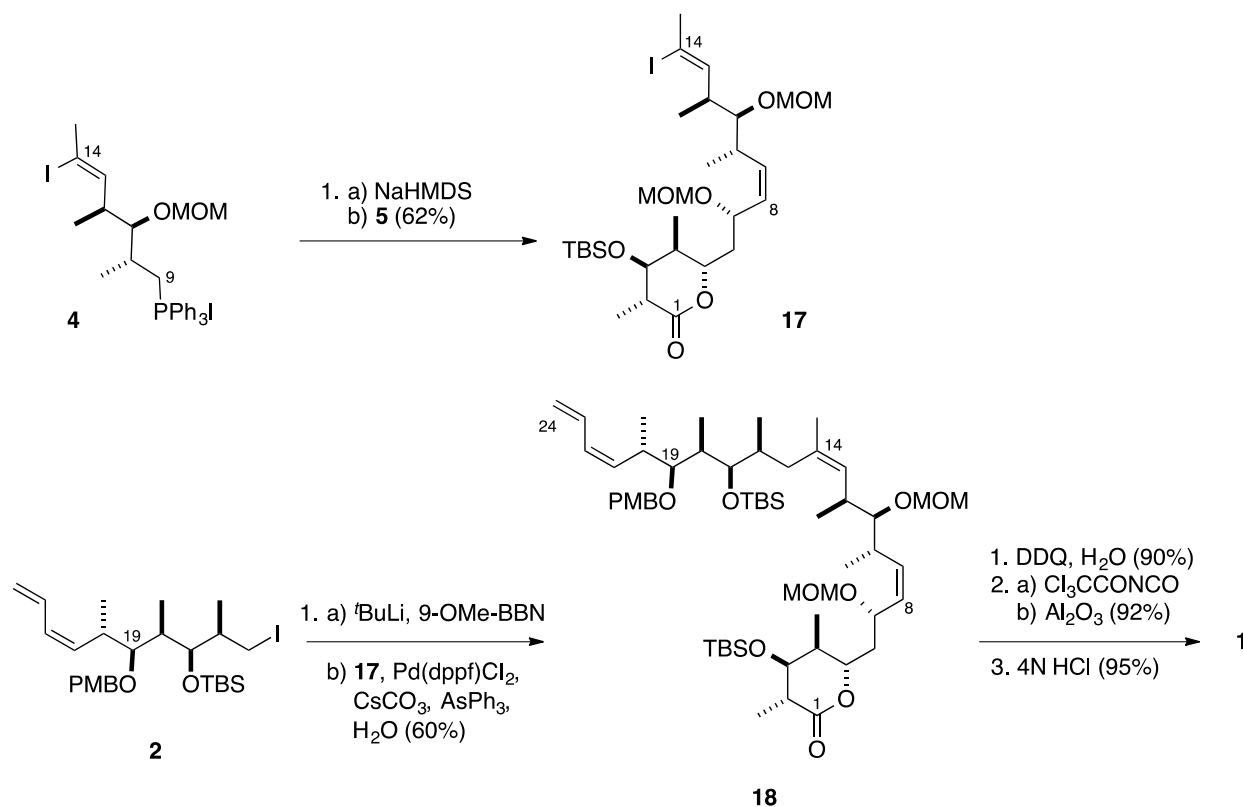
Scheme 4. Smith's fourth-generation synthesis of lactone intermediate **5**.

From the common precursor, synthesis of what would become the linker fragment, **4**, required only six additional steps (Scheme 5). Protection of the secondary alcohol followed by reduction of the amide allowed for the installation of the requisite trisubstituted vinyl iodide **16**. The conversion of **16** to Wittig salt **4** represented an improvement from earlier syntheses, which relied on high pressure conditions or led to undesirable cyclopentane-containing side products. This bifunctional intermediate also allowed for the direct sequential coupling to both carbamate and lactone fragments.



Scheme 5. Smith's fourth-generation synthesis of linker fragment **4**.

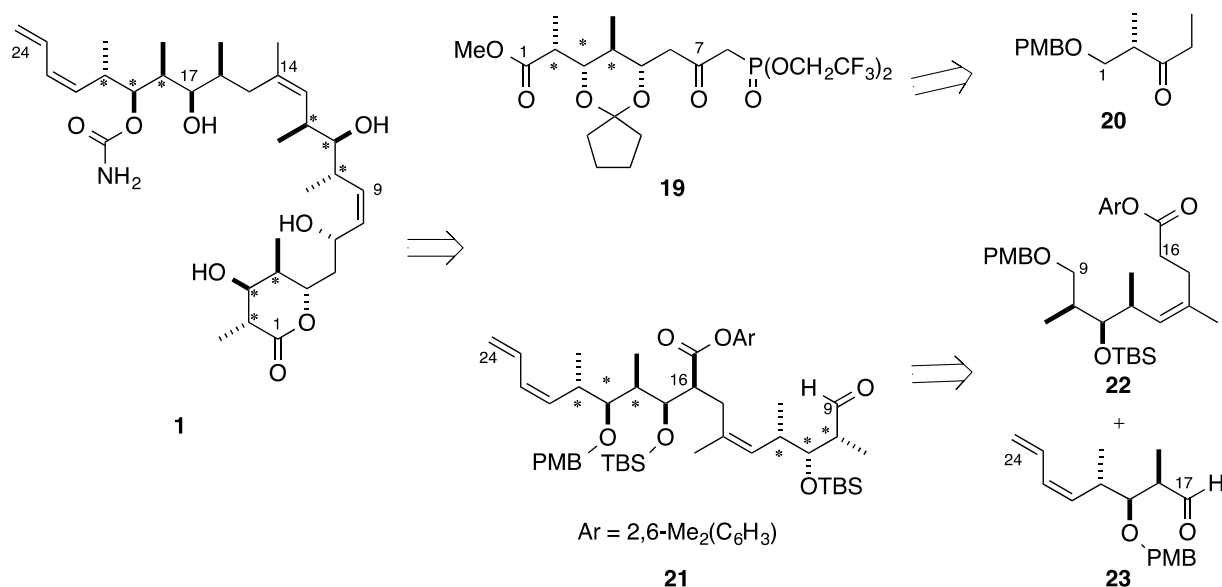
Coupling of the linker fragment **4** with the lactone **5** through the Wittig salt yielded vinyl iodide **17**, which could then be used in a Suzuki coupling reaction with diene **2** (Scheme 6). With the completed discodermolide backbone in place, only deprotection and installation of the carbamate was needed to furnish **1**. This process required only 17 linear steps, with a 9.0% overall yield.



Scheme 6. Smith's fourth-generation coupling of advanced intermediates to form **1**.

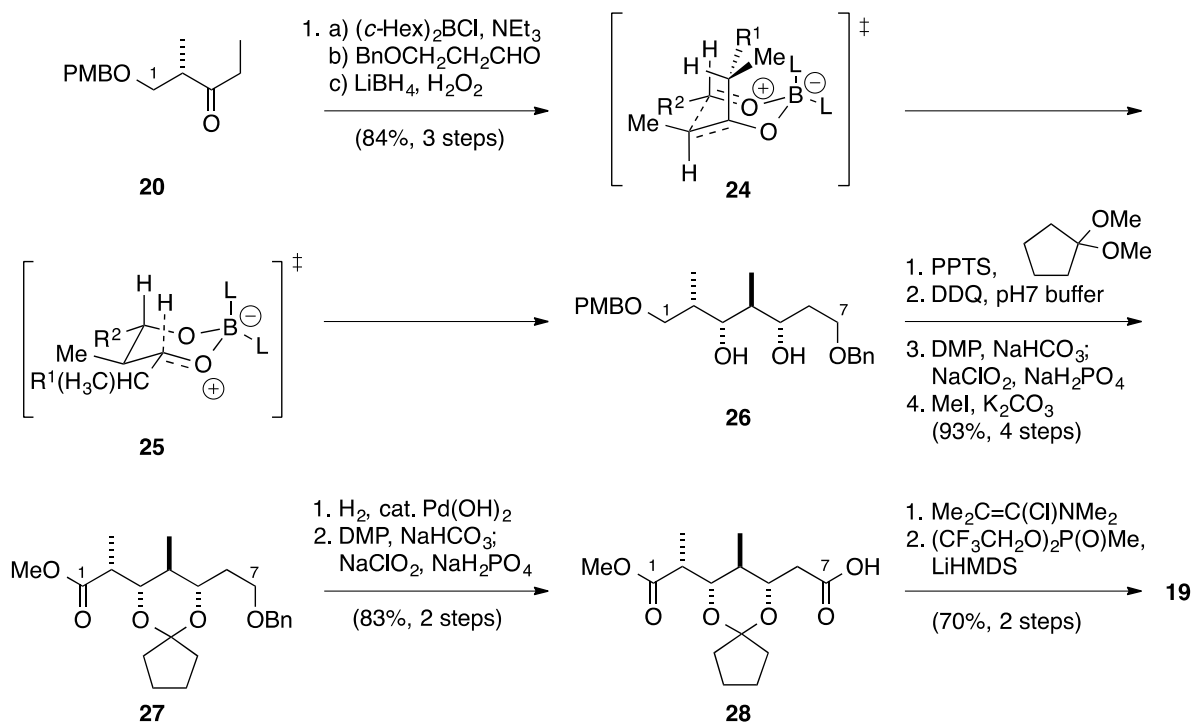
### 1.3.2 The Paterson Group Third-Generation Synthesis

The Paterson group reported their first total synthesis of discodermolide in 2000, five years after the Smith group's initial attempt.<sup>60</sup> Their early approach was also convergent, and relied on a novel boron-mediated aldol coupling to independently construct three advanced intermediates. Four years later, the group presented a third-generation approach that improved the overall convergence and streamlined the synthesis so it would be more amenable to an industrial scale.<sup>75</sup> The group envisioned a late stage Still-Gennari-type HWE olefination to join  $\beta$ -ketophosphonate **19** and aldehyde **21**, as can be seen in Scheme 7.



Scheme 7. Paterson's third-generation retrosynthetic plan.

The synthesis of  $\beta$ -ketophosphonate **19** began with installation of the stereotriad through a borane-mediated *anti*-aldol addition (Scheme 8). Here, the (*E*)-enol dicyclohexylborinate formed, allowing an aldol reaction via the chair-like transition state **24**. Reduction *in situ* of the resulting boron aldolate resulted in axial hydride delivery through transition state **25**, which minimizes steric interactions between cyclohexyl ligands and the benzyl ether group.<sup>80</sup> Conversion of *syn*-diol **26** to an acetal was followed by PMB deprotection, oxidation of the newly-formed primary alcohol, and methylation to **27**. In order to install the requisite phosphonate scaffold, the benzyl ether was removed through hydrogenolysis, and then oxidized. Finally, treatment of acid **28** with the Ghosez reagent generated the acid chloride, which was then converted to the desired phosphonate **19** through an acylation reaction.



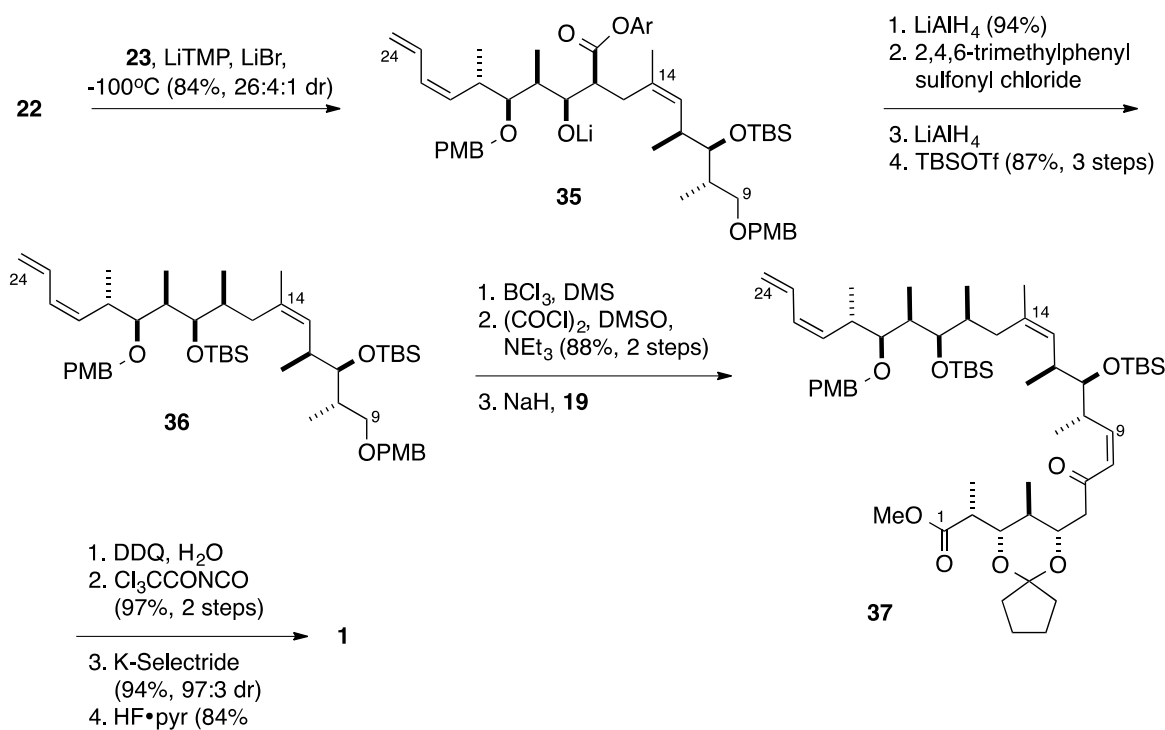
Scheme 8. Paterson's third-generation synthesis of  $\beta$ -ketophosphonate **19**.



Beginning from ethyl ketone **20**, intermediate **23** could be constructed in 11 steps (Scheme 9). Formation of the (*E*)-boron enolate of **20** and subsequent *anti*-selective aldol reaction established the stereochemistry of the methyl group at C18.  $\beta$ -Hydroxy-directed reduction of the ketone moiety produced a diol, whose terminal ether underwent methanolysis to provide a terminal alcohol. Glycol cleavage to form aldehyde **29** was followed by reduction, TBS protection of the primary alcohol, and DDQ-mediated acetal formation. Regioselective opening of the acetal effectively shifted the PMB group to the secondary alcohol, allowing the oxidation of the newly-deprotected terminal alcohol. Installation of the (*Z*)-diene occurred in a three-step process involving Nozaki-Hiyama-Kishi allylation to form the *anti*- $\beta$ -hydroxysilane **32**, then 1,2-*syn*-elimination, and finally oxidation to generate the desired aldehyde **23**.



Coupling of intermediates **22** and **23** began with enolization of the aryl ester moiety of **22** generated an (*E*)-lithium enolate, which then formed the desired 1,2-*anti* aldol adduct in the presence of **23** (Scheme 11). In order to transform the aryl ester at C16 into the desired methyl group, lithium aldolate **35** was subjected to an *in situ* reduction, sulfonation and subsequent deoxygenation. Protection of the secondary alcohol at C17 yielded **36**, then selective deprotection and oxidation of the primary alcohol gave a product that was ready for the final coupling stages. A Still-Gennari HWE reaction with phosphonate **19** produced the desired olefin with 10:1 *Z:E* selectivity. With the complete backbone of discodermolide in place, the group had only to carry out a final series of functional group manipulations. Thus, discodermolide was synthesized after deprotection, carbamate formation, 1,2-reduction at C7, and lactone cyclization steps.



Scheme 11. Endgame coupling strategy of Peterson's third-generation synthesis.

Overall, Paterson's third-generation synthesis of discodermolide relied on much of the chemistry previously developed within the group, like the preference for substrate-controlled over auxiliary-controlled reactions in order to achieve stereocontrol. The most notable modification was the relatively mild late-stage Still-Gennari-type HWE olefination. These improvements allowed for a milder endgame strategy, less reliance on boron-mediated aldol reactions, and minimized expense for scaled-up syntheses.

### 1.3.3 The Novartis 60-g Scale Synthesis

Due to the great promise of discodermolide as a novel chemotherapeutic agent, a practical synthesis was needed to advance it to clinical trials. Ultimately, process chemists for Novartis developed an approach that is a hybrid of both Smith and Paterson's routes.<sup>61–65</sup> In general, the

Smith route, including the usage of common precursor **6**, was utilized to form each of the three fragment regions. The Paterson methodology was responsible for late stage elaboration in the C1-C9 region. A very brief overview is provided below, in Figure 10. The efforts of the 43 Novartis chemists involved in this project culminated in about 60 g of pure discodermolide, synthesized over a total of 39 steps.

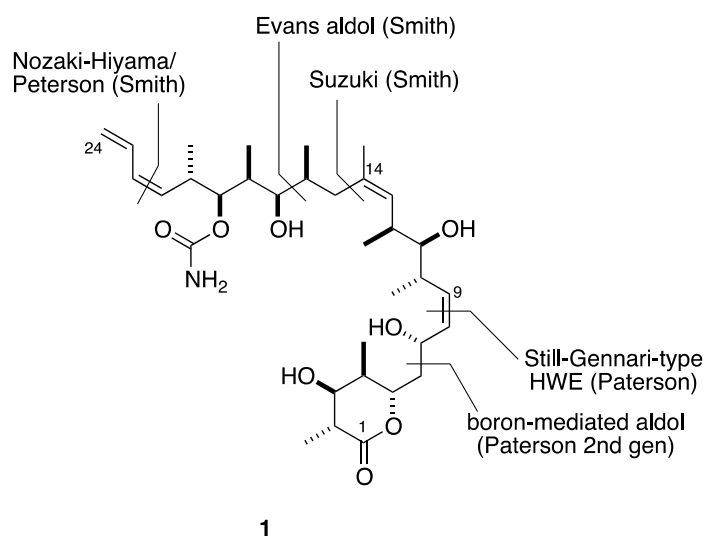


Figure 10. A summary of the approach taken by Novartis in their large-scale synthesis of **1**.

## 1.4 STRUCTURE ACTIVITY RELATIONSHIPS FOR DISCODERMOLIDE

### 1.4.1 Overview

In order to probe and optimize the biological activity of discodermolide, numerous SAR studies have been carried out. The results from analogue studies have allowed for the development of an extensive molecular activity map for the compound and for further optimization of binding

conformation profiles.<sup>56,81</sup> In order to simplify the analysis, the backbone of the discodermolide framework has been divided into three structurally distinct regions: the carbamate region in blue, the linker region in yellow, and the lactone region in yellow (Figure 11). Due to the variable antiproliferative activity in different cell lines and small changes from study to study, an exhaustive list of IC<sub>50</sub> values have been provided in a table (see Appendix) in their raw form and also relative to the parent compound for that particular study or cell line.

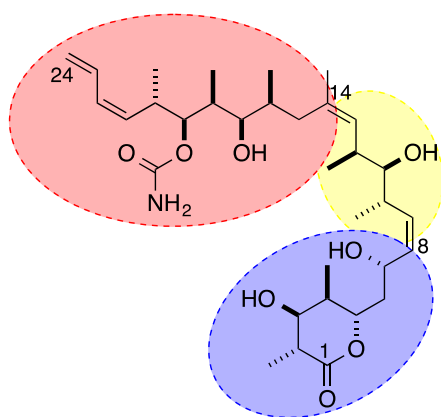


Figure 11. Distinctive regions of discodermolide for SAR analysis.

#### 1.4.2 Carbamate Fragment Analogues

Biological studies on discodermolide analogues have demonstrated the potential for great simplification and alteration to the carbamate portion of the molecule. Manipulation of the diene portion of the molecule was relatively well tolerated (Figure 12, Tables 3 and 8).<sup>7,82-87</sup> Hydrogenation of a single olefin was associated with a slight improvement in IC<sub>50</sub> and also removes a potential site for phase I metabolism (**38**, **39**).<sup>11</sup> However, with complete saturation (**41**), the compound lost significant potency in resistant cell lines. Addition of the bulky

photoaffinity probe (**48**, **49**) during conformational studies did not reduce activity in A549 cells, but complete replacement of the group with a benzyl or phenyl ether (**42**, **43**) significantly reduced its potency. This suggests the necessity of at least one olefin in this region, and also the ability to add bulky groups at the C24 position.

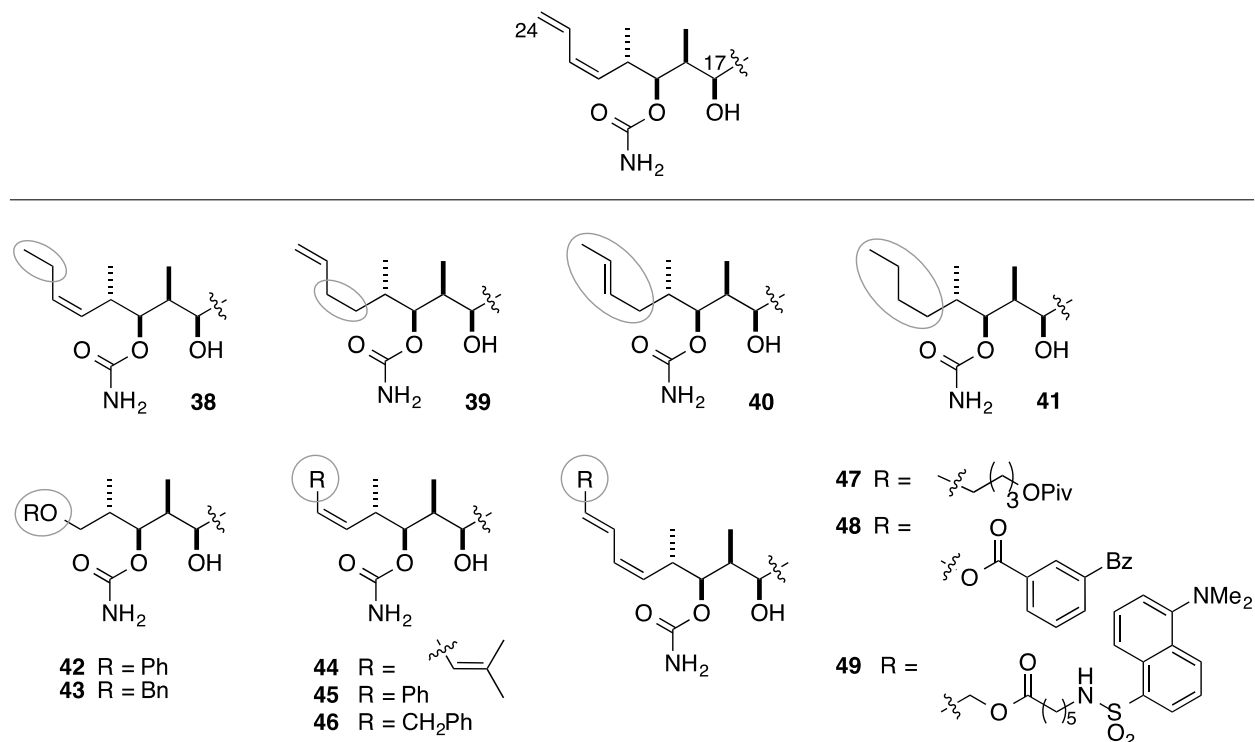


Figure 12. Modifications to the terminal diene.

Using large, mostly aromatic substitutions, the Smith group probed the electronic and steric limitations of the carbamate group at C19 (Figure 13, Tables 3 and 8).<sup>85,88</sup> Curiously, these analogues retained a significant degree of their potency, maintaining single or low-double digit nM IC<sub>50</sub> values. The most potent of these was the dimethylaniline moiety, whose potency was significantly greater than that of discodermolide in all cell lines except NCI/ADR. This scaffold is known to be metabolized rapidly *in vivo* by cytochrome P450, however. Less metabolically

labile isosteres, like imidazole **53** and morpholine **54**, did not have equivalent potency. Paclitaxel-discodermolide hybrid compounds **56-60** developed by Horwitz and Smith were appended with photoaffinity probes in order to study its binding mode.<sup>89</sup> These compounds all had enhanced antiproliferative activity of up to 8-fold compared to the parent. Further, the correlation between tether length and activity suggests that the groups are interacting with an aromatic pocket within tubulin rather than just enhancing the overall hydrophobicity of the compound.

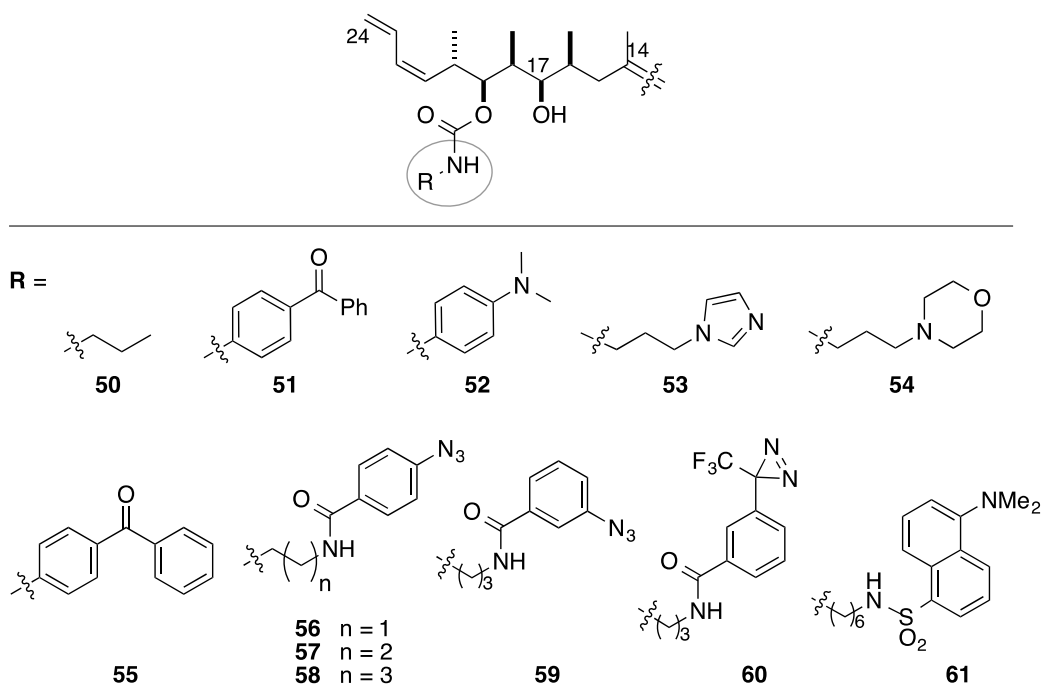


Figure 13. Modifications to the C19 carbamate group.

Other modifications to the carbamate region have also been extensively studied (Figure 14, Tables 3 and 8).<sup>7,84,90-93</sup> Complete removal of the methyl groups at C16 (**62**) or C14 (**64**), or of the carbamate group entirely (**65**) resulted in compounds with low nanomolar antiproliferative activity similar to the parent. For unknown reasons, though, these compounds are relatively

inactive in the NCI/ADR multidrug-resistant cell line. Epimerization of C16 or C17 in this region (**63**, **66**) significantly decreased activity, emphasizing the ability of these elements to maintain the conformational preferences of the molecule. More drastic alterations to the backbone included replacement of the C13-14 olefin with an amide linker (**68**) that resulted in sub-micromolar potency in A549 cells. In their efforts to attach an affinity binding probe to discodermolide, the Schreiber group explored extensions of C17 and C16. Whereas C17 tolerated the group with only a slight drop in cytotoxicity (**71**), C16 extensions such as **73** were not at all active.

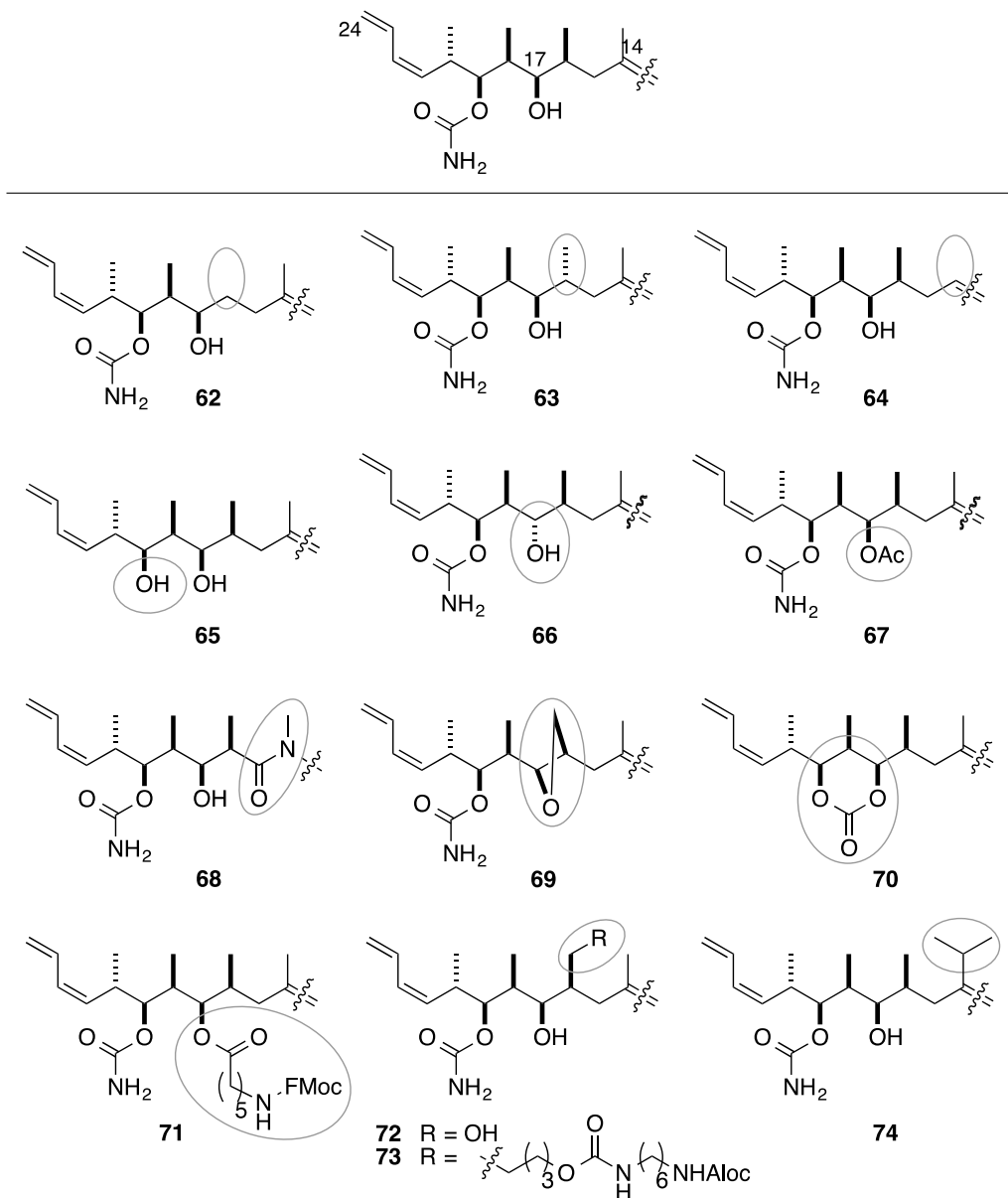


Figure 14. Modifications to the carbamate fragment.

### 1.4.3 Linker Fragment Analogues

In the final HCl-mediated global deprotection step of the Novartis synthesis, compounds **75-80** were isolated (Figure 15, Tables 4 and 9).<sup>94</sup> Of these, only **77** retained a modest potency

compared to the parent. Replacement of the C14-15 olefin and C14-methyl group with cyclopropane yielded a compound that was only 1-3 fold less active in MCF-7 and SKOV-3 cells, but significantly less active in the NCI/ADR multidrug resistant line.<sup>95</sup> This was comparable to the activity of the 14-normethyl analogue (**64**). It was hypothesized that the A<sup>1,3</sup>-strain imposed by the C14 methyl may be necessary to maintain a bioactive conformation that confers activity in MDR cell lines.<sup>95</sup>

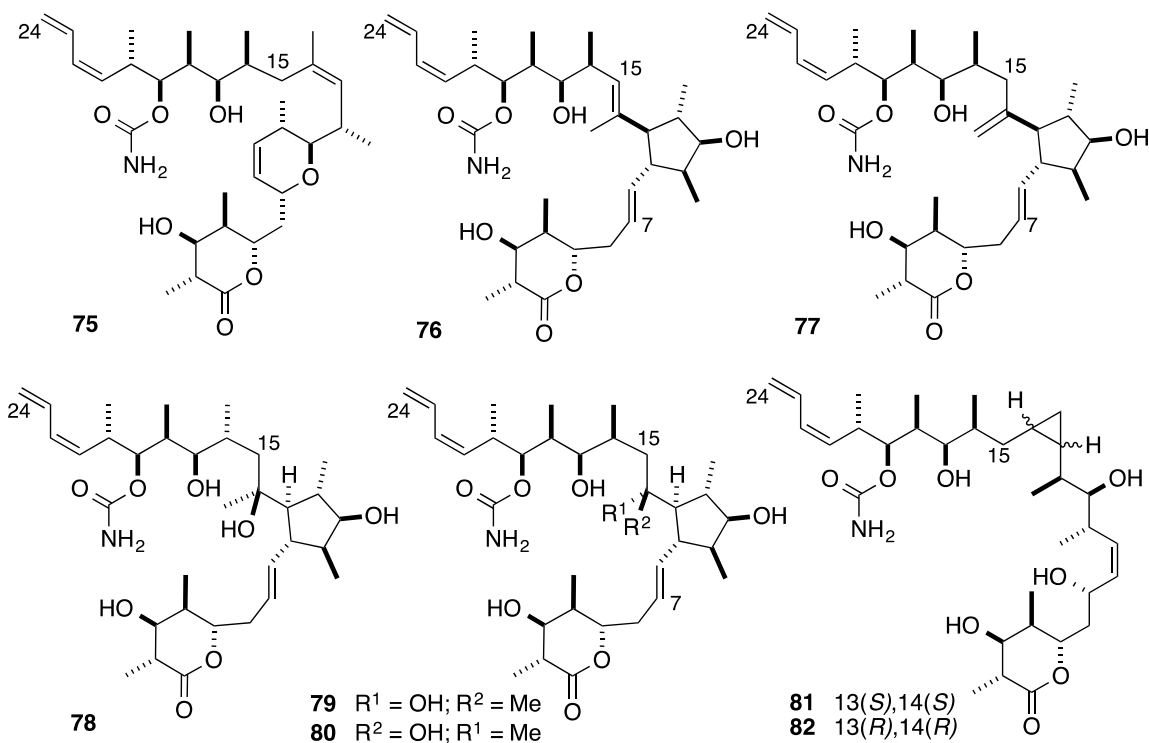


Figure 15. Cyclization of the linker region of discodermolide.

#### 1.4.4 Lactone Fragment Analogues

One of the most valuable findings in the many SAR studies of discodermolide was that the

structure of the lactone moiety could be drastically altered while still preserving low nanomolar antiproliferative activity (Figure 16, Tables 5 and 10).<sup>26,84,90,91,96-98</sup> Even contraction of the ring to form butyrolactone **89** yielded a compound that was more active than the parent. Forming a much-simplified lactone fragment through sequential removal of substituents in the C2-C7 region and hydrogenation (**83-93**, **95**) lead to compounds with improved or equivalent potency. Epimerization of the same stereogenic centers (**90-94**), however, led to a decrease in potency for all except analogue **93**. The lactone of the parent is known to adopt a twist-boat conformation, where substituents maintain an equatorial orientation and the overall ring is nearly planar.<sup>90,99</sup> Here, the olefin rigidifies the ring, and the double epimerization at C4 and C5 in **93** presumably allows the lactone to maintain its near-planarity.

More drastic alterations to the backbone of the lactone further demonstrated how tolerant it was of substitution and simplification. Outright removal of the C7 hydroxyl (**88**) only slightly reduced its cytotoxicity, and acetylation of hydroxyl groups present in this region yielded compounds with enhanced cytotoxicity (**96-99**), showing that H-bonding ability is not necessary for conformational requirements or binding interactions with tubulin. Surprisingly, thiophenyl acetals **100** and **101** had equivalent potency to discodermolide, regardless of their orientation. Even the naturally occurring linear methyl ester **102** retained double-digit nanomolar potency.

In polymerization studies carried out by Smith and Horwitz, it was shown that several analogues including **84** had a decreased ability to hypernucleate tubulin assembly.<sup>90</sup> For instance, average MT polymer length for cells treated with **84** were 5.1  $\mu\text{M}$ , which is more similar to Taxol (3.3  $\mu\text{M}$ ) than to discodermolide (0.78  $\mu\text{M}$ ). It still remains unclear which structural features are responsible for making discodermolide so efficient at microtubule polymerization when compared to paclitaxel, or what affect this has on cytotoxicity.

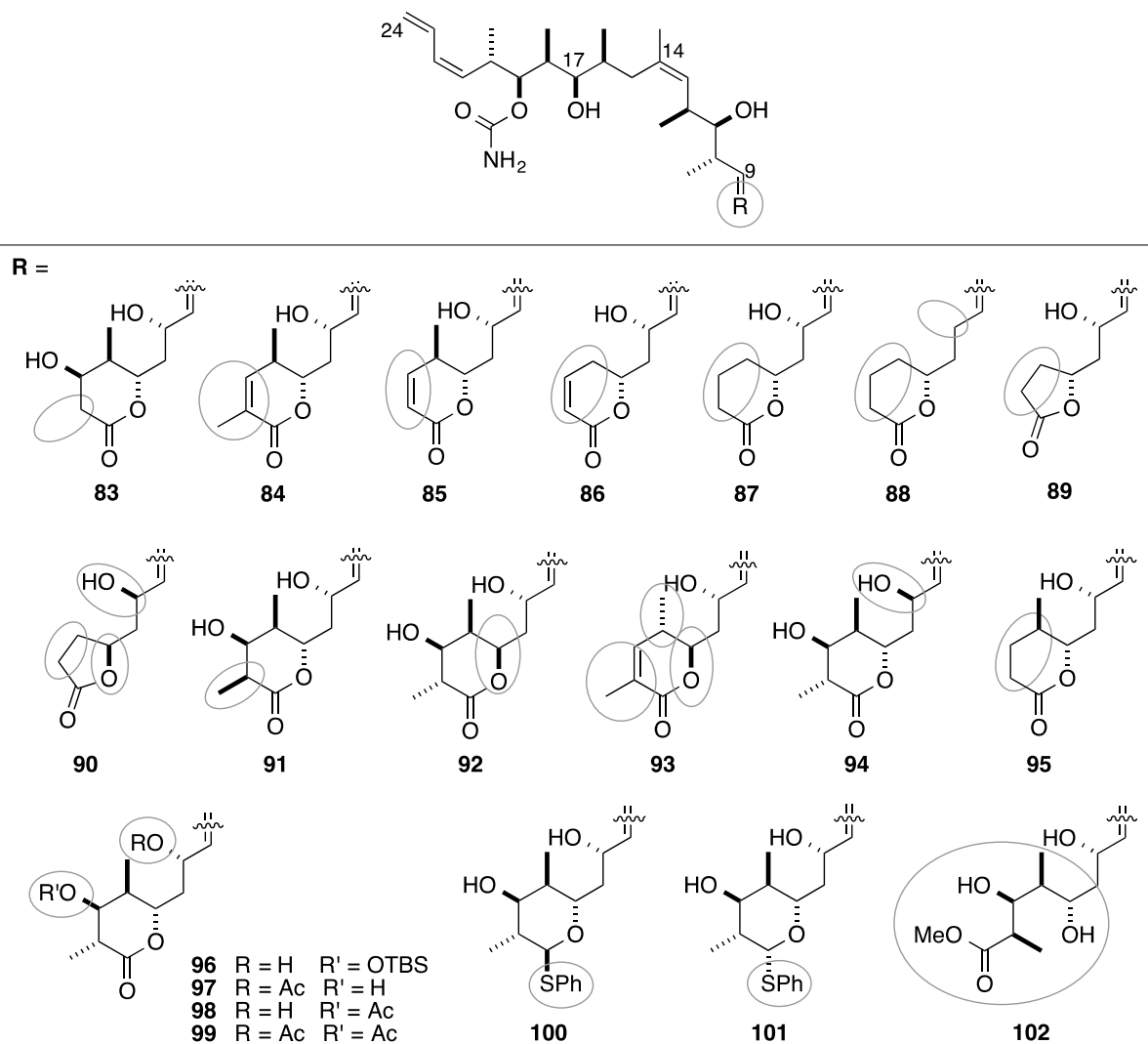


Figure 16. Synthetic analogues of the lactone group.

Progressing from the point mutations shown in Figure 16, more streamlined aromatic fragments were chosen to mimic the planar nature of the lactone in the parent (Figure 17, Tables 5 and 10).<sup>84,85,100-103</sup> With the exception of **121** and **122**, all of the fragments shown in Figure 17 also have the C7 hydroxyl group removed. Initial studies using the phenyl (**103**) and phenol (**108**) groups revealed sub-micromolar IC<sub>50</sub> values, but attempts at lead-optimization – regardless of steric or electronic manipulations – did not improve this value significantly or help to further

elucidate SAR for the region. The exception to this was the coumarin fragment (**120**), which showed antiproliferative activity equivalent to discodermolide. Both analogues containing a meta-hydroxyl substituent also performed well (**108** and **121**), suggesting that hydrogen bonding ability at this position may help improve activity. To date, **120** is the simplest substitution for the lactone region that allows the overall compound to maintain its low-nanomolar activity.

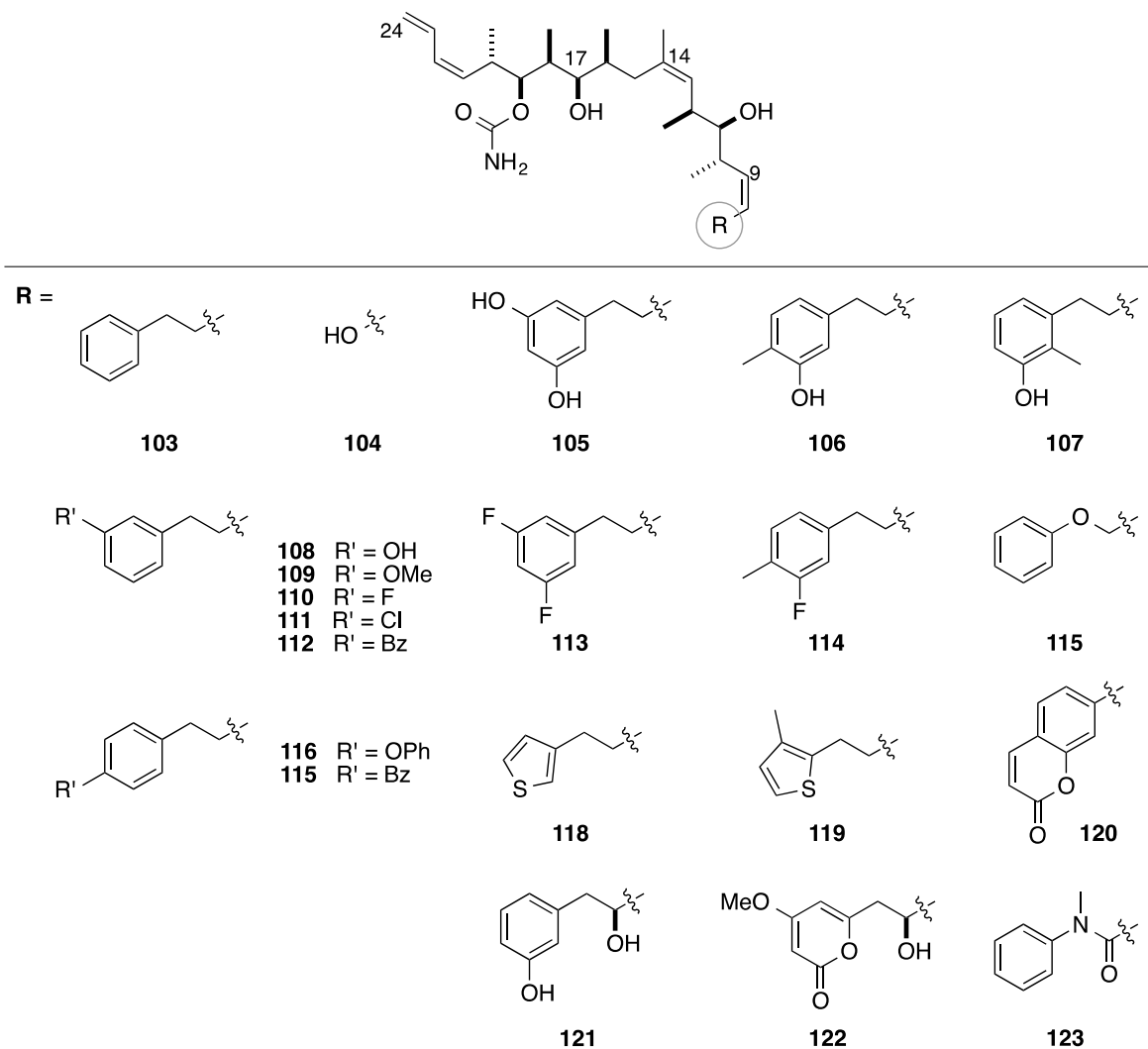


Figure 17. Streamlined analogues of the lactone group containing aromatic rings.

### 1.4.5 Analogues with Multiple Regions of Alteration

As more was learned about the SAR of discodermolide, more analogues were synthesized that incorporated several modifications into one structure. Major alterations to the compound often produced inactive species, but this was not always the case. In one of the most extreme cases of structural modification, truncated molecules **124-127** displayed relatively little inhibition, showing that both the lactone and the carbamate fragments are necessary to inhibit cell growth (Figure 18, Tables 6 and 11).<sup>82,84,86,93,101</sup>

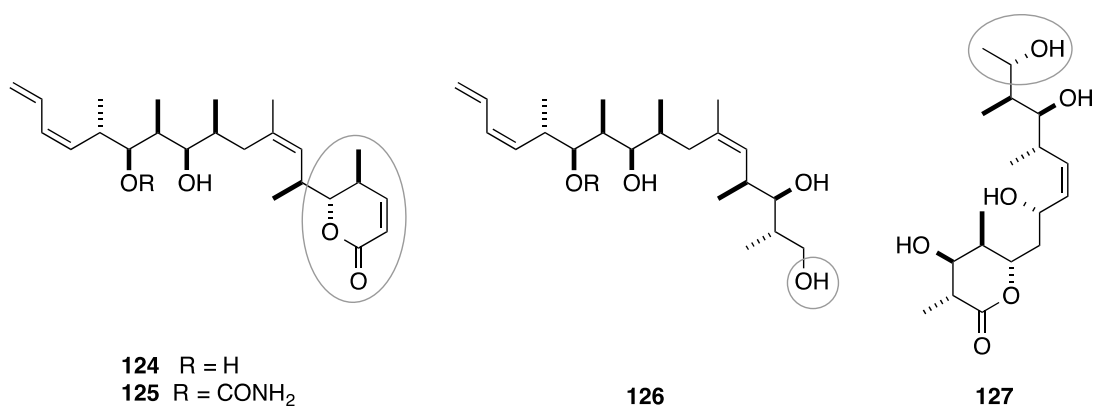


Figure 18. Truncation of the discodermolide backbone.

Complete saturation of the olefins within the carbon backbone resulted in the slight loss of activity for that congener (**128**).<sup>93</sup> However, nanomolar activity comparable to that of discodermolide was obtained when just one of these olefins was retained (**129**). Subsequent removal of the C7 hydroxyl group (**130**) severely reduced the cytotoxic activity observed (Figure 19, Tables 6 and 11).

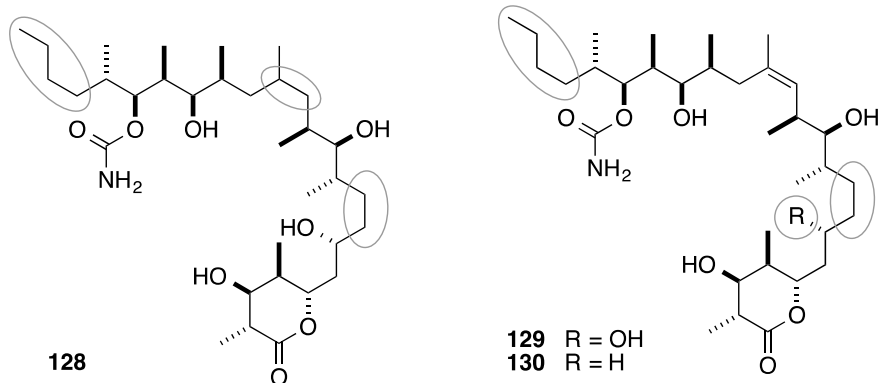


Figure 19. Saturation of discodermolide olefins.

It was hoped that acetylation of various hydroxyl groups would lead to a greater understanding of the electronic requirements for discodermolide's activity (Figure 20, Tables 6 and 11).<sup>84,93,98,104</sup> However, compounds **132-135** displayed a significant loss in activity compared to the parent. Compound **131** maintained a moderate, sub-micromolar, cytotoxicity. This difference is likely due in part to the acetylation of the C17 hydroxyl, which has been shown to severely lower activity (see Figure 14, **67**).<sup>7</sup>

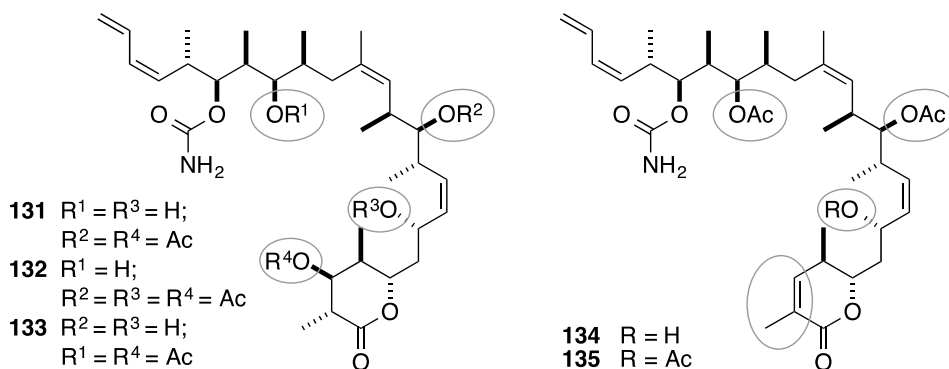


Figure 20. Acetylation of alcohol groups present in discodermolide.

Knowing that 14-normethyldiscodermolide and a saturated C-24 terminus did not negatively impact cell growth inhibition independently, these changes were paired with various lactone isosteres (Figure 21, Tables 6 and 11).<sup>77,102</sup> Improved activity was found with demethylation at C2 of the unsaturated fragment **137** when compared to **136**. A striking lack of activity was observed in the aromatic fragments assayed. This was surprising, especially considering that the corresponding phenol analogue (Figure 17, **108**) was so potent. Knowing how potent the previously-studied coumarin derivative was, a series of analogues were synthesized to probe the orientation and electronic requirements for the group. When combined with modifications to C14 and C23-24, only coumarin **141** displayed enhanced biological properties when compared to discodermolide.

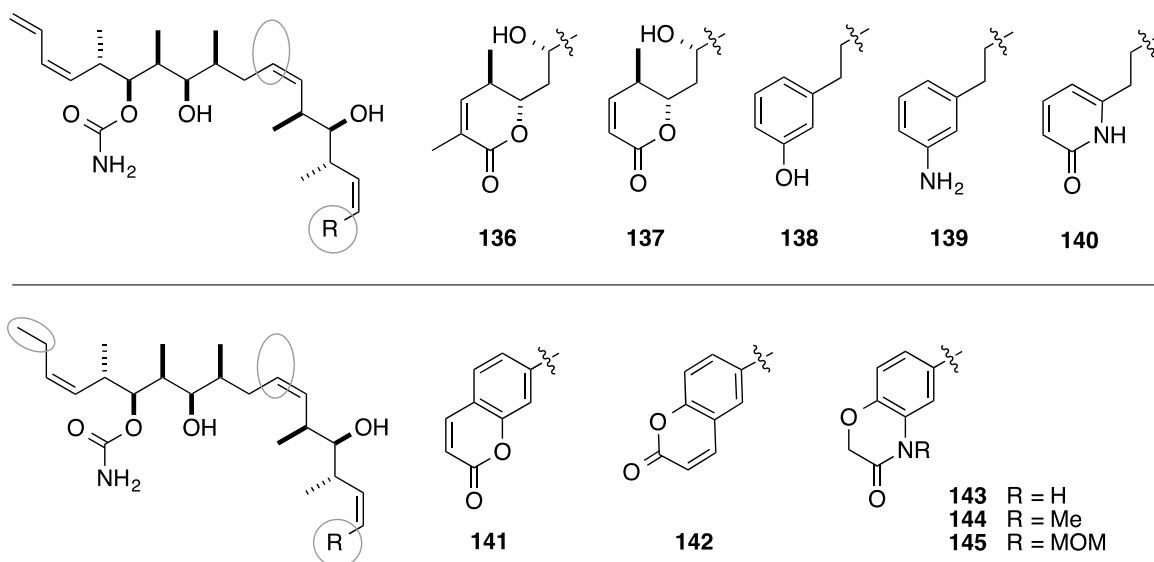


Figure 21. Investigation of lactone modifications coupled with C14 and/or C23-24 alterations.

In a series of studies within the Curran and Day groups, C14 demethylation was paired with modifications of the lactone and/or carbamate fragments.<sup>24,103,105,106</sup> These studies began

with the replacement of the lactone ring with a simple ester (Figure 22, Tables 7 and 12).<sup>24,105</sup> Of the compounds studied **146-173**, only seven showed activity below 5  $\mu\text{M}$  in at least one cell line assayed. The analogues shown in Figure 22 fared much worse than the previously-studied open-lactone analogue, **102**. These results suggest that the poor activity may be due to the high degree of modification across the compound or to the oversimplification of the lactone region, and not merely because of the open-lactone modification itself.

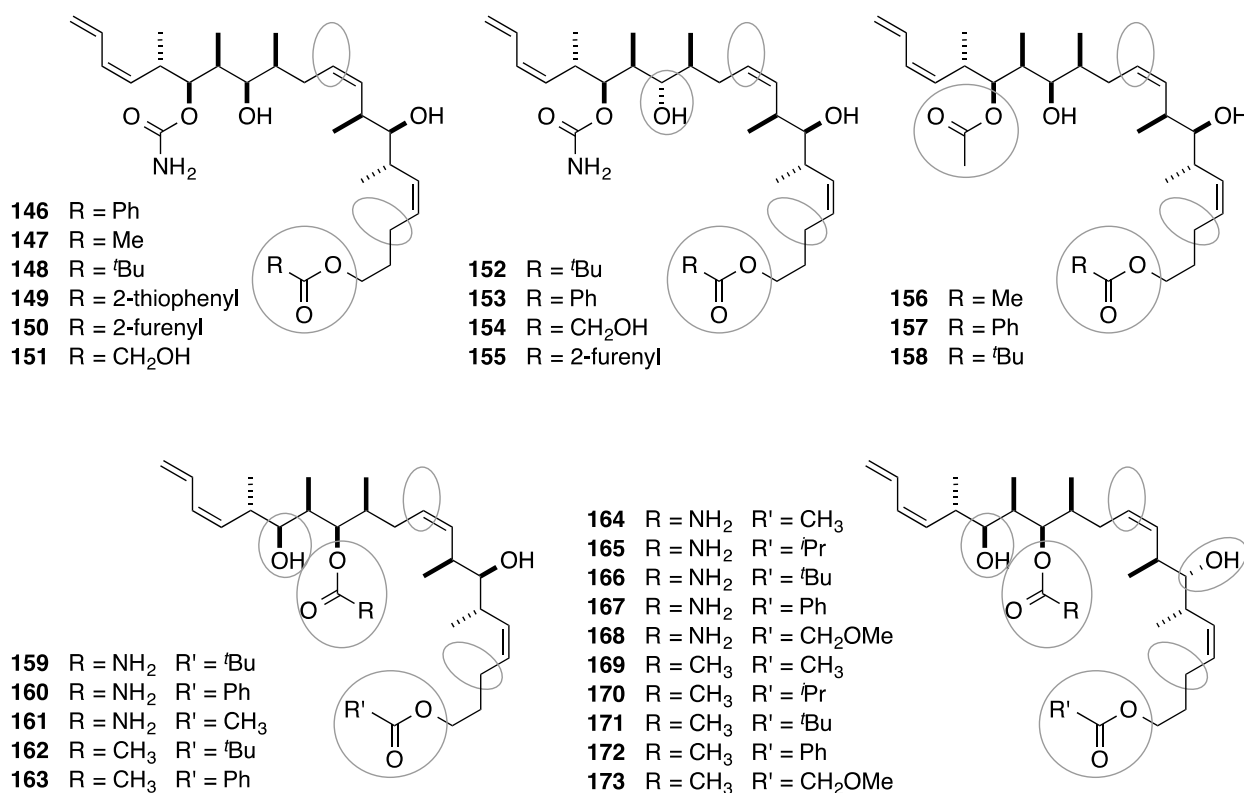


Figure 22. Carbamate and linker region modifications paired with a ring-opened lactone.

Although many of the compounds in Figure 22 exhibited  $\mu\text{M}$  GI<sub>50</sub>, *in vitro* bovine brain tubulin assembly assays showed them to be extremely weak tubulin hypernucleators.<sup>24,105</sup> This conflicting data prompted further investigation in the form of a high content cell-based assembly assay, which confirmed that the cells were indeed mitosis-blocking and cytotoxic. Results such

as these highlight difficulties that have been encountered when assaying discodermolide and its analogues; variations in activity are common across tubulin isotypes, cell lines, and *in vitro* assays.

Collaborators Day and Curran then moved on to manipulate further regions of the parent, leaving the lactone moiety largely intact (Figure 23, Tables 7 and 12). When the lactone motif was replaced with a simple ester, activity plummeted. Of the analogues shown in Figure 23, Replacement of the diene terminus (**176**, **177**, **179-182**) led to a substantial drop in activity. Notably, MOM protection (**175**) of the C3 hydroxyl group led to enhancement of growth inhibition while retaining sub-micromolar activity. This was presumably due to the extension of the lactone's H-bond acceptor that promoted a conformation with carbamate and lactone regions in close proximity.

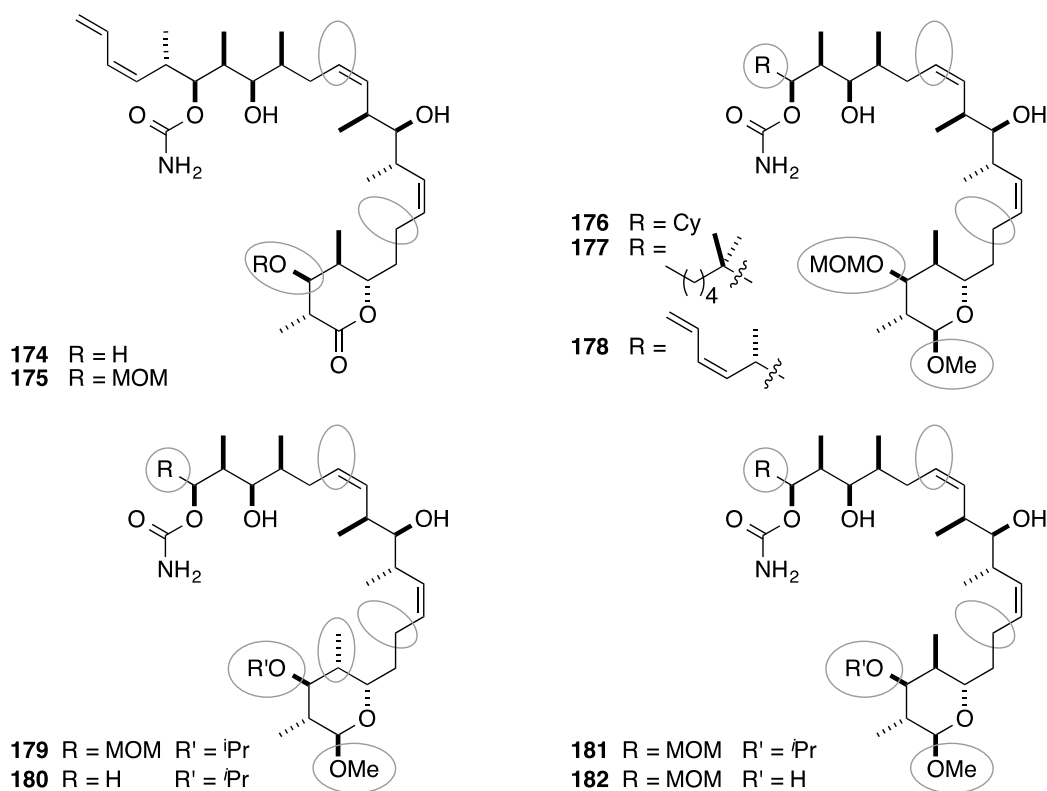


Figure 23. Carbamate and lactone fragment modifications.

#### 1.4.6 SAR Summary

Although discodermolide itself contains a great deal of complexity, analogue synthesis and SAR studies have proven that not all of components are essential for maintaining its biological activity. The ability to simplify various elements of the structure without diminishing its antiproliferative activity makes discodermolide an interesting target for further synthetic studies. Furthermore, alterations like these can be used to enhance metabolic stability, a likely cause of failure in Phase I clinical studies.<sup>10,11</sup> While the shortest linear sequence achieved during total syntheses is only 17 steps, this number reflects the convergence of the approach and is misleading when considering the complexity of the overall process. SAR studies such as these highlight the opportunity for significant simplifications to the structure – and, therefore, the

synthesis – that will help to enhance its clinical viability. A summary of the SAR profile of discodermolide is shown below, in Figure 24.

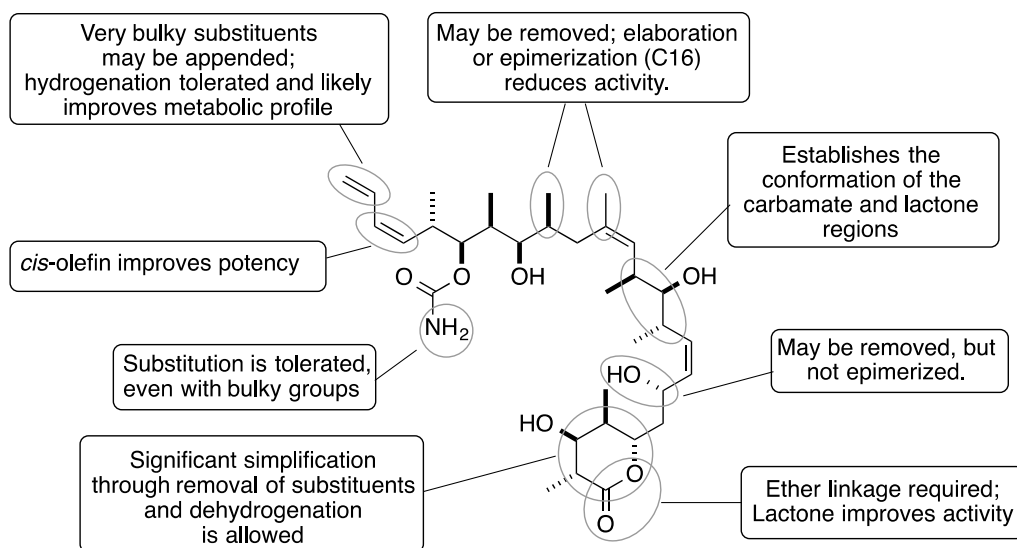


Figure 24. Summary of the SAR profile for discodermolide.

## 1.5 MODELING STUDIES OF DISCODERMOLIDE

Although there are 13 stereogenic centers and numerous rotatable sigma bonds, early modeling studies showed the three-dimensional conformation of discodermolide to be relatively rigid.<sup>2,107</sup>

In 2001, the Smith group carried out energy minimization and NMR studies of discodermolide in CD<sub>3</sub>CN, concluding that the structure in solution was very similar to that of the solid state (Figure 26, top).<sup>107</sup> Acetonitrile was chosen in order to maximize the stability of the compound while mimicking the inherent polarity of an aqueous biological environment. Even though the experiments were carried out in solution, the helical conformation is structurally enforced in

order to minimize A<sup>1,3</sup>-strain at C8-9, C13-14 and C21-22, and also *syn*-pentane interactions at C10-12, C16-18 and C18-21 (Figure 25).

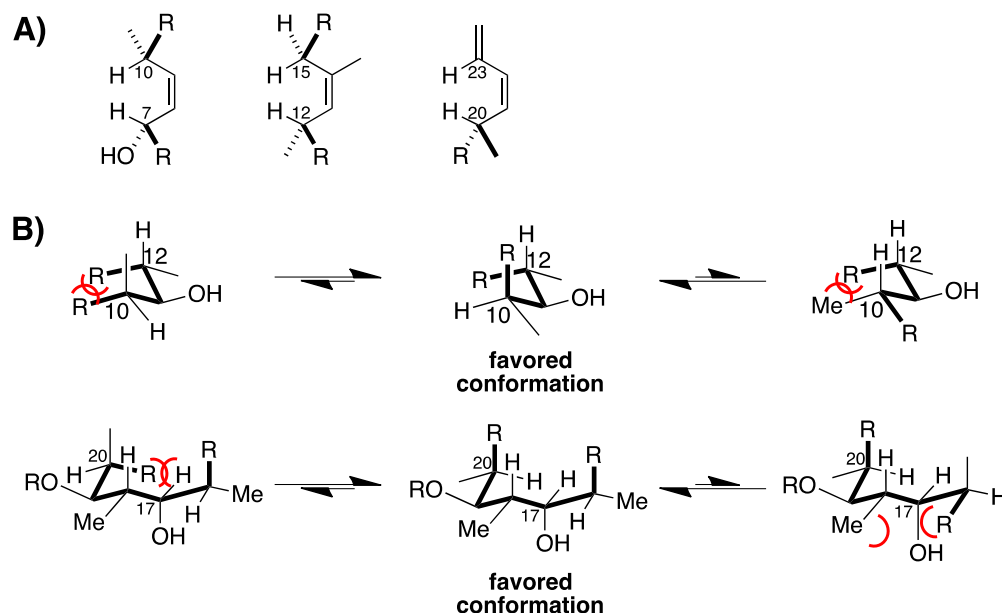


Figure 25. Conformational preferences are determined by strain minimization.

In the same year, the Snyder group also carried out NMR studies to determine the dynamic properties of discodermolide in solution.<sup>99</sup> These 2-D and NAMFIS (NMR analysis of molecular flexibility in solution) experiments were carried out in DMSO-*d*<sub>6</sub> to identify Boltzmann populations of rotamers in solution. They argued that a single solution conformation (as determined previously by the Smith group) was likely the result of signal averaging and represented a “virtual conformation” as a geometric average of distinct conformers. The group proposed a series of 14 rapidly interconverting structural conformations that are present in DMSO, with 68% of the population being described as having a corkscrew-like conformation (Figure 26, bottom).

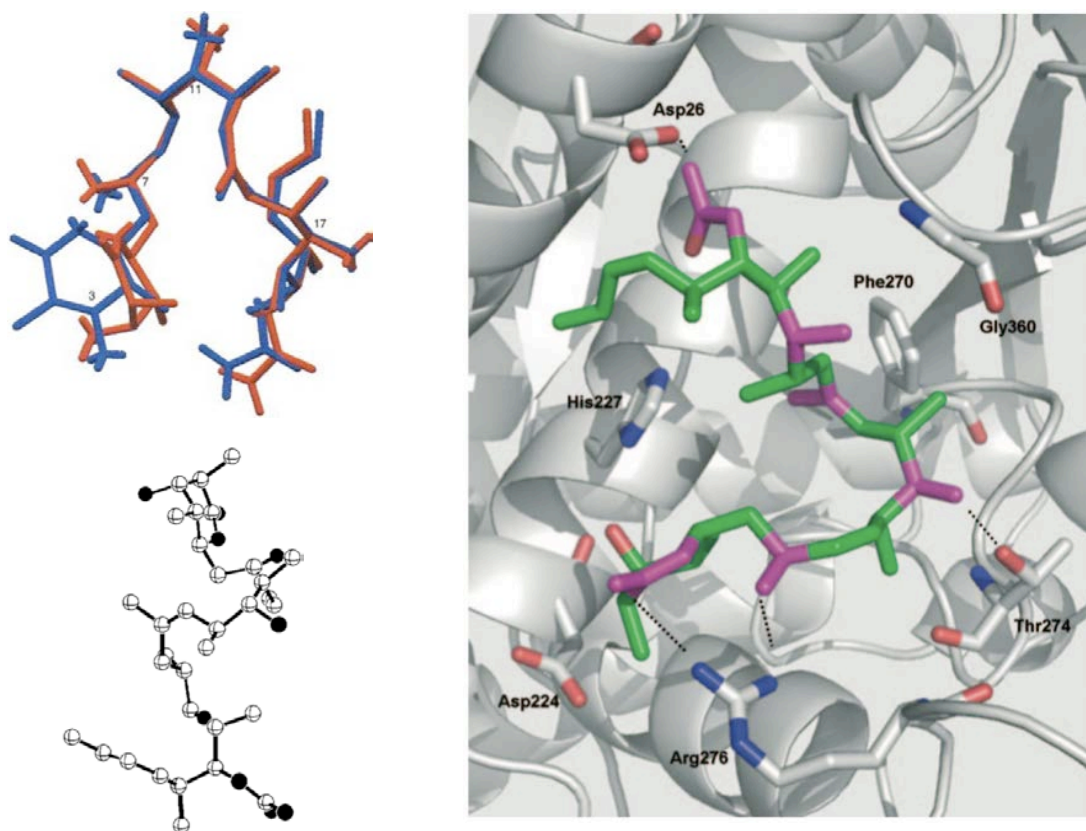


Figure 26. Conformational models of discodermolide.

Top: Smith's solution structure in  $\text{CD}_3\text{CN}$  (red) compared to the x-ray crystal structure (blue); bottom: Snyder's corkscrew solution structure in  $\text{DMSO}-d_6$ ; right: Three-dimensional model of discodermolide in the binding site, based on HQSAR screen. Fragments that were found to correlate with high cytotoxicity are labeled. *Image at top left adapted with permission from Ref. 107, copyright 2001 American Chemical Society; image at bottom left adapted with permission from Ref. 99, copyright 2001 American Chemical Society; image at right reproduced with permission from Wiley-VCH Verlag GmbH & Co. KGaA, Ref. 108, copyright 2009.*

Using more advanced spectroscopic and modeling techniques, several groups were later able to develop more precise models for conformation and binding. Competition binding experiments and photoaffinity labeling of discodermolide analogues provided confirmation that the preferred binding site of discodermolide was indeed the taxane site on tubulin, although multiple conformational contacts were not.<sup>45,109,110</sup> Later analogue studies involving paclitaxel-discodermolide-dictyostatin hybrids showed a decrease in activity, suggesting that this conclusion may not have been wholly accurate.<sup>111</sup> Previously-discussed HDX experiments by

Horwitz and Smith demonstrated that stabilized MT conformations differed, with solvent-exposed lateral sites that were only observed with discodermolide treatment.<sup>22</sup> This highlights difficulties that docking studies on MT stabilizers have experienced, largely as a result of reliance on the 3.5 Å resolution electron microscopy-derived structure of paclitaxel bound to the  $\alpha\beta$ -tubulin dimer (Shown in Figure 7).<sup>112</sup> Specifically:<sup>89</sup> (a) the MT backbone was likely distorted in the presence of paclitaxel, so does not precisely reflect the unbound structure; (b) Zn-induced crystalline sheets have been shown to have different conformations than those found *in vivo*; (c) the M-loop region, which is involved in paclitaxel binding, is poorly resolved; (d) lateral contacts between protofilaments are not present due to the aggregation state of the sample; (e) bovine brain tubulin was used to obtain this sample, although this tubulin isotype is different than that which is found in humans.

A study conducted by Dias and Andricopulo assembled a virtual set of fragments to develop a predictive quantitative SAR model (Hologram QSAR, or HQSAR).<sup>108</sup> This type of study differs significantly from others in that the researchers sought to develop a training set that could be used to predict IC<sub>50</sub> values and highlight structural features that were important for biological activity. Using their computational results and the PDB entries for bound paclitaxel and epothilones A (PDB IDs 1JFF and 1TVK, respectively), they were able to construct a three-dimensional model of discodermolide in the binding site. This model is shown in Figure 26 (right). The model agreed with previous studies that gave discodermolide a U-shaped structure, and placed the linker region away from the binding pocket.

Nine years after their original single-force field conformational analysis, the Snyder group suggested a pose for discodermolide in which the linker region pointed away from the binding site (Figure 27).<sup>113</sup> This came after extensive modeling using NAMFIS and docking

experiments with Glide, RosettaLigand, and AUTODOCK software. Specifically, C3 and C17 hydroxyl groups and the carbamate group form polar contacts with the M-loop while several nonpolar contacts to Leu361 are made with hydrophobic groups. The model was consistent with SAR data from known analogues and non-resistance to various cell lines containing  $\beta$ -tubulin mutations.<sup>9</sup> It also provided an alternative to established models, which could not always be used to rationalize SAR results. One of the most striking outcomes of these experiments is the understanding that major alterations, such as removal of hydroxyl groups or truncations of the structural backbone, would be possible without great loss of activity. Assuming that binding interactions were maintained, such alterations could be employed to improve the pharmacokinetic profile and enhance the viability of discodermolide as a therapeutic agent.

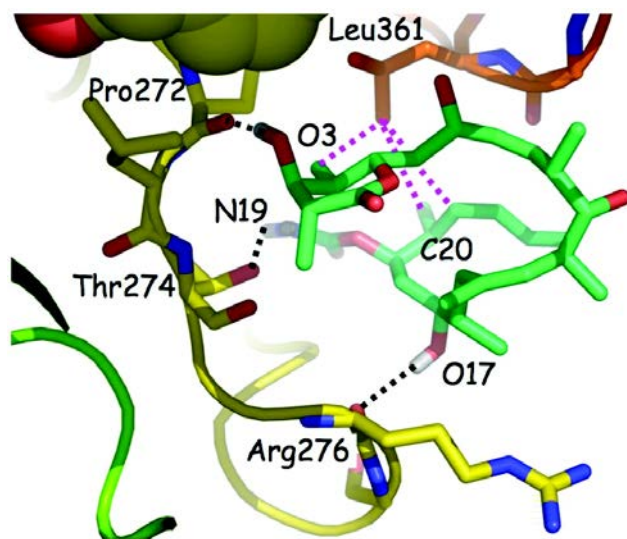


Figure 27. Proposed binding conformation of discodermolide.

Polar contacts are highlighted in black and nonpolar contacts are highlighted in magenta. *Reproduced with permission from Ref. 113, copyright 2010 American Chemical Society.*

## 2.0 RESEARCH PROJECT OVERVIEW

### 2.1.1 Hypothesis

Our group's interest in pursuing SAR development in this area was spurred by the need to further investigate the role of discodermolide's linker region. The majority of the SAR data for the linker has been collected from naturally occurring congeners or byproducts obtained during the course of other studies. As mentioned, it has been proposed that the linker region points away from the binding site while positioning the carbamate and lactone regions into it (Figures 26 and 27).<sup>113</sup> Further information is limited without a crystal structure of discodermolide in its tubulin binding pocket.

HQSAR studies were initially carried out by Mr. Daniel Brody of the Day lab in collaboration with the Andricopulo group to determine if significant alterations to the linker region could be made while maintaining the appropriate positioning of the carbamate and lactone regions.<sup>114</sup> Pleasingly, these computational models suggested that modifications to the linker portion of discodermolide may be well-tolerated. Based on the top hits of the HQSAR results, several virtual analogues were identified that allowed the carbamate and lactone regions to align well with the parent despite major structural changes. The best of these were predicted to have IC<sub>50</sub> values of ~100 nM against A549 lung carcinoma cell types in at least 3 of the 4 parameter models studies (Figure 28).

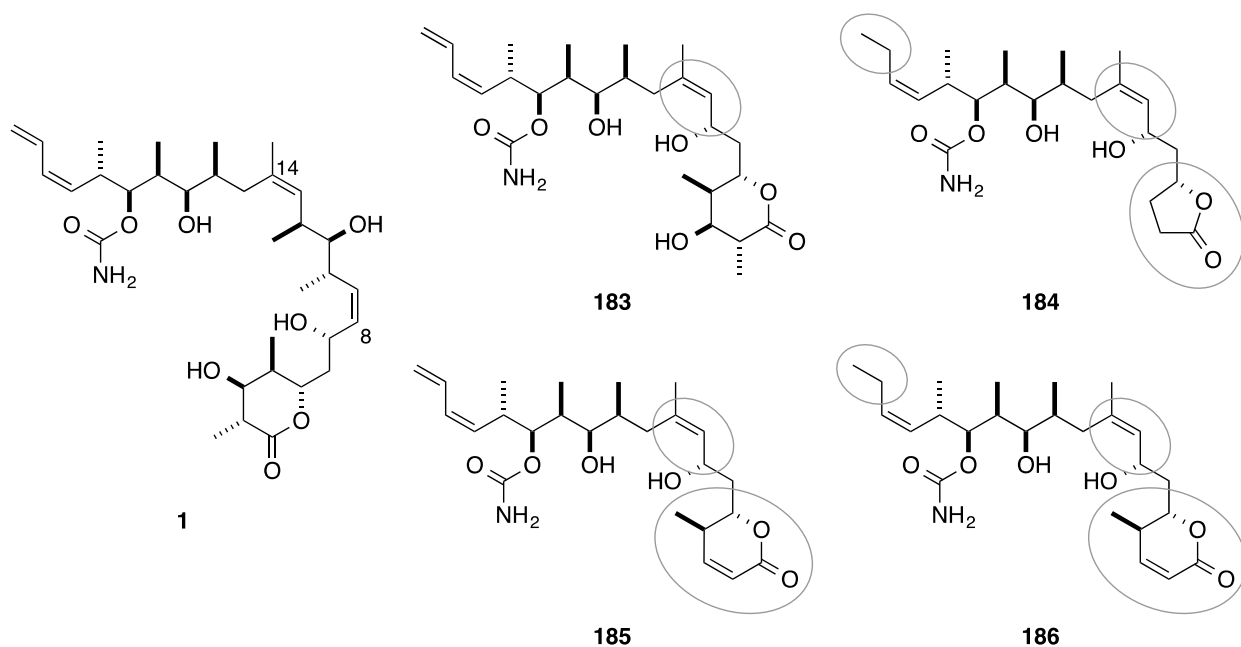


Figure 28. Discodermolide compared to the top performing hits from Day group HQSAR experiments. Modified regions are circled on the analogues.<sup>114</sup>

These promising results prompted further investigations with the long-term goal to synthesize simplified discodermolide analogues with novel linker regions and to assess their biological profiles. These analogues would be constructed with streamlined and more metabolically stable carbamate and lactone fragments. Two parallel projects were initiated in the Day group:

- 1) Replacement of C8-C14 with a truncated olefin linker (as shown in Figure 28).
- 2) Replacement of C8-C14 with a linker formed through multicomponent reactions.

The second of these two initiatives will be discussed at length herein.

Multicomponent reactions are atom-economical processes that have the potential to increase efficiency and variability when compared to traditional reaction sequences (Figure 29).<sup>115,116</sup> Although such reactions have been used frequently to construct complex

pharmacological agents, they have only recently been applied towards the synthesis of more elaborate natural products.<sup>117</sup> Isocyanide-based MCRs can provide a large library of drug-like molecules from a relatively small set of starting materials. The Ugi four-component reaction (Figure 29a) typically combines an isocyanide, a carbonyl-containing compound such as an aldehyde or ketone, an amine, and an acid in one pot to irreversibly deliver an  $\alpha$ -acylamino amide.<sup>118,119</sup> The van Leusen protocol (Figure 29b) involves treatment of a tosylmethyl isocyanate with an aldehyde and a primary amine leading to a 1,4-disubstituted imidazole.<sup>120</sup>

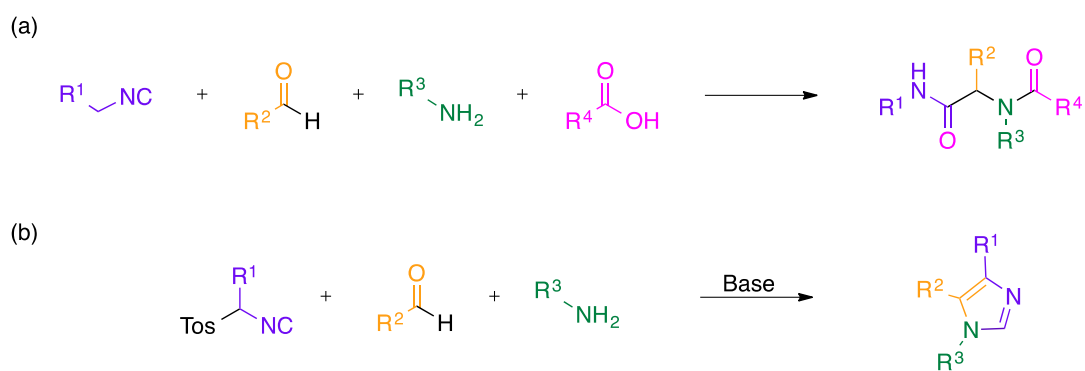


Figure 29. Reaction summary for (a) Ugi and (b) van Leusen MCR approaches.

### 2.1.2 Planned Research Approach

These two types of MCRs were envisioned to produce a series of discodermolide analogues with novel linker regions (Figure 30). First, carbamate and lactone fragments would need to be synthesized containing either an acid or amino terminus. Immediately before the Ugi MCR was carried out, the amino fragments could be converted to the less stable isocyanide and then paired with the other components to produce the product. In this way, MCR processes would be used to

join the carbamate and lactone regions together through either a peptide-like or imidazole linkage.

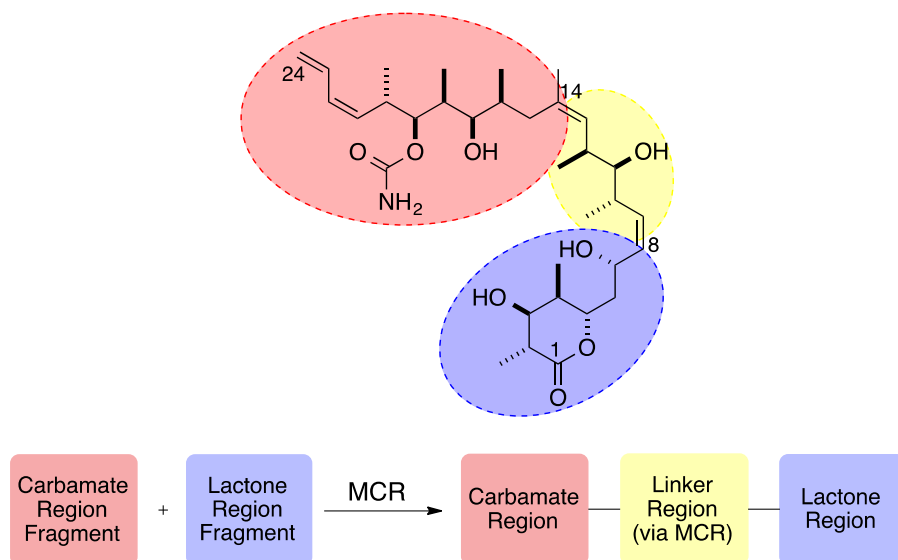


Figure 30. Design of discodermolide analogues joined by a linker through MCR.

The goal of this project was to construct precursor carbamate and lactone fragments containing amine and acid termini for later MCR coupling. Synthetic targets for the carbamate and lactone fragments were selected for their proven successes in previous SAR studies and simplicity of structure rather than pharmacological novelty (Figure 31, **187-189**, **192-195**). The imidazole linker formed through the van Leusen protocol (Figure 31, **190**) was chosen as an isostere for the truncated olefin linker used in our group's HQSAR experiments.<sup>114</sup> It also retains the ability to hydrogen bond, which has been hypothesized to aid in binding site interactions between tubulin and discodermolide.<sup>22</sup> The peptide-like Ugi linker (Figure 31, **191**) is much more flexible than that of the parent. However, the tertiary amide can be substituted with a bulky group such as isopropyl to impose a conformational bias. SAR studies have shown that some additional steric bulk is well-tolerated in this region, and according to the Snyder model

would be pointing away from the binding site, so this change would not likely have any steric effect on binding to the MT.<sup>84</sup> If necessary, interchanging the substituent at this position would be a straightforward method to manipulate PK properties such as solubility.

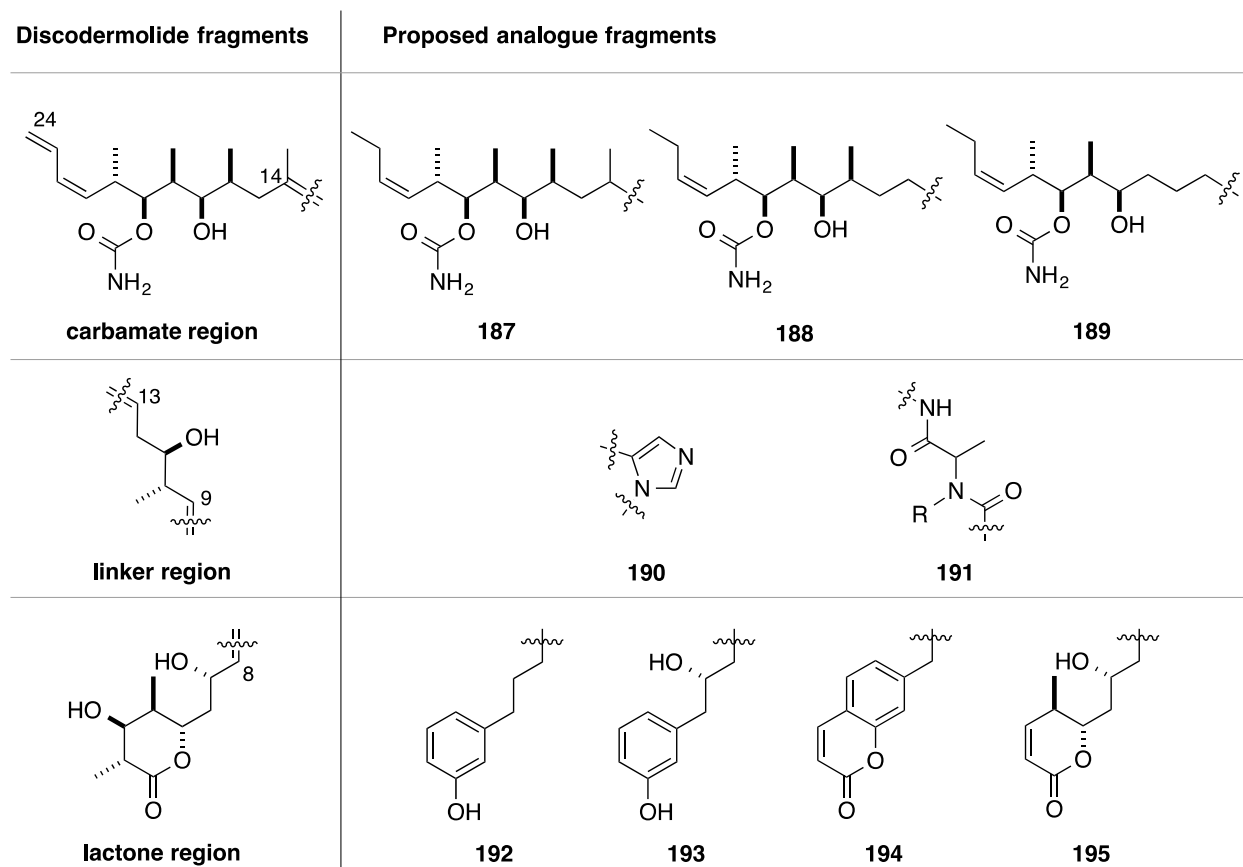
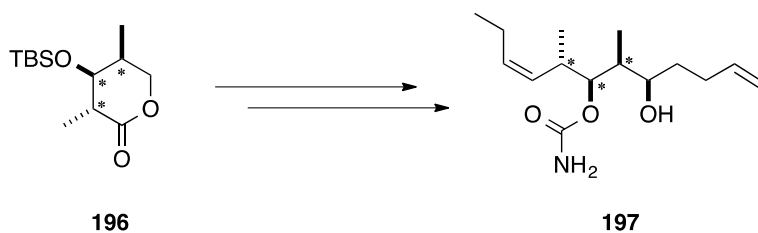


Figure 31. Fragments initially identified for this project's analogue studies.

Use of a multicomponent approach would allow for the synthesis of a broad variety of analogues through variation of the carbamate and lactone regions. For instance, a single carbamate fragment could be paired with any or all four of the lactone fragments shown above in parallel MCR experiments to yield up to four new analogues. Another advantage of the multicomponent approach is that the linker region could effectively be flipped through strategic



of the analogues should closely match that of the geometrically rigid parent structure. In the second phase of this project, a variety of MCR precursors were synthesized. A functionalized lactone containing the requisite stereotriad found in discodermolide was first synthesized as a common precursor to carbamate fragment analogues. This set the stage for the further carbamate fragment syntheses. Later work by Mr. Daniel Brody in the Day lab showed that this approach was feasible, successfully transforming the same common precursor lactone (**196**) into carbamate fragment **197** in 10 steps (Scheme 12).<sup>114</sup>



Scheme 12. Transformation of common precursor **196** into an advanced carbamate fragment.<sup>114</sup>

With the common precursor **196** synthesized and further carbamate fragments being explored elsewhere in the Day group, focus shifted to discodermolide's lactone region. Here, five lactone region fragments that contained amine or acid termini and one additional advanced fragment were successfully and efficiently completed.

## 3.0 RESULTS AND DISCUSSION

### 3.1 CONFORMATIONAL MODELS OF DISCODERMOLIDE ANALOGUES

Prior to the synthesis of individual fragments, a computational model of representative analogues was carried out. One of the fundamental characteristics of discodermolide is its relatively rigid framework, and the Snyder binding model postulates that the positioning of the carbamate and lactone regions specifically is crucial for its biological activity.<sup>113</sup> Therefore, the positioning of the carbamate and lactone regions in these analogue models needed to mimic that of the parent in order for them to be viable candidates for this MCR strategy.

Preliminary MM2 simulations of proposed analogues were conducted using Chem & Bio 3D 12.0 software. These computational models take into account factors that introduce strain or steric energy, including: bond stretching and bending, torsional strain, van der Waals interactions, and electrostatic interactions. The thermodynamic global minimum conformation from the MM2 experiment was then exported to MacPyMOL for rendering and visualization. Finally, the analogue structure was superposed on that of discodermolide and the three-dimensional space they occupied was compared.

Shown in Figure 33 are the structures and overlays that are the result of these computational models. In the three analogues shown, carbamate and lactone fragments are constant while the linker region is systematically altered. Only the linker region is then

responsible for any conformational differences between the three. Shown on the left is the product of a van Leusen reaction (**198**) and in the center and right are two Ugi reaction products (**199** and **200**). Pleasingly, the analogues exhibited a high degree of overlap with the parent, despite having structurally dissimilar linker regions, truncated carbamate fragments, and simplified lactone regions. This conformational similarity was encouraging and so the next phase of the project was initiated.

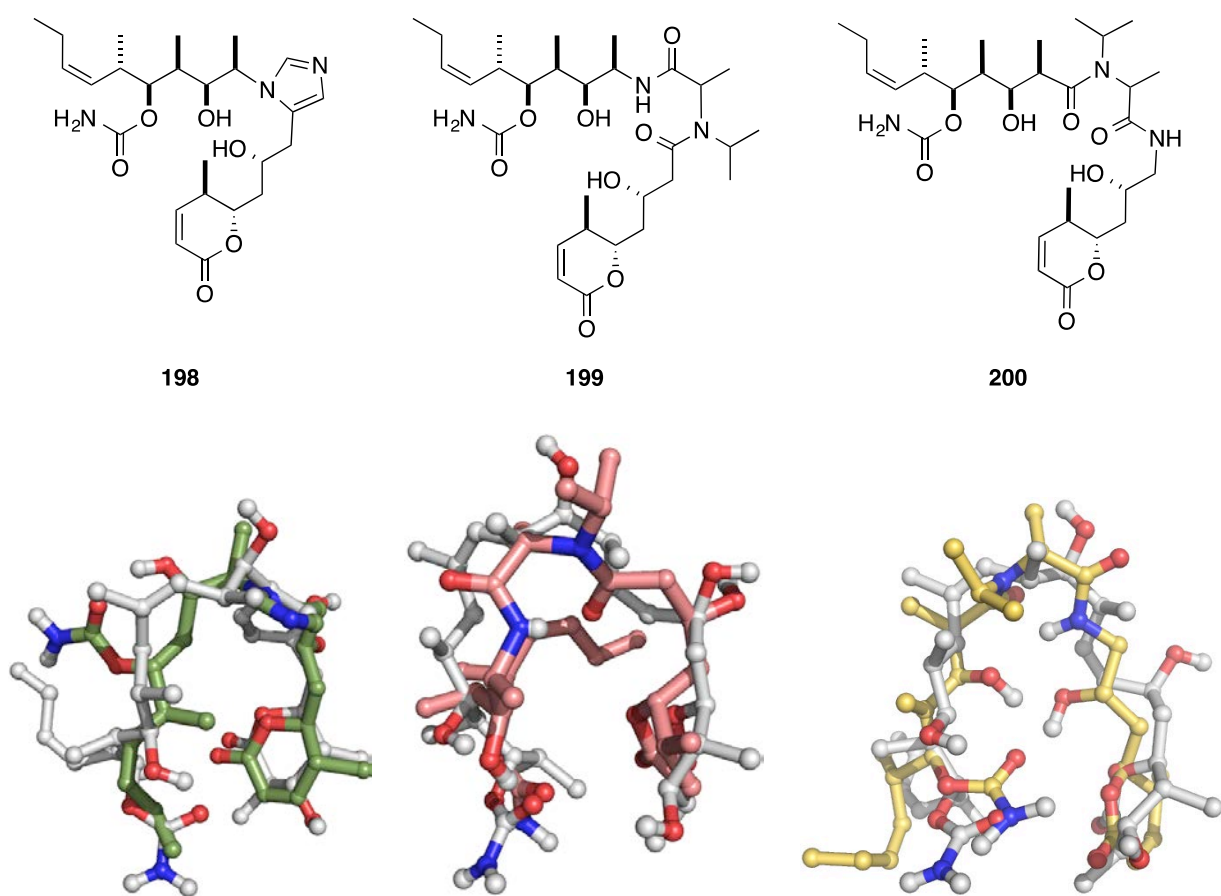
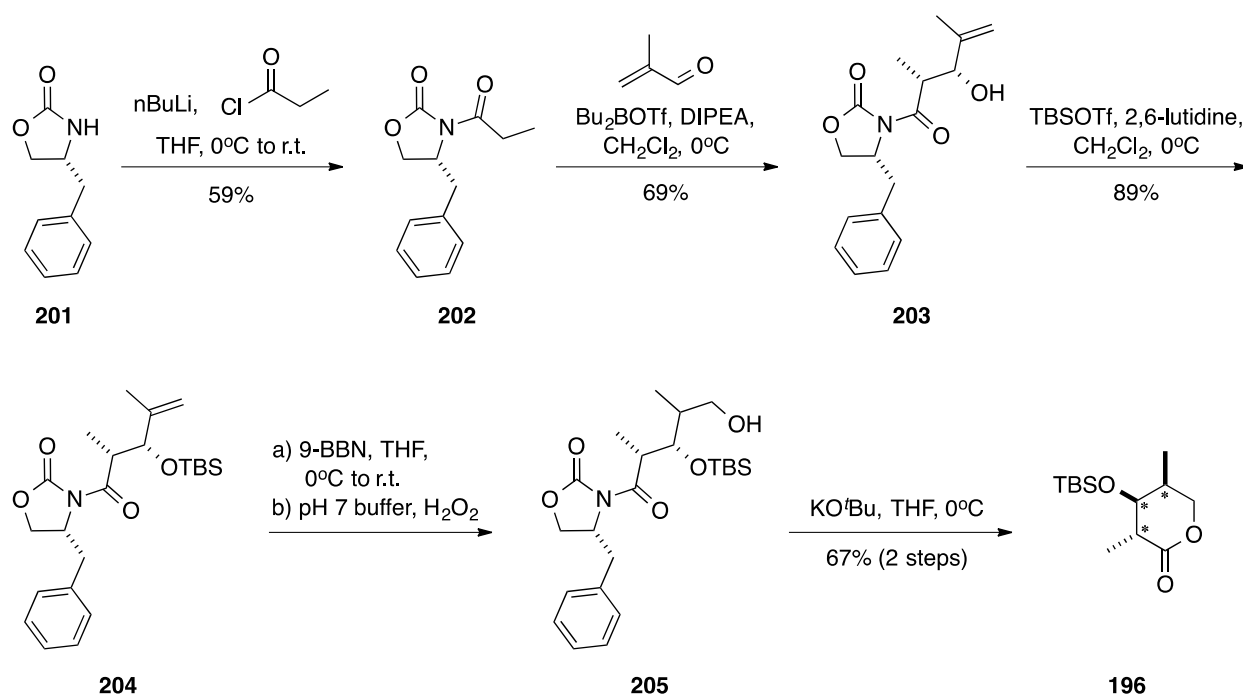


Figure 33. Overlay of sample MCR analogues **198-200** and discodermolide (white).

### 3.2 SYNTHESIS OF A CARBAMATE FRAGMENT COMMON PRECURSOR

A common precursor synthetic approach towards discodermolide has been used by a variety of groups in order to take advantage of its repeating stereotriad (see Chapter 1.3). This stereotriad has been shown to be essential for biological activity to remain intact (see Figures 14 and 16). Within the Day group, Mr. Daniel Brody had shown this strategy to be an effective means to obtain carbamate analogues in a parallel analogue synthesis project (see Scheme 12). In order to form this common precursor lactone **196**, a strategy developed within the Day group and by Novartis was employed (Scheme 13).<sup>121,122</sup>



Scheme 13. Synthesis of a discodermolide common precursor lactone.

Beginning with commercially available chiral oxazolidinone **201**, deprotonation with *n*-butyllithium and acylation with propionyl chloride led to the formation of the aldol precursor **202**

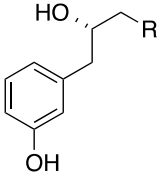
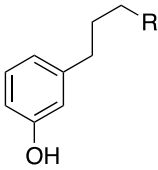
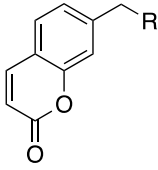
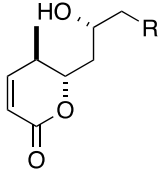
in 59% yield.<sup>123</sup> Carboximide **202** was transformed into a boron enolate with diisopropylethylamine and dibutylborontriflate, and immediately treated with methacrolein to produce **203** as a mixture of *syn* and *anti* adducts in a ratio of about 9:1. This ratio was determined through the calculation of vicinal coupling constants for the alpha and beta protons in the product's <sup>1</sup>H-NMR spectrum (*syn*:  $^3J_{\text{HH}} = 3.0 \text{ Hz}$ ).<sup>124,125</sup> The desired *syn* isomer was then easily isolated via flash chromatography in a 69% overall yield. Alkoxy oxazolidinone **203** was protected as a silyl ether and isolated in 89% yield without need for further purification. Treatment of the alkene moiety of **204** with 9-BBN and then peroxide provided the hydroboration-oxidation product **205**.<sup>122</sup> This unstable hydroxy imide was then immediately cyclized upon exposure to potassium *tert*-butoxide, giving lactone **196** in 67% yield over two steps. Overall, a single isomer of this common precursor was synthesized in 5 steps with a 24% yield. From here, the lactone **196** could serve as a key intermediate during the synthesis of carbamate fragment analogues.

### 3.3 SYNTHESIS OF LACTONE FRAGMENT PRECURSORS

#### 3.3.1 Summary of Fragment Syntheses

Once the carbamate region's common precursor had been synthesized, focus shifted towards the lactone region of discodermolide. Due to the variable stability of isocyanide compounds, the final two-step transformation of amine to isocyanide was strategically delayed until all other fragments were ready for MCR. Thus, the immediate substrates targeted for synthesis contained acid or amine termini. Overall, five fragments were completed, as summarized in Table 1 below.

Table 1: Summary of acid and amine lactone fragments syntheses.

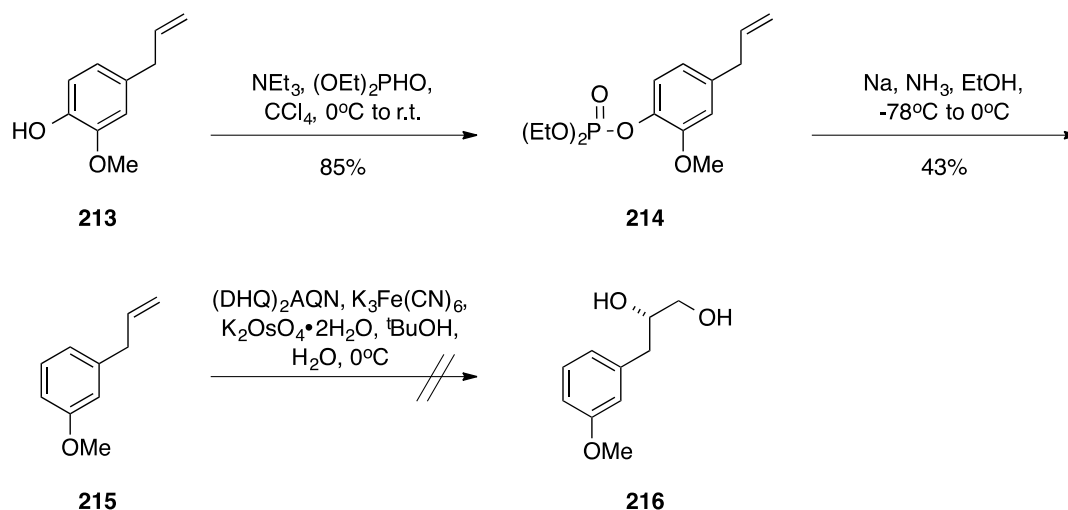
Targeted Fragment				
<b>R = COOH</b>	n/a	<b>207</b> 62% (3 steps)	<b>209</b> 59% (2 steps)	<b>211</b> partially completed
<b>R = NH<sub>2</sub></b>	<b>206</b> 64% (3 steps)	<b>208</b> 18% (46% BRSM) 5 steps	<b>210</b> 72% (2 steps)	<b>212</b> partially completed

### 3.3.2 Synthesis of the 3-(2-Hydroxypropyl)phenol Fragment **206**

Although the lactone region is known to interact with the MT binding pocket, there is a surprising amount of flexibility in the structural modifications that are allowed (see Figure 16). A *m*-hydroxy phenol substitution for the lactone isostere would enable hydrogen-bonding interactions that mimic the C3-hydroxyl group or the endocyclic oxygen of the parent. By itself, this substitution has been successful in SAR studies (**108**) but when combined with additional modifications, activity diminished to less than 17 times that of the parent (**138**).<sup>77,100</sup> The potential for an incredibly streamlined analogue was deemed worth that risk, and synthesis of MCR components was begun.

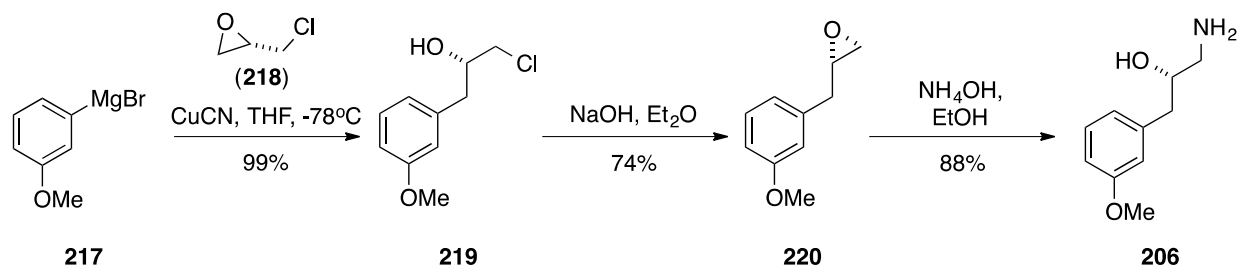
Initially, a cost-effective approach was taken towards the synthesis of phenol fragment **206**. Starting from the commercially available eugenol (**213**), successive phosphate protection and deprotection were used to yield the *m*-methoxybenzene intermediate **214** (Scheme 14).

Unfortunately, while **215** could be obtained in yields as high as 43%, the quantity recovered was often below 30%. A second-generation scheme was developed to circumvent the inconsistency of this approach and precautions associated with phosphate group removal on large scale.



Scheme 14. First-generation synthesis of fragment **206** via dihydroxylation.

This new route took advantage of the inherent chirality of the commercially-available (*S*)-(+)-epichlorohydrin (**218**) to establish the stereochemistry of the  $\beta$ -hydroxy group of **206**. In a first attempt, Grignard reagent **217** generated *in situ* was reacted with **218** to provide chlorohydrin **219**, then immediately reacted with sodium hydroxide to produce epoxide **220** in only 30% over two steps. A second attempt employing commercial Grignard reagent **217** and copper (I) cyanide significantly improved the efficiency of the process, increasing the yield to 99% for the first step (Scheme 15). The resulting chlorohydrin **219** was then treated with sodium hydroxide to produce epoxide **220** in 74% yield via an intramolecular  $\text{S}_{\text{N}}2$  reaction. Finally, the reaction of **220** with ammonium hydroxide gave the final  $\beta$ -hydroxyamine fragment **206** in 88% yield.

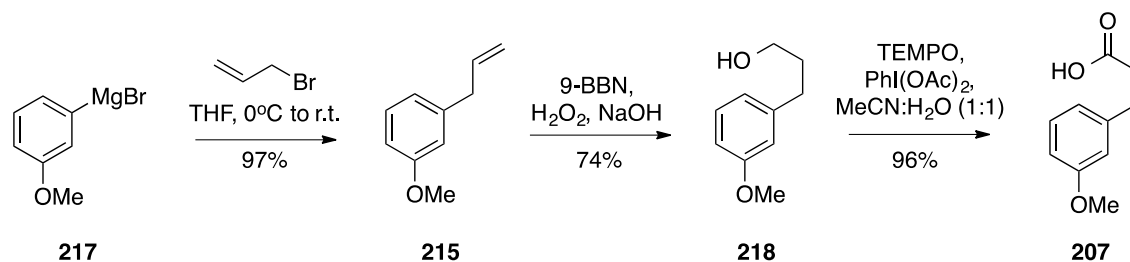


Scheme 15. Second-generation synthesis of  $\beta$ -hydroxyamine **206** via an epoxide intermediate.

### 3.3.3 Synthesis of 3-Propylphenol Fragments

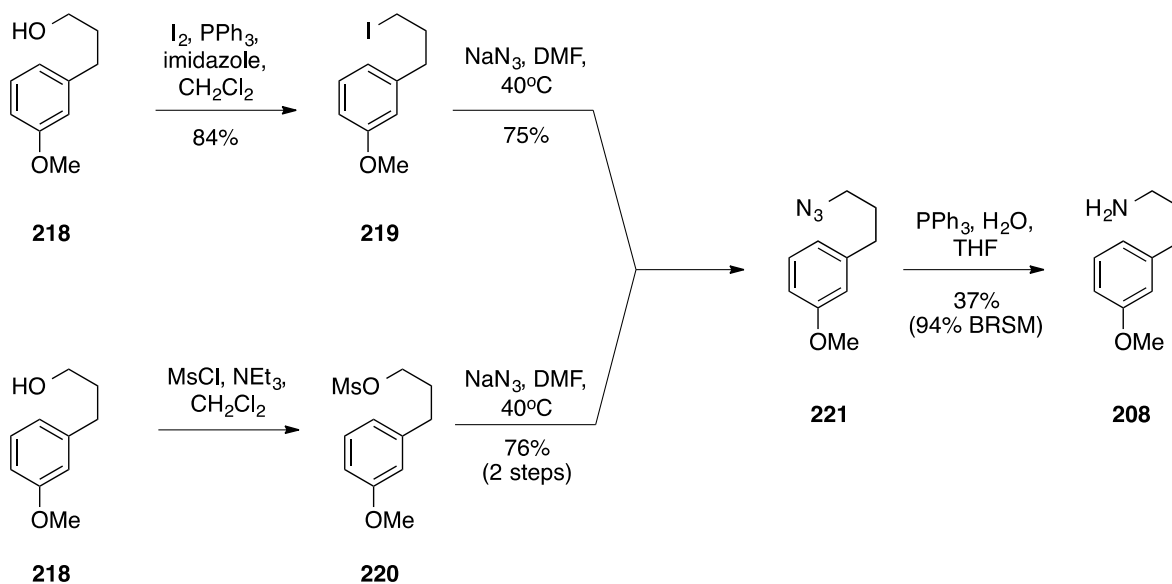
Early investigations by Smith and co-workers demonstrated that the  $\beta$ -hydroxy group of the phenol analogue was not necessary to maintain significant biological activity (Figure 17).<sup>100</sup> Despite the loss of a potential hydrogen bonding partner, analogues explored by the Smith group such as these maintained an  $IC_{50}$  of sub-200 nM in A549 and MCF-7 cells. Therefore, efforts were also made to synthesize a  $\beta$ -dehydroxy complement (**208** and **209**) to  $\beta$ -hydroxyamine fragment **206** described in the previous section.

A convergent strategy was used here to synthesize both acid and amine fragments from alcohol intermediate **218** (Schemes 16 and 17). A Grignard reaction coupling **217** with allyl bromide went smoothly on a multi-gram scale, producing **215** with a 97% yield after flash chromatography.<sup>126</sup> This was followed by a regioselective hydroboration reaction of **215** with 9-BBN and then peroxide that yielded alcohol intermediate **218** in 67%.<sup>126</sup> From here, TEMPO-mediated oxidation provided acid **207** in 97% yield.<sup>127</sup> Overall, the transformation required only three steps and produced the desired acid fragment **207** in 62% yield.



Scheme 16. Synthesis of acid fragment **207**.

From that same alcohol intermediate **218**, two routes were followed to obtain azide **221**, the precursor to the desired amine fragment **208** (Scheme 17). Many options are known for such functional group transformations as alcohol to amine. The simultaneous exploration of both routes was carried out in order to explore two of these options and determine which was most efficient. In the first route, alcohol **218** was reacted with triphenylphosphine and iodine to form iodide **219** in 84% yield. In this reaction, nucleophilic attack of the hydroxyl group on iodotriphenylphosphonium iodide results in the formation of an oxyphosphonium, which can then be displaced through substitution by *in situ* generated iodide anion.<sup>128</sup> Iodide **219** was then subjected to nucleophilic substitution by sodium azide to yield azide **221** in 75% yield. In the second route, the alcohol **218** was first protected through treatment with mesyl chloride to form mesylate **220**. This intermediate was then displaced by sodium azide to form **221** in 76% over two steps.<sup>129</sup> Overall, the second route was the more efficient of the two, and was used in later scale-up reactions. In order to form the desired amine, the azide **221** produced from these two routes was then reduced triphenylphosphine. This final reaction was sluggish and produced the target amine **208** in 37%, with the majority of unreacted starting material easily recovered.



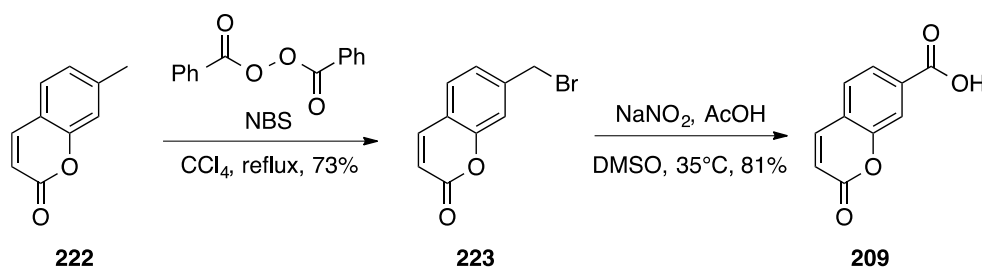
Scheme 17. Two routes towards the synthesis of amine fragment **208**.

### 3.3.4 Synthesis of Coumarin Fragments

The impressive biological activity of 7-substituted coumarin analogues of discodermolide demonstrates that this motif mimics that of the parent despite its simple structure (Figures 17 and 21).<sup>99,102,107</sup> Substitution at the 7-position is crucial (see Figure 21), presumably because it allows for proper alignment of the internal ester within the binding site. Overall, this is the most streamlined fragment of those being synthesized.

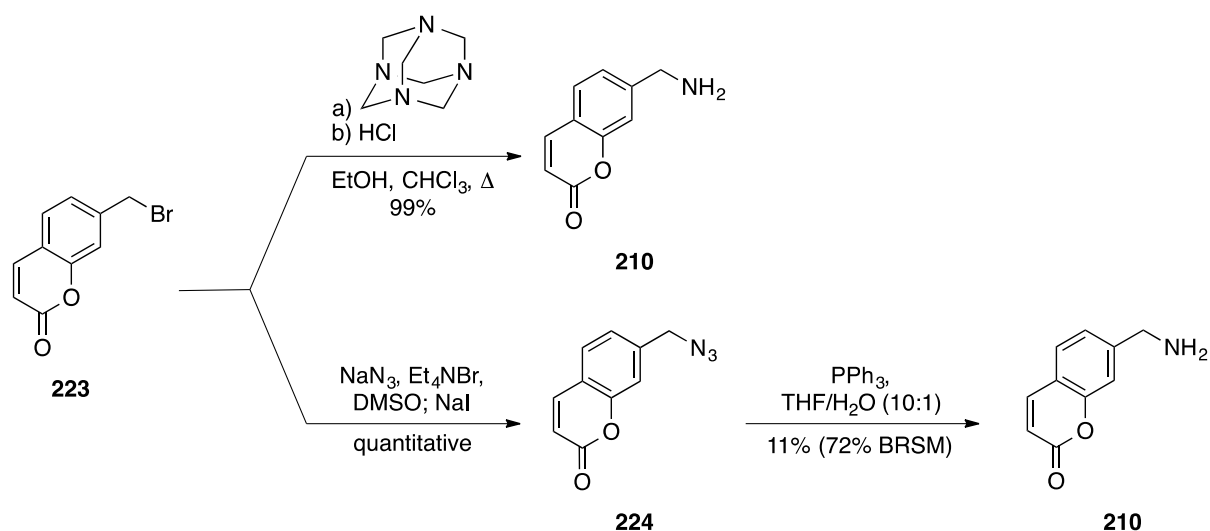
The synthesis of coumarin fragments with both acid (**209**) and amine (**210**) termini was undertaken. The formation of acid **209** was carried out in a straightforward 2-step process. First, bromination of 7-methylcoumarin using NBS and catalytic benzoyl peroxide gave bromide **223** in 73% yield. Although this yield is reported for the purified bromide **223**, the succinimide-contaminated crude product could also be used without further purification in the following step. With the bromide in hand, treatment with sodium nitrite and acetic acid provided the desired acid

fragment **209** in 81% yield. This reaction involves the initial displacement of the bromide by sodium nitrite. Under acidic conditions and in the presence of excess sodium nitrite, the nitroalkane intermediate becomes protonated, enabling the stepwise formation of the corresponding nitrolic acid, nitrile oxide, and then hydroxamic acid, which is finally hydrolyzed to yield the desired carboxylic acid.<sup>130</sup>



Scheme 18. Synthesis of the 7-carboxycoumarin fragment **209**.

From the bromide intermediate above (**223**), amine fragment **210** could also be rapidly synthesized. Initially, the Delépine protocol was used to form the amine through the reaction with hexamethylenetetramine to form the corresponding quaternary ammonium salt and immediate acid hydrolysis to convert the salt into amine **210** (Scheme 19, top).<sup>131,132</sup> On a 200 mg scale, this reaction was carried out in one step in a 99% yield. However, the method suffered from reduced and inconsistent yields during the scale-up process. Therefore, a pathway modified from 17 that relied on an azide intermediate was explored.



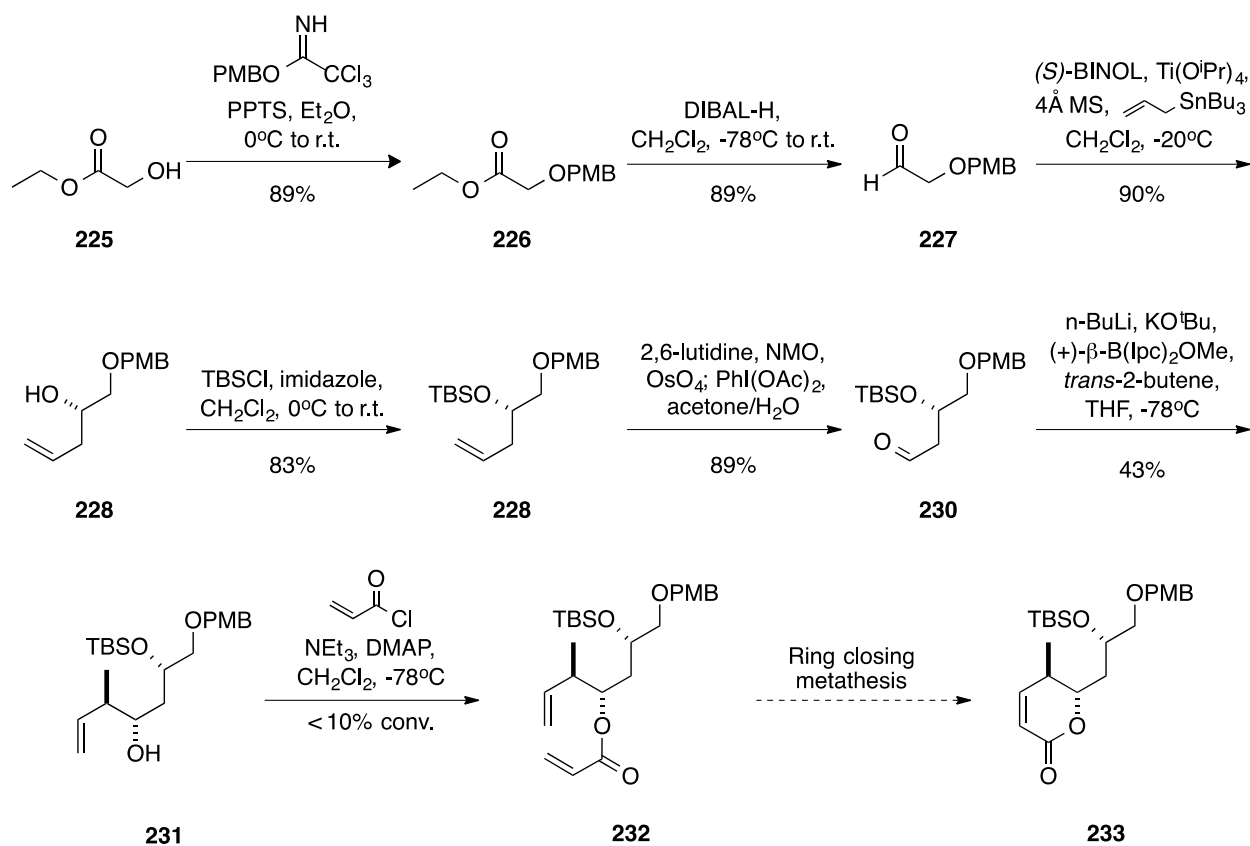
Scheme 19. Synthesis of the 7-aminocoumarin fragment **210**.

Bromide **223** was treated with sodium azide, sodium iodide and the phase transfer catalyst tetraethylammonium bromide to give azide **224** in quantitative yield via nucleophilic displacement of the *in situ*-generated iodide intermediate (Scheme 19, bottom). Staudinger reduction of azide **224** provided the completed amine fragment **210** in 11% yield.<sup>133</sup> This second pathway could be carried out on a multi-gram scale, but suffered from low yields due to poor solubility of the coumarin substrate in the reaction solution. Fortunately, much of the unreacted azide **224** could be easily re-isolated following completion of the Staudinger reaction.

### 3.3.5 Synthesis of 6,2-Normethyl-2,3-anhydro Lactone Fragments

The 2-normethyl-2,3-anhydro motif **195** was selected for its simplified structure and improved activity when substituted into the discodermolide framework (**85**, Figure 16).<sup>96</sup> While the lack of a C3-hydroxyl would prevent a potential H-bonding interaction with Pro272 within the binding

site, the Snyder model suggests that this could be overcome by higher-affinity hydrophobic interactions with tubulin's M-loop.<sup>113</sup> Another advantage is that when discodermolide's lactone region is substituted with this motif it becomes more cytotoxic in multi-drug resistant NCI/ADR cells.<sup>96</sup> The synthesis of this fragment was designed to enable late-stage differentiation for both the truncated olefin and the MCR synthetic routes from lactone **196** (Scheme 20).<sup>77</sup> Following the formation of this advanced intermediate, MCR fragments could be formed through PMB deprotection and subsequent functional group manipulations of the resulting alcohol using routes modified from those shown in Schemes 16 and 17.



Scheme 20. Synthesis of the 2-normethyl-2,3-anhydro fragment.

The synthesis began with a PMB protection of ethyl glycolate, using PPTS as a mild acid to yield **226** in 89%.<sup>77</sup> From here, the ester was reduced using DIBAL-H to furnish aldehyde **227** in 89% yield. This aldehyde was subjected to an allylation according to Keck's conditions to form homoallylic alcohol **228**.<sup>134</sup> The secondary alcohol resulting from this reaction was immediately protected as a silyl ether under standard conditions. Once the alcohol had been protected, focus shifted to extending the backbone of what would become the lactone ring. As an alternative to ozonolysis, the terminal olefin of **229** was subjected to (diacetoxyiodo)benzene-mediated oxidative cleavage to forming **230** in 89% yield.<sup>135</sup> In one pot, this method results in dihydroxylation of the olefin under Upjohn conditions followed by transformation to the aldehyde upon liberation of PhI and two equivalents of AcOH. This route enabled the advanced aldehyde intermediate **230** to be obtained in very high yields on a multi-gram scale (53% over five steps).

Following the protocol used by the Smith group during their SAR studies, Brown crotylation of aldehyde **230** enabled the rapid addition of two new stereocenters and the formation of *anti*-adduct **231** in 43% yield.<sup>77</sup> This crotylation product was isolated initially as an intractable mixture with the isopinocampheol byproduct of the reaction. Attempts at performing the subsequent acylation reaction resulted in <10% conversion of starting material by NMR, likely a result of those impurities. Similar difficulties in the separation of unwanted byproducts during diisopinocampheylborane-mediated allylation and crotylation reactions have been extensively reported, although more intensive purification processes have been met with success for others.<sup>136</sup>

From intermediate **232**, ring-closing metathesis would lead to closure of the lactone ring, and further functional group manipulations of the protected terminal alcohol would yield the

desired functionalized tether. Because of its use in previous SAR studies, this lactone-forming step has a synthetic precedent in the Smith group (75% using Grubbs second generation catalyst under standard metathesis conditions).<sup>77</sup> Therefore, following optimization of the acylation product's purification, this remaining key step would not likely hinder future synthetic efforts.

## 4.0 SUMMARY

The past two decades of research on discodermolide have yielded an incredible amount of knowledge about the compound, but still leave many questions to be answered. With a single digit nM  $IC_{50}$  similar to paclitaxel, an estimated 160-fold greater aqueous solubility than paclitaxel, an identified high affinity binding site, and an effectiveness even in drug resistant cell lines where paclitaxel and epothilone B fail, discodermolide is an extremely viable lead compound for future studies. The SAR profile summarized in Chapter 1 demonstrates that simplifying the structure of discodermolide can lead to a potent analogue with a more streamlined synthesis. MCR strategies will make analogue synthesis more efficient, requiring only one coupling step that simultaneously establishes the linker region, and the ability to interchange components (carbamate and lactone fragments) to efficiently generate diversity. The daunting task of establishing 13 stereogenic centers, four olefins, a completely functionalized lactone, and managing the multiple coupling stages can therefore be eased. Finally, because unwanted toxicity of discodermolide in high doses is thought to stem from drug metabolites, analogue synthesis is a good means to explore the reasons for and mitigate this effect.

The overarching goal of this project is to design a straightforward synthesis for structurally simplified fragments, and to join these via MCR chemistry to form discodermolide analogues with a novel linker region. Significant progress has been made toward s the completion of this goal. Once an MCR route to analogue synthesis had been decided upon,

initial modeling studies helped to understand the three dimensional configuration of these analogues compared to that of the parent. The high degree of overlap between proposed analogues and discodermolide led to the beginning of the synthetic phase of the project.

The synthesis of five separate fragments to mimic the lactone region of discodermolide have been described. These syntheses require on average only 3 steps to obtain, and have been carried out on a multi-gram scale. This efficiency is of particular importance for making a drug synthetically feasible on an industrial scale. The 2-normethyl-2,3-anhydro fragment is in its advanced stages of construction, and needs only a precedented metathesis reaction to be completed before functional group manipulations to differentiate between acid and amine will complete the sequence. In addition, a common precursor lactone to precede the synthesis of carbamate fragment analogues has also been achieved. Although this project was halted prematurely, the MCR approach is still one that is promising for future SAR investigations of discodermolide.

## 5.0 EXPERIMENTAL

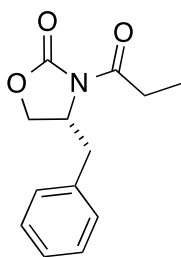
### Modeling Experimental

Model analogues, like those shown in Figure 33, were constructed using ChemDraw Ultra 12.0, converted to .mol format using Chem3D Pro 12.0. From there, PyMOL was used for 3D rendering of analogues, overlay with discodermolide was carried out using the lactone ring and the carbamate stereotriad carbons with the pair fitting wizard.

### Synthesis Experimental

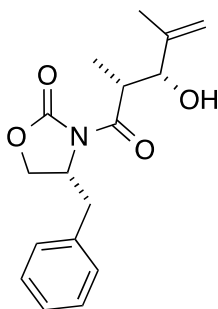
All reactions were performed under an inert atmosphere of N<sub>2</sub> gas in oven-dried glassware using anhydrous solvents, unless otherwise noted. Methylene chloride (CH<sub>2</sub>Cl<sub>2</sub>) was distilled from calcium hydride. Tetrahydrofuran (THF) was obtained from sodium/benzophenone distillation. All other anhydrous solvents were purchased from Sigma-Aldrich. All reactions were monitored by thin-layer chromatography (TLC) carried out on 0.25 mm EMD silica gel plates (60F-254) using heat or UV light (254 nm) for visualization and *p*-anisaldehyde in ethanol, or 0.2% ninhydrin in ethanol as developing agents. TSI silica gel (230–400 mesh) was used for flash chromatography. <sup>1</sup>H- and <sup>13</sup>C- NMR spectra were recorded on a Bruker Avance II Ultrashield Plus 600 equipped with a cryoprobe at 600 and 150 MHz, respectively. Chemical shift values are in ppm relative to residual solvent signal. The following abbreviations are used to indicate the multiplicities: s = singlet, d = doublet, t = triplet, q = quartet, m = multiplet, br = broad. FT-

IR spectra were recorded on a Bruker Alpha FT-IR spectrometer. Low-resolution mass spectra were obtained on an Applied Biosciences API 2000 ESI- triple quadrupole mass spectrometer with a Shimadzu UFLC inlet system. Additional mass spectra were recorded on a Waters Super Critical Fluid Chromatograph with a 3100 MS Detector using a solvent system of methanol and CO<sub>2</sub> on a Regis Cell OD column.

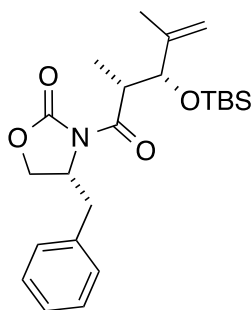


**Preparation of 202.** Chiral auxiliary **201** (1.00 g, 5.64 mmol) was dissolved in THF (22.6 mL) and the solution was cooled to 0 °C. Then, n-BuLi (3.9 mL, 1.6 M in hexanes) was slowly added, followed by propionyl chloride (0.59 mL, 6.7 mmol). The reaction solution was allowed to warm slowly to r.t. and stirred at that temperature for 19 h. The reaction was quenched through the addition of sat. aq. NH<sub>4</sub>Cl (23 mL). The layers were separated, and the aqueous layer was extracted with Et<sub>2</sub>O (2 x 23 mL). The combined organic layers were washed with 1 M HCl (2 x 23 mL), 1 M NaOH (2 x 23 mL), and brine (23 mL). The organic layer was dried over MgSO<sub>4</sub>, filtered, and concentrated *in vacuo*. The residue was purified by chromatography on SiO<sub>2</sub> (0–100% EtOAc in hexanes) to afford **202** (0.78 g, 59%) as a faintly yellow solid. R<sub>f</sub> = 0.24 (10% EtOAc in hexanes); <sup>1</sup>H NMR (600 MHz, CDCl<sub>3</sub>) δ 7.35 (t, *J* = 7.2, 2H), 7.29 (t, *J* = 7.2 Hz, 1H), 7.22 (d, *J* = 7.2 Hz, 2H), 4.70 (m, 1H), 4.22 (dd, *J* = 9.0, 16.8 Hz, 1H), 4.18 (dd, *J* = 3.0, 9.0 Hz, 1H), 3.32 (dd, *J* = 3.0, 13.2, 1H), 3.03 (m, 2H), 2.79 (dd, *J* = 9.6, 13.8 Hz, 1H), 1.22

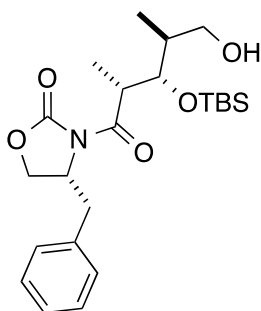
(t,  $J = 7.2$  Hz, 3H);  $^{13}\text{C}$  NMR (150 MHz,  $\text{CDCl}_3$ )  $\delta$  174.24, 153.67, 135.47, 129.57, 129.11, 127.50, 66.36, 55.33, 38.08, 29.35, 8.44.



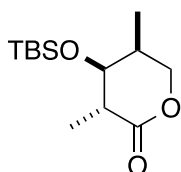
**Preparation of 203.** The acylated chiral auxiliary **202** (0.962 g, 4.12 mmol) was dissolved in  $\text{CH}_2\text{Cl}_2$  (9 mL) and cooled to 0 °C before *n*-dibutylboron triflate (4.9 mL, 1 M in  $\text{CH}_2\text{Cl}_2$ ) and DIPEA (0.93 mL, 5.3 mmol) were slowly added. The solution was then cooled to -78 °C and methacrolein (0.77 mL, 9.3 mmol) was slowly added. After stirring for 20 min, the solution was warmed to 0 °C and stirred an additional 1.5 h. Workup proceeded with the addition of pH 7 buffer (5 mL), MeOH (9 mL), and  $\text{H}_2\text{O}_2$  (30% in  $\text{H}_2\text{O}$ , 5 mL) in MeOH (14 mL). The solution was stirred at 0 °C for 1 h, and then partially concentrated *in vacuo*. The resulting slurry was extracted with  $\text{Et}_2\text{O}$  (3 x 10 mL), the organic layer was washed with brine and dried over  $\text{MgSO}_4$  and concentrated *in vacuo*. The crude product was purified by chromatography on  $\text{SiO}_2$  (0–100% EtOAc in hexanes) to afford **203** (0.901 g, 69%) as a single diastereomer, as a white solid.  $^1\text{H}$  NMR (600 MHz,  $\text{CDCl}_3$ )  $\delta$  7.35 (t,  $J = 7.2$ , 2H), 7.30 (t,  $J = 7.2$  Hz, 1H), 7.22 (d,  $J = 7.2$  Hz, 2H), 5.13 (s, 1H), 4.99 (s, 1H), 4.73 (m, 1H), 4.43 (s, 1H), 4.26 (dd,  $J = 9.0$ , 16.8 Hz, 1H), 4.21 (dd,  $J = 3.0$ , 9.0 Hz, 1H), 3.99 (qd,  $J = 3.0$ , 7.2 Hz, 1H), 3.29 (dd,  $J = 3.6$ , 13.8 Hz, 1H), 2.93 (d,  $J = 3.0$  Hz, 1H), 2.82 (dd,  $J = 9.6$ , 13.2 Hz, 1H), 1.74 (s, 3H), 1.20 (d,  $J = 7.2$  Hz, 3H).



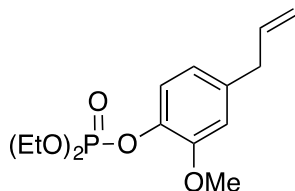
**Preparation of 204.** To the stirring solution of auxiliary **203** (0.754 g, 2.48 mmol) in  $\text{CH}_2\text{Cl}_2$  (4 mL) at 0 °C was slowly added 2,6-lutidine (0.40 mL, 3.5 mmol) and then TBSOTf (0.63 mL, 2.7 mmol) dropwise. After 2 h of stirring, an additional portion of 2,6-lutidine was added (0.40 mL), and stirring continued at 0 °C for an additional 1 h. The reaction was quenched through the addition of 1 M HCl (4.5 mL) and hexane (9 mL). The aqueous layer was extracted with hexanes (3 x 10 mL) and the combined organic layers were washed with 1 M HCl (10 mL) and  $\text{NaHCO}_3$ . The organic layer was dried with  $\text{MgSO}_4$ , filtered, and concentrated *in vacuo*. The crude white residue of **204** (0.924 g, 89%) was submitted for NMR analysis and used in the following step without further purification. The NMR shows only slight contamination with compound **203** and *tert*-butyl dimethylsilanol.  $^1\text{H}$  NMR (600 MHz,  $\text{CDCl}_3$ )  $\delta$  7.34 (t,  $J = 7.2$ , 2H), 7.28 (t,  $J = 6.6$  Hz, 1H), 7.22 (d,  $J = 7.2$  Hz, 2H), 4.94 (s, 1H), 4.84 (s, 1H), 4.59 (m, 1H), 4.36 (d,  $J = 6.6$  Hz, 1H), 4.17 (dd,  $J = 2.4, 9.0$  Hz, 1H), 4.15 (dd,  $J = 9.0, 16.8$  Hz, 1H), 4.05 (pentet,  $J = 6.6$  Hz, 1H), 3.29 (dd,  $J = 3.0, 13.2$ , 1H), 2.79 (dd,  $J = 10.2, 13.2$  Hz, 1H), 1.72 (s, 3H), 1.22 (d,  $J = 7.2$  Hz, 3H), 0.91 (s, 9H), 0.02 (s, 3H), -0.01 (s, 3H).



**Preparation of 205.** To a stirring solution of alkene **204** (0.478 g, 1.14 mmol) in THF (3.0 mL) at 0 °C was added 9-borabicyclo[3.3.1]nonane (4.6 mL, 0.5 M in THF) dropwise. The solution was stirred at that temperature for 15 minutes and was then allowed to slowly warm to r.t. over 5.5 h. The solution was then cooled to 0 °C and then the following were sequentially added: a pre-mixed solution of EtOH (3.0 mL) and THF (3.0 mL), pH 7 phosphate buffer (3.0 mL), and H<sub>2</sub>O<sub>2</sub> (30% in H<sub>2</sub>O, 3.0 mL). The resulting mixture was stirred vigorously at 0 °C and stirring continued overnight at r.t. Workup of the reaction was carried out through the addition of hexanes (10 mL) and Na<sub>2</sub>S<sub>2</sub>O<sub>3</sub> (10 mL). The aqueous layer was extracted with hexanes (2 x 10 mL), the combined organic layers were washed with brine (10 mL), dried over MgSO<sub>4</sub>, filtered and concentrated *in vacuo*. The crude residue of **205** (0.595 g) was submitted for NMR analysis to confirm the disappearance of olefin peaks (singlets at 4.94 and 4.84 ppm) and was used in the following step without further purification.

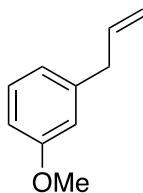


**Preparation of 196.** Potassium *tert*-butoxide (6 mg, 0.05 mmol) was added to a solution of **205** (0.595 g, 1.37 mmol) in THF (14 mL) and the resulting solution was stirred for 1.5 h. The reaction was then diluted with hexanes (35 mL) and quenched with brine (30 mL). The organic layer was then dried over MgSO<sub>4</sub>, filtered, and concentrated *in vacuo*. The crude product was purified by chromatography on SiO<sub>2</sub> (0–100% EtOAc in hexanes) to afford **196** (0.237 g, 67%) as a white solid. <sup>1</sup>H NMR (600 MHz, CDCl<sub>3</sub>) δ 4.27 (t, *J* = 10.2 Hz, 1H), 4.14 (dd, *J* = 4.8, 10.8 Hz, 1H), 3.68 (m, 1H), 2.64 (m, 1H), 2.20 (m, 1H), 1.30 (d, *J* = 7.2 Hz, 3H), 0.96 (d, *J* = 7.2 Hz, 3H), 0.89 (s, 9H), 0.08 (s, 3H), 0.06 (s, 3H); <sup>13</sup>C NMR (150 MHz, CDCl<sub>3</sub>) δ 173.95, 73.64, 70.24, 43.77, 30.43, 25.83, 18.11, 16.41, 12.18, –4.44, –4.63; *m/z* (ESI) [M + H]<sup>+</sup> 259.1.



**Preparation of 214.** To a stirring solution of eugenol (3.10 mL, 20.0 mmol) in CCl<sub>4</sub> (67 mL) at 0 °C was added diethyl phosphite (2.70 mL, 20.98 mmol). Triethylamine was then added dropwise, the solution was allowed to warm to room temperature by removal of the ice bath. After 20 h, an additional portion of diethyl phosphite (0.39 mL, 3.0 mmol) was added. Stirring was continued for an additional 24 h, after which the solution was diluted with CH<sub>2</sub>Cl<sub>2</sub> (40 mL), washed with H<sub>2</sub>O (100 mL), then 10% HCl (100 mL), brine (100 mL), dried over Na<sub>2</sub>SO<sub>4</sub>, filtered, and concentrated *in vacuo*. The residue was purified by chromatography on SiO<sub>2</sub> (0–

100% EtOAc in hexanes) to afford **214** (5.087 g, 85%) as a colorless oil.  $R_f = 0.44$  (25% EtOAc in hexanes);  $^1\text{H}$  NMR (600 MHz,  $\text{CDCl}_3$ )  $\delta$  7.19 (dd,  $J = 7.2, 1.2$  Hz, 1H), 6.76 (s, 1H), 6.72 (dd,  $J = 8.4, 1.8$  Hz, 1H), 5.97 (ddt,  $J = 17.4, 10.2, 6.6$  Hz, 1H), 5.10 (dd,  $J = 17.4, 1.8$  Hz, 1H), 5.08 (dd,  $J = 10.2, 1.8$ ), 4.26 (dq,  $J = 7.2$  Hz, 4H), 3.85 (s, 3H), 3.35 (d,  $J = 6.6$  Hz, 2H), 1.36 (t,  $J = 7.2, 6\text{H}$ );  $^{13}\text{C}$  NMR (150 MHz,  $\text{CDCl}_3$ )  $\delta$  150.56, 138.29, 137.85, 137.21, 121.21, 120.77, 116.17, 113.10, 64.56, 56.01, 40.06, 16.21.

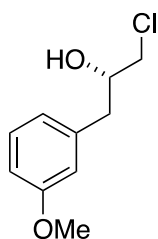


### Preparation of **215**.

**Method A:** Gaseous ammonia (~20 mL after condensation) was passed through a  $\text{K}_2\text{CO}_3$  drying tube and condensed into a dried 3-necked flask outfitted with an additional  $\text{K}_2\text{CO}_3$  drying tube. To this solution was added **214**, and then pieces of sodium (0.427 g, 18.6 mmol), rinsed with dried hexanes, were added over 5 minutes. A color change was observed, and EtOH was added to quench the reaction after 5 minutes. A stream of  $\text{N}_2$  was used to remove ammonia at 0 °C, and crude orange oil was diluted in  $\text{Et}_2\text{O}$  (30 mL). This solution was washed with  $\text{H}_2\text{O}$  (30 mL), the aqueous layer was extracted with  $\text{Et}_2\text{O}$  (3 x 20 mL), and the combined organic layers were washed with brine (20 mL). The resulting organic solution was dried over  $\text{Na}_2\text{SO}_4$ , filtered, and concentrated *in vacuo*. The residue was purified by chromatography on  $\text{SiO}_2$  (0–100%

EtOAc in hexanes) to afford **215** (0.566 g, 43%) as a faintly yellow oil.  $R_f = 0.80$  (75% EtOAc in hexanes).

**Method B:** To a stirring solution of 3-methoxyphenylmagnesium bromide (30.0 mL, 1M in THF) in THF (30 mL) at 0 °C was added slowly, in portions, allyl bromide. The resulting solution was stirred at 25 °C for 24 h before being partitioned between Et<sub>2</sub>O (20 mL) and sat. aq. NH<sub>4</sub>Cl (20 mL). The layers were separated and the aqueous layer was extracted with Et<sub>2</sub>O (2 x 20 mL). The combined organic layers were washed with brine (20 mL), dried over MgSO<sub>4</sub>, filtered and concentrated *in vacuo*. The residue was purified by chromatography on SiO<sub>2</sub> (0–100% EtOAc in hexanes) to afford **215** (4.29 g, 97%) as a faintly yellow oil.  $R_f = 0.53$  (10% EtOAc in hexanes); <sup>1</sup>H NMR (600 MHz, CDCl<sub>3</sub>) δ 6.86 (d,  $J = 8.4$  Hz, 1H), 6.70 (m, 2H), 5.99 (ddt,  $J = 7.2, 10.2, 17.4$  Hz, 1H), 5.48 (s, 1H), 5.09 (dd,  $J = 1.8, 17.4$  Hz, 1H), 5.06 (dd,  $J = 1.8, 10.2$  Hz, 1H), 3.88 (s, 3H), 3.33 (d,  $J = 6.6$  Hz, 2H); <sup>13</sup>C NMR (150 MHz, CDCl<sub>3</sub>) δ 146.56, 144.03, 137.96, 132.06, 121.31, 115.67, 114.36, 111.21, 55.99, 40.04.

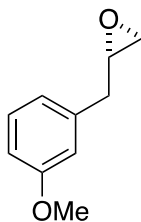


### Preparation of 219.

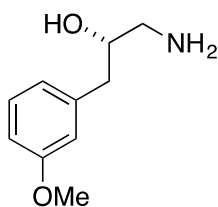
**Method A:** Magnesium turnings (0.130 g, 5.35 mmol) were stirred in a solution of THF (13 mL) in a dried flask filled with N<sub>2</sub> for 10 minutes. Then, 3-bromoanisole (1.00 g, 5.35 mmol) was added in small portions via syringe, followed by I<sub>2</sub> (0.046 g, 0.182 mmol). The

solution was brought to reflux (~70 °C), and stirred for 16 h. At this point, the oil bath was removed, and the solution was allowed to cool to r.t. before an ice bath was applied. Once the reaction solution was 0 °C, the reflux condenser was removed. A solution of (*S*)-(+)-epichlorohydrin (0.33 mL, 4.3 mmol) in THF (8.5 mL) was added dropwise to the stirring mixture. The ice bath was removed, and stirring continued for an additional 2 h. The reaction was quenched with 1M HCl (5 mL) and extracted with Et<sub>2</sub>O (3 x 8 mL), and then the combined organic layers were dried over Na<sub>2</sub>SO<sub>4</sub>, filtered, and concentrated *in vacuo*. The crude material (1.32 g) was isolated as a yellow oil, and used immediately in the subsequent reaction.

**Method B:** A solution of 3-methoxyphenylmagnesium bromide (24.0 mL, 1M in THF) was added dropwise to a stirred mixture of (*S*)-(+)-epichlorohydrin (1.56 mL, 20.0 mmol) and CuCN (0.179 g, 2.00 mmol) in THF (22 mL) that had been pre-cooled to -78 °C. The resulting solution was allowed to warm to -20 °C over a period of 3 h. The reaction mixture was poured into a solution of sat. aq. NH<sub>4</sub>Cl (25 mL) and Et<sub>2</sub>O (25 mL) and stirred vigorously. The layers were separated, and the aqueous layer was extracted with additional Et<sub>2</sub>O (3 x 50 mL). The combined organic layers were washed with brine (50 mL), then dried over MgSO<sub>4</sub>, filtered, and concentrated *in vacuo*. The faintly yellow residue was purified by chromatography on SiO<sub>2</sub> (0–100% EtOAc in hexanes) to afford **219** (3.967 g, 99%) as a colorless oil. *R*<sub>f</sub> = 0.27 (20% EtOAc in hexanes); <sup>1</sup>H NMR (600 MHz, CDCl<sub>3</sub>) δ; 7.28 (t, *J* = 7.8 Hz, 1H), 6.85 (m, 3H), 4.10 (m, 1H), 3.83 (s, 3H), 3.66 (dd, *J* = 4.2, 11.4 Hz, 1H), 3.52 (dd, *J* = 6.0, 11.4 Hz, 1H), 2.88 (d, *J* = 6.6 Hz, 2H), 2.21 (d, *J* = 6.6 Hz), 2.31 (br s, 1H); <sup>13</sup>C NMR (150 MHz, CDCl<sub>3</sub>) δ 159.86, 138.63, 129.83, 121.73, 115.16, 112.19, 72.24, 55.29, 49.28, 40.69; *m/z* (APCI) [M - Cl]<sup>+</sup> 165.

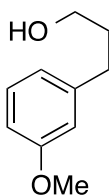


**Preparation of 220.** Crushed NaOH pellets (0.548 g, 13.7 mmol) were added to a flask containing **219** (0.500 g, 2.492 mmol) in Et<sub>2</sub>O (2.8 mL). This sample was stirred for 20 h at 25 °C, whereupon H<sub>2</sub>O (3 mL) was added. The aqueous layer was extracted with Et<sub>2</sub>O (3 x 4 mL), then the combined organic layers were dried over MgSO<sub>4</sub>, filtered, and concentrated *in vacuo*. The residue was purified by chromatography on SiO<sub>2</sub> (5–100% EtOAc in hexanes) to afford **220** (0.304 g, 74%) as a colorless oil.  $R_f = 0.60$  (20% EtOAc in hexanes); <sup>1</sup>H NMR (600 MHz, CDCl<sub>3</sub>) δ 7.25 (t,  $J = 7.8$  Hz, 1H), 6.85 (d,  $J = 7.2$  Hz, 1H), 6.81 (m, 2H), 3.81 (s, 3H), 3.17 (m, 1H), 2.92 (dd,  $J = 15.0, 5.4$  Hz, 1H), 2.81 (t,  $J = 4.2$  Hz, 1H), 2.81 (dd,  $J = 15, 5.4$  Hz, 1H), 2.57 (dd,  $J = 4.8, 3.0$ ); <sup>13</sup>C NMR (150 MHz, CDCl<sub>3</sub>) δ 159.85, 138.90, 129.66, 121.47, 114.89, 112.11, 55.33, 52.54, 47.07, 38.98;  $m/z$  (APCI) [M + 1]<sup>+</sup> 165.



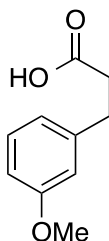
**Preparation of 206.** Epoxide **220** (0.104 g, 0.633 mmol) and a solution of NH<sub>4</sub>OH (25% in H<sub>2</sub>O, 4.2 mL) were stirred in EtOH (4 mL) at 25 °C for 22 h. The solution was then heated to 70 °C, and stirred for an additional 23 h, at which point the solution was concentrated to ~1 mL. The

solution was extracted with  $\text{CH}_2\text{Cl}_2$  (3 x 2 mL), and the combined organic layers were dried over  $\text{Na}_2\text{SO}_4$ , filtered, and concentrated *in vacuo* to afford **206** (0.101 g, 88%).  $^1\text{H}$  NMR (600 MHz,  $\text{CDCl}_3$ )  $\delta$  7.24 (m, 1H), 6.82 (d,  $J = 7.8$  Hz, 1H), 6.78 (m, 2H), 3.80 (s, 3H), 3.78 (m, 1H), 2.87 (br s, 1H), 2.74 (dd,  $J = 7.2, 1.8$  Hz), 2.61 (br s, 1H), 1.27 (t,  $J = 7.2$  Hz, 1H).

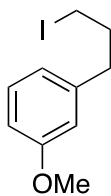


**Preparation of 218.** To a stirring solution of alkene **215** (4.01 g, 27.0 mmol) in THF (108 mL) at  $0^\circ\text{C}$  was added dropwise 9-borabicyclo[3.3.1]nonane (85.0 mL, 42.5 mmol). The resulting solution was stirred at r.t. for 4 h. The solution was cooled to  $0^\circ\text{C}$ , then the following were sequentially added: a solution of EtOH and THF (35 mL each), pH 7 phosphate buffer (70 mL), and  $\text{H}_2\text{O}_2$  (30% in  $\text{H}_2\text{O}$ , 70 mL). This mixture was stirred at  $0^\circ\text{C}$  for 30 min and at r.t. for 10 h. To quench the reaction, diethyl ether (75 mL) and 20%  $\text{Na}_2\text{S}_2\text{O}_3$  (110 mL) were added. The aqueous layer was extracted with  $\text{CH}_2\text{Cl}_2$  (2 x 50 mL), then the combined organic layers were washed with brine, dried over  $\text{Na}_2\text{SO}_4$ , filtered, and concentrated *in vacuo*. The residue was purified by chromatography on  $\text{SiO}_2$  (0–100% EtOAc in hexanes) to afford **218** (3.01 g, 67%) as a colorless oil.  $R_f = 0.35$  (50 % EtOAc in hexanes);  $^1\text{H}$  NMR (600 MHz,  $\text{CDCl}_3$ )  $\delta$  7.22 (t,  $J = 7.8$  Hz, 1H), 6.81 (d,  $J = 7.2$  Hz, 1H), 6.75 (m, 2H), 3.80 (s, 3H), 3.69 (t,  $J = 6.0$  Hz, 1H), 2.70 (t,  $J = 7.8$  Hz, 1H), 1.92 (tt,  $J = 6.6, 7.8$  Hz, 1H), 1.66 (br s, 1H);  $^{13}\text{C}$  NMR (150 MHz,  $\text{CDCl}_3$ )  $\delta$

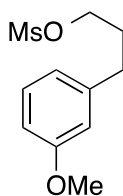
159.70, 143.59, 129.48, 120.94, 114.28, 111.17, 62.34, 55.24, 34.20, 32.23;  $m/z$  (ESI)  $[M + 1]^+$  167.1,  $[M - H_2O]^+$  149.2.



**Preparation of 207.** TEMPO (0.036 g, 0.23 mmol) and  $\text{PhI}(\text{OAc})_2$  (0.806 g, 2.50 mmol) were added to a stirring solution of **218** (0.189 g, 1.14 mmol) in MeCN (6 mL) and  $\text{H}_2\text{O}$  (6 mL), and the reaction solution was stirred at 25 °C for 24 h. The reaction was then quenched by the addition of  $\text{Na}_2\text{S}_2\text{O}_3$  (10% in  $\text{H}_2\text{O}$ , 10 mL). The aq layer was extracted with EtOAc (3 x 10 mL). The combined organic layers were washed with brine, dried over  $\text{Na}_2\text{SO}_4$ , filtered and concentrated *in vacuo*. The residue was purified by chromatography on  $\text{SiO}_2$  (0–100% EtOAc in hexanes) to afford **207** (0.196 g, 96%) as a yellow oil.  $R_f = 0.58$  (50% EtOAc in hexanes);  $^1\text{H}$  NMR (600 MHz,  $\text{CDCl}_3$ )  $\delta$  7.25 (t,  $J = 7.8$  Hz, 1H);  $^{13}\text{C}$  NMR (150 MHz,  $\text{CDCl}_3$ )  $\delta$  201.75, 159.94, 142.09, 129.76, 120.75, 114.30, 111.66, 55.31, 45.34, 28.30; IR (neat) 3253 (broad), 2937, 1720, 1600, 1583, 1257, 1151, 1036, 778, 694  $\text{cm}^{-1}$ ;  $m/z$  (ESI)  $[M + 1]^+$  181.2,  $[M + \text{Na}]^+$  203.9.

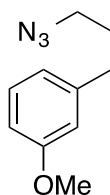


**Preparation of 219.** Triphenylphosphine (0.710 g, 2.71 mmol) and I<sub>2</sub> (0.687 g, 2.71 mmol) were dissolved in CH<sub>2</sub>Cl<sub>2</sub> at 0 °C and stirred for 10 min. Imidazole (0.307 g, 4.51 mmol) was then added, and the solution was stirred for another 10 min. Then alcohol **218** in 1 mL CH<sub>2</sub>Cl<sub>2</sub> was added dropwise. The ice bath was removed and stirring continued at r.t. for 3 h. At that time, sat. aq. Na<sub>2</sub>S<sub>2</sub>O<sub>3</sub> (20 mL) was added. The aqueous layer was extracted with CH<sub>2</sub>Cl<sub>2</sub> (3 x 10 mL); the combined organic layers were washed with brine (20 mL), dried over Na<sub>2</sub>SO<sub>4</sub>, filtered and concentrated *in vacuo*. The residue was purified by chromatography on SiO<sub>2</sub> (0–100% EtOAc in hexanes) to afford **219** (0.427 g, 86%) as an orange oil. R<sub>f</sub> = 0.73 (50% EtOAc in hexanes); <sup>1</sup>H NMR (600 MHz, CDCl<sub>3</sub>) δ 7.23 (t, *J* = 7.8 Hz, 1H), 6.80 (m, 3H), 3.81 (s, 3H), 3.18 (t, *J* = 7.2 Hz, 2H), 2.72 (t, *J* = 7.2 Hz, 2H), 2.15 (pentet, *J* = 7.2 Hz, 2H); <sup>13</sup>C NMR (150 MHz, CDCl<sub>3</sub>) δ 159.69, 142.05, 129.51, 120.97, 114.35, 111.41, 55.20, 36.24, 34.77, 6.58.



**Preparation of 220.** Methanesulfonyl chloride (0.21 mL, 2.7 mmol) and NEt<sub>3</sub> (0.50 mL, 3.6 mmol) were sequentially added to a stirring solution of **218** (0.300 g, 1.81 mmol) in CH<sub>2</sub>Cl<sub>2</sub> (18

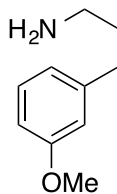
mL). The reaction was stirred at r.t. for 3 h before it was quenched by the addition of sat. aq. NaHCO<sub>3</sub> (20 mL). The aqueous layer of the resulting solution was extracted with CH<sub>2</sub>Cl<sub>2</sub> (3 x 20 mL), the organic layer was washed with brine (20 mL), dried over Na<sub>2</sub>SO<sub>4</sub>, filtered, and concentrated. The crude orange oil (**220**) was used in the next reaction without any further purification. R<sub>f</sub> = 0.44 (50% EtOAc in hexanes); <sup>1</sup>H NMR (600 MHz, CDCl<sub>3</sub>) δ 7.23 (t, *J* = 7.2 Hz, 1H), 6.79 (m, 3H), 4.24 (t, 6.0 Hz, 2H), 3.80 (s, 3H), 3.00 (s, 3H), 2.74 (t, *J* = 7.2 Hz, 2H), 2.10 (pentet, *J* = 6.6 Hz, 2H); <sup>13</sup>C NMR (150 MHz, CDCl<sub>3</sub>) δ 159.92, 142.02, 129.72, 120.93, 114.41, 111.68, 69.24, 55.31, 37.49, 31.69, 30.66; *m/z* (ESI) [M + Na]<sup>+</sup> 267.1.



### Preparation of **221**

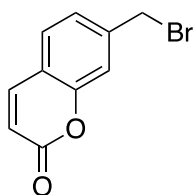
**Method A:** To a solution of iodide **219** (0.420 g, 1.52 mmol) in DMF (1.5 mL) was added NaN<sub>3</sub> (0.198 g, 3.04 mmol). This mixture was then stirred at 25 °C for 1 h and then at 40 °C for an additional 20 h. The reaction was then quenched by the addition of sat. aq. NaHCO<sub>3</sub> (20 mL) and sat. aq. Na<sub>2</sub>S<sub>2</sub>O<sub>3</sub> (20 mL). The aqueous layer was extracted with CH<sub>2</sub>Cl<sub>2</sub> (5 x 15 mL), the combined organic layers were washed with H<sub>2</sub>O (3 x 10 mL) and brine (10 mL), then dried over Na<sub>2</sub>SO<sub>4</sub>, filtered and concentrated *in vacuo*. The residue was purified by chromatography on SiO<sub>2</sub> (0–100% EtOAc in hexanes) to afford **221** (0.291 g, 75%) as a colorless oil.

**Method B:** To a solution of mesylate **220** (0.441 g, 1.81 mmol) in DMF (1.8 mL) was added NaN<sub>3</sub> (0.469 g, 7.22 mmol). This mixture was then stirred at 25 °C for 1 h and then at 40 °C for an additional 24 h. The reaction was then quenched by the addition of sat. aq. NaHCO<sub>3</sub> (20 mL) and sat. aq. Na<sub>2</sub>S<sub>2</sub>O<sub>3</sub> (20 mL). The aqueous layer was extracted with CH<sub>2</sub>Cl<sub>2</sub> (5 x 15 mL), the combined organic layers were washed with H<sub>2</sub>O (3 x 10 mL) and brine (10 mL), then dried over Na<sub>2</sub>SO<sub>4</sub>, filtered and concentrated *in vacuo*. The residue was purified by chromatography on SiO<sub>2</sub> (0–100% EtOAc in hexanes) to afford **221** (0.345 g, 76%) as a colorless oil. R<sub>f</sub> = 0.67 (50% EtOAc in hexanes); <sup>1</sup>H NMR (600 MHz, CDCl<sub>3</sub>) δ 7.23 (t, *J* = 7.8 Hz, 1H), 6.79 (m, 2H), 3.81 (s, 3H), 3.30 (t, *J* = 6.6 Hz, 2H), 2.70 (t, *J* = 7.2 Hz, 2H), 1.94 (pentet, *J* = 7.2 Hz).

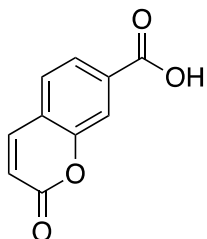


**Preparation of 208.** H<sub>2</sub>O (0.16 mL) and then triphenylphosphine (1.17 g, 4.45 mmol) were added to a solution of azide **221** (.340 g, 1.78 mmol) in THF (18 mL) at 25 °C. The mixture was heated to 40 °C, then stirred 20 h. An additional 1.6 mL of H<sub>2</sub>O was added, and the mixture was stirred for another 24 h. After concentrating the solution, it was dissolved in CH<sub>2</sub>Cl<sub>2</sub> (10 mL) and washed with 1 M HCl (3 x 10 mL), allowing for unreacted starting material to be collected (0.105 g). The aqueous layer was extracted with EtOAc (3 x 10 mL), and then 3 M NaOH was added to the aqueous layer until the pH reached 10. The aqueous layer was then extracted with

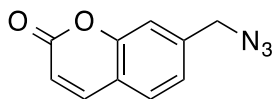
CH<sub>2</sub>Cl<sub>2</sub> (3 x 10 mL). The combined organic layers were dried over Na<sub>2</sub>SO<sub>4</sub>, filtered and concentrated *in vacuo*. The residue was purified by chromatography on SiO<sub>2</sub> (0–100% EtOAc in hexanes) to afford **208** (0.11 g, 37%, 94% BRSM) as a faintly yellow oil. R<sub>f</sub> = 0.18 (50% EtOAc in hexanes); <sup>1</sup>H NMR (600 MHz, CDCl<sub>3</sub>) δ 7.20 (t, *J* = 7.2 Hz, 1H), 6.78 (m, 2H), 3.79 (s, 3H), 2.74 (br t, *J* = 6.0 Hz, 2H), 2.64 (t, *J* = 7.2 Hz, 2H), 1.96 (br s, 2H), 1.81 (pentet, *J* = 7.2 Hz, 2H); <sup>13</sup>C NMR (150 MHz, CDCl<sub>3</sub>) δ 159.76, 143.83, 129.44, 120.93, 114.29, 111.16, 55.26, 41.79, 35.19, 33.41; *m/z* (ESI) [M + 1]<sup>+</sup> 166.2, [M – NH<sub>3</sub>]<sup>+</sup> 149.1, [M – CH<sub>2</sub>NH<sub>3</sub>]<sup>+</sup> 136.1.



**Preparation of 223.** To a solution of 7-methylcoumarin (4.00 g, 25.0 mmol) in CCl<sub>4</sub> (125 mL), *N*-bromosuccinimide (4.57 g, 25.7 mmol) and benzoyl peroxide (0.363 g, 1.50 mmol) were sequentially added. The reaction solution was heated to reflux, and stirred 24 h. When the reaction had finished, the solution was concentrated *in vacuo*, and purified by chromatography on SiO<sub>2</sub> (10–100% EtOAc in hexanes) to afford **223** (4.33 g, 73%) as a pale yellow solid. R<sub>f</sub> = 0.19 (25% EtOAc in hexanes); <sup>1</sup>H NMR (600 MHz, CDCl<sub>3</sub>) δ 7.70 (d, *J* = 9.6 Hz, 1H), 7.47 (d, *J* = 7.8 Hz, 1H), 7.35 (s, 1H), 7.32 (dd, *J* = 7.8, 1.8 Hz, 1H), 6.44 (d, *J* = 9.6 Hz, 1H), 4.52 (s, 2H); <sup>13</sup>C NMR (150 MHz, CDCl<sub>3</sub>) δ 160.65, 154.21, 142.94, 142.12, 128.43, 125.34, 118.85, 117.39, 117.29, 31.95; *m/z* (APCI) [M + 1]<sup>+</sup> 239, [M + 3]<sup>+</sup> 241.

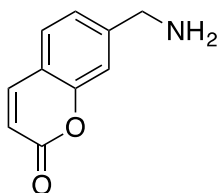


**Preparation of 209.** To a solution of crude bromide **223** (4.330 g, 18.11 mmol) in DMSO (50 mL) was added sodium nitrite (5.17 g, 74.9 mmol) and acetic acid (13.6 mL, 237 mmol). The mixture was heated to 100 °C and stirred for 4 h. Once the mixture cooled to 25 °C, a 37% HCl solution was added dropwise until the pH reached 1.5. The solution was extracted with Et<sub>2</sub>O (6 x 80 mL); the combined organic layers were then washed with H<sub>2</sub>O (300 mL), dried over Na<sub>2</sub>SO<sub>4</sub>, filtered, and concentrated *in vacuo* to afford **209** (2.80 g, 81%) as a pale yellow solid. NMR shows slight contamination with succinimide. <sup>1</sup>H NMR (600 MHz, DMSO-*d*<sub>6</sub>) δ 8.11 (d, *J* = 9.6 Hz, 1H), 7.84 (dd, *J* = 7.8, 1.2 Hz, 1H), 7.80 (d, *J* = 7.8 Hz, 1H), 7.77 (s, 1H), 6.59 (d, *J* = 9.6 Hz, 1H); <sup>13</sup>C NMR (150 MHz, DMSO-*d*<sub>6</sub>) δ 166.22, 159.65, 153.20, 143.46, 133.59, 128.87, 124.89, 122.18, 118.35, 116.88; *m/z* (APCI) [M + 1]<sup>+</sup> 191.



**Preparation of 224.** To a solution of sodium azide (0.139 g, 2.14 mmol) in DMSO (4 mL) was sequentially added bromide **223** and then tetraethylammonium bromide (2 mg, 10 μmol). The solution was then stirred 20 h at r.t. At this point, sodium iodide (0.087 g, 0.58 mmol) was

added and the reaction was stirred for an additional 24 h. Workup was carried out through the addition of water (10 mL). The aqueous layer was extracted with CH<sub>2</sub>Cl<sub>2</sub> (3 x 10 mL), the combined organic layers were then washed with water (2 x 10 mL) and brine (10 mL), dried over Na<sub>2</sub>SO<sub>4</sub>, filtered and concentrated *in vacuo*. The crude orange solid (**224**) was used in the following step without further purification. <sup>1</sup>H NMR (600 MHz, DMSO-*d*<sub>6</sub>) δ 7.88 (d, *J* = 9.0 Hz, 1H), 7.67 (d, *J* = 7.8 Hz, 1H), 7.45 (m, 2H), 6.60 (d, *J* = 9.6 Hz, 1H), 4.61 (s, 2H); <sup>13</sup>C NMR (150 MHz, DMSO-*d*<sub>6</sub>) δ 160.70, 154.28, 143.12, 140.02, 128.49, 124.06, 118.65, 117.09, 116.32, 54.15; *m/z* (APCI) [M + 1]<sup>+</sup> 202.

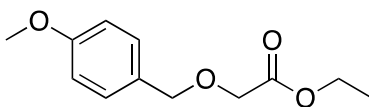


### Preparation of 210.

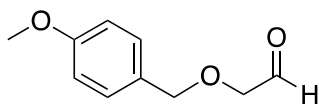
**Method A:** Bromide **223** (0.200 g, 0.837 mmol) in CHCl<sub>3</sub> (4 mL) was added to a stirring solution of hexamethylenetetramine (0.164 g, 1.17 mmol) in EtOH (6 mL). The resulting solution was stirred at 25 °C for 24 h, heated at 80 °C for 4 h, and then stirred for an additional 12 h at 25 °C. The precipitate was filtered and washed with cold EtOH. The solid residue was collected and diluted with additional EtOH (7.4 mL), then 12 N HCl (0.27 mL) was added slowly, and the biphasic solution was stirred at 55 °C for 30 min. The mixture was cooled to room temperature and concentrated overnight. The solid residue was diluted with hexanes (3

mL) and stirred for 15 min. Filtration, followed by two days under vacuum furnished **210** as an orange solid (0.146 g, 99%).

**Method B:** Water (0.16 mL) and then triphenylphosphine (1.17 g, 4.47 mmol) were added to a solution of azide **224** (0.360 g, 1.79 mmol) in THF (18 mL) at 25 °C. The mixture was heated to 40 °C, then stirred 20 h. An additional 1.6 mL of H<sub>2</sub>O was added, and the mixture was stirred for another 24 h. After concentrating the solution, it was dissolved in CH<sub>2</sub>Cl<sub>2</sub> (10 mL) and washed with 1 M HCl (3 x 10 mL), allowing for unreacted starting material to be collected (0.304 g). The aqueous layer was extracted with EtOAc (3 x 10 mL), and then 3 M NaOH was added to the aqueous layer until the pH reached 10. The aqueous layer was then extracted with CH<sub>2</sub>Cl<sub>2</sub> (3 x 10 mL). The combined organic layers were dried over Na<sub>2</sub>SO<sub>4</sub>, filtered and concentrated *in vacuo*. The residue was purified by chromatography on SiO<sub>2</sub> (0–100% EtOAc in hexanes) to afford **210** (0.035 g, 11%, 72% BRSM). NMR was initially taken with CDCl<sub>3</sub> as the solvent, and the sample was concentrated before taking an additional NMR using DMSO-*d*<sub>6</sub>. The reported NMR spectra show CDCl<sub>3</sub> contamination. <sup>1</sup>H NMR (600 MHz, DMSO-*d*<sub>6</sub>) δ 8.61 (br s, 2H), 8.10 (d, *J* = 9.0 Hz, 1H), 7.77 (d, *J* = 7.8 Hz), 7.59 (s, 1H), 7.48 (dd, *J* = 7.8, 1.2 Hz, 1H), 6.54 (d, *J* = 9.6 Hz, 1H), 4.15 (br s, 2H); <sup>13</sup>C NMR (150 MHz, DMSO-*d*<sub>6</sub>) δ 159.83, 153.30, 143.92, 138.38, 128.58, 125.03, 118.53, 116.61, 116.57, 41.63; *m/z* (ESI) [M + H]<sup>+</sup> 176.0, [M – NH<sub>3</sub>]<sup>+</sup> 159.0.

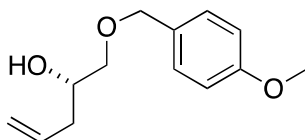


**Preparation of 226.** Ethyl glycolate (1.03 mL, 10.8 mmol) was diluted into a solution of anhydrous  $\text{CH}_2\text{Cl}_2$  (5 mL) and cyclohexanes (10 mL), and then cooled to  $0^\circ\text{C}$ . To this solution was added dropwise *para*-methoxy benzyl trichloroacetimidate (3.67 mL, 13.0 mmol) in  $\text{CH}_2\text{Cl}_2$  (1.00 mL), followed by pyridinium *para*-toluenesulfonate (0.272 g, 1.08 mmol) in one portion. The mixture was warmed to  $25^\circ\text{C}$  after removal of the ice bath and stirred for 20 h, after which it was filtered through a plug of silica (3 mL) that was subsequently flushed with 20% EtOAc in hexanes solution (15 mL). The filtrate was washed with  $\text{NaHCO}_3$  (10 mL), dried over  $\text{Na}_2\text{SO}_4$ , filtered, and concentrated *in vacuo*. The residue was purified by chromatography on  $\text{SiO}_2$  (5–100% EtOAc in hexanes) to afford **226** (2.43 g, 89%) as a colorless oil.  $R_f = 0.30$  (25% EtOAc in hexanes);  $^1\text{H NMR}$  (600 MHz,  $\text{CDCl}_3$ )  $\delta$  7.30 (d,  $J = 8.4$  Hz, 2H), 6.89 (d,  $J = 8.4$  Hz, 2H), 4.57 (s, 2H), 4.21 (q,  $J = 7.2$  Hz, 2H), 4.06 (s, 2H), 3.81 (s, 3H), 1.30 (t,  $J = 6.6$ , 3H);  $^{13}\text{C NMR}$  (150 MHz,  $\text{CDCl}_3$ )  $\delta$  170.60, 159.63, 129.94, 129.30, 114.01, 73.093, 67.04, 60.99, 55.42, 14.35.



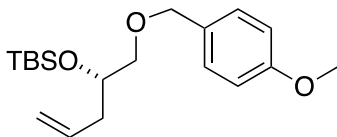
**Preparation of 227.** To a stirring solution of **226** (0.280 g, 1.25 mmol) in anhydrous  $\text{CH}_2\text{Cl}_2$  (6 mL) under  $\text{N}_2$  at  $-15^\circ\text{C}$  was added dropwise diisobutylaluminum hydride (1.87 mL, 1M in toluene, 1.87 mmol) and stirred 1.5 h. The reaction solution was quenched with 0.20 mL methanol, saturated aqueous sodium potassium tartrate (8 mL) was added, and the solution was allowed to warm to  $25^\circ\text{C}$  while stirring vigorously. The organic layer was separated and the aqueous layer was extracted with  $\text{CH}_2\text{Cl}_2$  (3 x 8 mL). The combined organic layers were washed

with brine (10 mL), dried over Na<sub>2</sub>SO<sub>4</sub>, filtered, and concentrated *in vacuo*. The residue was purified by chromatography on SiO<sub>2</sub> (0–100% EtOAc in hexanes) to afford **227** (0.170 g, 76%) as a colorless oil. R<sub>f</sub> = 0.45 (50% EtOAc in hexanes); <sup>1</sup>H NMR (600 MHz, CDCl<sub>3</sub>) δ 9.71 (s, 1H), 7.30 (d, *J* = 8.4 Hz, 2H), 6.91 (d, *J* = 8.4 Hz, 2H), 4.57 (s, 2H), 4.07 (s, 2H), 3.81 (s, 3H); <sup>13</sup>C NMR (150 MHz, CDCl<sub>3</sub>) δ 200.80, 159.77, 129.93, 128.98, 114.13, 75.15, 73.49, 55.44.



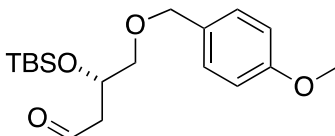
**Preparation of 228.** A flask fitted with a reflux condenser was charged with crushed and oven-dried 4Å molecular sieves (3.43 g), a 0.10 M solution of (*S*)-1,1'-bi-2-naphthol (0.508 g, 1.78 mmol) in CH<sub>2</sub>Cl<sub>2</sub> (17.8 mL), a 1.0 M solution of titanium isopropoxide (0.27 mL, 0.888 mmol) in CH<sub>2</sub>Cl<sub>2</sub> (0.90 mL), and a 1.0 M solution of trifluoroacetic acid (4.8 μL, 0.0622 mmol) in CH<sub>2</sub>Cl<sub>2</sub> (60 μL). The reaction mixture was stirred and heated at reflux for 1 h and then allowed to cool to 25 °C. A 3.0 M solution of aldehyde **227** (1.60 g, 8.88 mmol) in CH<sub>2</sub>Cl<sub>2</sub> (3.0 mL) was added, using an additional 0.1 mL CH<sub>2</sub>Cl<sub>2</sub> to transfer the remaining aldehyde residue to the reaction flask. The mixture was stirred for 30 min before cooling to -78 °C. Allyltributylstannane (3.6 mL, 11.543 mmol) was added dropwise at this temperature to the mixture, and stirred an additional 10 minutes at -78 °C before being transferred to a -20 °C freezer, where it was manually agitated daily. After 6 days, the reaction mixture was filtered over a pad of Celite (4 mL), which was flushed with CH<sub>2</sub>Cl<sub>2</sub> (10 mL). The filtrate was then quenched with NaHCO<sub>3</sub> (10 mL) and stirred for 1 h before separating the layers. The aqueous

layer was extracted with CH<sub>2</sub>Cl<sub>2</sub> (2 x 10 mL), the combined organic layers were washed with brine (10 mL), dried over Na<sub>2</sub>SO<sub>4</sub>, filtered, and concentrated *in vacuo* to give the crude product as a red-orange oil. The residue was purified by chromatography on SiO<sub>2</sub> (0–100% EtOAc in hexanes) to afford **228** (1.78 g, 90%) as a colorless oil. R<sub>f</sub> = 0.53 (50% EtOAc in hexanes); <sup>1</sup>H NMR (600 MHz, CDCl<sub>3</sub>) δ 7.27 (d, *J* = 8.4 Hz, 2 H), 6.90 (d, *J* = 8.4 Hz, 2H), 5.86 (ddt, *J* = 10.2, 16.8, 7.2 Hz, 1H), 5.13 (dd, *J* = 3.3, 16.8 Hz, 1H), 5.10 (dd, *J* = 3.3, 10.2 Hz, 1H), 4.49 (s, 2H), 3.88 (m, 1H), 3.81 (s, 3H), 3.50 (dd, *J* = 3.0, 9.6 Hz, 1H), 3.36 (dd, *J* = 7.2, 9.6 Hz, 1H), 2.30 (d, *J* = 3.6 Hz, 1 H), 2.27 (t, *J* = 7.2 Hz, 2H); <sup>13</sup>C NMR (150 MHz, CDCl<sub>3</sub>) δ 159.44, 134.39, 130.17, 129.53, 117.79, 113.98, 73.73, 73.17, 55.41, 38.03.

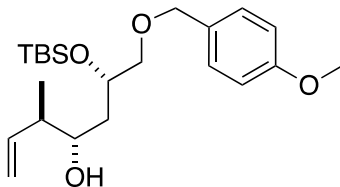


**Preparation of 229.** To a stirring solution of **228** (1.75 g, 7.87 mmol) and imidazole (1.07 g, 15.7 mmol) in CH<sub>2</sub>Cl<sub>2</sub> (78 mL) was cooled to 0 °C and then *tert*-butyldimethylsilyl chloride (1.78 g, 11.8 mmol) was quickly added. The reaction solution was stirred at 25 °C for 12 h, and was then diluted with diethyl ether (100 mL), washed with H<sub>2</sub>O (2 x 100 mL) and brine (100 mL), dried over MgSO<sub>4</sub>, filtered, and concentrated *in vacuo*. The residue was purified by chromatography on SiO<sub>2</sub> (5–100% EtOAc in hexanes) to afford **229** (2.20 g, 83%) as a colorless oil. R<sub>f</sub> = 0.60 (25% EtOAc in hexanes); <sup>1</sup>H NMR (600 MHz, CDCl<sub>3</sub>) δ 7.26 (d, *J* = 8.4 Hz, 2H), 6.88 (d, *J* = 8.4 Hz, 2H), 5.85 (ddt, *J* = 10.2, 16.8, 7.2 Hz, 1H), 5.07 (d, *J* = 16.8 Hz, 1H), 5.04 (d, *J* = 10.2 Hz, 1H), 4.45 (d, *J* = 0.06 Hz, 2H), 3.88 (m, 1H), 3.81 (s, 3H), 3.37 (dd, *J* = 1.8, 5.4

Hz, 2H), 2.36 (ddd,  $J = 6.6, 6.6, 13.2$  Hz, 1H), 2.23 (ddd,  $J = 6.6, 6.6, 13.2$  Hz, 1H), 0.88 (s, 9H), 0.05 (s, 3H), 0.04 (s, 3H);  $^{13}\text{C}$  NMR (150 MHz,  $\text{CDCl}_3$ )  $\delta$  159.23, 135.16, 130.71, 129.35, 117.11, 113.84, 74.10, 73.10, 71.34, 55.42, 39.54, 26.01, 18.33, -4.31, -4.56.

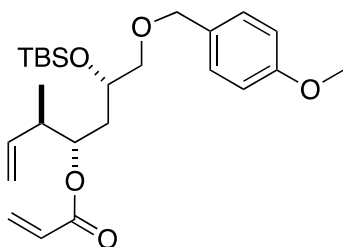


**Preparation of 230.** To a stirred solution of **229** (0.073 g, 0.22 mmol) in acetone (0.67 mL) and  $\text{H}_2\text{O}$  (67  $\mu\text{L}$ ) was added 2,6-lutidine (50.3  $\mu\text{L}$ , 0.434 mmol), 4-methylmorpholine N-oxide (0.038 g, 0.326 mmol), and osmium tetroxide (1.1 mg, 4.34  $\mu\text{mol}$ ). This solution was stirred 14 h, then (diacetoxyiodo)benzene (0.105 g, 0.326 mmol) was added, and the mixture was stirred an additional 3 h. The reaction mixture was quenched with saturated aqueous  $\text{Na}_2\text{S}_2\text{O}_3$  (7 mL), the aqueous layer was extracted with EtOAc, the combined organic layers were washed with saturated aqueous  $\text{CuSO}_4$  (2 x 14 mL), dried over  $\text{Na}_2\text{SO}_4$ , filtered, and concentrated *in vacuo*. The residue was purified by chromatography on  $\text{SiO}_2$  (0–100% EtOAc in hexanes) to afford **230** (0.065 g, 89%) as a colorless oil.  $R_f = 0.50$  (25% EtOAc in hexanes);  $^1\text{H}$  NMR (600 MHz,  $\text{CDCl}_3$ )  $\delta$  9.79 (s, 1H), 7.24 (d,  $J = 9.0$  Hz, 2H), 6.88 (d,  $J = 8.4$  Hz, 2H), 4.45 (d,  $J = 1.8$  Hz, 2H), 4.36 (m, 1H), 3.81 (s, 3H), 3.49 (dd,  $J = 5.4, 9.6$  Hz, 1H), 3.37 (dd,  $J = 6.6, 9.6$  Hz, 1H), 2.66 (ddd,  $J = 2.4, 5.4, 15.6$  Hz, 1H), 2.58 (ddd,  $J = 2.4, 6.6, 15.6$  Hz, 1H), 0.86 (s, 9H), 0.06 (s, 3H), 0.06 (s, 3H);  $^{13}\text{C}$  NMR (150 MHz,  $\text{CDCl}_3$ )  $\delta$  201.70, 159.39, 130.17, 129.44, 113.93, 73.82, 73.20, 67.48, 55.42, 49.12, 25.87, 18.16, -4.32, -4.83.



**Preparation of 231.** To a solution of potassium *tert*-butoxide (0.020 g, 0.18 mmol) and *trans*-2-butene (0.022 mL, 0.25 mmol), stirring at -78 °C in THF (0.17 mL), was added dropwise *n*-BuLi (0.106 mL, 2.4 M in hexanes, 0.170 mmol). The resulting mixture was stirred for 20 min at -45 °C, before being cooled once again to -78 °C. A solution of (+)- $\beta$ -methoxy diisopinocampheylborane (0.063 g, 0.201 mmol) in THF (100  $\mu$ L) was added, and stirring continued at this temperature for 35 min. To this mixture was quickly added  $\text{BF}_3 \cdot \text{OEt}_2$  and then a solution of aldehyde **230** (0.040 g, 0.118 mmol) in THF (0.05 mL). The reaction was quenched after stirring for 4 h by the addition of 3N NaOH (0.11 mL) and then  $\text{H}_2\text{O}_2$  (30% in  $\text{H}_2\text{O}$ , 0.11 mL). The cooling bath was removed, and the reaction mixture was then stirred 12 h at 25 °C. After dilution with EtOAc (2 mL) and brine (2 mL), the aqueous layers were washed with EtOAc (3 x 2 mL), the combined organic layers were dried over  $\text{MgSO}_4$ , filtered, and concentrated *in vacuo*. The residue was purified by careful chromatography on  $\text{SiO}_2$  (2.5–100% EtOAc in hexanes) to afford **231** (0.020 g, 42%) as a colorless oil.  $R_f = 0.53$  (25% EtOAc in hexanes);  $^1\text{H}$  NMR (600 MHz,  $\text{CDCl}_3$ )  $\delta$  7.25 (d,  $J = 8.4$ , 2H), 6.88 (d,  $J = 8.4$ , 2H), 5.83 (ddd,  $J = 16.8, 10.8, 7.8$  Hz, 1H), 5.08 (dd,  $J = 10.2, 1.2$  Hz, 1H), 5.08 (dd  $J = 16.8, 1.2$  Hz, 1H), 4.49 (d,  $J = 11.4$  Hz, 1H), 4.14 (ddd,  $J = 10.8, 6.0, 5.4$  Hz, 1H), 3.81 (s, 3H), 3.72 (m, 1H), 3.47 (dd,  $J = 9.6, 5.4$  Hz, 1H), 3.06 (br s, 1H), 2.21 (m, 1H), 1.69 (ddd,  $J = 14.4, 5.4, 1.8$  Hz, 1H), 1.63 (ddd,  $J = 14.4, 10.8, 4.2$  Hz, 1H), 1.03 (d,  $J = 7.2$ , 3H), 0.88 (s, 9H), 0.08 (s, 3H), 0.06 (s, 3H);  $^{13}\text{C}$  NMR

(150 MHz, CDCl<sub>3</sub>)  $\delta$  159.36, 140.83, 130.31, 129.47, 115.42, 113.92, 73.39, 73.10, 71.53, 70.35, 55.45, 44.34, 37.78, 25.98, 18.22, 15.94, -4.41, -4.90.



**Preparation of 232.** To a stirred solution of alkene **231** (15 mg, 0.038 mmol) in CH<sub>2</sub>Cl<sub>2</sub> (0.5 mL) was added 4-(dimethylamino)pyridine (0.3 mg, 0.003 mmol), and the resulting solution was then cooled from 25 °C to -78 °C. Triethylamine (13.2  $\mu$ L) was added and then acryloyl chloride (6.2  $\mu$ L) was added. The solution was diluted with CH<sub>2</sub>Cl<sub>2</sub> after 2 h, quenched with the addition of brine, and warmed to 25 °C. The aqueous layer was extracted with CH<sub>2</sub>Cl<sub>2</sub>, the combined organic layers were dried over Na<sub>2</sub>SO<sub>4</sub>, filtered, and concentrated *in vacuo* to afford a 10.5:1 mixture of **231** to **232** (21 mg mixture, <8%) as a yellow oil.  $R_f$  = 0.47 (25% EtOAc in hexanes.  $m/z$  (APCI) [M +1]<sup>+</sup> 449.

## APPENDIX A

### ANTIPROLIFERATIVE ACTIVITY OF DISCODERMOLIDE ANALOGUES

This appendix has been included to accompany the SAR studies discussed in Section 1.4 of this document. It begins with Table 2, which summarizes the notable features of each of the cell lines involved in these SAR studies. The remaining tables include all antiproliferative data for these analogues in each of the cell lines that were assayed. Tables are organized by the figure in which they appeared in Section 1.4. Due to the range of measured  $IC_{50}$  values for the parent compound in each study, the data is presented in two forms.

- 1) Antiproliferative data is presented as a ratio of [activity of analogue]/[activity of parent, as measured in that particular study]. A heat map was generated to color code the individual analogues according to their activity when compared to the parent; analogues that perform as well or better than the parent are shaded green, and analogues that perform significantly worse than the parent are shaded red.
- 2) Unprocessed data is presented, showing the antiproliferative activity of both the analogue and the parent for each figure without further calculations performed.

Table 2. Characterization of cell lines used in discodermolide SAR studies.

<b>Cell Line</b>	<b>Notes</b>
1A9	Human ovarian carcinoma
1A9-PTX22	Paclitaxel-resistant human ovarian carcinoma; contains $\beta$ -tubulin mutation A364T
2008	Human ovarian cystadenocarcinoma
A549	Human non-small cell lung adenocarcinoma
CCRF-CEM	Human acute lymphocytic leukemia
HCT116	Human colorectal carcinoma
MCF-7	Human breast ductal carcinoma
MDA-MB231	Human breast carcinoma
MG63	Human osteosarcoma
MIP101	Undifferentiated human colon carcinoma
NCI/ADR	Multidrug-resistant OVCAR-8 human ovarian carcinoma (originally named MCF-7/ADR); expresses high levels of MDR1 and P-glycoprotein)
P388	Murine lymphocytic leukemia
PANC-1	Human pancreatic ductal carcinoma
PC-3	Human prostate adenocarcinoma
SKOV-3	Human ovarian adenocarcinoma
VERO	Normal (non-cancerous) kidney epithelial cell line of the African green monkey

Table 3. IC<sub>50</sub> values for carbamate fragment analogues, presented as a ratio of analogue to parent.

		Ref.	A549	P388	HCT 116	MIP 101	1A9	1A9-PTX2 2	MCF-7	NCI/A DR	SKOV-3	MG63	MDA-A1	MDA-MB231
Figure 12	38	82-84	0.40		0.57	0.70	0.30	0.67						
	39	82-84	0.16		0.29	2.50	0.10	0.67						
	40	82-84	0.20		0.14	13.00	0.30	1.00						
	41	91	0.40	0.11	21.43	80.00	3.00	8.33						
	42	82-84	2.40		5.71	360	2.00	1.67						
	43	82-84	12.00		28.57	380	3.00	30.00						
	44	87			0.26								1.47	0.24
	45	87			3.80								42.48	7.05
	46	87			64.20								82.32	64.68
	47	7										11.67		
	48	85	0.91											
49	85	0.81												
Figure 13	50	88	2.45						0.96	Inactive	1.62			
	51	88	0.45						0.30	Inactive	0.38			
	52	88	0.23						0.07	1.88	0.09			
	53	88	2.64						1.18	Inactive	1.48			
	54	88	1.36						0.36	Inactive	0.67			
	55	85	0.37											
	56	89	0.60						0.46					
	57	89	0.13						0.24					
	58	89	0.40						0.34					
	59	89	0.11						0.21					
	60	89	0.28						0.24					
61	85	0.31												
Figure 14	62	7										1.67		
	63	7										50.00		
	64	84,88	2.27		4.29	20.00	2.00	8.33		34.17	1.67			
	65	91	3.66	0.14	0.57	6.00	1.00	5.00						
	66	7										Inactive		
	67	7,93	Inactive	Inactive								11.67		
	68	82-84	16.40		1857	2000	400	1000						
	69	92	n/a											
	70	92	n/a											
	71	7										11.67		
	72	92	n/a											
73	7										Inactive			
74	87			0.46								20.79	1.12	

Table 4. IC<sub>50</sub> values for linker fragment analogues, presented as a ratio of analogue to parent.

		Ref.	A549	P388	MCF-7	NCI/A DR	SKOV-3	PANC-1	VERO
Figure 15	75	94	97.33	30.30	750.00	258.82		63.88	0.12
	76	94	442.67	64.55	875.00	Inactive		134.08	0.73
	77	94	6.67	5.76	54.17	200.00		6.73	0.02
	78	94	Inactive	231.82	3062.50	Inactive		Inactive	0.38
	79	94	56.00	73.33	983.33	Inactive		61.84	0.14
	80	94	176.00	63.33	720.83	Inactive		Inactive	0.55
	81	95	11.03		3.29	22.22	2.04		
	82	95	7.24		2.71	22.22	1.30		

Table 5. IC<sub>50</sub> values for lactone fragment analogues, presented as a ratio of analogue to parent.

		Ref.	A549	P388	HCT 116	MIP 101	1A9	1A9-PTX2 2	MCF-7	NCI/A DR	SKOV-3	MG63	CCRF-CEM	PANC-1	VERO	
Figure 16	83	91	2.40	4.91	4.29	19.00	26.00	3.33								
	84	77,90,93	0.09	0.96	0.04	3.00	1.00	1.67	0.20	1.93	0.16		0.19			
	85	90,96	0.17						0.08	0.40			0.17			
	86	90,96	0.36						0.11	2.63			0.24			
	87	90,96	1.64		1.00	6.00	0.60	1.17	0.30	Inactive			0.18			
	88	90,96	7.27						0.82	1.38			0.39			
	89	90,96	0.22						0.10	1.46			0.14			
	90	90,96	90.91						13.93	Inactive			19.38			
	91	91	1.20	3.83	5.71	7.00	3.00	6.67								
	92	84	6.00		14.29	100.00	10.00	50.00								
	93	90,96	0.35						0.16	1.46			0.25			
	94	84	20.00		14.29	100.00	20.00	50.00								
	95	90,96	0.27						0.10	0.63			0.09			
	96	94	132.67	23.94					400.00	164.71					54.08	0.014
	97	98	0.01	0.11	0.01	0.30	0.30	0.03								
	98	98	0.16	0.36	0.03	1.40	0.40	0.17								
99	98	0.04	0.02	0.03	1.00	2.00	0.33									
100	7										1.00					
101	7										0.67					
102	91		1.89	8.57	0.60	4.00	3.33									
Figure 17	103	100	23.18						17.14	2.33	16.67					
	104	101,	5.20		57.14	130.00	7.00	11.67								
	105	100	14.09						5.71	Inactive	2.14					
	106	100	181.82						27.50	16.67	19.52					
	107	100	41.36						17.50	4.17	12.86					
	108	77,100	8.64						4.64	1.63	1.90					
	109	100	27.27						11.79	2.08	17.62					
	110	100	29.55						13.21	2.08	19.05					
	111	100	26.36						14.29	2.71	18.10					
	112	85	13.15													
	113	100	45.45						21.43	8.33	17.14					
	114	100	181.82						35.71	16.67	47.62					
	115	82-84			28.57	40.00	30.00	16.67								
	116	100	454.55						142.86	41.67	476.19					
	117	85	4.67													
	118	100	181.82						30.36	16.67	20.95					
119	100	35.91						13.21	2.58	17.62						
120	102							0.46	0.73	1.76						
121	87			3.20									4.23	45.71		
122	82-84	128.00		85.71	650.00	30.00	66.67									
123	82-84			114.29	320.00	50.00	66.67									

Table 6. IC<sub>50</sub> values for analogues with multiple regions of alteration, presented as a ratio of analogue to parent.

		Ref.	A549	P388	HCT 116	MIP 101	1A9	1A9-PTX2 2	MCF-7	NCI/A DR	SKOV-3
Figure 18	124	93	Inactive	Inactive							
	125	93	270.96	105.31							
	126	82-84	40.00		571.43	600.00	100.00	333.33			
	127	82-84	348.00		1714.29	5800.00	4900.00	1833.33			
Fig. 19	128	93	0.80	8.83	7.14	51.00	4.00	25.00			
	129	93	1.20	0.97	2.86	110.00	0.20	8.33			
	130	93	Inactive	Inactive							
Figure 20	131	98,104	13.20	2.94	4.29	52.00	4.00	55.00			
	132	98,104	33.20	4.74	88.57	520.00	49.00	466.67			
	133	98,104	40.00	32.83	142.86	550.00	330.00	550.00			
	134	84,93	196.00	Inactive	871.43	1000.00	2000.00	883.33			
	135	84,94	560.00	202.17	2000.00	1900.00	Inactive	2333.33			
Figure 21	136	77	24.36						6.61	Inactive	3.90
	137	77	13.64						1.61	Inactive	2.38
	138	77	Inactive						Inactive	Inactive	Inactive
	139	77	Inactive						Inactive	Inactive	37.62
	140	77	Inactive						Inactive	Inactive	Inactive
	141	102							0.58	0.88	1.40
	142	102							61.54	12.69	72.00
	143	102							16.54	3.23	31.60
	144	102							61.54	12.31	96.00
	145	102							115.38	15.38	116.00

Table 7. Analogues with measured GI<sub>50</sub> values, rather than IC<sub>50</sub> values, presented as a ratio of analogue to parent.

		Ref.	MDA-MB 231	PC-3	2008
<b>Figure 22</b>	<b>146</b>	24	450.00	164.18	106.94
	<b>147</b>	24	750.00	98.51	80.56
	<b>148</b>	24	162.50	44.78	20.83
	<b>149</b>	24	500.00	223.88	98.61
	<b>150</b>	24	468.75	208.96	88.89
	<b>151</b>	24	2562.50	Inactive	333.33
	<b>152</b>	105	1500.00	343.28	375.00
	<b>153</b>	105	1250.00	343.28	291.67
	<b>154</b>	105	Inactive	Inactive	Inactive
	<b>155</b>	105	1187.50	298.55	277.78
	<b>156</b>	105	1375.00	373.13	208.33
	<b>157</b>	105	1250.00	313.43	277.78
	<b>158</b>	105	425.00	208.96	194.44
	<b>159</b>	105	687.50	298.51	37.50
	<b>160</b>	105	937.50	223.88	291.67
	<b>161</b>	105	Inactive	Inactive	Inactive
	<b>162</b>	105	1250.00	298.51	80.56
	<b>163</b>	105	1562.50	373.13	41.67
	<b>164</b>	105	Inactive	Inactive	Inactive
	<b>165</b>	105	Inactive	Inactive	430.56
<b>166</b>	105	1375.00	492.54	458.33	
<b>167</b>	105	1562.50	298.51	361.11	
<b>168</b>	105	Inactive	Inactive	Inactive	
<b>169</b>	105	Inactive	Inactive	Inactive	
<b>170</b>	105	750.00	Inactive	Inactive	
<b>171</b>	105	1437.50	641.79	569.44	
<b>172</b>	105	437.50	388.06	402.78	
<b>173</b>	105	Inactive	Inactive	Inactive	
<b>Figure 23</b>	<b>174</b>	106	131.25	111.94	72.22
	<b>175</b>	106	54.38	26.87	9.03
	<b>176</b>	106	150.00	Inactive	402.78
	<b>177</b>	106	1437.50	567.16	583.33
	<b>178</b>	106	212.50	223.88	65.28
	<b>179</b>	106	Inactive	Inactive	Inactive
	<b>180</b>	106	Inactive	Inactive	Inactive
	<b>181</b>	106	2875.00	Inactive	Inactive
	<b>182</b>	106	1875.00	Inactive	Inactive



Table 9. IC<sub>50</sub> values (nM) for discodermolide (left) and linker fragment analogues (right).

		Ref.	A549		P388		MCF-7		NCI/ADR		SKOV-3		PANC-1		VERO	
<b>Figure 15</b>	<b>75</b>	94	15	1460	33	1000	2.4	1800	17	4400			49	3130	30000	3650
	<b>76</b>	94	15	6640	33	2130	2.4	2100	17	>5000			49	6570	30000	21900
	<b>77</b>	94	15	100	33	190	2.4	130	17	3400			49	330	30000	690
	<b>78</b>	94	15	>5000	33	7650	2.4	7350	17	>5000			49	>5000	30000	11400
	<b>79</b>	94	15	840	33	2420	2.4	2360	17	>5000			49	3030	30000	4300
	<b>80</b>	94	15	2640	33	2090	2.4	1730	17	>5000			49	>5000	30000	16600
	<b>81</b>	95	29	320			14	46	180	4000	54	110				
	<b>82</b>	95	29	210			14	38	180	4000	54	70				



Table 11. IC<sub>50</sub> values (nM) for discodermolide (left) and analogues with multiple modifications (right).

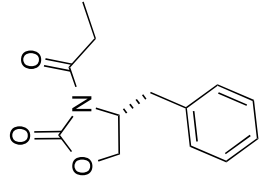
		Ref.	A549	P388	HCT116	MIP101	1A9	1A9-PTX22	MCF-7	NCI/ADR	SKOV-3
Figure 18	124	93	25 >12787	35 >12787							
	125	93	25 6774	35 3686							
	126	82-84	25 1000		7 4000	10 6000	10 1000	6 2000			
	127	82-84	25 8700		7 12000	10 58000	10 49000	6 11000			
Figure 19	128	93	25 20	35 309	7 50	10 510	10 40	6 150			
	129	93	25 30	35 33.8	7 20	10 1100	10 2	6 50			
	130	93	25 >8292	35 >8292							
Figure 20	131	98,104	25 330	35 103	7 30	10 520	10 40	6 330			
	132	98,104	25 830	35 166	7 620	10 5200	10 490	6 2800			
	133	98,104	25 1000	35 1149	7 1000	10 5500	10 3300	6 3300			
	134	84,93	25 4900	35 >7587	7 6100	10 10000	10 20000	6 5300			
	135	84,94	25 14000	35 7076	7 14000	10 19000	10 >18000	6 14000			
Figure 21	136	77	22 536						28 185	240 >1000	21 82
	137	77	22 300						28 45	240 >1000	21 50
	138	77	22 >5000						28 >5000	240 >5000	21 >5000
	139	77	22 >1000						28 >1000	240 >1000	21 790
	140	77	22 >1000						28 >1000	240 >1000	21 >1000
	141	102							26 15	260 230	25 35
	142	102							26 1600	260 3300	25 1800
	143	102							26 430	260 840	25 790
	144	102							26 1600	260 3200	25 2400
	145	102							26 3000	260 4000	25 2900

Table 12. GI<sub>50</sub> values (nM) for discodermolide (left) and analogues with multiple modifications (right).

		Ref.	MDA-MB231	PC-3	2008
<b>Figure 22</b>	<b>146</b>	24	16 7200	67 11000	72 7700
	<b>147</b>	24	16 12000	67 6600	72 5800
	<b>148</b>	24	16 2600	67 3000	72 1500
	<b>149</b>	24	16 8000	67 15000	72 7100
	<b>150</b>	24	16 7500	67 14000	72 6400
	<b>151</b>	24	16 41000	67 >50000	72 24000
	<b>152</b>	105	16 24000	67 23000	72 27000
	<b>153</b>	105	16 20000	67 23000	72 21000
	<b>154</b>	105	16 >50000	67 >50000	72 >50000
	<b>155</b>	105	16 19000	67 20003	72 20000
	<b>156</b>	105	16 22000	67 25000	72 15000
	<b>157</b>	105	16 20000	67 21000	72 20000
	<b>158</b>	105	16 6800	67 14000	72 14000
	<b>159</b>	105	16 11000	67 20000	72 2700
	<b>160</b>	105	16 15000	67 15000	72 21000
	<b>161</b>	105	16 >50000	67 >50000	72 >50000
	<b>162</b>	105	16 20000	67 20000	72 5800
	<b>163</b>	105	16 25000	67 25000	72 3000
	<b>164</b>	105	16 >50000	67 >50000	72 >50000
	<b>165</b>	105	16 >50000	67 >50000	72 31000
<b>166</b>	105	16 22000	67 33000	72 33000	
<b>167</b>	105	16 25000	67 20000	72 26000	
<b>168</b>	105	16 >50000	67 >50000	72 >50000	
<b>169</b>	105	16 >50000	67 >50000	72 >50000	
<b>170</b>	105	16 12000	67 >50000	72 >50000	
<b>171</b>	105	16 23000	67 43000	72 41000	
<b>172</b>	105	16 7000	67 26000	72 29000	
<b>173</b>	105	16 >50000	67 >50000	72 >50000	
<b>Figure 23</b>	<b>174</b>	106	16 2100	67 7500	72 5200
	<b>175</b>	106	16 870	67 1800	72 650
	<b>176</b>	106	16 2400	67 >50000	72 29000
	<b>177</b>	106	16 23000	67 38000	72 42000
	<b>178</b>	106	16 3400	67 15000	72 4700
	<b>179</b>	106	16 >50000	67 >50000	72 >50000
	<b>180</b>	106	16 >50000	67 >50000	72 >50000
	<b>181</b>	106	16 46000	67 >50000	72 >50000
	<b>182</b>	106	16 30000	67 >50000	72 >50000

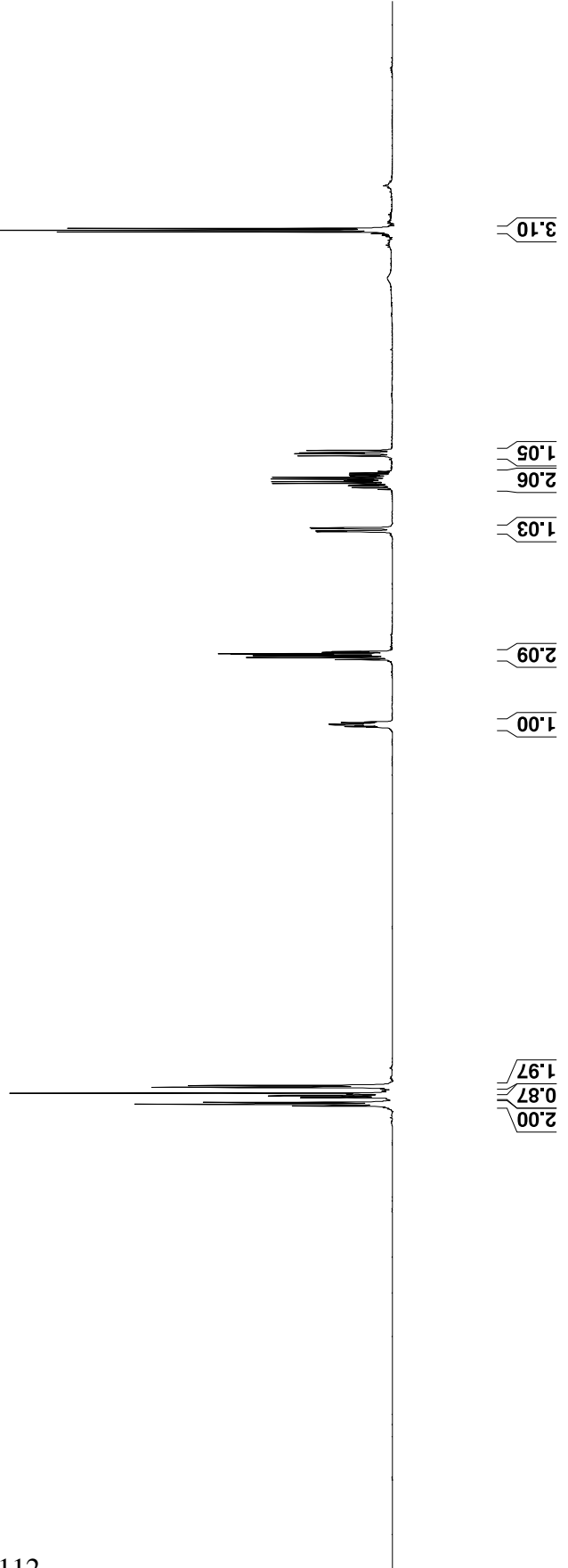
## **APPENDIX B**

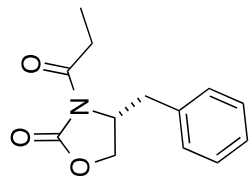
### **EXPERIMENTAL SPECTRA**



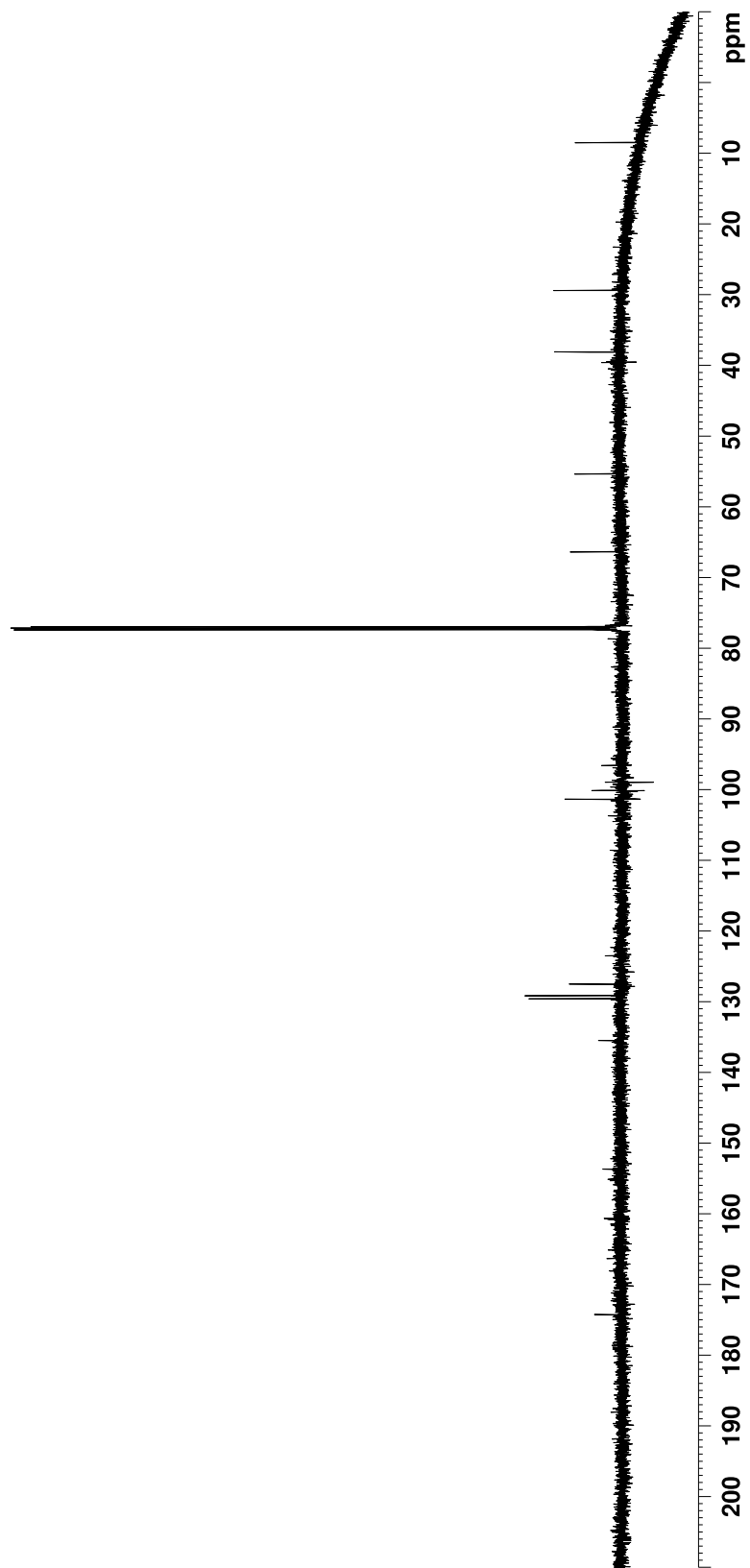
202

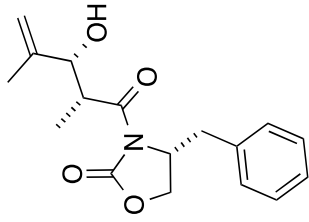
96  
3.001  
3.014  
3.026  
3.295  
3.300  
3.317  
3.322  
4.162  
4.167  
4.177  
4.182  
4.191  
4.204  
4.219  
4.656  
4.661  
4.667  
4.668  
4.673  
4.677  
4.682  
4.684  
4.689  
4.695  
7.206  
7.218  
7.278  
7.290  
7.324  
7.337  
7.349



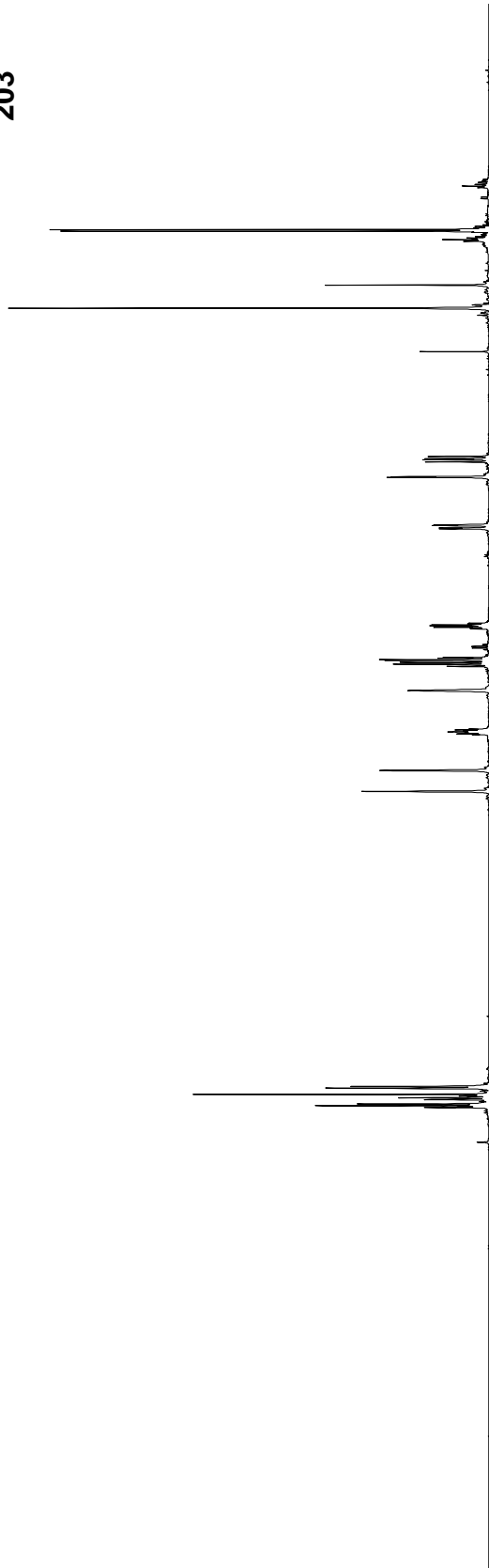


202

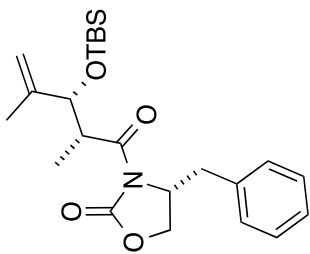




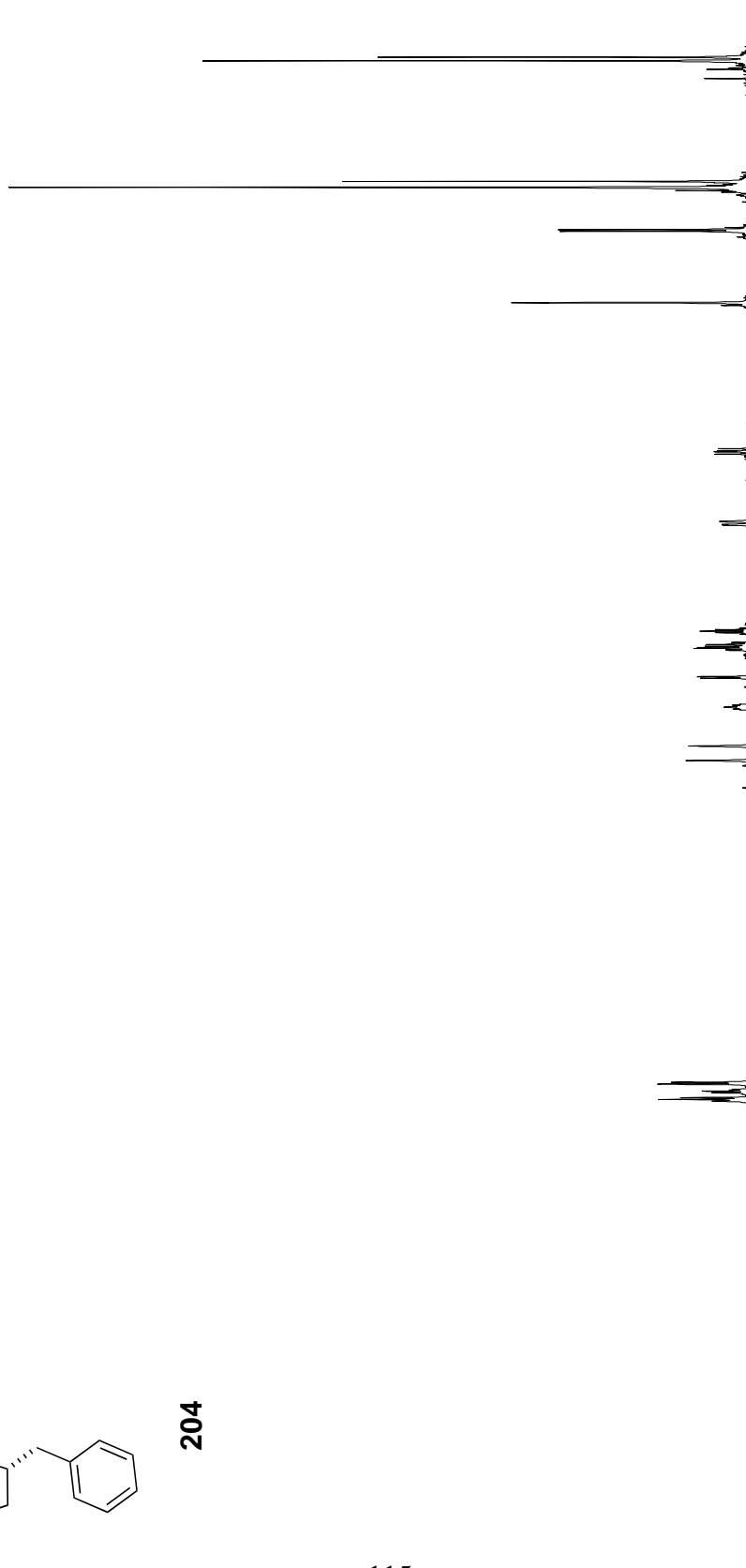
203

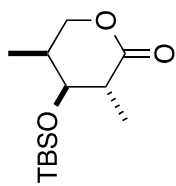


00



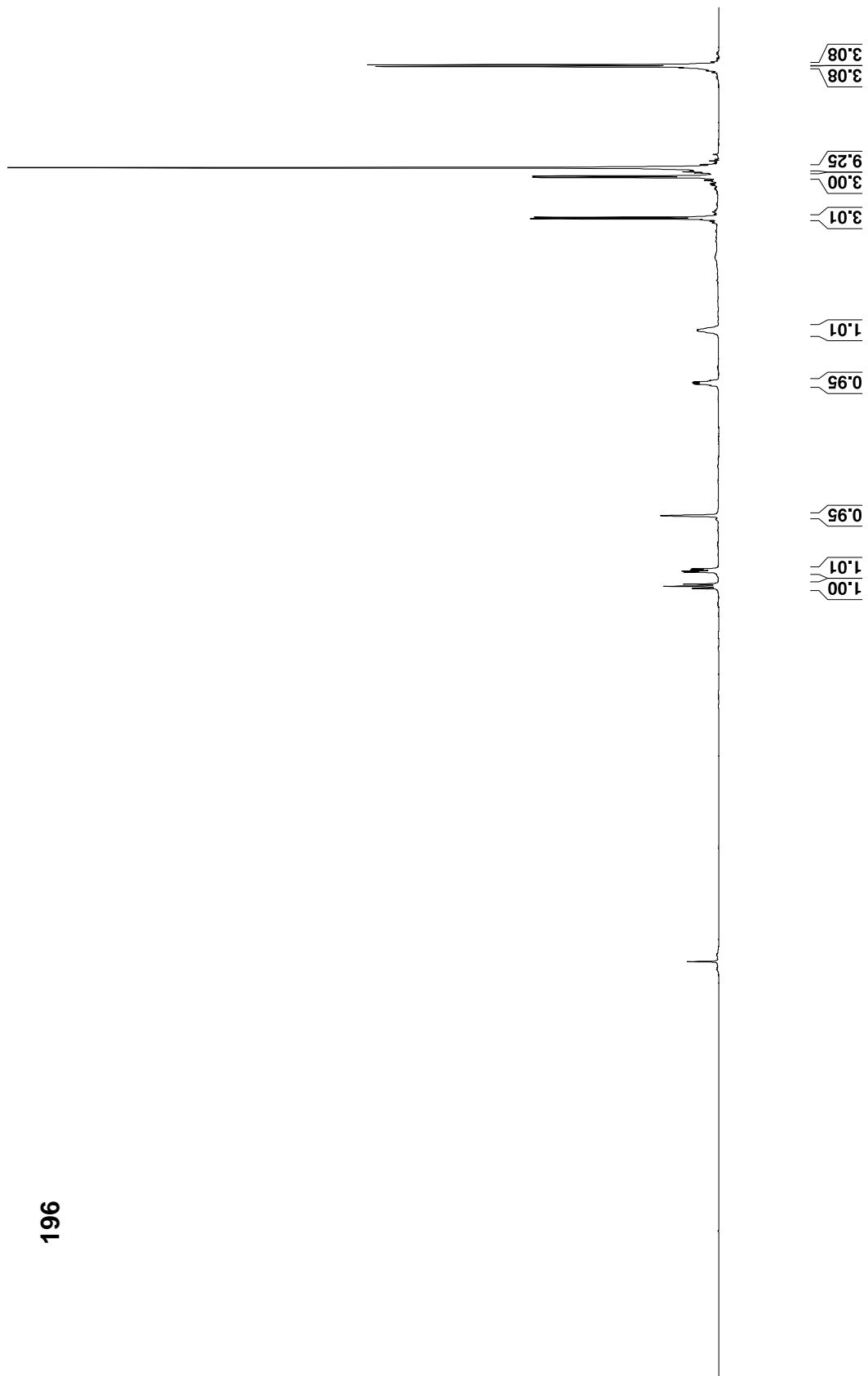
204

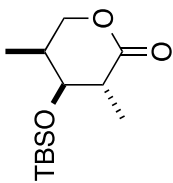




196

4.265  
4.248  
31





173.954

196

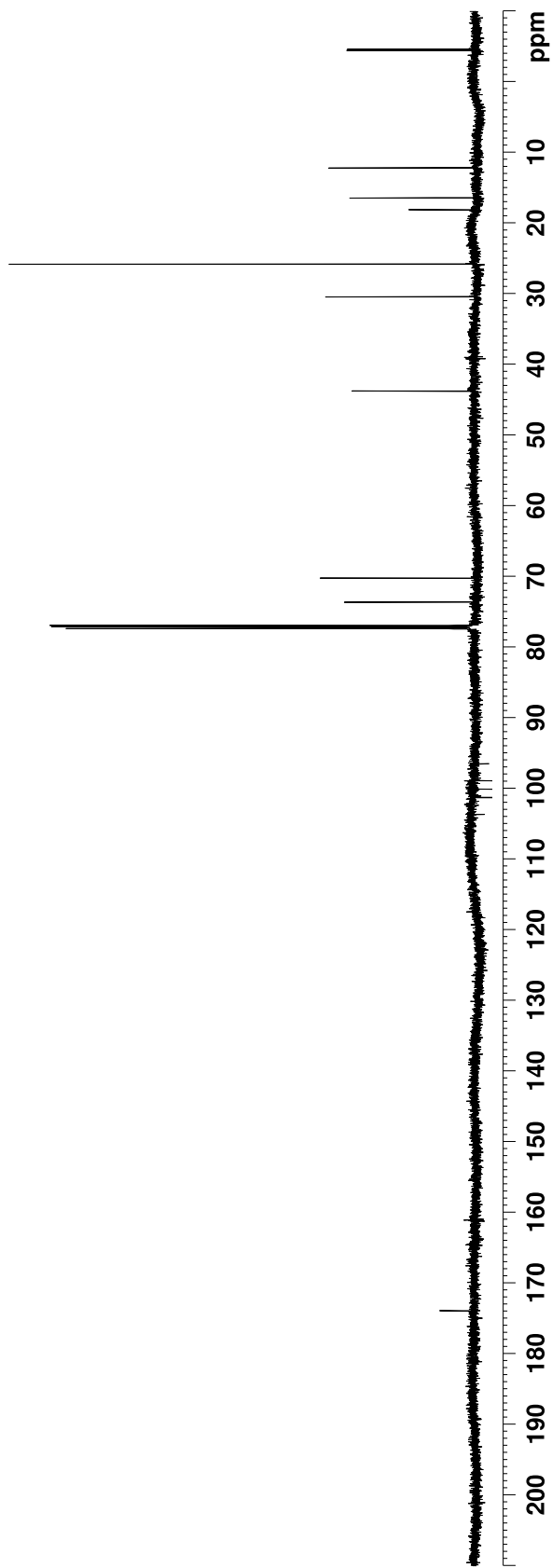
-4.444  
-4.631

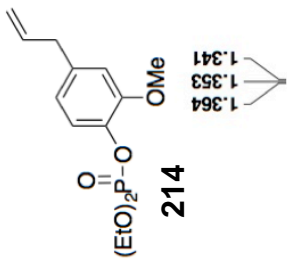
12.178  
16.414  
18.106

25.826  
30.431

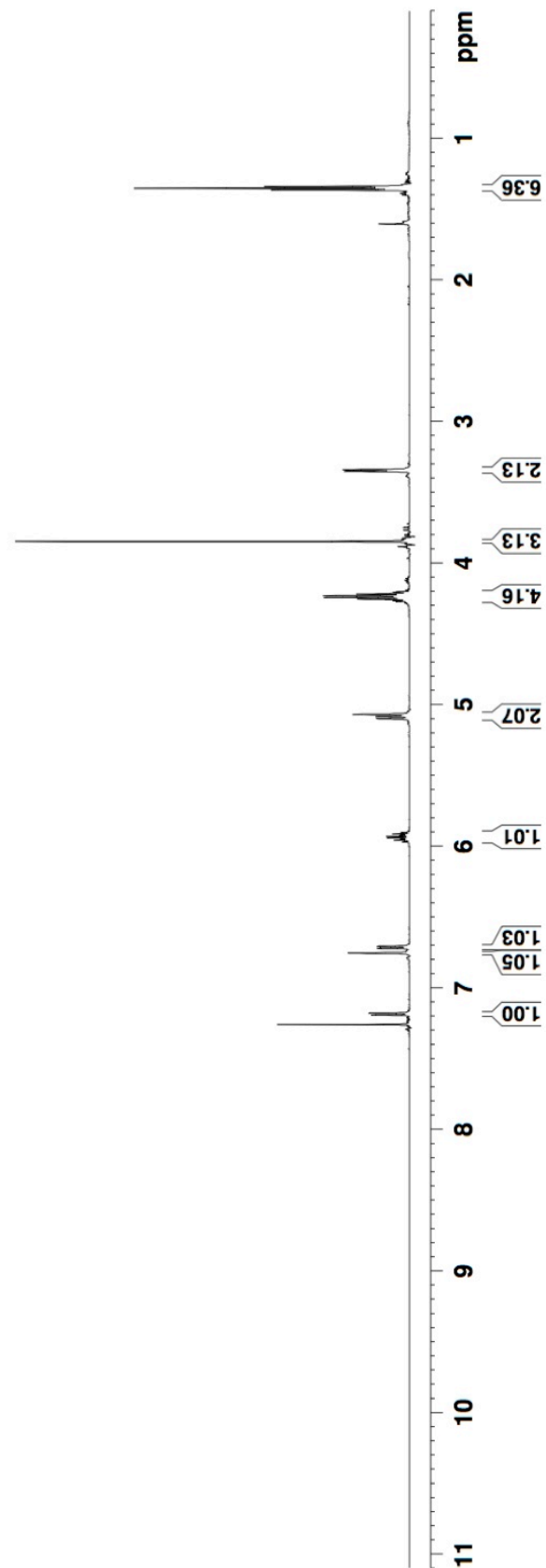
43.767

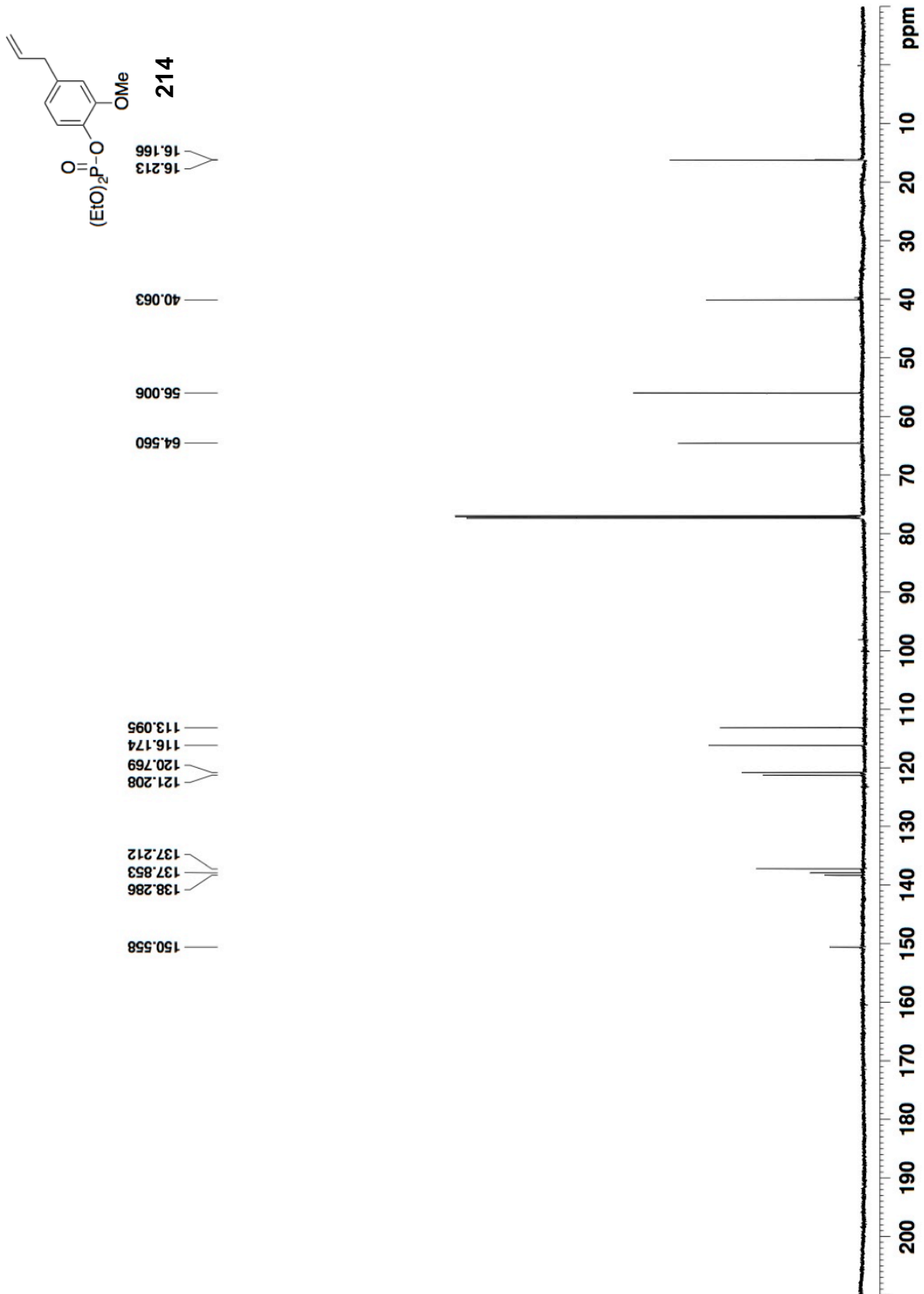
70.237  
73.635

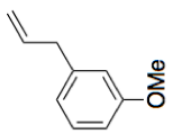




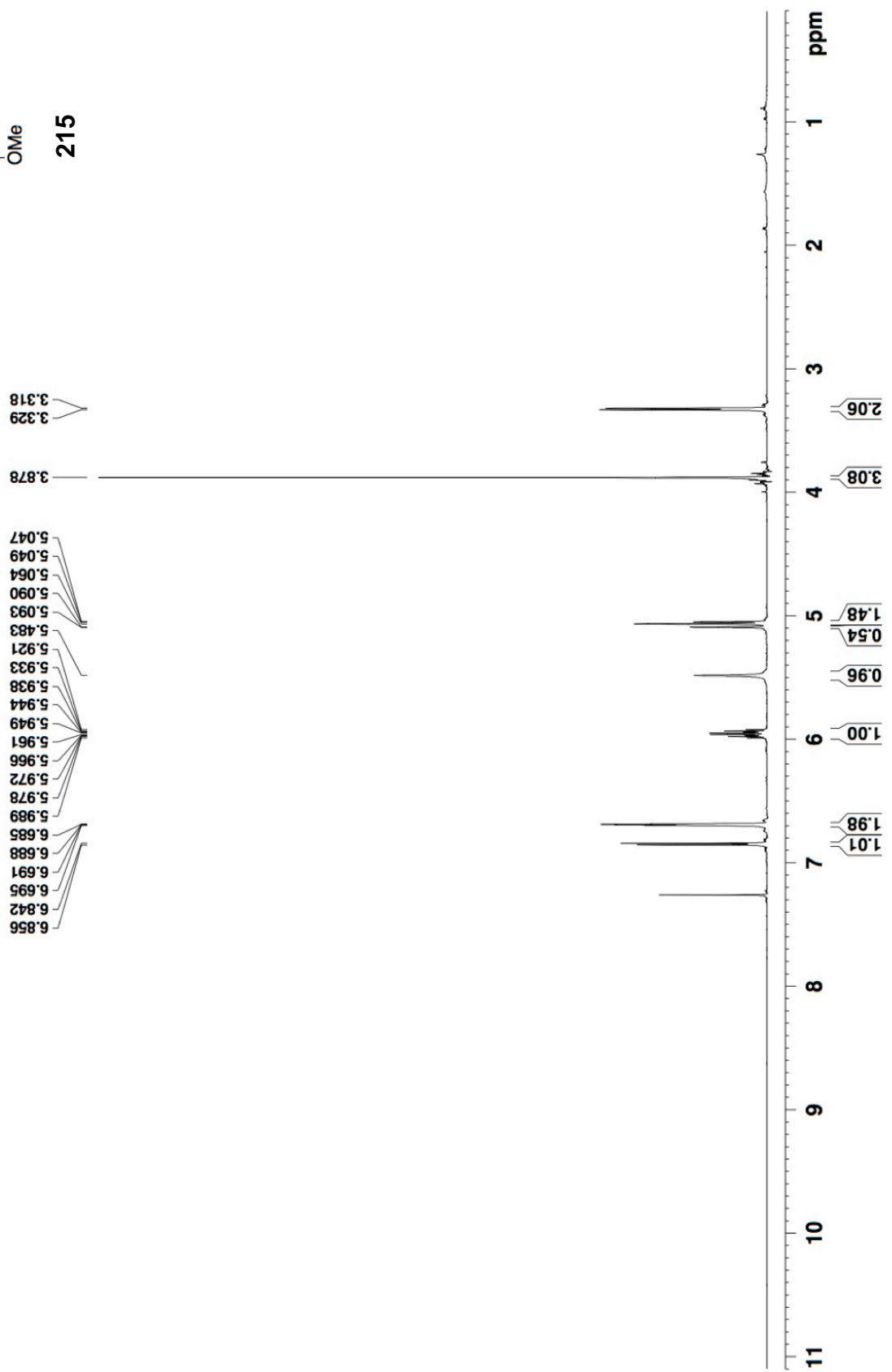
- 1.364
- 1.353
- 1.341
- 3.339
- 3.350
- 3.847
- 4.203
- 4.208
- 4.220
- 4.231
- 4.243
- 4.255
- 4.267
- 4.271
- 5.067
- 5.068
- 5.082
- 5.084
- 5.097
- 5.100
- 5.902
- 5.913
- 5.919
- 5.924
- 5.930
- 5.941
- 5.947
- 5.952
- 5.958
- 5.969
- 6.706
- 6.709
- 6.720
- 6.723
- 6.755
- 7.178
- 7.180
- 7.192
- 7.193

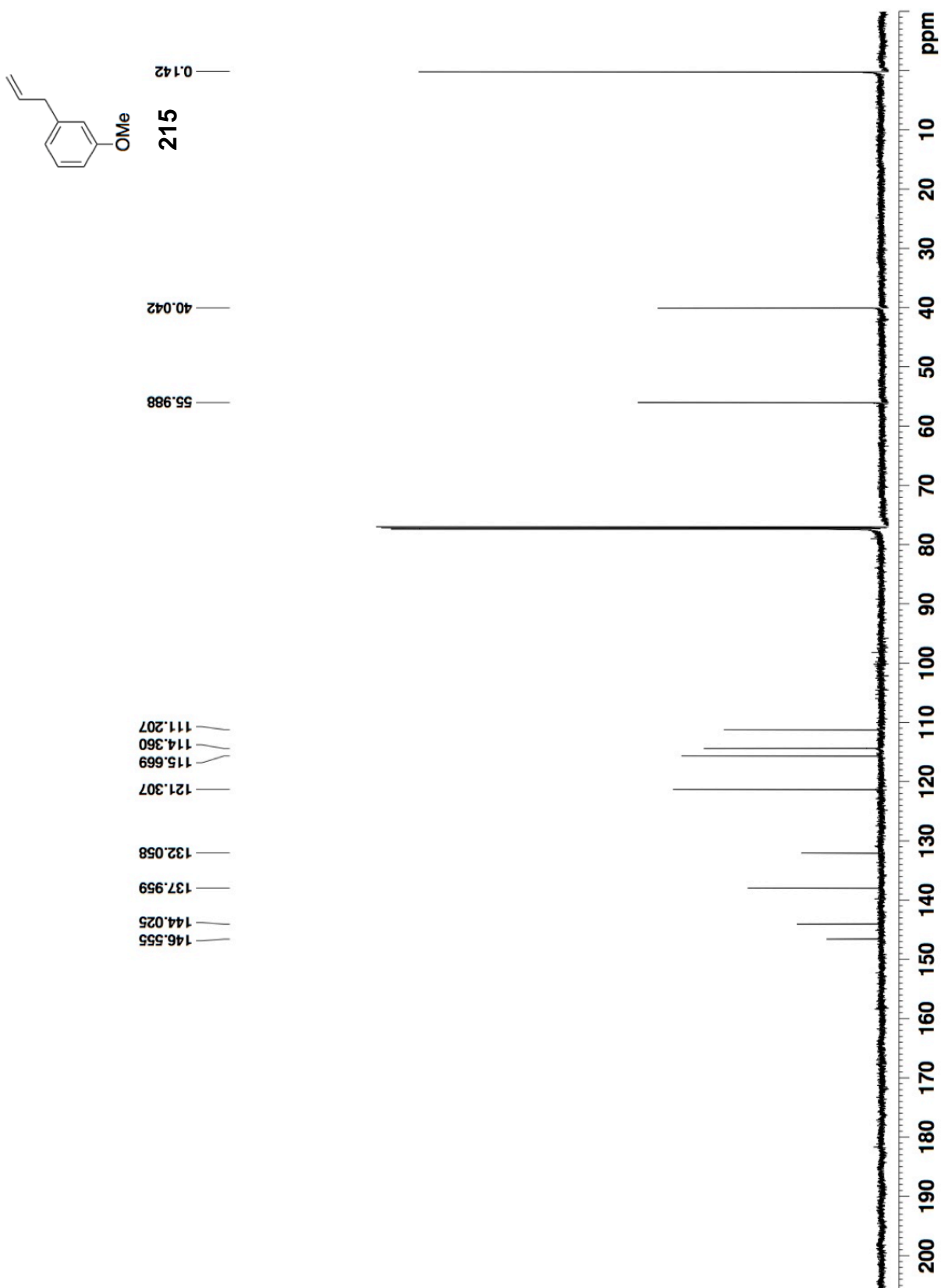


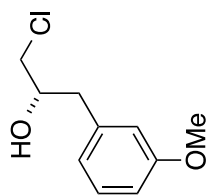




215

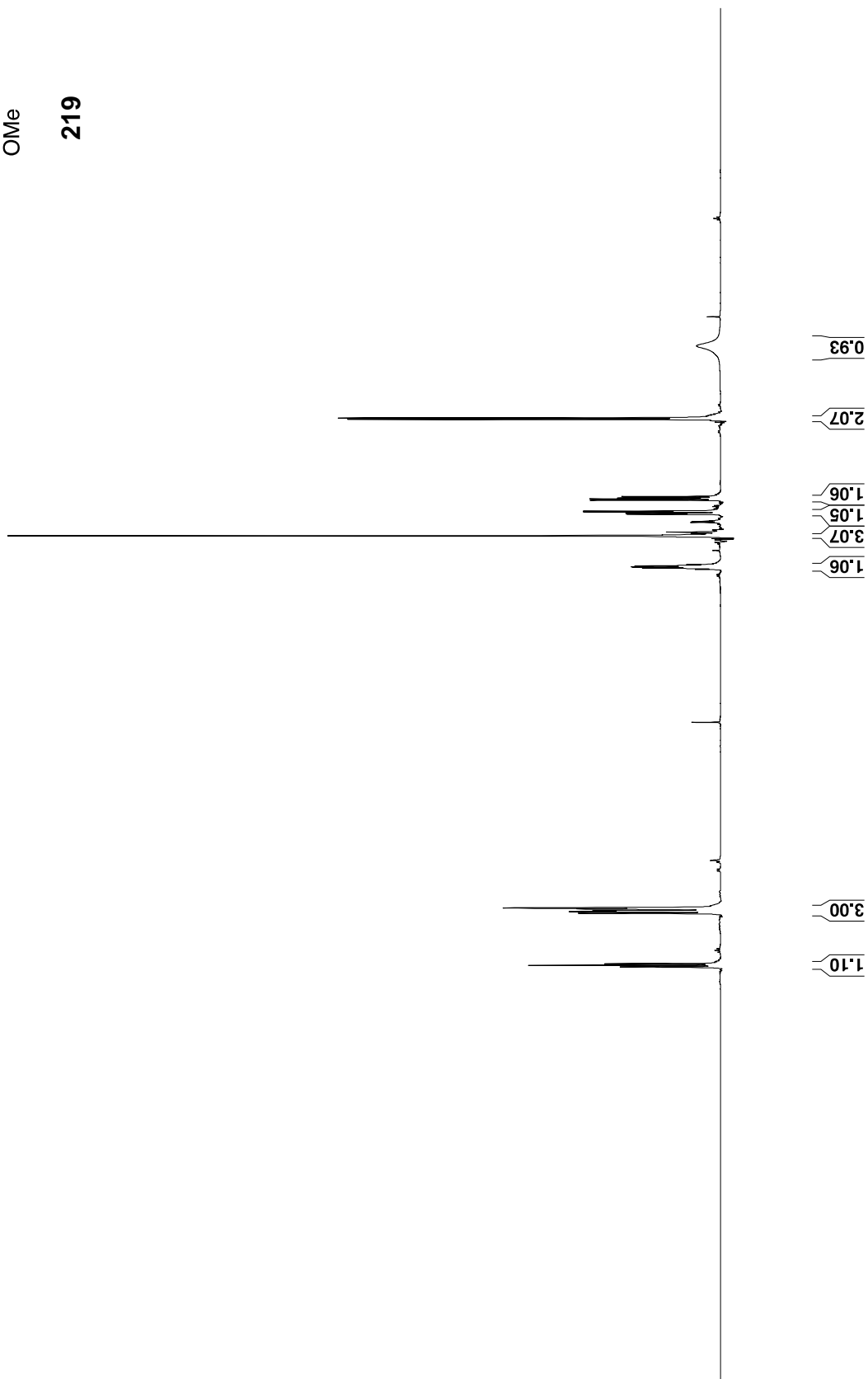


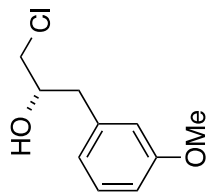




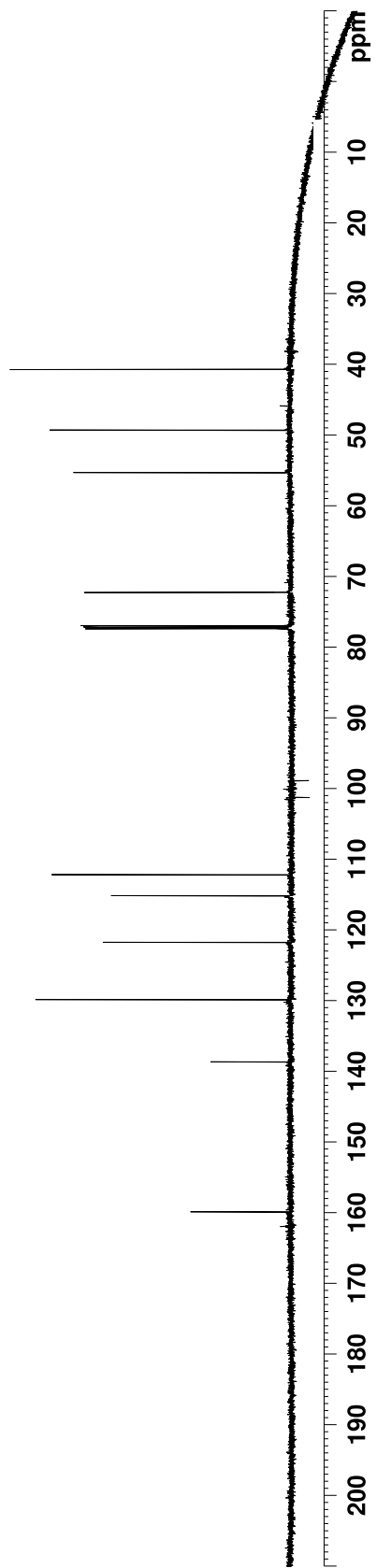
219

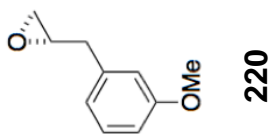
7.282  
7.269  
7.256  
6.852  
6.839  
6.832





219

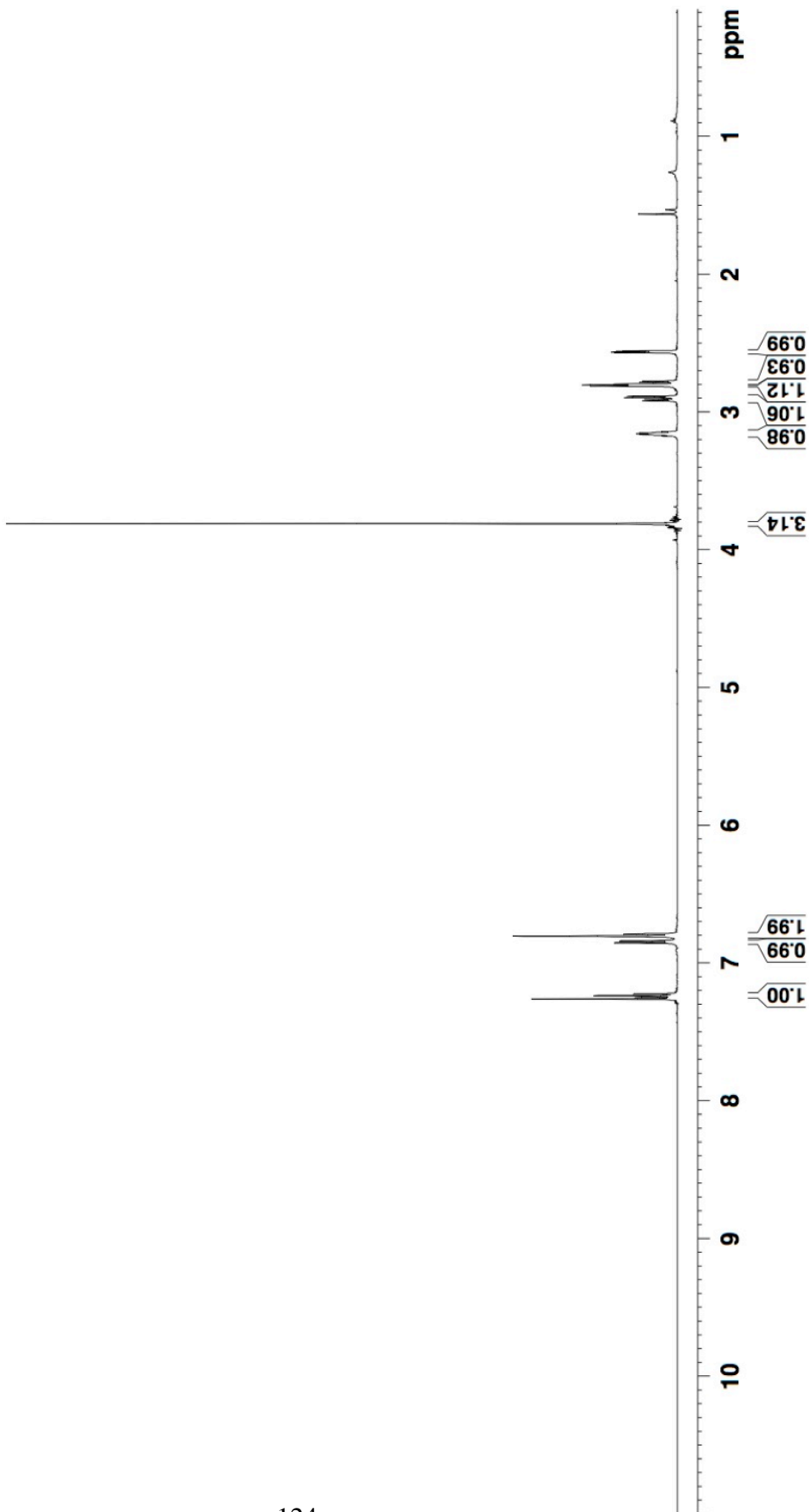


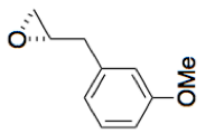


220

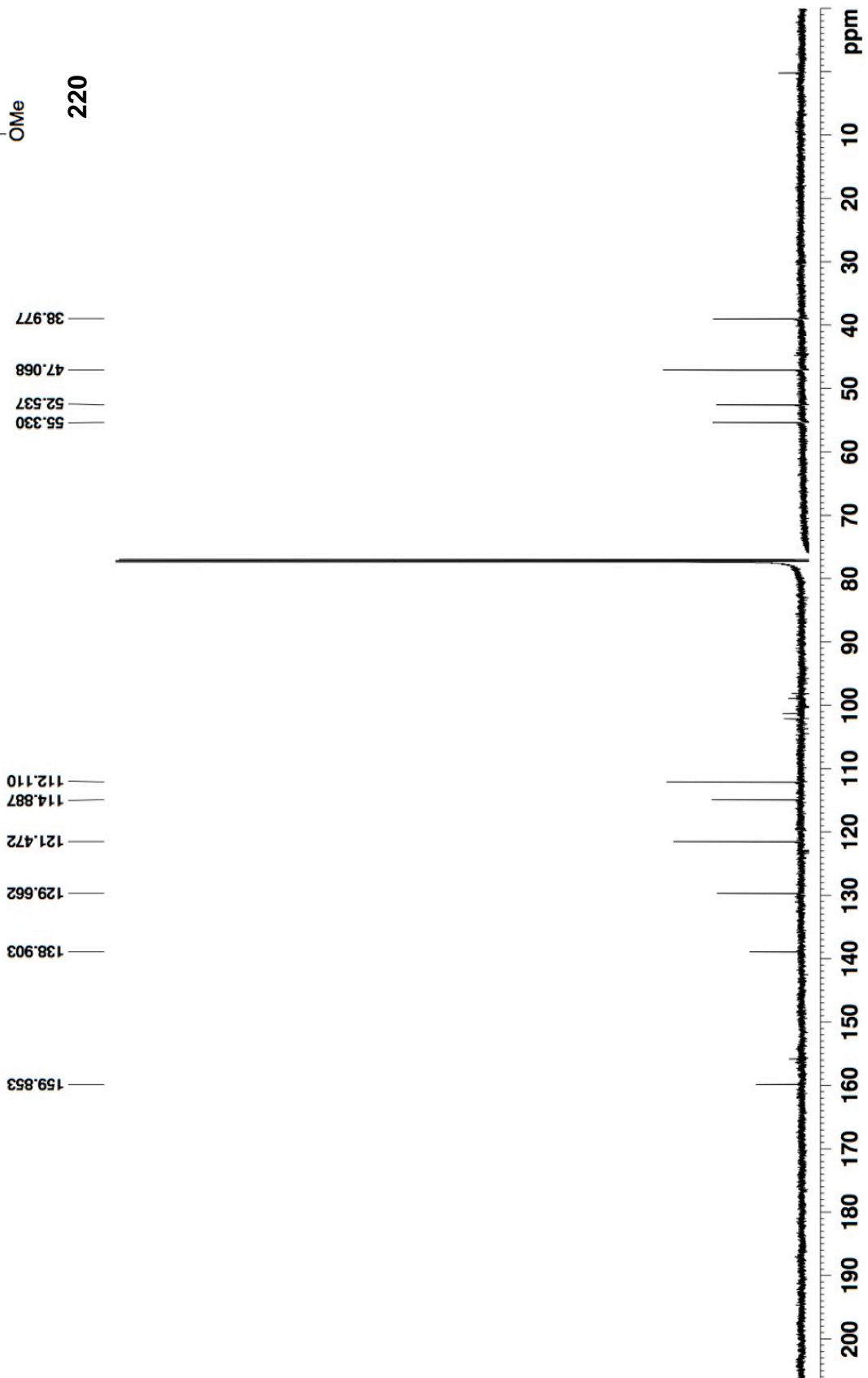
- 2.556
- 2.560
- 2.564
- 2.569
- 2.776
- 2.785
- 2.796
- 2.803
- 2.810
- 2.884
- 2.894
- 2.909
- 2.918
- 3.143
- 3.149
- 3.152
- 3.157
- 3.158
- 3.162
- 3.165
- 3.172
- 3.810

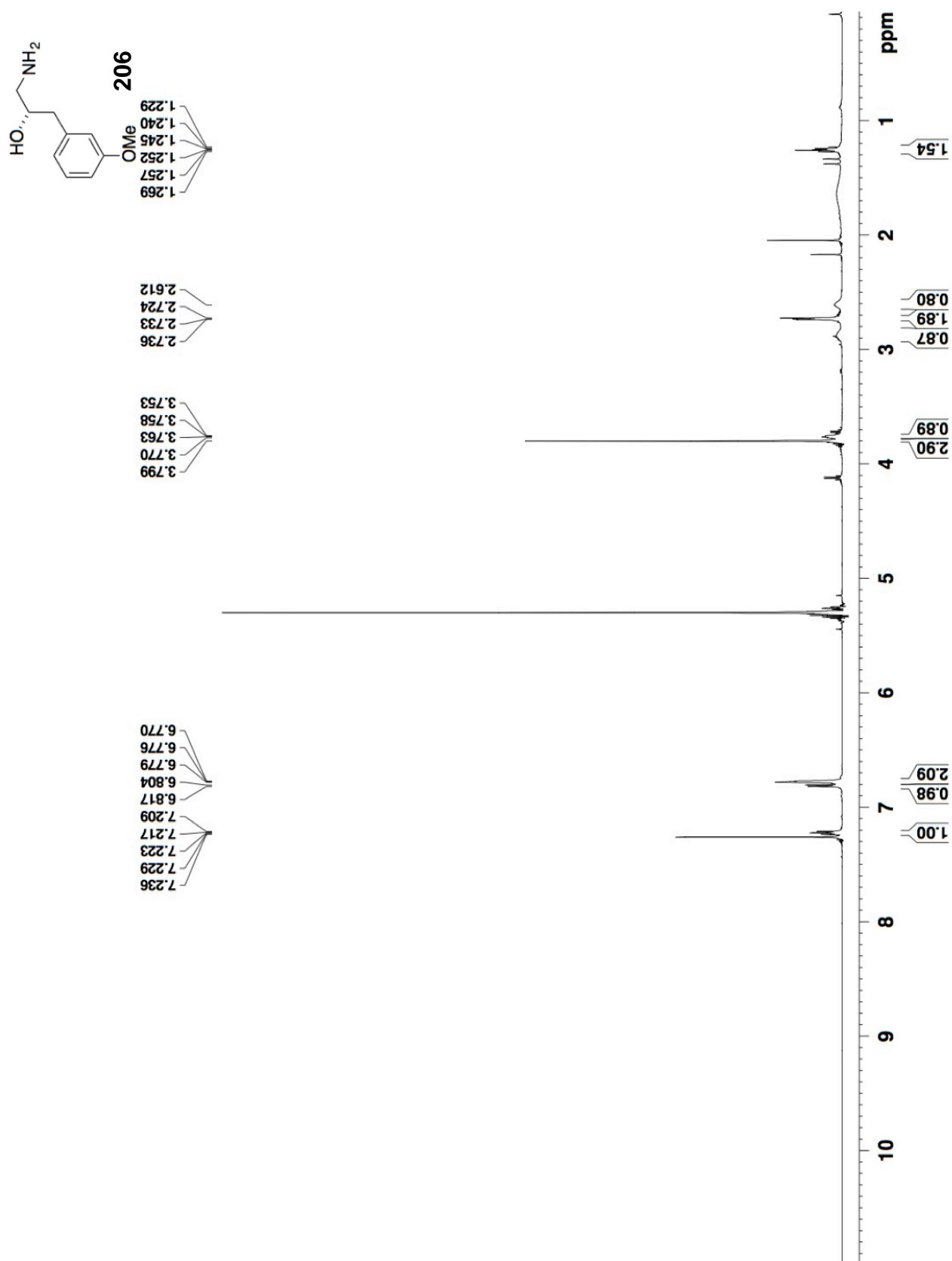
- 6.787
- 6.791
- 6.805
- 6.841
- 6.853
- 7.224
- 7.237
- 7.250

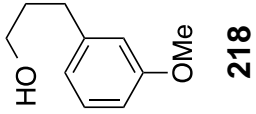




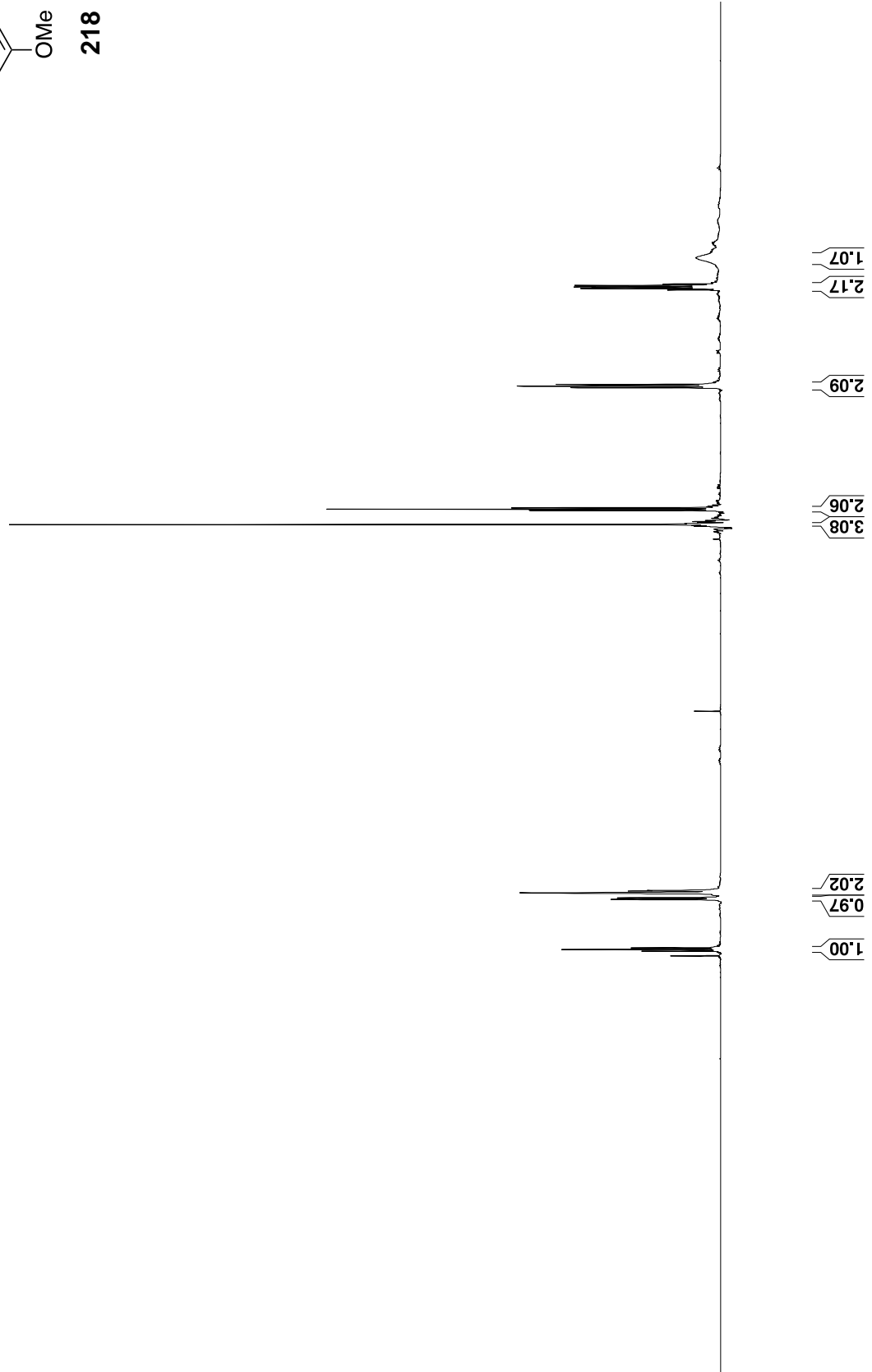
220

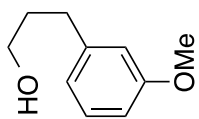




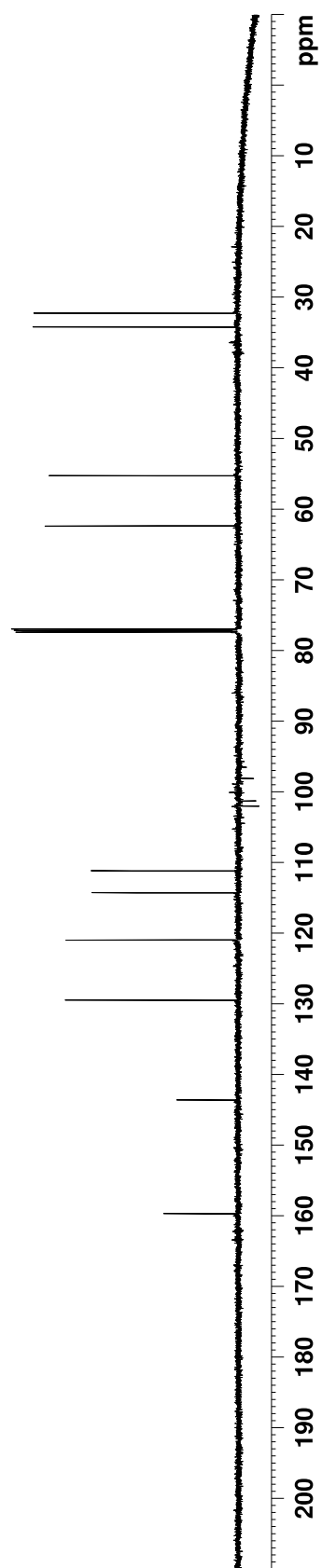


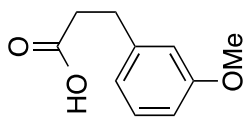
7.222  
7.209  
97



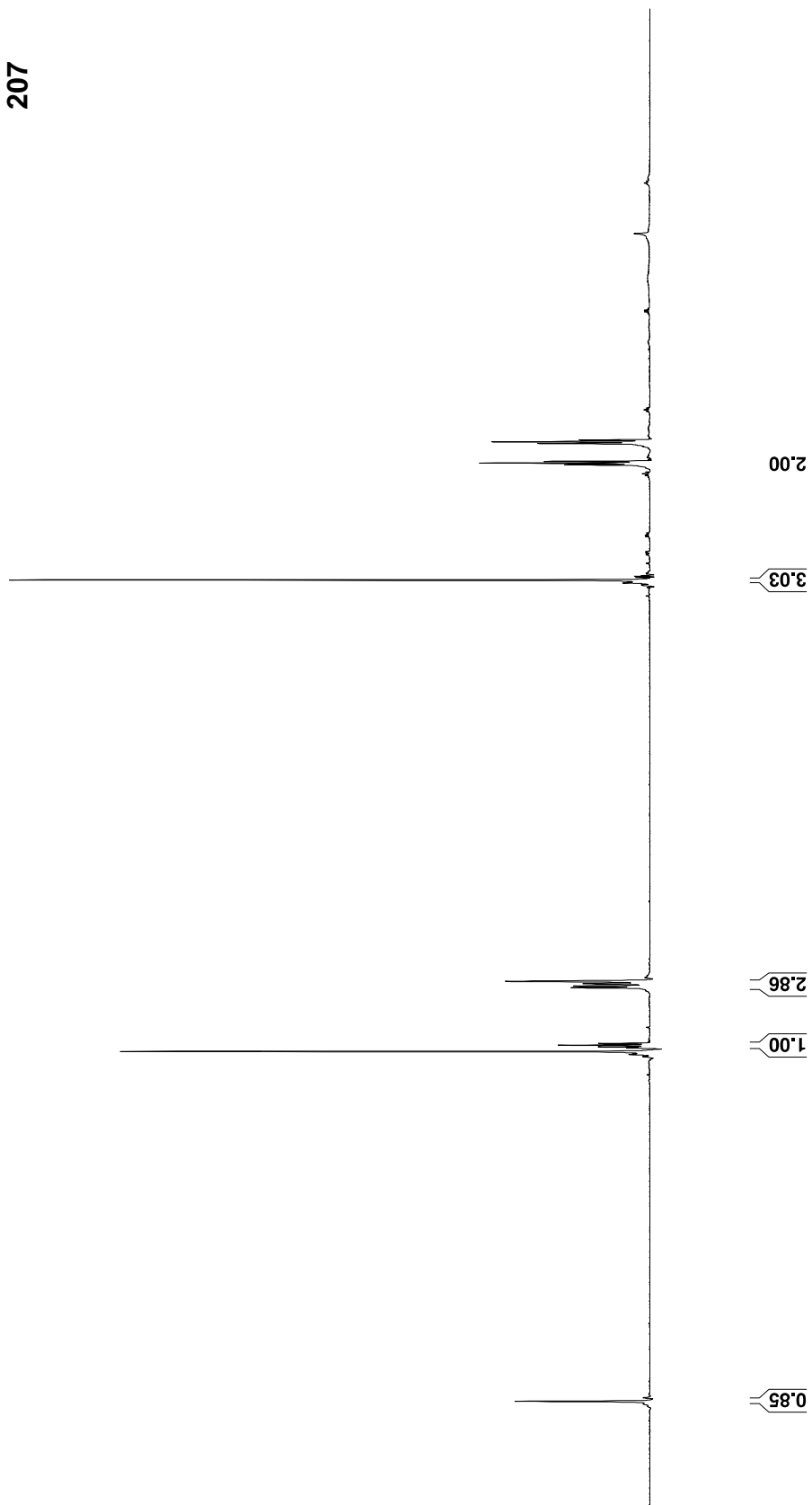


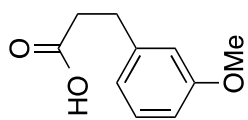
218



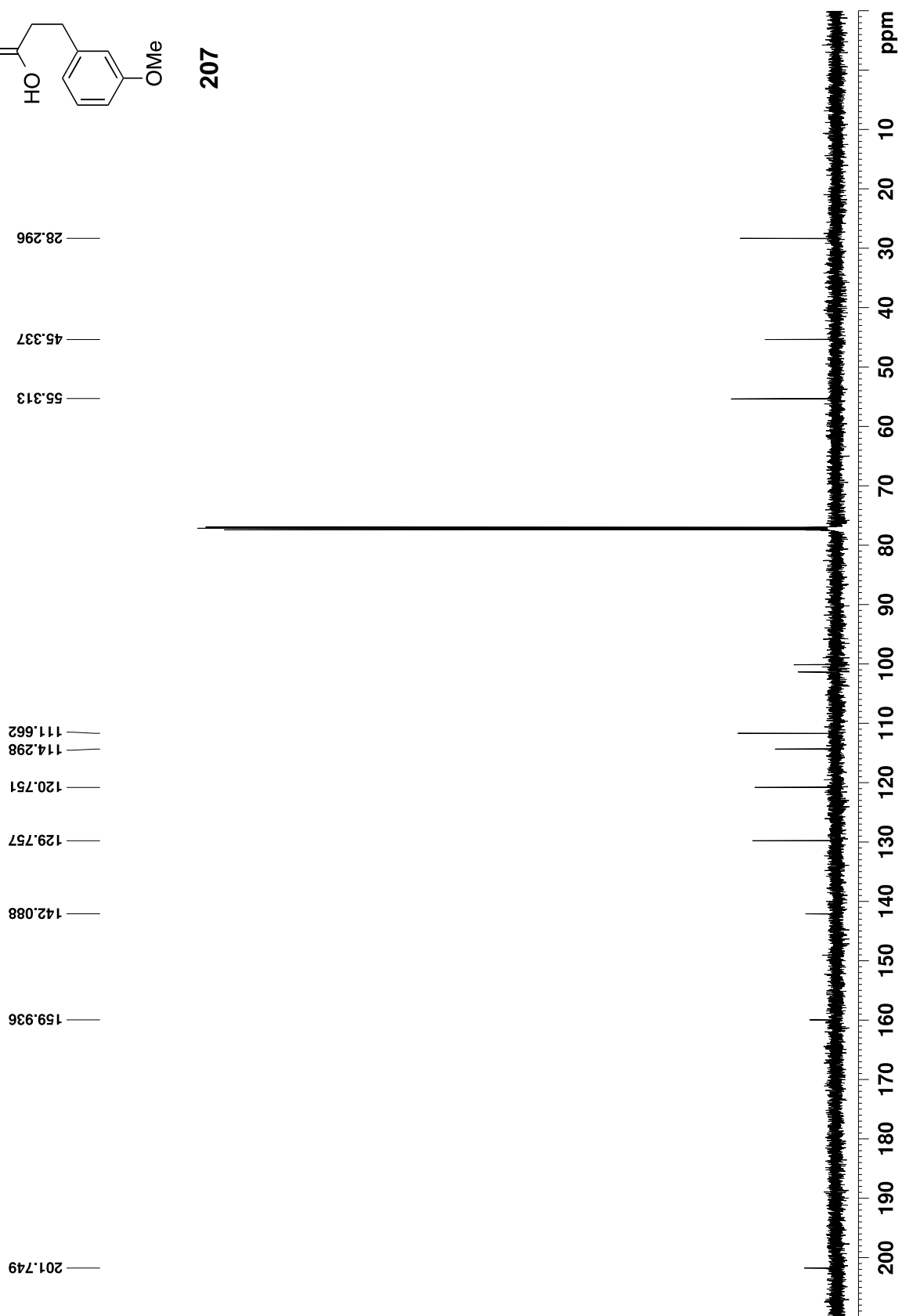


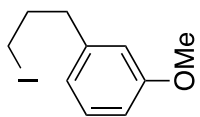
207



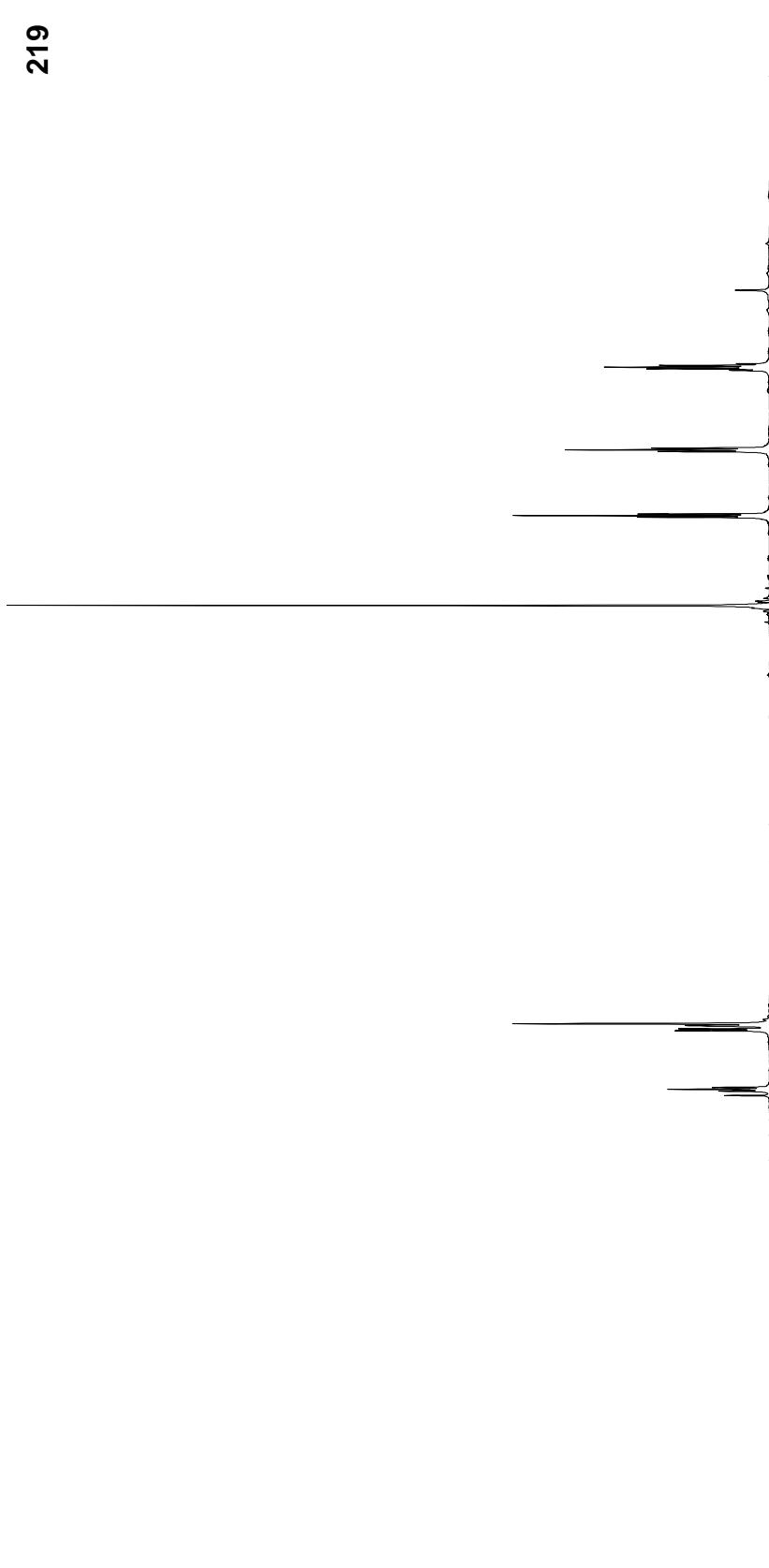


207

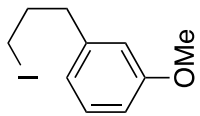




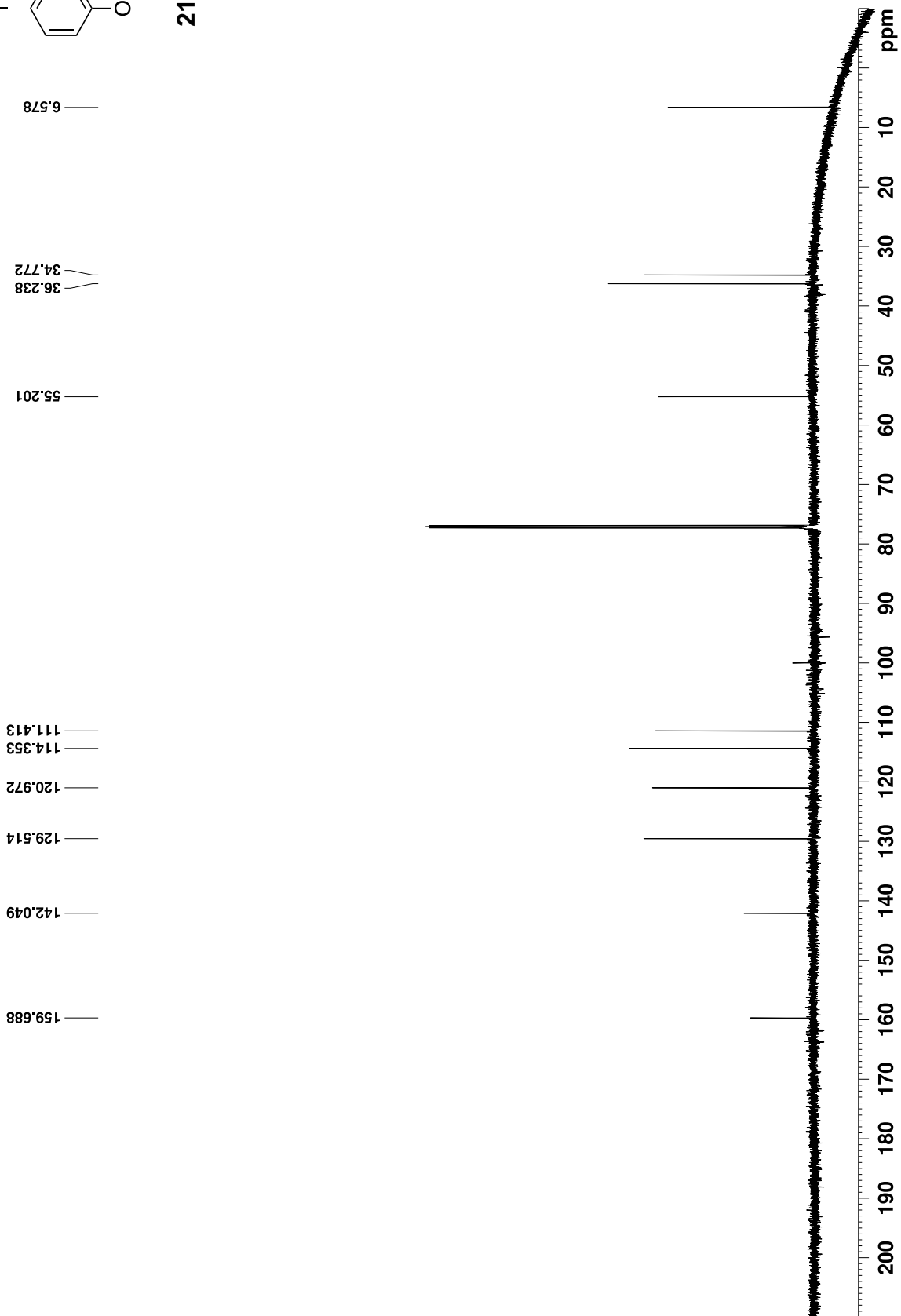
219

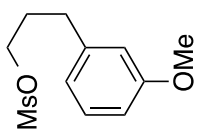


94

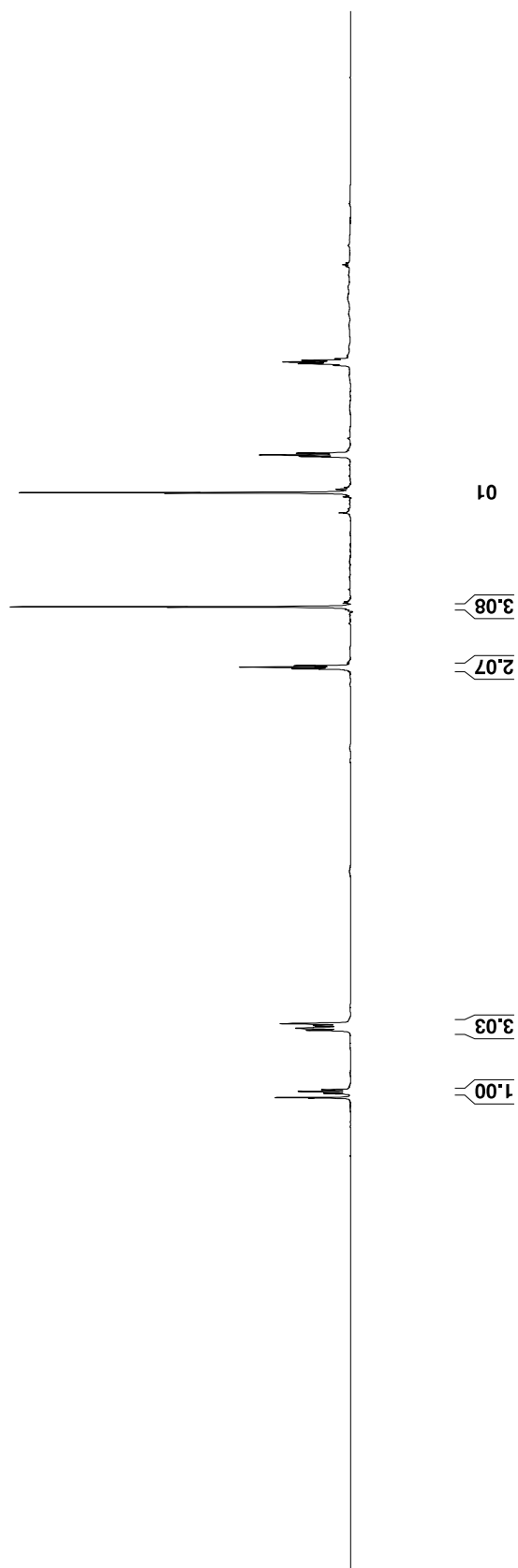


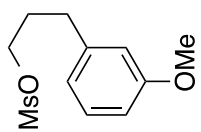
219





220





220

30.658  
31.691  
37.490

55.310

69.241

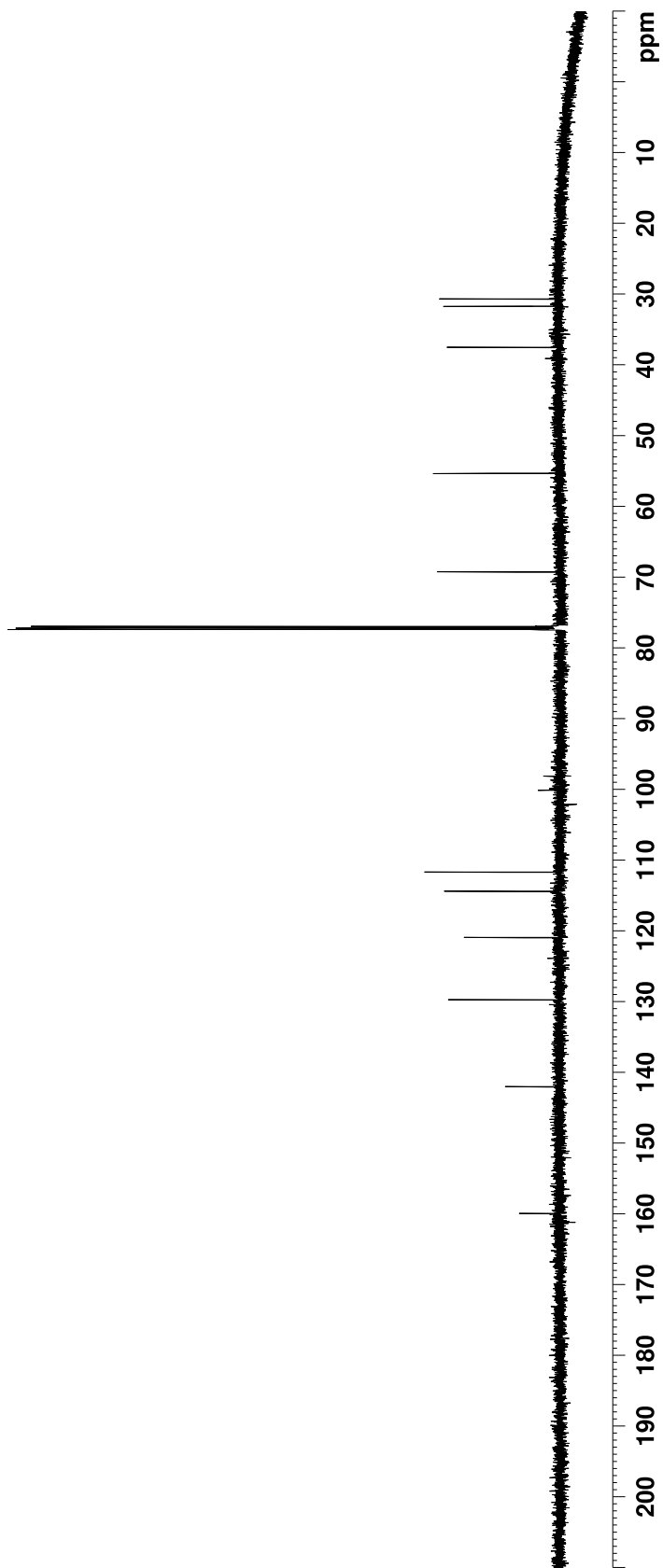
111.682  
114.409

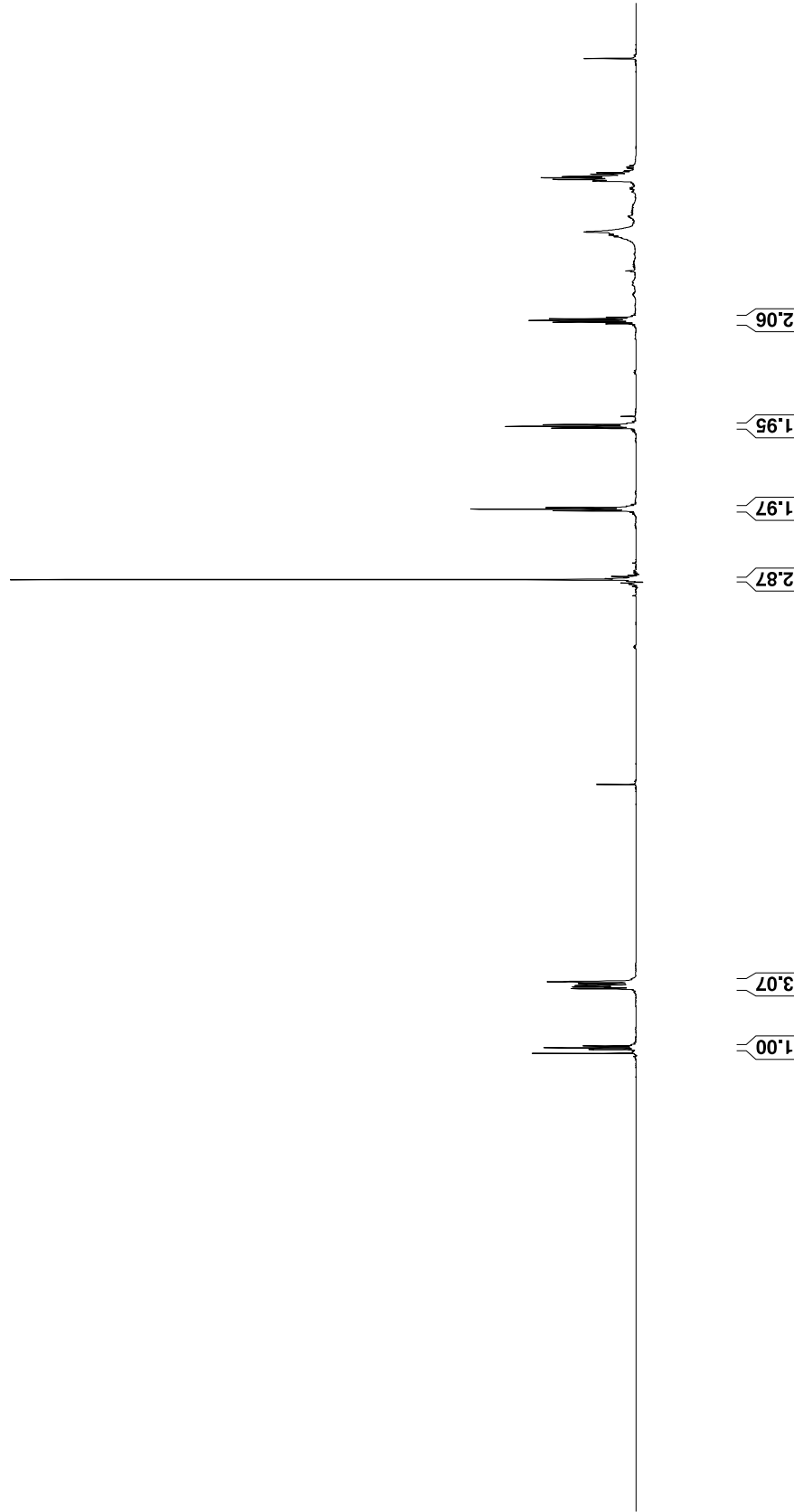
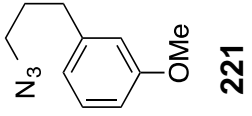
120.933

129.717

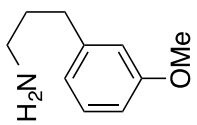
142.017

159.915

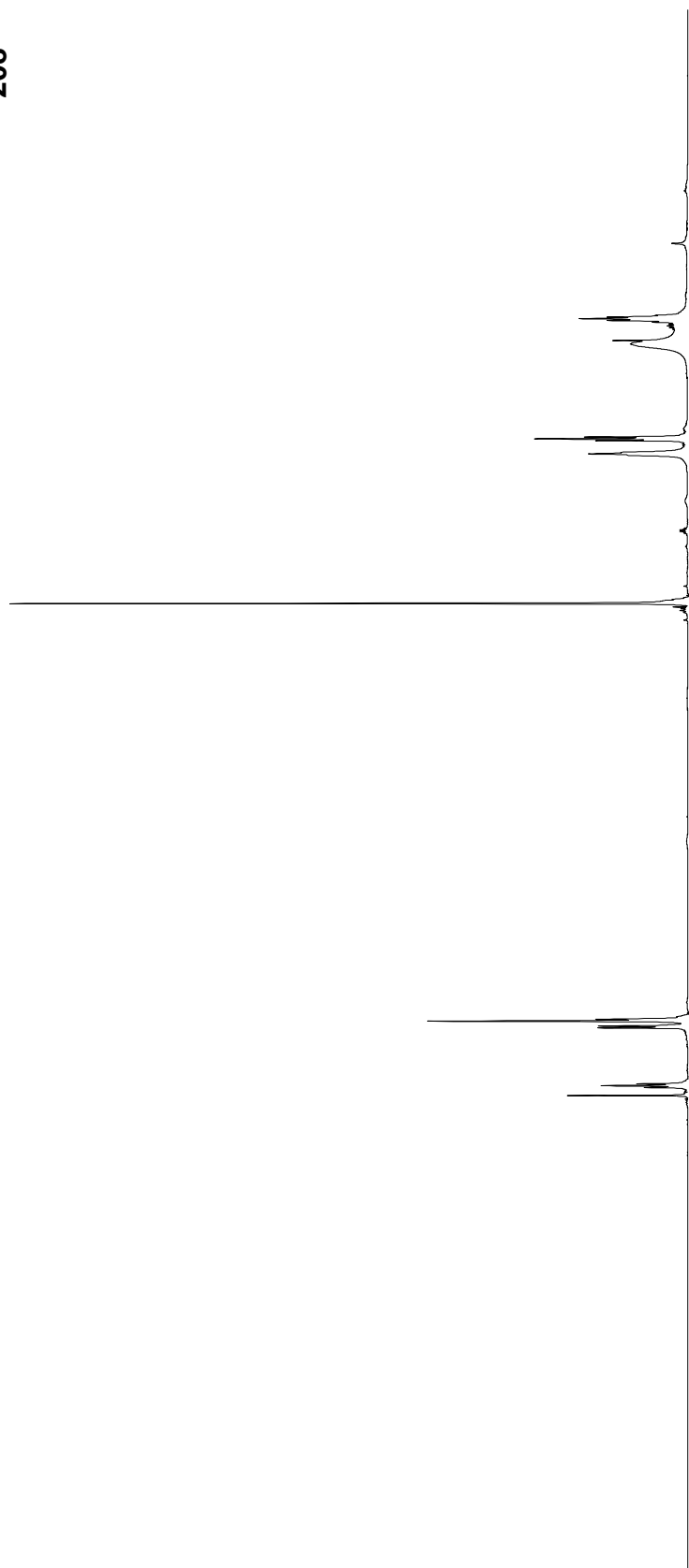




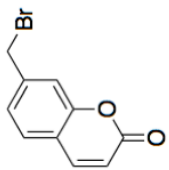
3



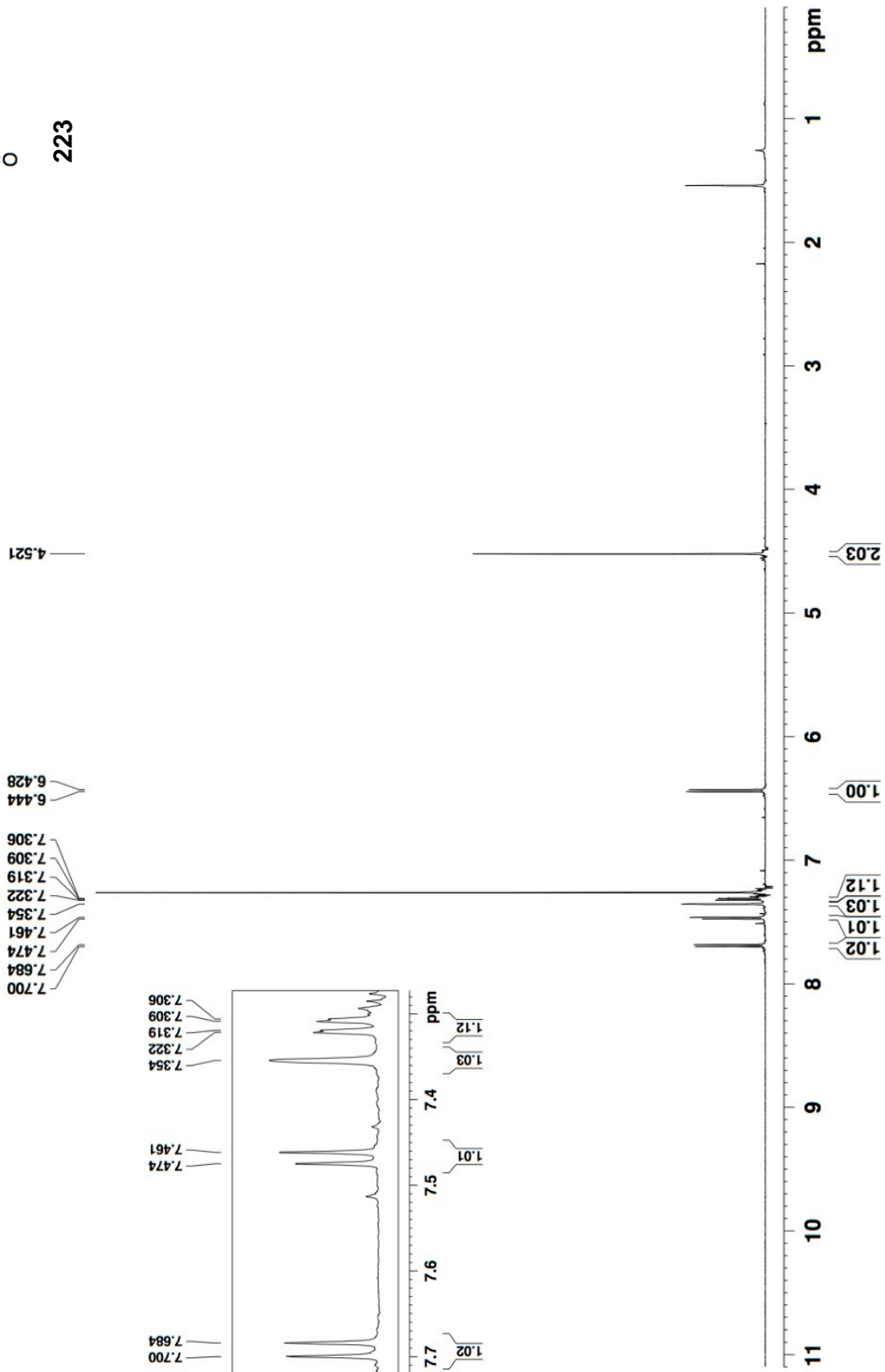
208

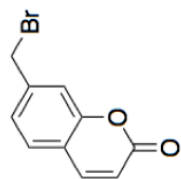


0



223

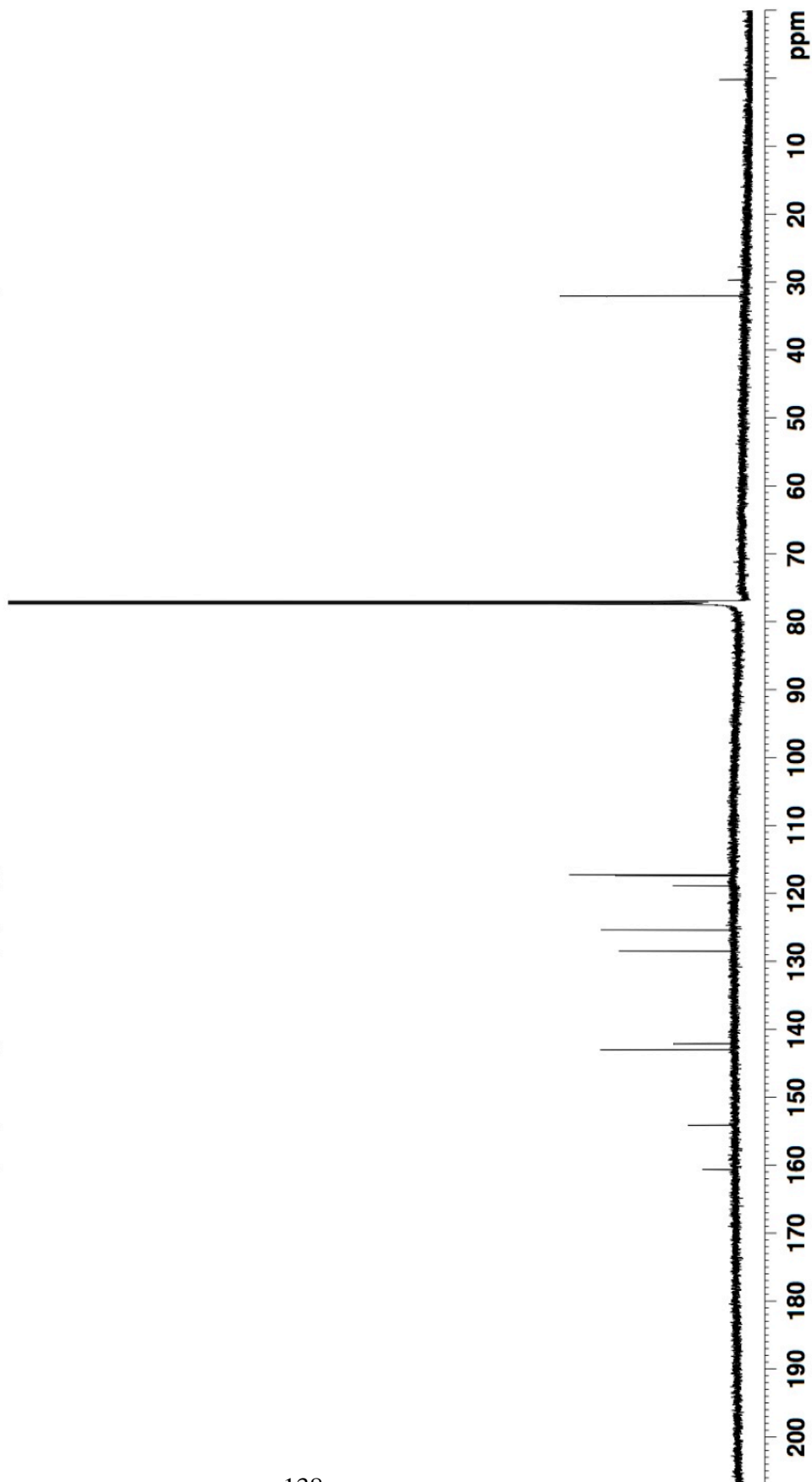


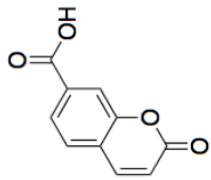


223

31.995

160.627  
154.091  
143.006  
142.095  
128.446  
125.358  
118.817  
117.371  
117.246





209

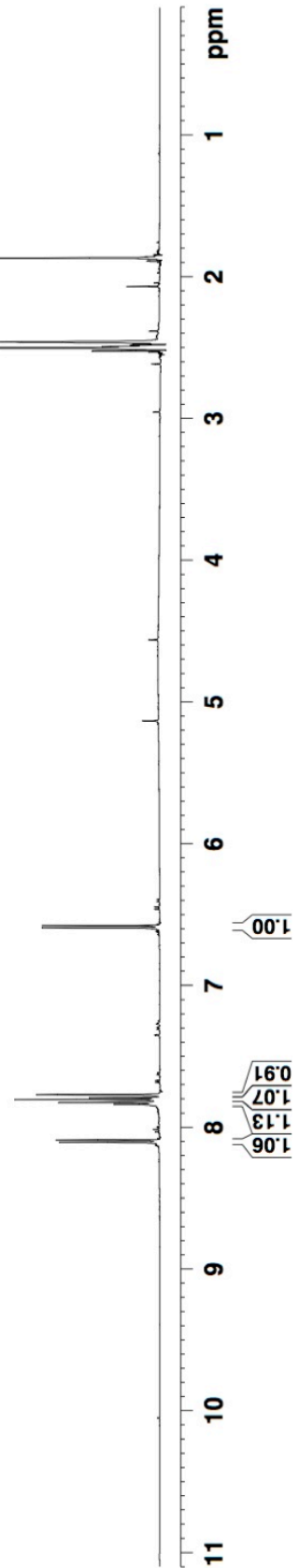
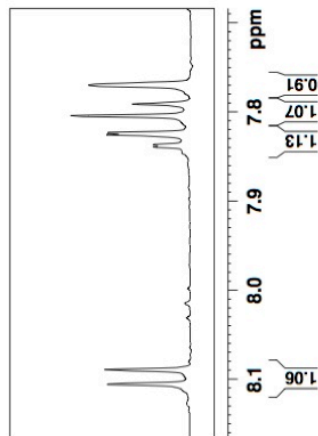
1.866  
2.458  
2.461  
2.464  
2.500

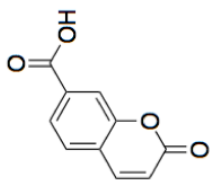
6.577  
6.593

7.770  
7.791  
7.804  
7.824  
7.826  
7.837  
7.839  
8.089  
8.105

7.770  
7.791  
7.804  
7.824  
7.826  
7.837  
7.839

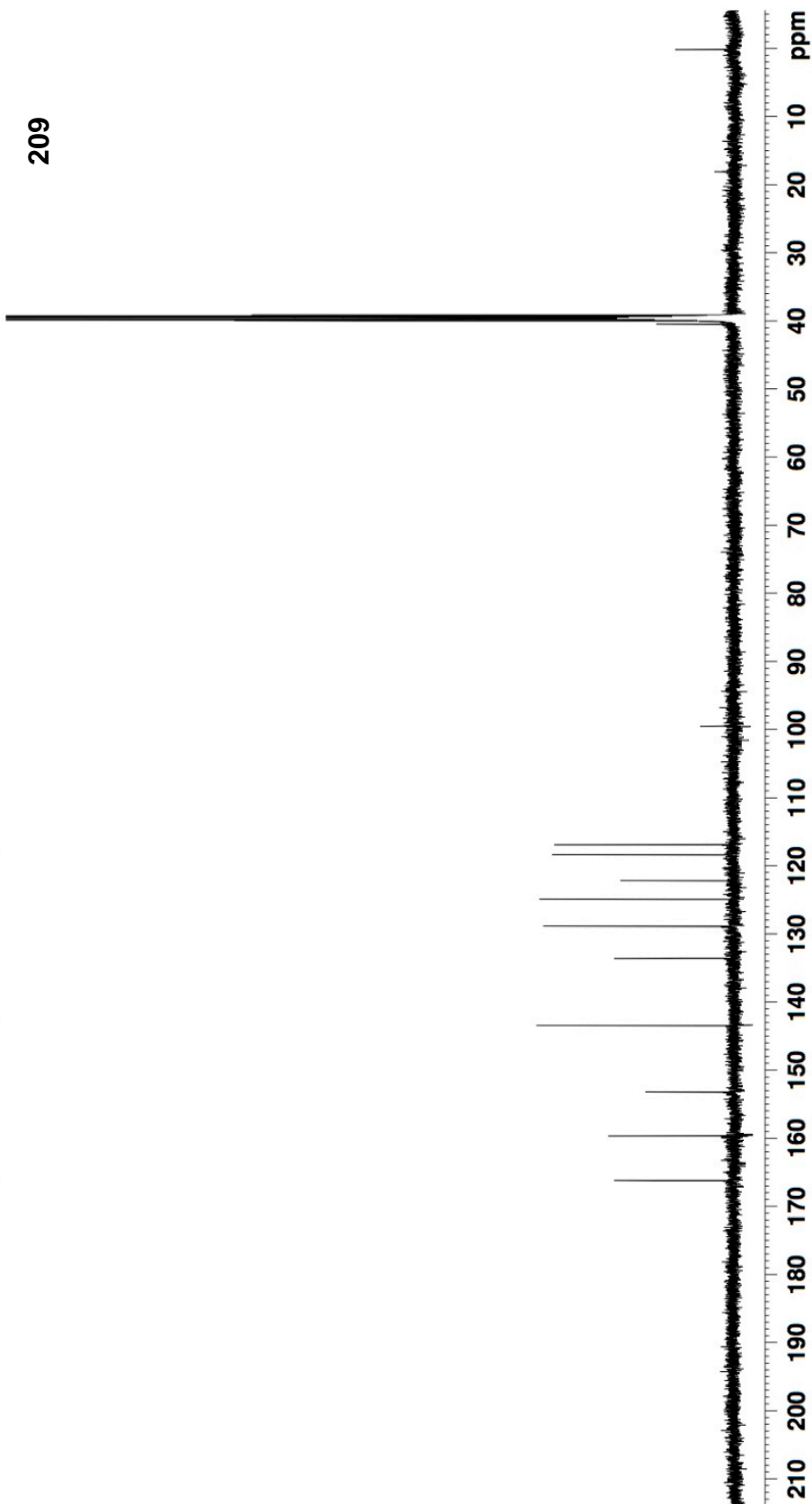
8.089  
8.105

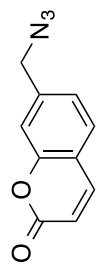




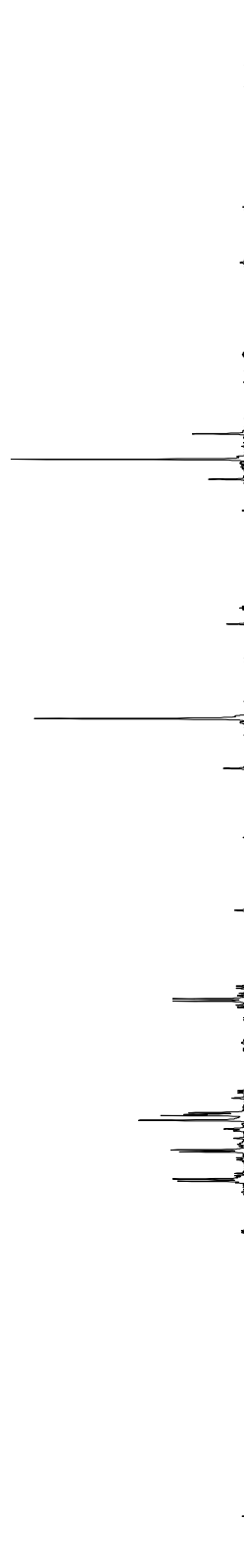
209

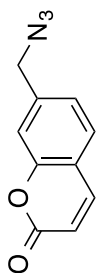
- 116.888
- 118.351
- 122.175
- 124.894
- 128.870
- 133.577
- 143.460
- 153.205
- 159.651
- 166.208





224

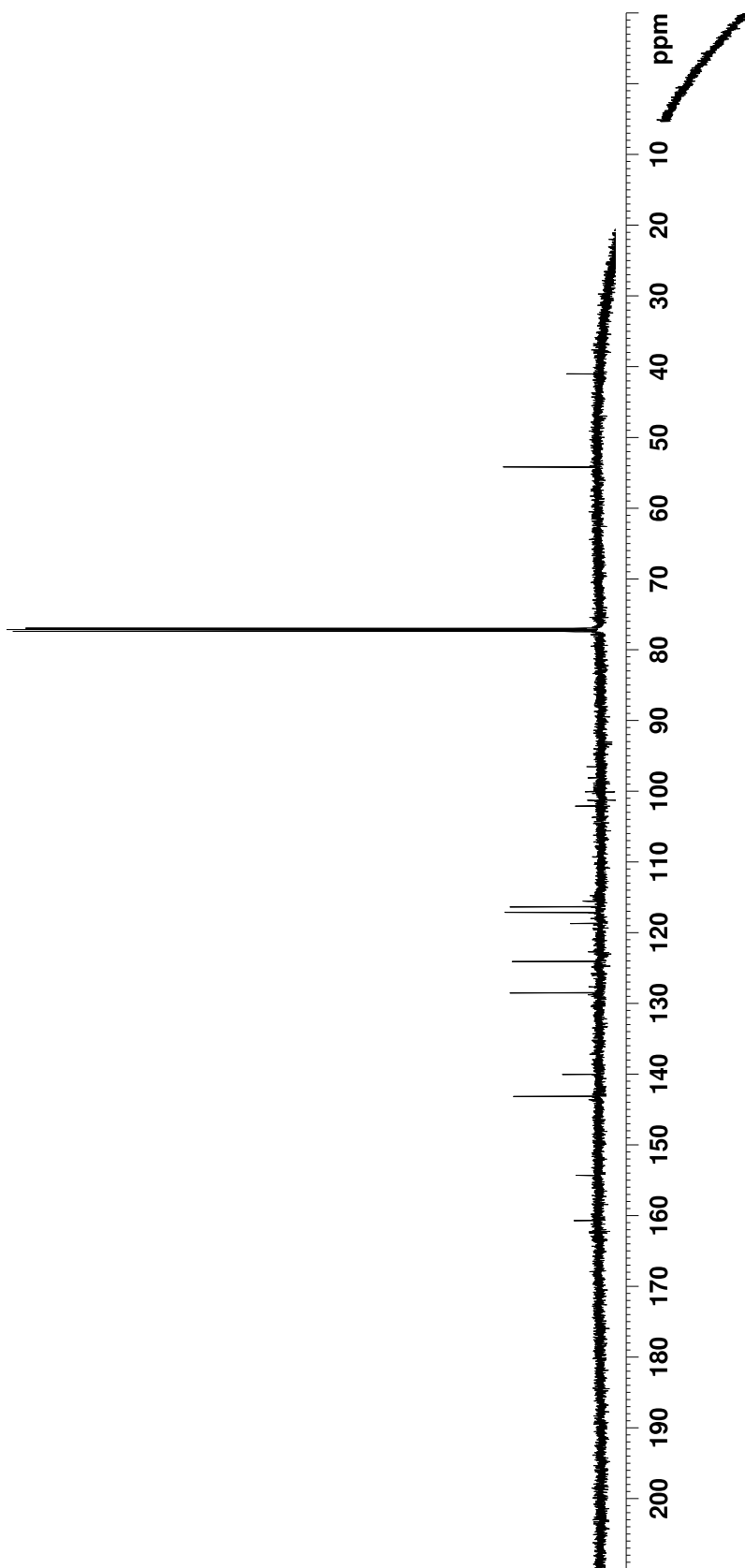


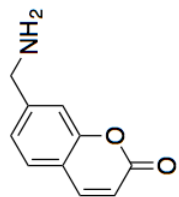


224

54.145

160.702  
154.278  
143.121  
140.022  
128.485  
124.062  
118.654  
117.092  
116.321





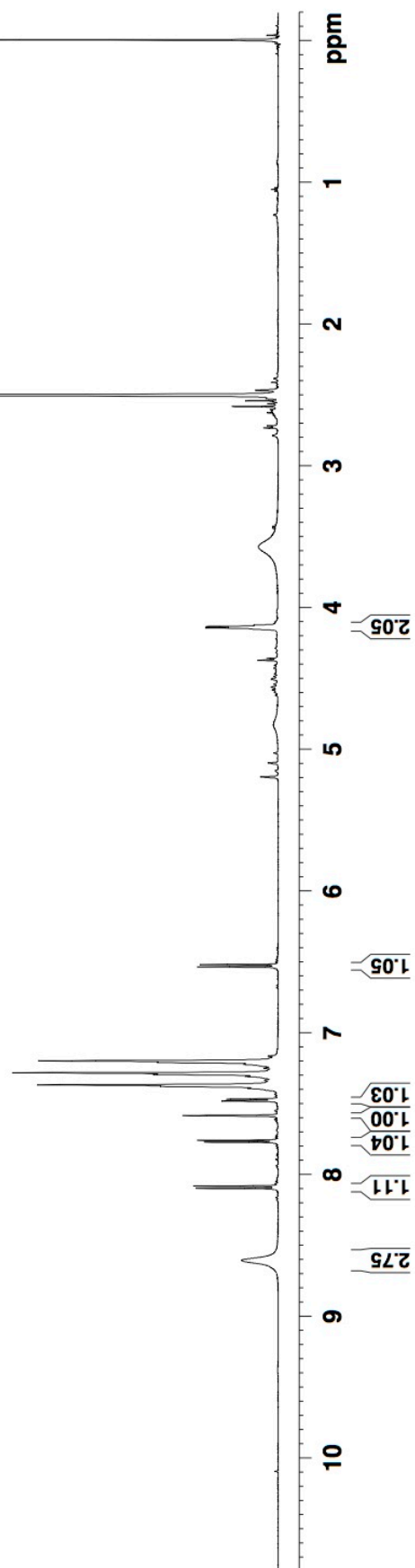
210

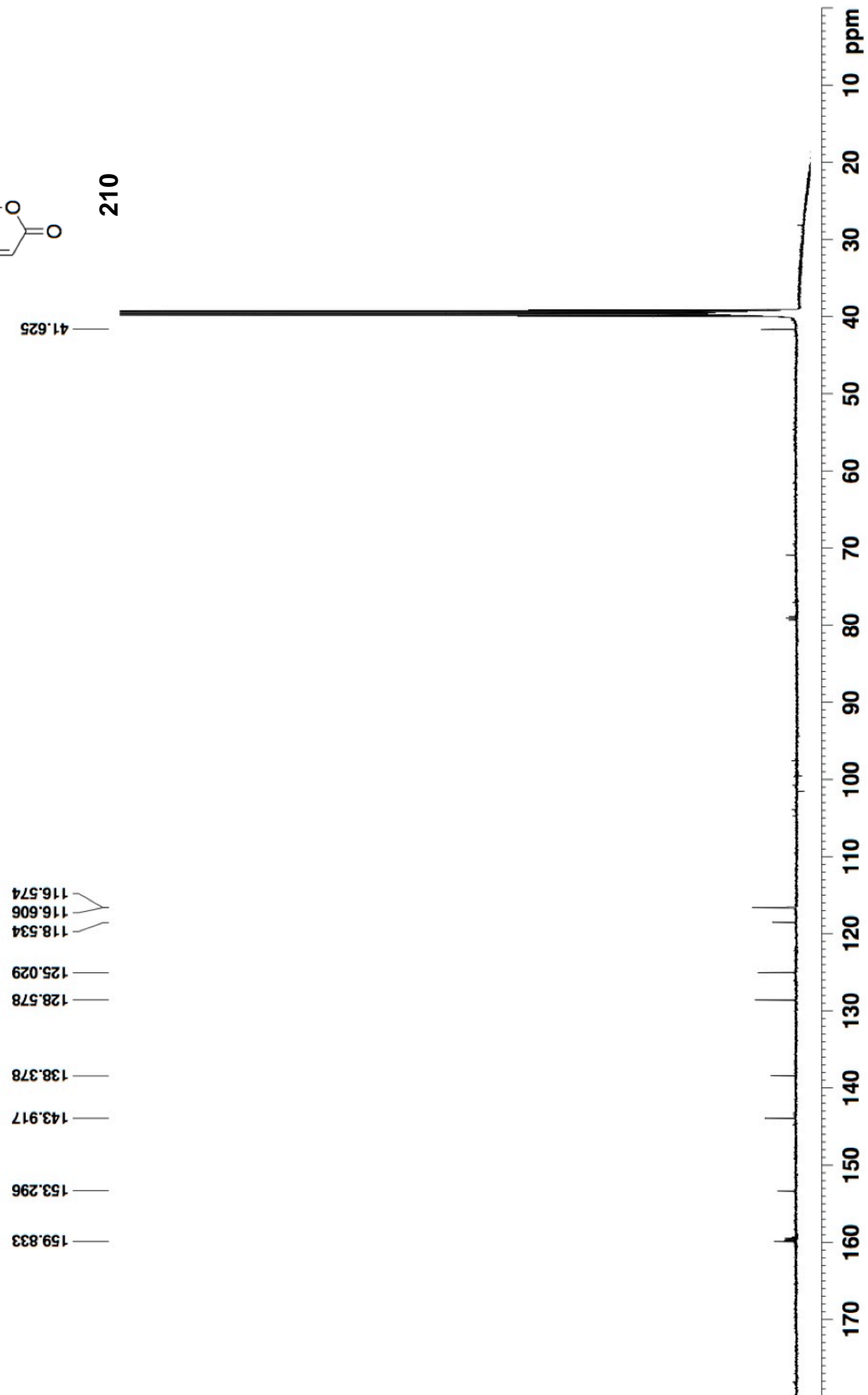
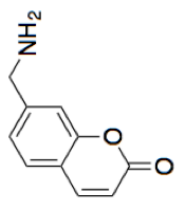
4.152  
4.143  
4.133  
4.124

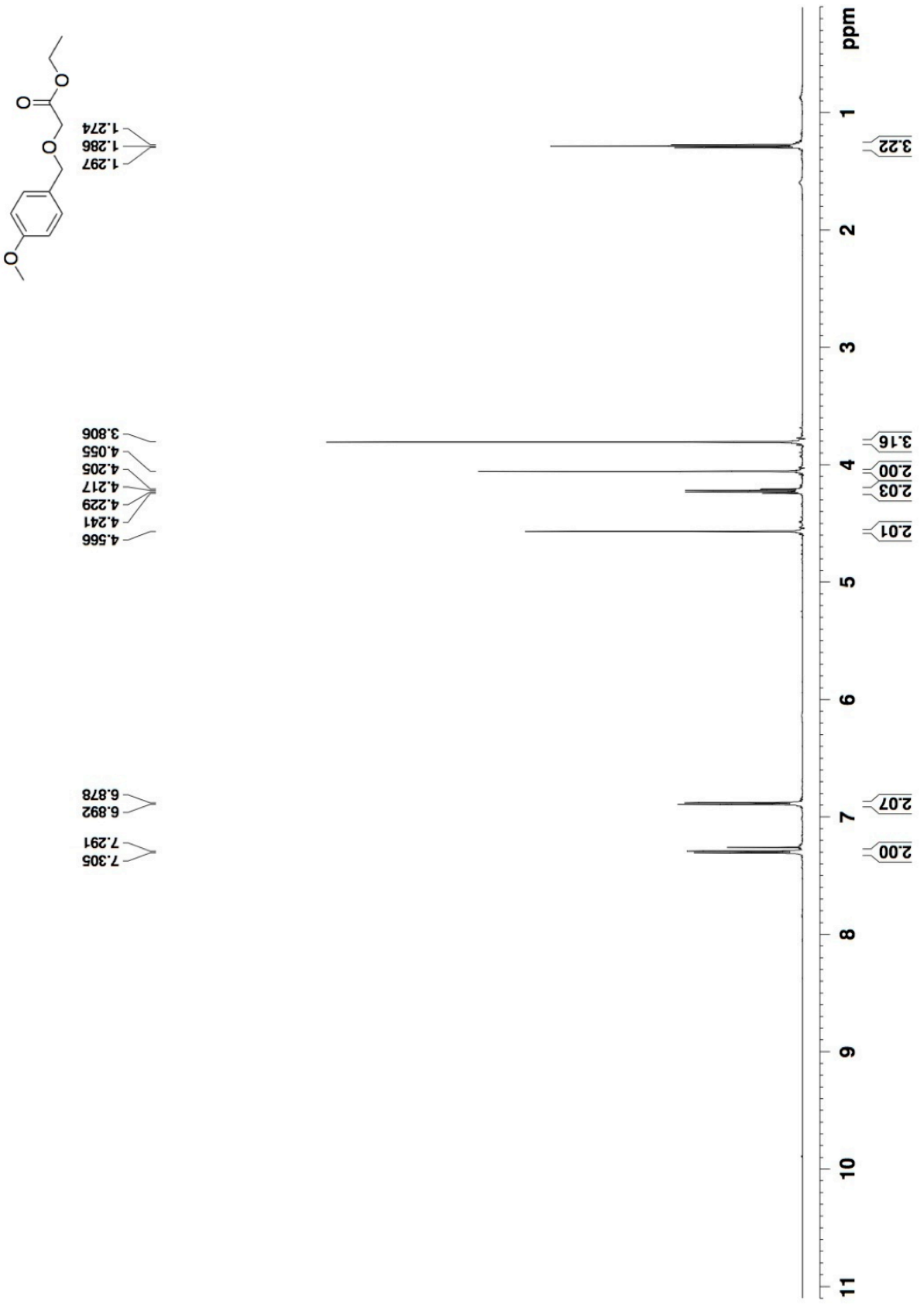
6.535  
6.519

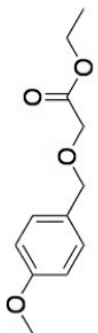
7.468  
7.481  
7.585  
7.758  
7.772  
8.082  
8.098

8.606



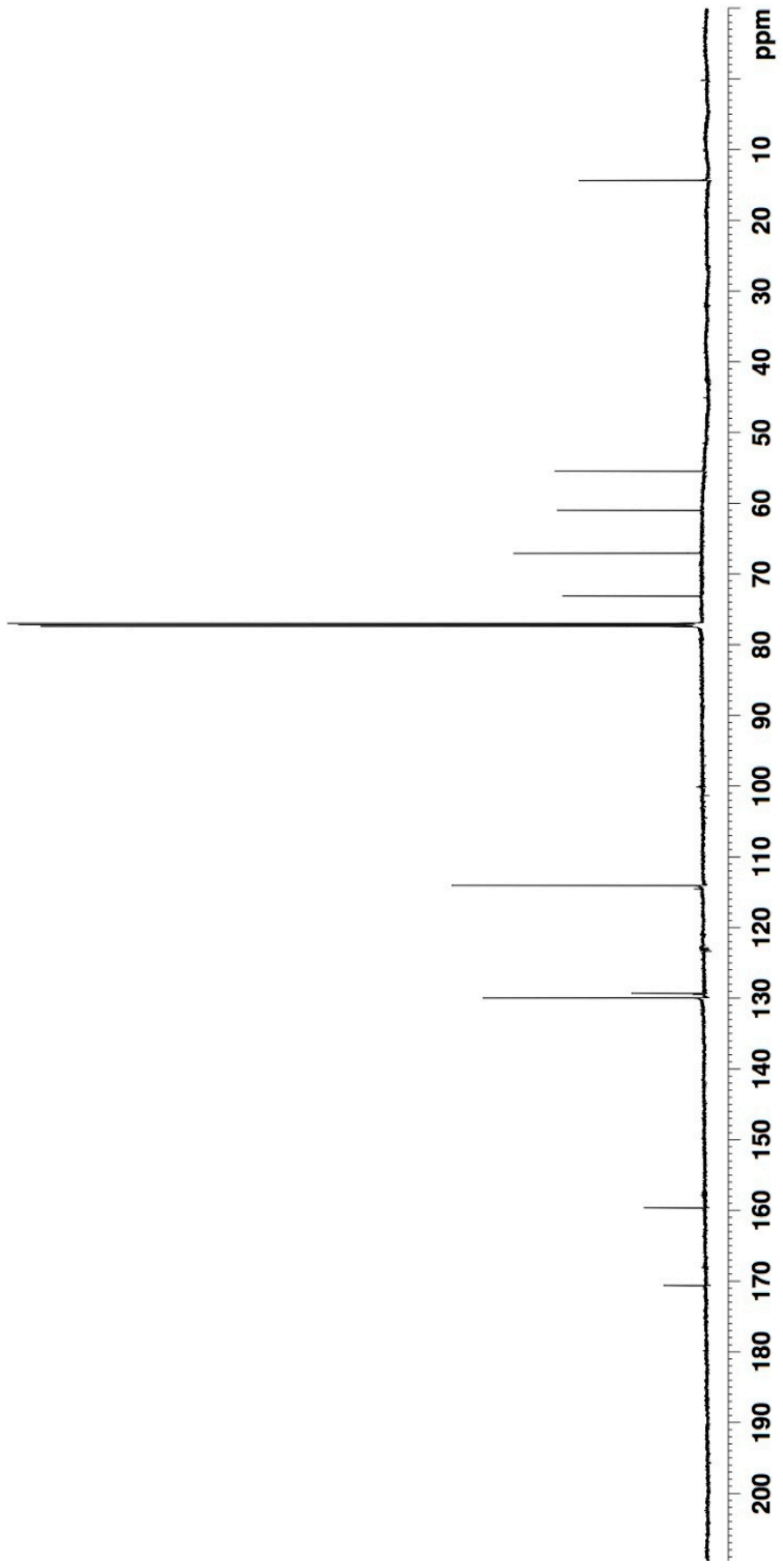


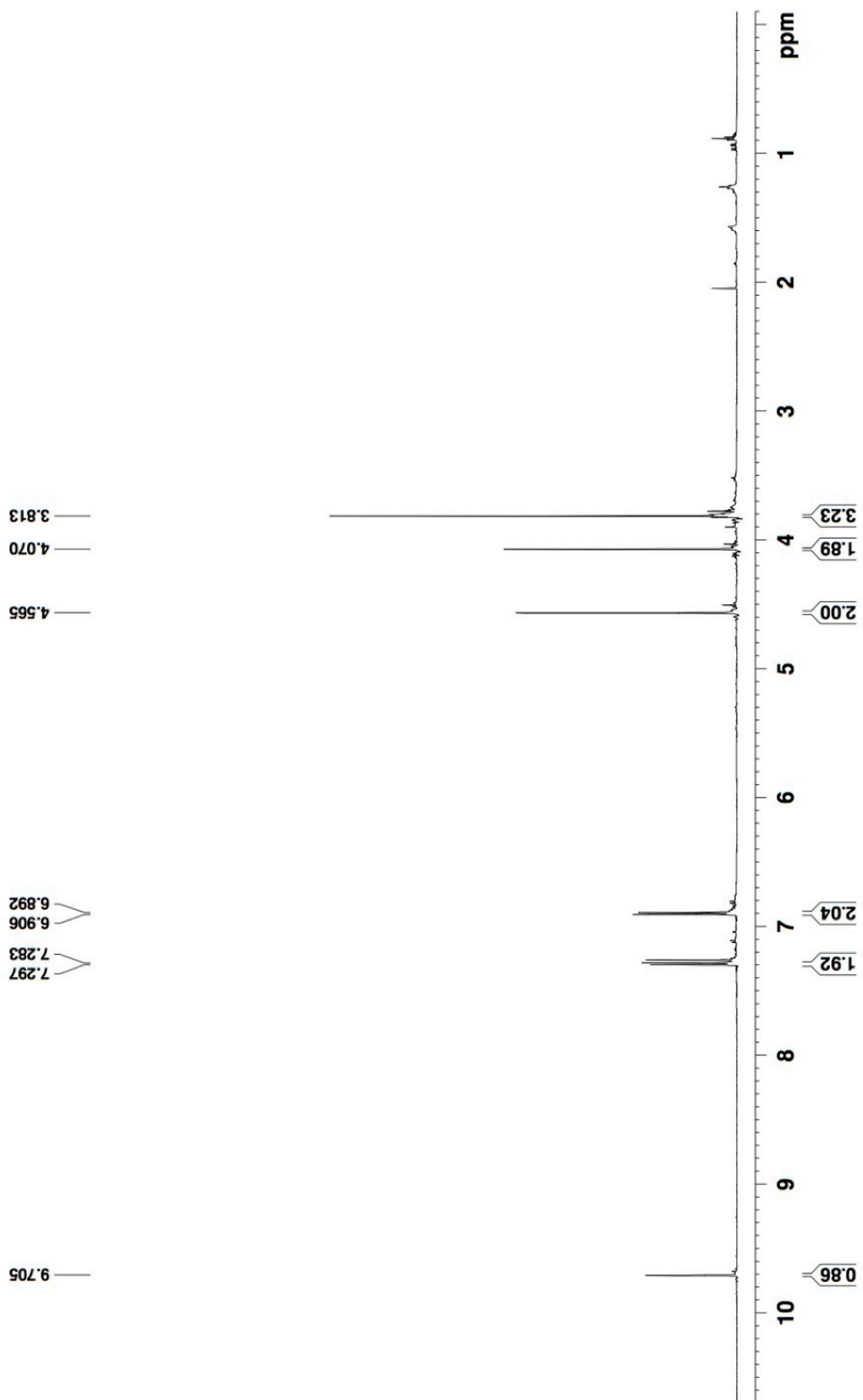
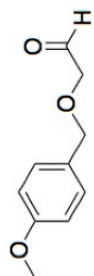


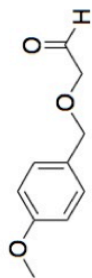


226

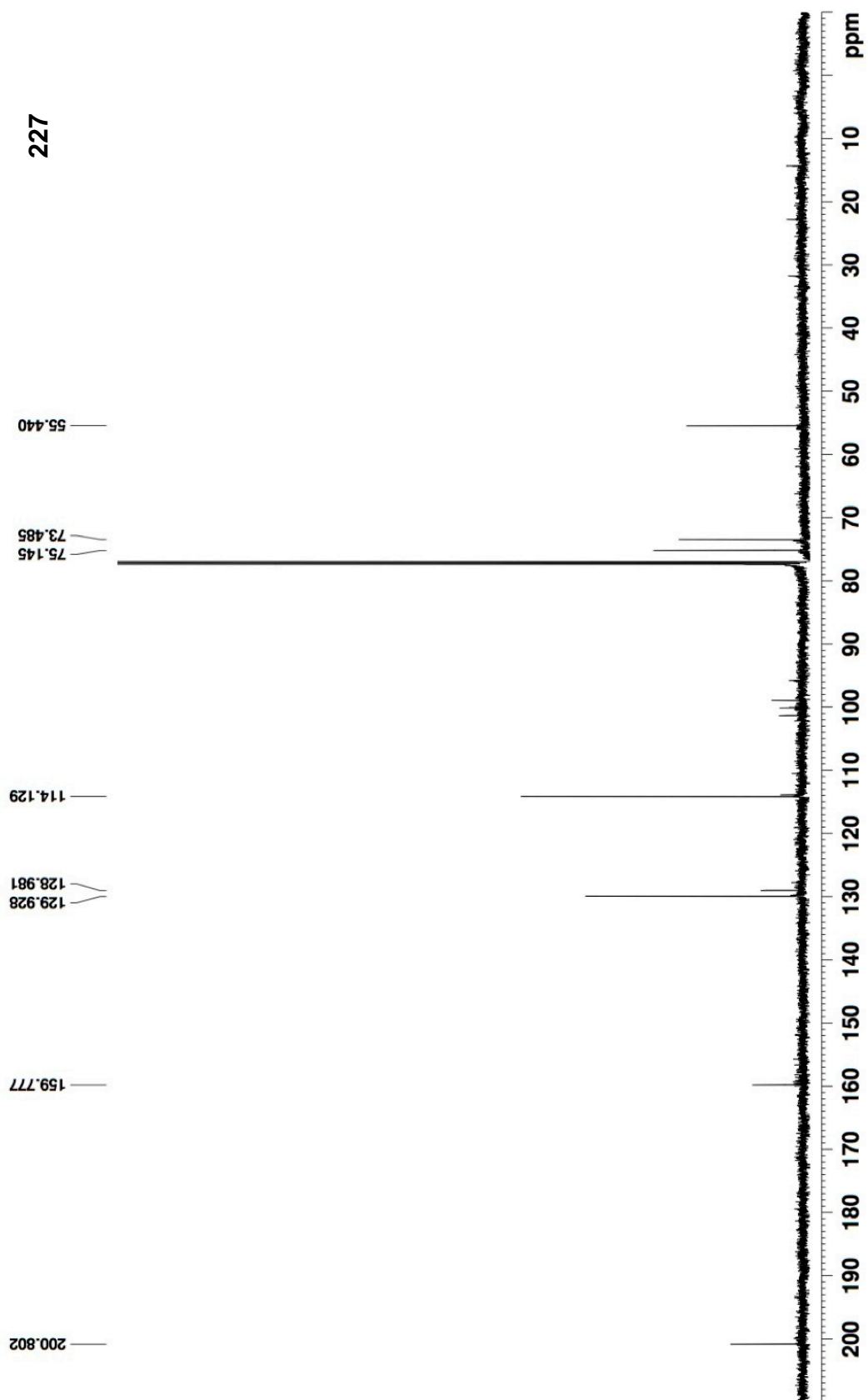
- 14.354
- 55.422
- 60.993
- 67.039
- 73.093
- 114.010
- 129.937
- 129.295
- 159.630
- 170.599

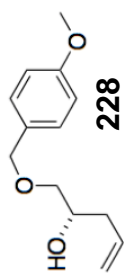




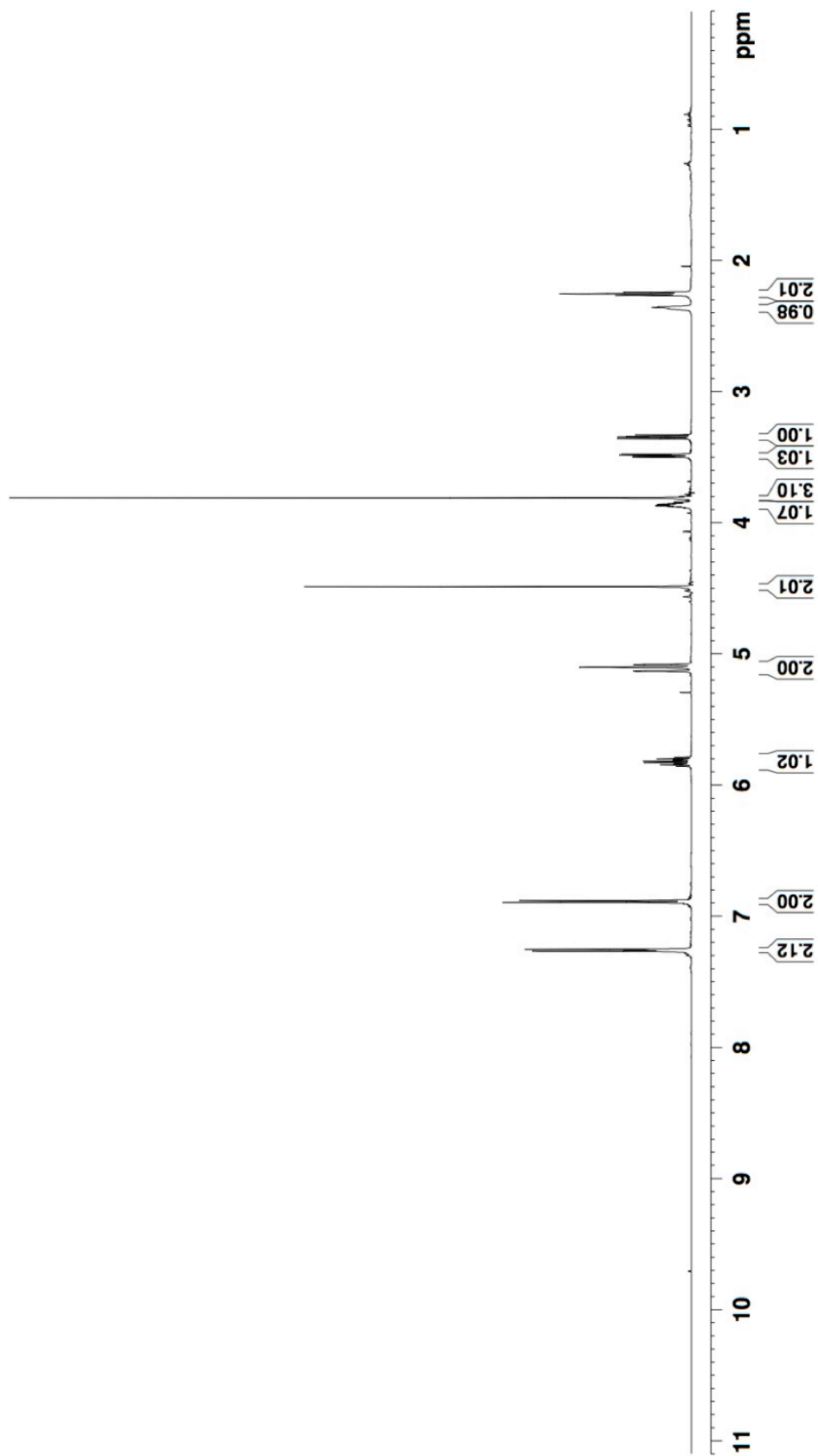


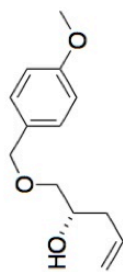
227





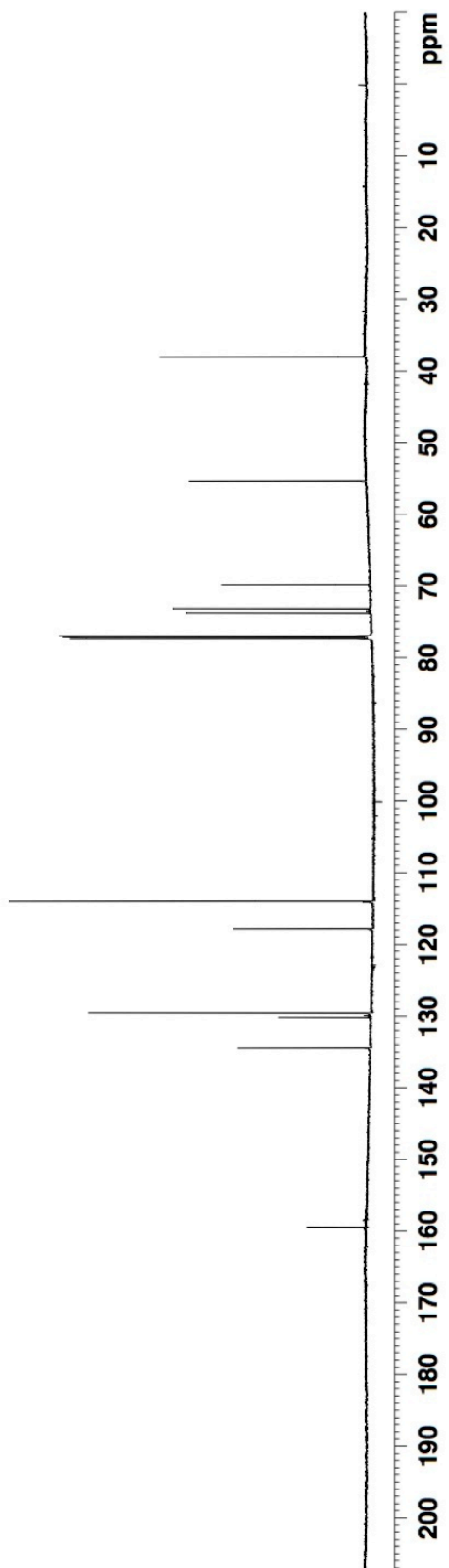
7.267  
7.253  
6.894  
6.880  
5.856  
5.844  
5.839  
5.832  
5.827  
5.816  
5.811  
5.804  
5.799  
5.787  
5.130  
5.127  
5.099  
5.082  
4.485  
3.886  
3.880  
3.874  
3.869  
3.863  
3.857  
3.852  
3.846  
3.840  
3.808  
3.498  
3.492  
3.482  
3.476  
3.358  
3.345  
3.342  
3.330  
2.369  
2.357  
2.352  
2.264  
2.252  
2.241

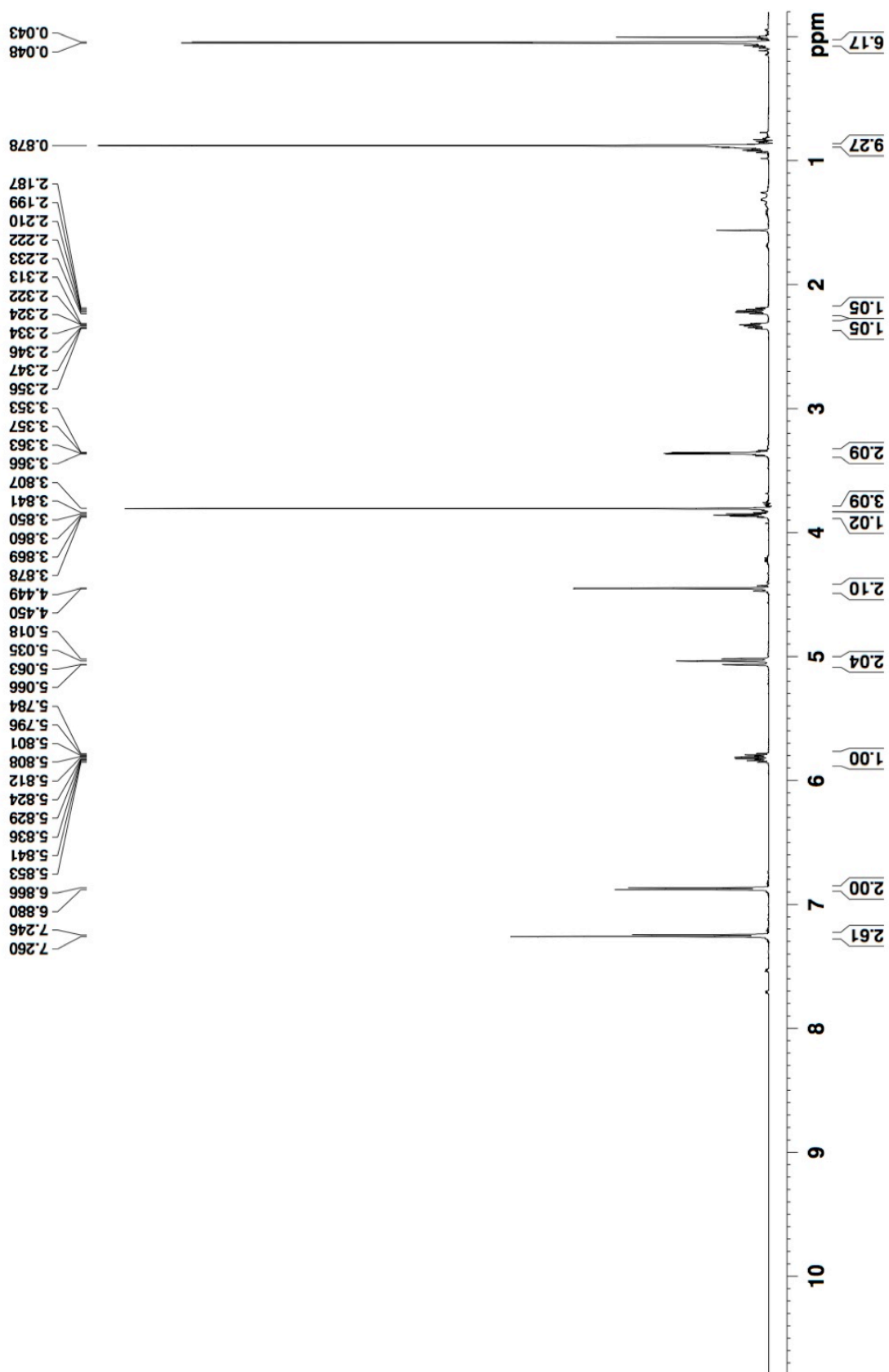
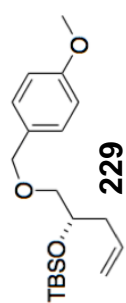




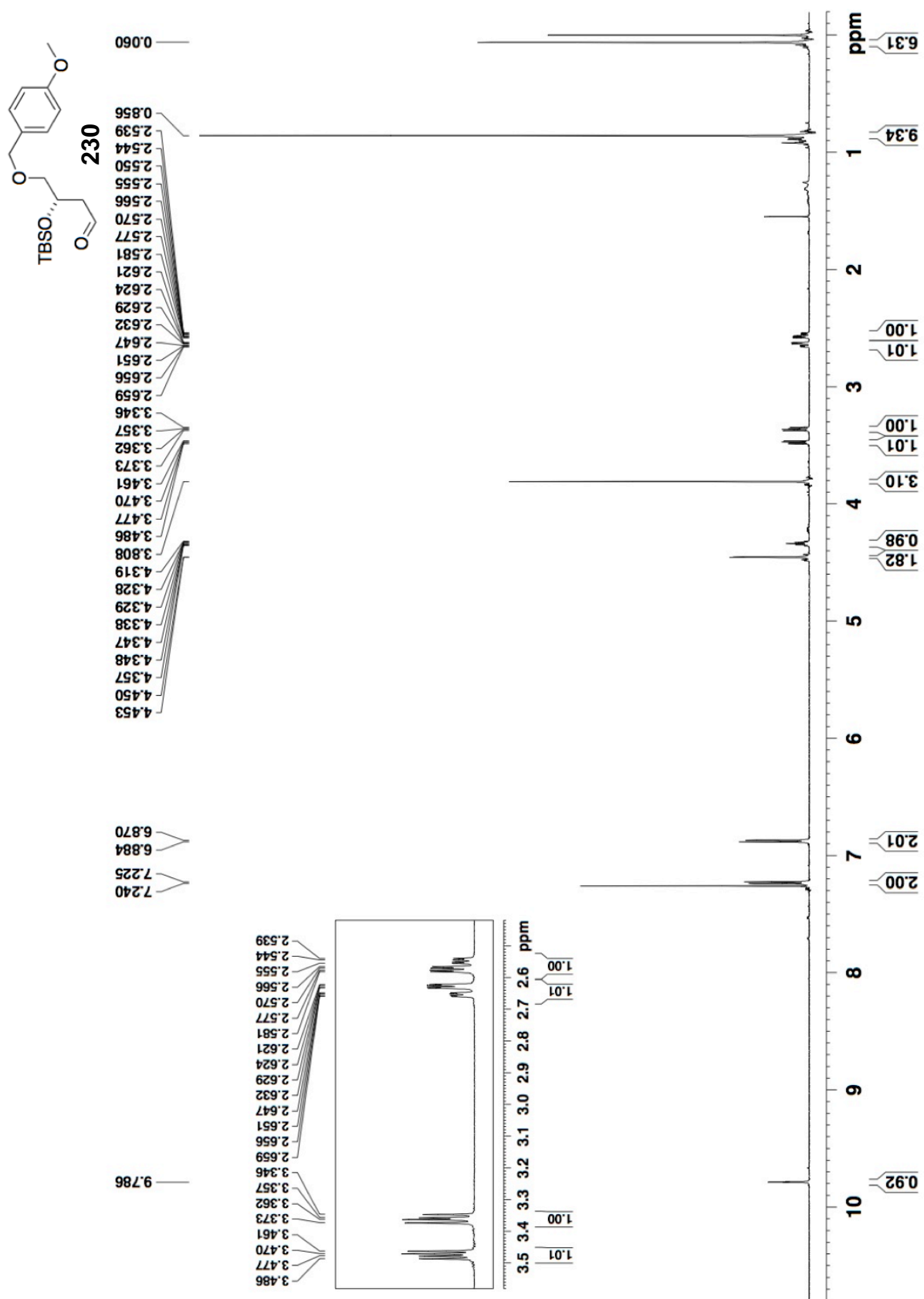
228

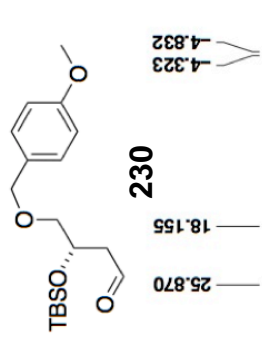
- 38.029
- 55.408
- 69.821
- 73.165
- 73.725
- 113.976
- 117.793
- 129.528
- 130.170
- 134.389
- 159.437



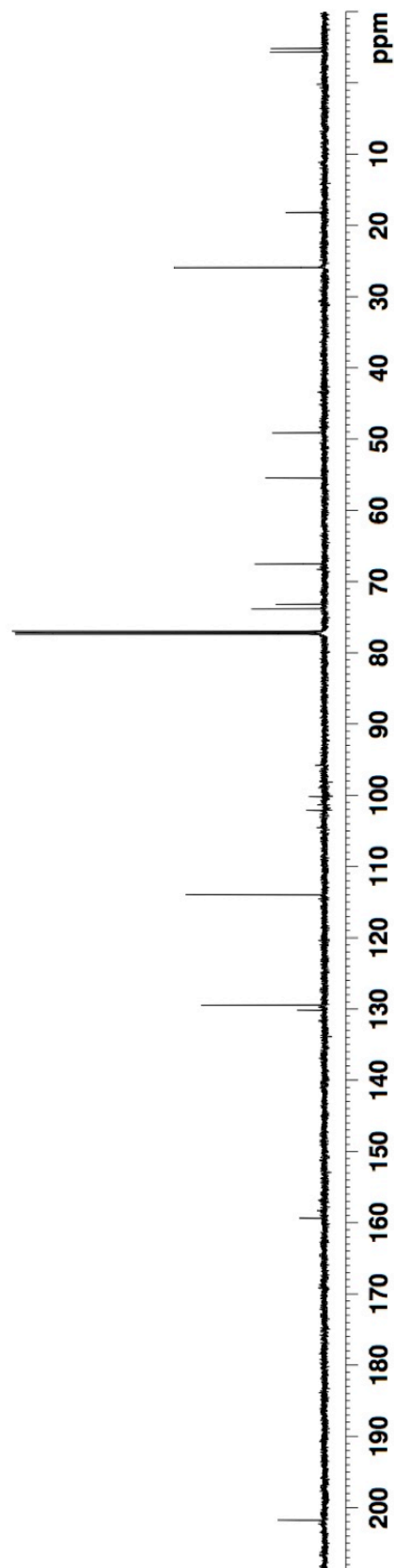




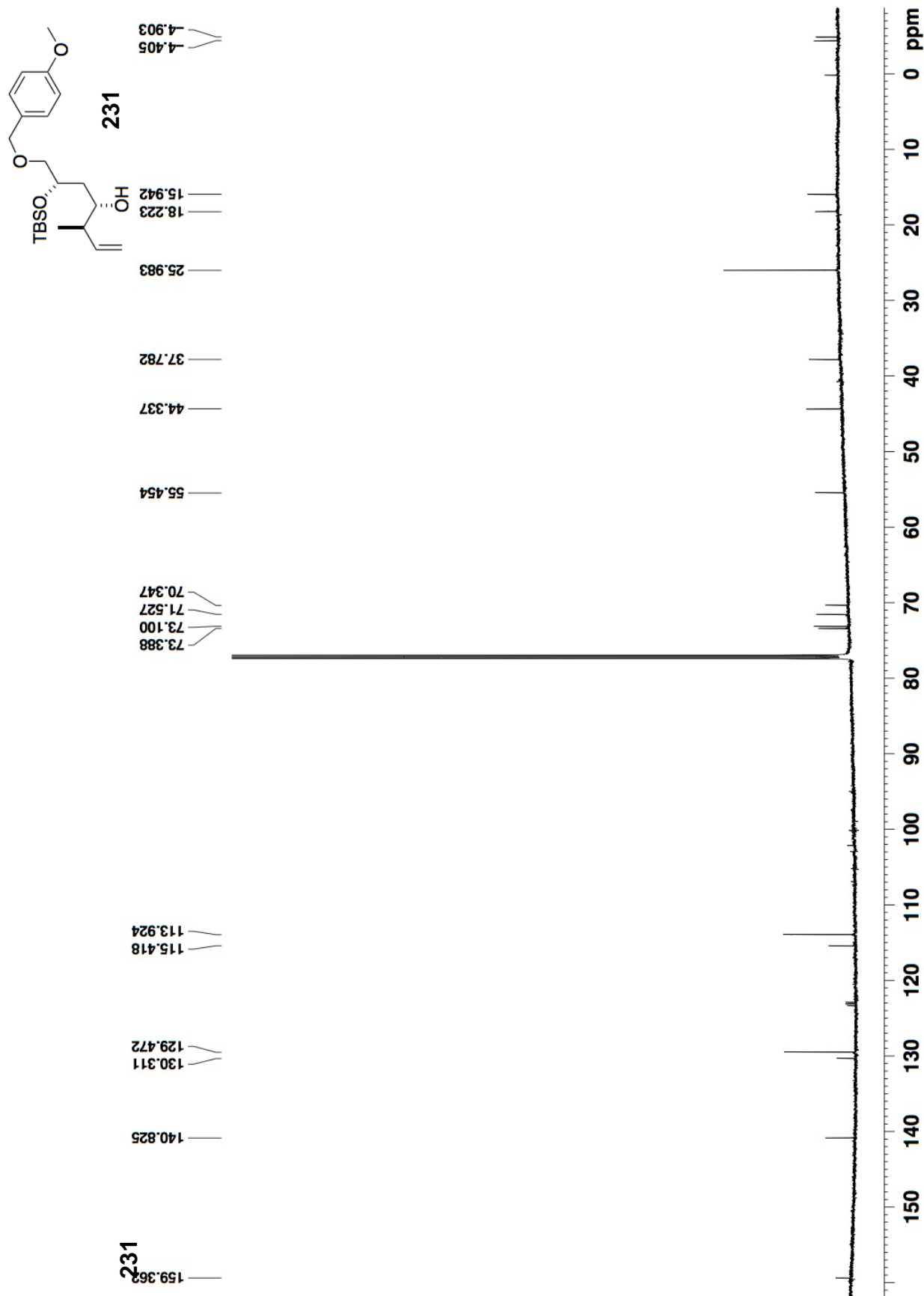


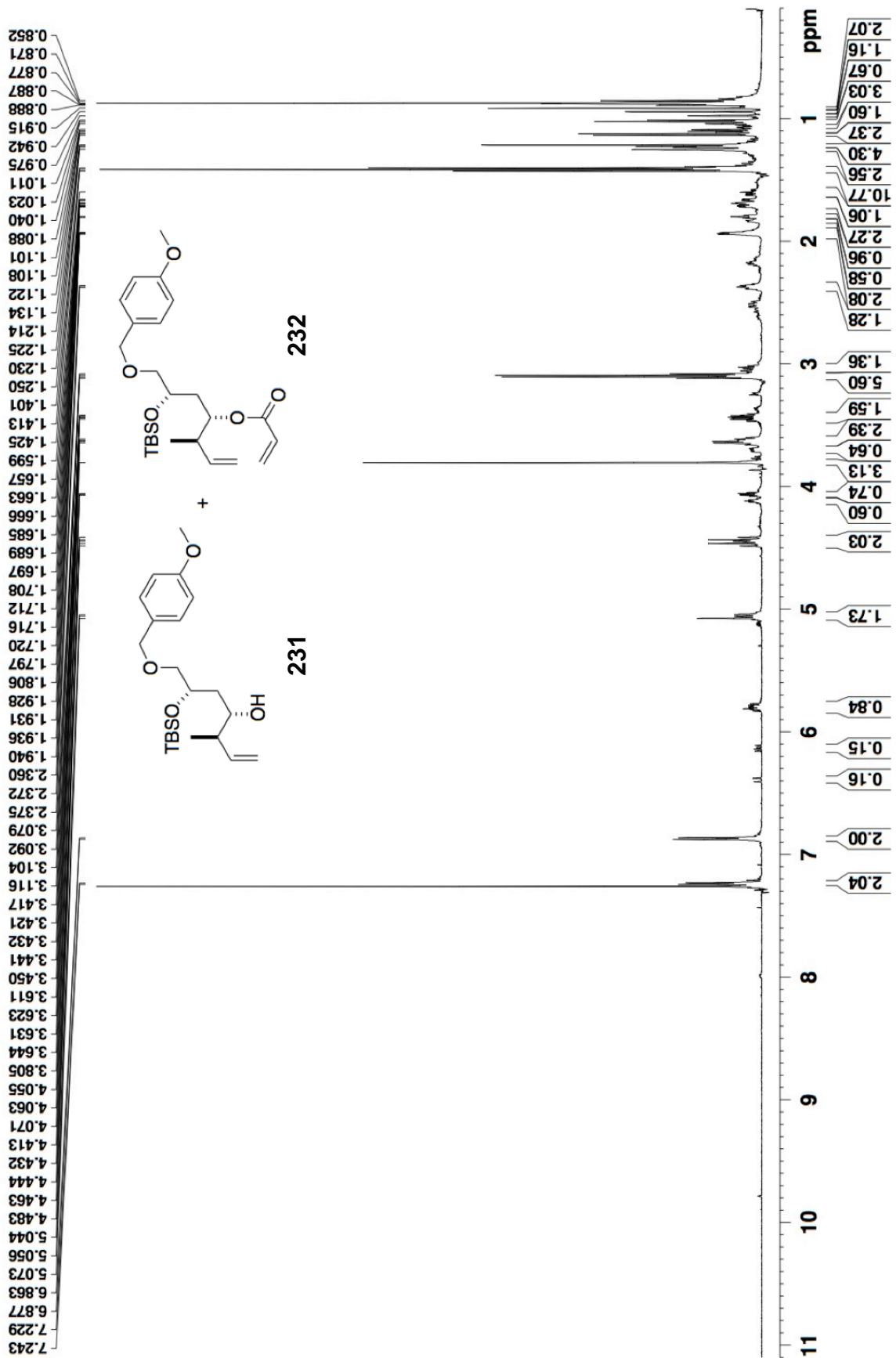


230









## BIBLIOGRAPHY

- (1) Nuijen, B.; Bouma, M.; Manada, C.; Jimeno, J. M.; Schellens, J. H. M.; Bult, A.; Beijnen, J. H. Pharmaceutical Development of Anticancer Agents Derived from Marine Sources. *Anticancer. Drugs* **2000**, *11*, 793–811.
- (2) Gunasekera, S. P.; Gunasekera, M.; Longley, R. E.; Schulte, G. K. Discodermolide: A New Bioactive Polyhydroxylated Lactone from the Marine Sponge *Discodermia Dissoluta*. *J. Org. Chem.* **1990**, *55*, 4912–4915.
- (3) Longley, R. E.; Caddigan, D.; Harmody, D.; Gunasekera, M.; Gunasekera, S. P. Discodermolide-A New, Marine-Derived Immunosuppressive Compound: II. in Vivo Studies. *Transplantation* **1991**, *52*, 656–661.
- (4) Longley, R. E.; Caddigan, D.; Harmody, D.; Gunasekera, M.; Gunasekera, S. P. Discodermolide-A New, Marine-Derived Immunosuppressive Compound: I. in Vitro Studies. *Transplantation* **1991**, *52*, 650–655.
- (5) Longley, R. E.; Gunasekera, S. P.; Faherty, D.; McLane, J.; Dumont, F. Immunosuppression by Discodermolide. *Ann. N. Y. Acad. Sci.* **1993**, *696*, 94–107.
- (6) Alberts, B.; Johnson, A.; Lewis, J.; Raff, M.; Roberts, K.; Walter, P. *Molecular Biology of the Cell*; Garland Science Taylor & Francis Group, 2002.
- (7) Hung, D. T.; Nerenberg, J. B.; Schreiber, S. L. Syntheses of Discodermolides Useful for Investigating Microtubule Binding and Stabilization. *J. Am. Chem. Soc.* **1996**, *118*, 11054–11080.
- (8) Ter Haar, E.; Kowalski, R. J.; Hamel, E.; Lin, C. M.; Longley, R. E.; Gunasekera, S. P.; Rosenkranz, H. S.; Day, B. W. Discodermolide, A Cytotoxic Marine Agent That Stabilizes Microtubules More Potently Than Taxol. *Biochemistry* **1996**, *35*, 243–250.
- (9) Kowalski, R. J.; Giannakakou, P.; Gunasekera, S. P.; Longley, R. E.; Day, B. W.; Hamel, E. The Microtubule-Stabilizing Agent Discodermolide Competitively Inhibits the Binding of Paclitaxel (Taxol) to Tubulin Polymers, Enhances Tubulin Nucleation Reactions More Potently than Paclitaxel, and Inhibits the Growth of Paclitaxel-Resistant Cells. *Mol. Pharmacol.* **1997**, *52*, 613–622.

- (10) Mita, A.; Lockhart, A. C.; Chen, T.-L.; Bochinski, K.; Curtright, J.; Cooper, W.; Hammond, L.; Rothenberg, M.; Rowinsky, E.; Sharma, S. A Phase I Pharmacokinetic (PK) Trial of XAA296A (Discodermolide) Administered Every 3 Wks to Adult Patients with Advanced Solid Malignancies. *ASCO Meet. Abstr.* **2004**, *22*, 2025.
- (11) Fan, Y.; Schreiber, E. M.; Day, B. W. Human Liver Microsomal Metabolism of (+)-Discodermolide. *J. Nat. Prod.* **2009**, *72*, 1748–1754.
- (12) Akhmanova, A.; Steinmetz, M. O. Tracking the Ends: A Dynamic Protein Network Controls the Fate of Microtubule Tips. *Nat. Rev. Mol. Cell Biol.* **2008**, *9*, 309+.
- (13) Zhai, Y.; Kronebusch, P. J.; Simon, P. M.; Borisy, G. G. Microtubule Dynamics at the G2/M Transition: Abrupt Breakdown of Cytoplasmic Microtubules at Nuclear Envelope Breakdown and Implications for Spindle Morphogenesis. *J. Cell Biol.* **1996**, *135*, 201–214.
- (14) Pepperkok, R.; Bré, M. H.; Davoust, J.; Kreis, T. E. Microtubules Are Stabilized in Confluent Epithelial Cells but Not in Fibroblasts. *J. Cell Biol.* **1990**, *111*, 3003–3012.
- (15) Rusan, N. M.; Fagerstrom, C. J.; Yvon, A.-M. C.; Wadsworth, P. Cell Cycle-Dependent Changes in Microtubule Dynamics in Living Cells Expressing Green Fluorescent Protein-A Tubulin. *Mol. Biol. Cell* **2001**, *12*, 971–980.
- (16) Jordan, M. A.; Wilson, L. Microtubules as a Target for Anticancer Drugs. *Nat. Rev. Cancer* **2004**, *4*, 253–265.
- (17) Jordan, M. A.; Thrower, D.; Wilson, L. Mechanism of Inhibition of Cell Proliferation by Vinca Alkaloids. *Cancer Res.* **1991**, *51*, 2212–2222.
- (18) Jordan, M. A. Mechanism of Action of Antitumor Drugs That Interact with Microtubules and Tubulin. *Curr. Med. Chem. Anti-Cancer Agents* **2002**, *2*, 1–17.
- (19) Na, G. C.; Timasheff, S. N. Stoichiometry of the Vinblastine-Induced Self-Association of Calf Brain Tubulin. *Biochemistry* **1980**, *19*, 1347–1354.
- (20) Yang, H.; Ganguly, A.; Cabral, F. Inhibition of Cell Migration and Cell Division Correlates with Distinct Effects of Microtubule Inhibiting Drugs. *J. Biol. Chem.* **2010**, *285*, 32242–32250.
- (21) Nogales, E.; Grayer Wolf, S.; Khan, I. A.; Luduena, R. F.; Downing, K. H. Structure of Tubulin at 6.5 Å and Location of the Taxol-Binding Site. *Nature* **1995**, *375*, 424–427.
- (22) Khrapunovich-Baine, M.; Menon, V.; Verdier-Pinard, P.; Smith, A. B.; Angeletti, R. H.; Fiser, A.; Horwitz, S. B.; Xiao, H. Distinct Pose of Discodermolide in Taxol Binding Pocket Drives a Complementary Mode of Microtubule Stabilization. *Biochemistry* **2009**, *48*, 11664–11677.

- (23) Derry, W. B.; Wilson, L.; Jordan, M. A. Substoichiometric Binding of Taxol Suppresses Microtubule Dynamics. *Biochemistry* **1995**, *34*, 2203–2211.
- (24) Minguez, J. M.; Giuliano, K. A.; Balachandran, R.; Madiraju, C.; Curran, D. P.; Day, B. W. Synthesis and High Content Cell-Based Profiling of Simplified Analogues of the Microtubule Stabilizer (+)-Discodermolide 1 Supported by National Cancer Institute Grant CA78039. 1. *Mol. Cancer Ther.* **2002**, *1*, 1305–1313.
- (25) Harbor Branch Oceanographic Institute. Sponges, Medicine, and the Nobel Chemistry Connection <http://www.fau.edu/hboi/disco.php> (accessed Dec 7, 2011).
- (26) Hung, D. T.; Chen, J.; Schreiber, S. L. (+)-Discodermolide Binds to Microtubules in Stoichiometric Ratio to Tubulin Dimers, Blocks Taxol Binding and Results in Mitotic Arrest. *Chem. Biol.* **1996**, *3*, 287–293.
- (27) Martello, L. A.; McDaid, H. M.; Regl, D. L.; Yang, C.-P. H.; Meng, D.; Pettus, T. R. R.; Kaufman, M. D.; Arimoto, H.; Danishefsky, S. J.; Smith, A. B.; et al. Taxol and Discodermolide Represent a Synergistic Drug Combination in Human Carcinoma Cell Lines. *Clin. Cancer Res.* **2000**, *6*, 1978–1987.
- (28) Honore, S.; Kamath, K.; Braguer, D.; Wilson, L.; Briand, C.; Jordan, M. A. Suppression of Microtubule Dynamics by Discodermolide by a Novel Mechanism Is Associated with Mitotic Arrest and Inhibition of Tumor Cell Proliferation. *Mol. Cancer Ther.* **2003**, *2*, 1303–1311.
- (29) Gonçalves, A.; Braguer, D.; Kamath, K.; Martello, L.; Briand, C.; Horwitz, S.; Wilson, L.; Jordan, M. A. Resistance to Taxol in Lung Cancer Cells Associated with Increased Microtubule Dynamics. *Proc. Natl. Acad. Sci.* **2001**, *98*, 11737–11742.
- (30) Canales, A.; Rodríguez-Salarichs, J.; Trigili, C.; Nieto, L.; Coderch, C.; Andreu, J. M.; Paterson, I.; Jiménez-Barbero, J.; Díaz, J. F. Insights into the Interaction of Discodermolide and Docetaxel with Tubulin. Mapping the Binding Sites of Microtubule-Stabilizing Agents by Using an Integrated NMR and Computational Approach. *ACS Chem. Biol.* **2011**, *6*, 789–799.
- (31) Buey, R. M.; Calvo, E.; Barasoain, I.; Pineda, O.; Edler, M. C.; Matesanz, R.; Cerezo, G.; Vanderwal, C. D.; Day, B. W.; Sorensen, E. J.; et al. Cyclostreptin Binds Covalently to Microtubule Pores and Luminal Taxoid Binding Sites. *Nat. Chem. Biol.* **2007**, *3*, 117–125.
- (32) Buey, R. M.; Barasoain, I.; Jackson, E.; Meyer, A.; Giannakakou, P.; Paterson, I.; Mooberry, S.; Andreu, J. M.; Díaz, J. F. Microtubule Interactions with Chemically Diverse Stabilizing Agents: Thermodynamics of Binding to the Paclitaxel Site Predicts Cytotoxicity. *Chem. Biol.* **2005**, *12*, 1269–1279.

- (33) Buey, R. M.; Díaz, J. F.; Andreu, J. M.; O'Brate, A.; Giannakakou, P.; Nicolaou, K. C.; Sasmal, P. K.; Ritzén, A.; Namoto, K. Interaction of Epothilone Analogs With the Paclitaxel Binding Site: Relationship Between Binding Affinity, Microtubule Stabilization, and Cytotoxicity. *Chem. Biol.* **2004**, *11*, 225–236.
- (34) Diaz, J. F.; Valpuesta, J. M.; Chacon, P.; Diakun, G.; Andreu, J. M. Changes in Microtubule Protofilament Number Induced by Taxol Binding to an Easily Accessible Site. *J. Biol. Chem.* **1998**, *273*, 33803–33810.
- (35) Huang, G. S.; Lopez-Barcons, L.; Freeze, B. S.; Smith, A. B.; Goldberg, G. L.; Horwitz, S. B.; McDaid, H. M. Potentiation of Taxol Efficacy by Discodermolide in Ovarian Carcinoma Xenograft-Bearing Mice. *Clin. Cancer Res.* **2006**, *12*, 298–304.
- (36) He, L.; Huang Yang, C.-P.; Horwitz, S. B. Mutations in B-Tubulin Map to Domains Involved in Regulation of Microtubule Stability in Epothilone- Resistant Cell Lines I. *Mol. Cancer Ther.* **2001**, *1*, 3–10.
- (37) Photiou, A.; Shah, P.; Leong, L. K.; Moss, J.; Retsas, S. In Vitro Synergy of Paclitaxel (Taxol) and Vinorelbine (navelbine) against Human Melanoma Cell Lines. *Eur. J. Cancer* **1997**, *33*, 463–470.
- (38) Knick, V. C.; Eberwein, D. J.; Miller, C. G. Vinorelbine Tartrate and Paclitaxel Combinations: Enhanced Activity Against In Vivo P388 Murine Leukemia Cells. *J. Natl. Cancer Inst.* **1995**, *87*, 1072–1077.
- (39) Carles, G.; Braguer, D.; Sabeur, G.; Briand, C. The Effect of Combining Antitubulin Agents on Differentiated and Undifferentiated Human Colon Cancer Cells. *Anticancer. Drugs* **1998**, *9*, 209–222.
- (40) Garcia, P.; Braguer, D.; Carles, G.; Briand, C. Simultaneous Combination of Microtubule Depolymerizing and Stabilizing Agents Acts at Low Doses. *Anticancer. Drugs* **1995**, *6*, 533–544.
- (41) Giannakakou, P.; Villalba, L.; Li, H.; Poruchynsky, M.; Fojo, T. Combinations of Paclitaxel and Vinblastine and Their Effects on Tubulin Polymerization and Cellular Cytotoxicity: Characterization of a Synergistic Schedule. *Int. J. Cancer* **1998**, *75*, 57–63.
- (42) Seidman, A. D.; Scher, H. I.; Petrylak, D.; Dershaw, D. D.; Curley, T. Estramustine and Vinblastine: Use of Prostate Specific Antigen as a Clinical Trial End Point for Hormone Refractory Prostatic Cancer. *J. Urol.* **1992**, *147*, 931–934.
- (43) Hudes, G. R.; Nathan, F.; Khater, C.; Haas, N.; Cornfield, M.; Giantonio, B.; Greenberg, R.; Gomella, L.; Litwin, S.; Ross, E.; et al. Phase II Trial of 96-Hour Paclitaxel plus Oral Estramustine Phosphate in Metastatic Hormone-Refractory Prostate Cancer. *J. Clin. Oncol.* **1997**, *15*, 3156–3163.

- (44) Honore, S.; Kamath, K.; Braguer, D.; Horwitz, S. B.; Wilson, L.; Briand, C.; Jordan, M. A. Synergistic Suppression of Microtubule Dynamics by Discodermolide and Paclitaxel in Non-Small Cell Lung Carcinoma Cells. *Cancer Res.* **2004**, *64*, 4957–4964.
- (45) Xia, S.; Kenesky, C. S.; Rucker, P. V.; Smith, A. B.; Orr, G. A.; Horwitz, S. B. A Photoaffinity Analogue of Discodermolide Specifically Labels a Peptide in B-Tubulin $\dagger$ . *Biochemistry* **2006**, *45*, 11762–11775.
- (46) Chou, T.-C.; Talalay, P. Quantitative Analysis of Dose-Effect Relationships: The Combined Effects of Multiple Drugs or Enzyme Inhibitors. *Adv. Enzyme Regul.* **1984**, *22*, 27–55.
- (47) Klein, L. E.; Freeze, B. S.; Smith, A. B.; Horwitz, S. B. The Microtubule Stabilizing Agent Discodermolide Is a Potent Inducer of Accelerated Cell Senescence. *Cell Cycle* **2005**, *4*, 501–507.
- (48) Gewirtz, D. A.; Holt, S. E.; Elmore, L. W. Accelerated Senescence: An Emerging Role in Tumor Cell Response to Chemotherapy and Radiation. *Biochem. Pharmacol.* **2008**, *76*, 947–957.
- (49) Chao, S. K.; Lin, J.; Brouwer-Visser, J.; Smith, A. B.; Horwitz, S. B.; McDaid, H. M. Resistance to Discodermolide, a Microtubule-Stabilizing Agent and Senescence Inducer, Is 4E-BP1-dependent. *Proc. Natl. Acad. Sci.* **2011**, *108*, 391–396.
- (50) Collado, M.; Serrano, M. The Power and the Promise of Oncogene-Induced Senescence Markers. *Nat. Rev. Cancer* **2006**, *6*, 472–476.
- (51) Cobb, M. H.; Ross, E. M. Cell Communication: Principles of Cell Signaling. In *Cells*; Lewin, B.; Cassimeris, L.; Lingappa, V. R.; Plopper, G., Eds.; Jones and Bartlett Publishers: Sudbury, Massachusetts, 2007; pp. 587–643.
- (52) Nerenberg, J. B.; Hung, D. T.; Somers, P. K.; Schreiber, S. L. Total Synthesis of the Immunosuppressive Agent (-)-Discodermolide. *J. Am. Chem. Soc.* **1993**, *115*, 12621–12622.
- (53) Hung, D. T.; Nerenberg, J. B.; Schreiber, S. L. Distinct Binding and Cellular Properties of Synthetic (+)- and (-)-Discodermolides. *Chem. Biol.* **1994**, *1*, 67–71.
- (54) Smith, A. B.; Qiu, Y.; Jones, D. R.; Kobayashi, K. Total Synthesis of (-)-Discodermolide. *J. Am. Chem. Soc.* **1995**, *117*, 12011–12012.
- (55) Paterson, I.; Florence, G. The Chemical Synthesis of Discodermolide Tubulin-Binding Agents. In; Carlomagno, T., Ed.; Springer Berlin/Heidelberg, 2009; Vol. 286, pp. 73–119.
- (56) Smith, A. B.; Freeze, B. S. (+)-Discodermolide: Total Synthesis, Construction of Novel Analogues, and Biological Evaluation. *Tetrahedron* **2008**, *64*, 261–298.

- (57) Harried, S. S.; Yang, G.; Strawn, M. A.; Myles, D. C. Total Synthesis of (–)-Discodermolide: An Application of a Chelation-Controlled Alkylation Reaction. *J. Org. Chem.* **1997**, *62*, 6098–6099.
- (58) Marshall, J. A.; Johns, B. A. Total Synthesis of (+)-Discodermolide. *J. Org. Chem.* **1998**, *63*, 7885–7892.
- (59) Smith, A. B.; Kaufman, M. D.; Beauchamp, T. J.; LaMarche, M. J.; Arimoto, H. Gram-Scale Synthesis of (+)-Discodermolide. *Org. Lett.* **1999**, *1*, 1823–1826.
- (60) Paterson, I.; Florence, G. J.; Gerlach, K.; Scott, J. P. Total Synthesis of the Antimicrotubule Agent (+)-Discodermolide Using Boron-Mediated Aldol Reactions of Chiral Ketones. *Angew. Chemie Int. Ed.* **2000**, *39*, 377–380.
- (61) Mickel, S. J.; Sedelmeier, G. H.; Niederer, D.; Daeffler, R.; Osmani, A.; Schreiner, K.; Seeger-Weibel, M.; B<sup>1</sup>rod, B.; Schaer, K.; Gamboni, R.; et al. Large-Scale Synthesis of the Anti-Cancer Marine Natural Product (+)-Discodermolide. Part 1: Synthetic Strategy and Preparation of a Common Precursor. *Org. Process Res. Dev.* **2003**, *8*, 92–100.
- (62) Mickel, S. J.; Sedelmeier, G. H.; Niederer, D.; Schuerch, F.; Grimler, D.; Koch, G.; Daeffler, R.; Osmani, A.; Hirni, A.; Schaer, K.; et al. Large-Scale Synthesis of the Anti-Cancer Marine Natural Product (+)-Discodermolide. Part 2: Synthesis of Fragments C1-6 and C9-14. *Org. Process Res. Dev.* **2003**, *8*, 101–106.
- (63) Mickel, S. J.; Sedelmeier, G. H.; Niederer, D.; Schuerch, F.; Koch, G.; Kuesters, E.; Daeffler, R.; Osmani, A.; Seeger-Weibel, M.; Schmid, E.; et al. Large-Scale Synthesis of the Anti-Cancer Marine Natural Product (+)-Discodermolide. Part 3: Synthesis of Fragment C15-21. *Org. Process Res. Dev.* **2003**, *8*, 107–112.
- (64) Mickel, S. J.; Sedelmeier, G. H.; Niederer, D.; Schuerch, F.; Seger, M.; Schreiner, K.; Daeffler, R.; Osmani, A.; Bixel, D.; Loiseleur, O.; et al. Large-Scale Synthesis of the Anti-Cancer Marine Natural Product (+)-Discodermolide. Part 4: Preparation of Fragment C7-24. *Org. Process Res. Dev.* **2003**, *8*, 113–121.
- (65) Mickel, S. J.; Niederer, D.; Daeffler, R.; Osmani, A.; Kuesters, E.; Schmid, E.; Schaer, K.; Gamboni, R.; Chen, W.; Loeser, E.; et al. Large-Scale Synthesis of the Anti-Cancer Marine Natural Product (+)-Discodermolide. Part 5: Linkage of Fragments C1-6 and C7-24 and Finale. *Org. Process Res. Dev.* **2003**, *8*, 122–130.
- (66) Loiseleur, O.; Koch, G.; Cercus, J.; Schürch, F. A Formal Synthesis of (+)-Discodermolide. *Org. Process Res. Dev.* **2005**, *9*, 259–271.
- (67) Arefolov, A.; Panek, J. S. Crotylsilane Reagents in the Synthesis of Complex Polyketide Natural Products: Total Synthesis of (+)-Discodermolide. *J. Am. Chem. Soc.* **2005**, *127*, 5596–5603.

- (68) Smith, A. B.; Freeze, B. S.; Xian, M.; Hirose, T. Total Synthesis of (+)-Discodermolide: A Highly Convergent Fourth-Generation Approach. *Org. Lett.* **2005**, *7*, 1825–1828.
- (69) Smith, A. B.; Beauchamp, T. J.; LaMarche, M. J.; Kaufman, M. D.; Qiu, Y.; Arimoto, H.; Jones, D. R.; Kobayashi, K. Evolution of a Gram-Scale Synthesis of (+)-Discodermolide. *J. Am. Chem. Soc.* **2000**, *122*, 8654–8664.
- (70) Smith, A. B.; Freeze, B. S.; Brouard, I.; Hirose, T. A Practical Improvement, Enhancing the Large-Scale Synthesis of (+)-Discodermolide: A Third-Generation Approach. *Org. Lett.* **2003**, *5*, 4405–4408.
- (71) Harried, S. S.; Lee, C. P.; Yang, G.; Lee, T. I. H.; Myles, D. C. Total Synthesis of the Potent Microtubule-Stabilizing Agent (+)-Discodermolide. *J. Org. Chem.* **2003**, *68*, 6646–6660.
- (72) Marshall, J. A.; Lu, Z.-H.; Johns, B. A. Synthesis of Discodermolide Subunits by SE2<sup>+</sup> Addition of Nonracemic Allenylstannanes to Aldehydes. *J. Org. Chem.* **1998**, *63*, 817–823.
- (73) de Lemos, E.; Porée, F.-H.; Commerçon, A.; Betzer, J.-F.; Pancrazi, A.; Ardisson, J. A-Oxygenated Crotyltitanium and Dyotropic Rearrangement in the Total Synthesis of Discodermolide. *Angew. Chemie Int. Ed.* **2007**, *46*, 1917–1921.
- (74) Paterson, I.; Delgado, O.; Florence, G. J.; Lyothier, I.; Scott, J. P.; Sereinig, N. 1,6-Asymmetric Induction in Boron-Mediated Aldol Reactions: Application to a Practical Total Synthesis of (+)-Discodermolide. *Org. Lett.* **2003**, *5*, 35–38.
- (75) Paterson, I.; Lyothier, I. Total Synthesis of (+)-Discodermolide: An Improved Endgame Exploiting a Still–Gennari-Type Olefination with a C1–C8 B-Ketophosphonate Fragment†. *Org. Lett.* **2004**, *6*, 4933–4936.
- (76) Paterson, I.; Delgado, O.; Florence, G. J.; Lyothier, I.; O’Brien, M.; Scott, J. P.; Sereinig, N. A Second-Generation Total Synthesis of (+)-Discodermolide: The Development of a Practical Route Using Solely Substrate-Based Stereocontrol. *J. Org. Chem.* **2004**, *70*, 150–160.
- (77) Smith, A. B.; Freeze, B. S.; Lamarche, M. J.; Hirose, T.; Brouard, I.; Xian, M.; Sundermann, K. F.; Shaw, S. J.; Burlingame, M. A.; Horwitz, S. B.; et al. Design, Synthesis, and Evaluation of Analogues of (+)-14-Normethyldiscodermolide. *Org. Lett.* **2005**, *7*, 315–318.
- (78) Ikeda, Y.; Ukai, J.; Ikeda, N.; Yamamoto, H. Stereoselective Synthesis of (z)- and (e)-1,3-Alkadienes from Aldehydes Using Organotitanium and Lithium Reagents. *Tetrahedron* **1987**, *43*, 723–730.

- (79) Mukaiyama, T.; Narasaka, K.; Banno, K. NEW ALDOL TYPE REACTION. *Chem. Lett.* **1973**, 2, 1011–1014.
- (80) Paterson, I.; Perkins, M. V. Studies in Polypropionate Synthesis: Stereoselective Synthesis of (–)-Denticulatin A and B. *Tetrahedron Lett.* **1992**, 33, 801–804.
- (81) Shaw, S. J. The Structure Activity Relationship of Discodermolide Analogues. *Mini Rev. Med. Chem.* **2008**, 8, 276–284.
- (82) Kinder Jr., F. R.; Bair, K. W.; Ramsey, T. M.; Sabio, M. L. Certain Substituted Polyketides, Pharmaceutical Compositions Containing Them and Their Use in Treating Tumors. WIPO patent 2,003,014,102, 2003.
- (83) Kinder Jr., F. R. Process for Preparing Discodermolide and Analogues Thereof. WIPO patent 2,002,012,220, 2002.
- (84) Kinder Jr., F. R.; Bair, K. W.; Chen, W.; Florence, G. J.; Francavilla, C.; Geng, P.; Gunasekera, S.; Lassota, P. T.; Longley, R.; Palermo, M.; et al. Poster #3650. *American Association for Cancer Research 93rd Annual Meeting*, 2002.
- (85) Smith, A. B.; Rucker, P. V.; Brouard, I.; Freeze, B. S.; Xia, S.; Horwitz, S. B. Design, Synthesis, and Biological Evaluation of Potent Discodermolide Fluorescent and Photoaffinity Molecular Probes. *Org. Lett.* **2005**, 7, 5199–5202.
- (86) Kinder Jr., F. R.; Kapa, P. K.; Loeser, E. M. Certain Salts of Discodermolide Acid, Pharmaceutical Compositions Containing Them and Their Use in Treating Tumors. WIPO patent 2,002,098,843, 2003.
- (87) De Lemos, E.; Agouridas, E.; Sorin, G.; Guerreiro, A.; Commerçon, A.; Pancrazi, A.; Betzer, J.-F.; Lannou, M.-I.; Ardisson, J. Conception, Synthesis, and Biological Evaluation of Original Discodermolide Analogues. *Chem. – A Eur. J.* **2011**, 17, 10123–10134.
- (88) Smith, A. B.; Freeze, B. S.; LaMarche, M. J.; Hirose, T.; Brouard, I.; Rucker, P. V.; Xian, M.; Sundermann, K. F.; Shaw, S. J.; Burlingame, M. A.; et al. Design, Synthesis, and Evaluation of Carbamate-Substituted Analogues of (+)-Discodermolide. *Org. Lett.* **2005**, 7, 311–314.
- (89) Smith, A. B.; Sugawara, K.; Atasoylu, O.; Yang, C.-P. H.; Horwitz, S. B. Design and Synthesis of (+)-Discodermolide–Paclitaxel Hybrids Leading to Enhanced Biological Activity. *J. Med. Chem.* **2011**, 54, 6319–6327.
- (90) Martello, L. A.; LaMarche, M. J.; He, L.; Beauchamp, T. J.; Smith III, A. B.; Horwitz, S. B. The Relationship between Taxol and (+)-Discodermolide: Synthetic Analogs and Modeling Studies. *Chem. Biol.* **2001**, 8, 843–855.

- (91) Gunasekera, S. P.; Paul, G. K.; Longley, R. E.; Isbrucker, R. A.; Pomponi, S. A. Five New Discodermolide Analogues from the Marine Sponge Discodermia Species. *J. Nat. Prod.* **2002**, *65*, 1643–1648.
- (92) Paterson, I.; Delgado, O. Synthesis of Novel Discodermolide Analogues with Modified Hydrogen-Bonding Donor/acceptor Sites. *Tetrahedron Lett.* **2003**, *44*, 8877–8882.
- (93) Gunasekera, S. P.; Longley, R. E.; Isbrucker, R. A. Semisynthetic Analogues of the Microtubule-Stabilizing Agent Discodermolide: Preparation and Biological Activity. *J. Nat. Prod.* **2002**, *65*, 1830–1837.
- (94) Gunasekera, S. P.; Mickel, S. J.; Daeffler, R.; Niederer, D.; Wright, A. E.; Linley, P.; Pitts, T. Synthetic Analogues of the Microtubule-Stabilizing Agent (+)-Discodermolide: Preparation and Biological Activity. *J. Nat. Prod.* **2004**, *67*, 749–756.
- (95) Smith, A. B.; Xian, M.; Liu, F. Design, Total Synthesis, and Evaluation of C(13)–C(14) Cyclopropane Analogues of (+)-Discodermolide. *Org. Lett.* **2005**, *7*, 4613–4616.
- (96) Shaw, S. J.; Sundermann, K. F.; Burlingame, M. A.; Myles, D. C.; Freeze, B. S.; Xian, M.; Brouard, I.; Smith, A. B. Toward Understanding How the Lactone Moiety of Discodermolide Affects Activity. *J. Am. Chem. Soc.* **2005**, *127*, 6532–6533.
- (97) Paterson, I.; Perkins, M. V. Total Synthesis of (–)-Denticulatins A and B Using Efficient Methods of Acyclic Stereocontrol. *Tetrahedron* **1996**, *52*, 1811–1834.
- (98) Gunasekera, S. P.; Longley, R. E.; Isbrucker, R. A. Acetylated Analogues of the Microtubule-Stabilizing Agent Discodermolide: Preparation and Biological Activity. *J. Nat. Prod.* **2001**, *64*, 171–174.
- (99) Monteagudo, E.; Cicero, D. O.; Cornett, B.; Myles, D. C.; Snyder, J. P. The Conformations of Discodermolide in DMSO. *J. Am. Chem. Soc.* **2001**, *123*, 6929–6930.
- (100) Burlingame, M. A.; Shaw, S. J.; Sundermann, K. F.; Zhang, D.; Petryka, J.; Mendoza, E.; Liu, F.; Myles, D. C.; LaMarche, M. J.; Hirose, T.; et al. Design, Synthesis and Cytotoxicity of 7-Deoxy Aryl Discodermolide Analogues. *Bioorganic Med. Chem. Lett.* **2004**, *14*, 2335–2338.
- (101) Paterson, I.; Florence, G. J.; Gerlach, K.; Scott, J. P.; Sereinig, N. A Practical Synthesis of (+)-Discodermolide and Analogues: Fragment Union by Complex Aldol Reactions. *J. Am. Chem. Soc.* **2001**, *123*, 9535–9544.
- (102) Shaw, S. J.; Menzella, H. G.; Myles, D. C.; Xian, M.; Smith III, A. B. Coumarin-Derived Discodermolide Analogues Possessing Equivalent Antiproliferative Activity to the Natural Product—a Further Simplification of the Lactone Region. *Org. Biomol. Chem.* **2007**, *5*, 2753–2755.

- (103) Curran, D. P.; Furukawa, T. Simultaneous Preparation of Four Truncated Analogues of Discodermolide by Fluorous Mixture Synthesis. *Org. Lett.* **2002**, *4*, 2233–2235.
- (104) Isbrucker, R.; Gunasekera, S. P.; Longley, R. Structure-Activity Relationship Studies of Discodermolide and Its Semisynthetic Acetylated Analogs on Microtubule Function and Cytotoxicity. *Cancer Chemother. Pharmacol.* **2001**, *48*, 29–36.
- (105) Minguez, J. M.; Kim, S. Y.; Giuliano, K. A.; Balachandran, R.; Madiraju, C.; Day, B. W.; Curran, D. P. Synthesis and Biological Assessment of Simplified Analogues of the Potent Microtubule Stabilizer (+)-Discodermolide. *Bioorg. Med. Chem.* **2003**, *11*, 3335–3357.
- (106) Choy, N.; Shin, Y.; Nguyen, P. Q.; Curran, D. P.; Balachandran, R.; Madiraju, C.; Day, B. W. Simplified Discodermolide Analogues: Synthesis and Biological Evaluation of 4-Epi-7-Dehydroxy-14,16-Didemethyl-(+)-Discodermolides as Microtubule-Stabilizing Agents. *J. Med. Chem.* **2003**, *46*, 2846–2864.
- (107) Smith, A. B.; LaMarche, M. J.; Falcone-Hindley, M. Solution Structure of (+)-Discodermolide. *Org. Lett.* **2001**, *3*, 695–698.
- (108) Salum, L. B.; Dias, L. C.; Andricopulo, A. D. Fragment-Based QSAR and Molecular Modeling Studies on a Series of Discodermolide Analogs as Microtubule-Stabilizing Anticancer Agents. *QSAR Comb. Sci.* **2009**, *28*, 325–337.
- (109) Canales, A.; Matesanz, R.; Gardner, N. M.; Andreu, J. M.; Paterson, I.; Díaz, J. F.; Jiménez-Barbero, J. The Bound Conformation of Microtubule-Stabilizing Agents: NMR Insights into the Bioactive 3D Structure of Discodermolide and Dictyostatin. *Chem. – A Eur. J.* **2008**, *14*, 7557–7569.
- (110) Sánchez-Pedregal, V. M.; Kubicek, K.; Meiler, J.; Lyothier, I.; Paterson, I.; Carlomagno, T. The Tubulin-Bound Conformation of Discodermolide Derived by NMR Studies in Solution Supports a Common Pharmacophore Model for Epothilone and Discodermolide. *Angew. Chemie Int. Ed.* **2006**, *45*, 7388–7394.
- (111) Paterson, I.; Naylor, G. J.; Fujita, T.; Guzman, E.; Wright, A. E. Total Synthesis of a Library of Designed Hybrids of the Microtubule-Stabilising Anticancer Agents Taxol, Discodermolide and Dictyostatin. *Chem. Commun.* **2010**, *46*, 261–263.
- (112) Löwe, J.; Li, H.; Downing, K. H.; Nogales, E. Refined Structure of A $\beta$ -Tubulin at 3.5 Å Resolution. *J. Mol. Biol.* **2001**, *313*, 1045–1057.
- (113) Jogalekar, A. S.; Kriel, F. H.; Shi, Q.; Cornett, B.; Cicero, D.; Snyder, J. P. The Discodermolide Hairpin Structure Flows from Conformationally Stable Modular Motifs. *J. Med. Chem.* **2010**, *53*, 155–165.
- (114) Brody, D. M. Synthesis of Simplified Discodermolide Analogues. Masters Thesis, University of Pittsburgh, Pittsburgh, PA, 2013.

- (115) Dömling, A.; Ugi, I. Multicomponent Reactions with Isocyanides. *Angew. Chemie Int. Ed.* **2000**, *39*, 3168–3210.
- (116) Dömling, A.; Wang, W.; Wang, K. Chemistry and Biology Of Multicomponent Reactions. *Chem. Rev.* **2012**.
- (117) Pando, O.; Stark, S.; Denkert, A.; Porzel, A.; Preusentanz, R.; Wessjohann, L. A. The Multiple Multicomponent Approach to Natural Product Mimics: Tubugis, N-Substituted Anticancer Peptides with Picomolar Activity. *J. Am. Chem. Soc.* **2011**, *133*, 7692–7695.
- (118) Ugi, I.; Meyr, R. Neue Darstellungsmethode Für Isonitrile. *Angew. Chemie* **1958**, *70*, 702–703.
- (119) Ugi, I.; Meyr, R. Isonitrile, I. Darstellung von Isonitrilen Aus Monosubstituierten Formamiden Durch Wasserabspaltung. *Chem. Ber.* **1960**, *93*, 239–248.
- (120) Van Leusen, A. M.; Wildeman, J.; Oldenziel, O. H. Chemistry of Sulfonylmethyl Isocyanides. 12. Base-Induced Cycloaddition of Sulfonylmethyl Isocyanides to Carbon,nitrogen Double Bonds. Synthesis of 1,5-Disubstituted and 1,4,5-Trisubstituted Imidazoles from Aldimines and Imidoyl Chlorides. *J. Org. Chem.* **1977**, *42*, 1153–1159.
- (121) Day, B. W.; Kangani, C. O.; Avor, K. S. Convenient Syntheses of (2R,3S,4R)-3-(tert-Butyldimethylsilyloxy)-2,4-Dimethyl-5-Oxopentanoic Acid Methoxymethylamide from Methacrolein. Preparation of C1-C7 and C17-C24 Fragments of (+)-Discodermolide. *Tetrahedron: Asymmetry* **2002**, *13*, 1161–1165.
- (122) Loiseleur, O.; Koch, G.; Wagner, T. A Practical Building Block for the Synthesis of Discodermolide. *Org. Process Res. Dev.* **2004**, *8*, 597–602.
- (123) Gage, J. R.; Evans, D. A. (S)-4-(phenylmethyl)-2-Oxazolidinone. *Org. Synth.* **1993**, *68*, 77.
- (124) Evans, D. A.; Fitch, D. M. Enantioselective Synthesis of the Elaiophylin Aglycon. *J. Org. Chem.* **1997**, *62*, 454–455.
- (125) Bifulco, G.; Dambruoso, P.; Gomez-Paloma, L.; Riccio, R. Determination of Relative Configuration in Organic Compounds by NMR Spectroscopy and Computational Methods. *Chem. Rev.* **2007**, *107*, 3744–3779.
- (126) Yan, B.; Spilling, C. D. Stereospecific Pd(O)-Catalyzed Malonate Additions to Allylic Hydroxy Phosphonate Derivatives: A Formal Synthesis of (-)-Enterolactone. *J. Org. Chem.* **2004**, *69*, 2859–2862.
- (127) Epp, J. B.; Widlanski, T. S. Facile Preparation of Nucleoside-5'-Carboxylic Acids. *J. Org. Chem.* **1998**, *64*, 293–295.

- (128) Garegg, P. J.; Regberg, T.; Stawinski, J.; Stromberg, R. A Phosphorus Nuclear Magnetic Resonance Spectroscopic Study of the Conversion of Hydroxy Groups into Iodo Groups in Carbohydrates Using the Iodine-Triphenylphosphine-Imidazole Reagent. *J. Chem. Soc. Perkin Trans. 2* **1987**, 271–274.
- (129) Umezawa, T.; Sueda, M.; Kamura, T.; Kawahara, T.; Han, X.; Okino, T.; Matsuda, F. Synthesis and Biological Activity of Kalkitoxin and Its Analogues. *J. Org. Chem.* **2011**, *77*, 357–370.
- (130) Matt, C.; Wagner, A.; Mioskowski, C. Novel Transformation of Primary Nitroalkanes and Primary Alkyl Bromides to the Corresponding Carboxylic Acids. *J. Org. Chem.* **1997**, *62*, 234–235.
- (131) Bottini, A. T.; Dev, V.; Klinck, J. 2-Bromoallylamine. *Org. Synth.* **1973**, *5*, 121.
- (132) Nodiff, A. E.; Hulsizer, J. M.; Tanabe, K. No Title. *Chem. Ind.* **1974**, 962.
- (133) Shen, J.; Woodward, R.; Kedenburg, J. P.; Liu, X.; Chen, M.; Fang, L.; Sun, D.; Wang, P. G. Histone Deacetylase Inhibitors through Click Chemistry. *J. Med. Chem.* **2008**, *51*, 7417–7427.
- (134) Keck, G. E.; Krishnamurthy, D. Catalytic Assymmetric Allylation Reactions: (S)-1-(phenylmethoxy)-4-Penten-2-Ol. *Org. Synth.* **1998**, *75*, 12.
- (135) Nicolaou, K. C.; Adsool, V. A.; Hale, C. R. H. An Expedient Procedure for the Oxidative Cleavage of Olefinic Bonds with PhI(OAc)<sub>2</sub>, NMO, and Catalytic OsO<sub>4</sub>. *Org. Lett.* **2010**, *12*, 1552–1555.
- (136) Roush, W. R.; Sun, H. Synthesis of (+)-B-Allyldiisopinocampheylborane and Its Reaction with Aldehydes. *Org. Synth.* **2011**, *88*, 87.
- (137) de Lemos, E.; Porée, F.-H.; Bourin, A.; Barbion, J.; Agouridas, E.; Lannou, M.-I.; Commerçon, A.; Betzer, J.-F.; Pancrazi, A.; Ardisson, J. Total Synthesis of Discodermolide: Optimization of the Effective Synthetic Route. *Chem. – A Eur. J.* **2008**, *14*, 11092–11112.